Accurate calculations using explicitly correlated wave functions

by
Pål Dahle

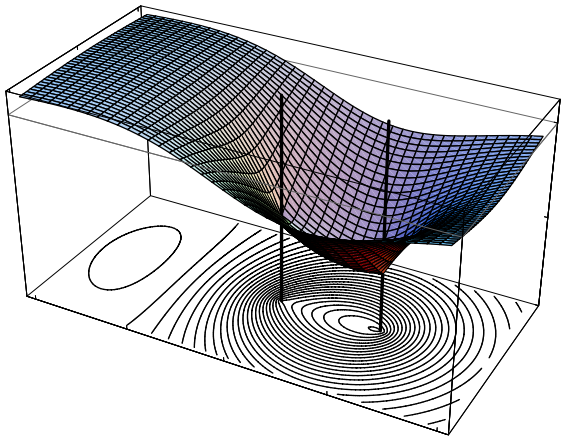

Dissertation presented for the degree of
doctor philosophiae

Department of Chemistry
Faculty of Mathematics and Natural Sciences
University of Oslo
Norway
2004

Preface

This thesis is based on research done in the period 1997–2001 while I was working as a teaching assistant at the Department of Chemistry, University of Oslo. Parts of the research have also been done at the San Diego Supercomputer Center (SDSC) and the University of California, San Diego (UCSD) where I worked with Peter Taylor and his research group the spring of 1997 and the autumn of 1998. My position as a teaching assistant ended December 2001, and in January 2002 I entered a new position as a research scientist at the Norwegian Computing Center (NR). Since I started to write the thesis late 2001 I was not able to complete it before I entered my new position, and the writing of this thesis has therefore been a major part time project ever since.

The results that are presented herein are based on research made in collaboration with Peter Taylor, Trygve Helgaker, Dan Jonsson, B. Joakim Persson, and Robert Polly, and their contributions will be summarised below.

The original idea of expanding pair functions using both the conventional virtual orbitals expansion and a set of Gaussian-type geminals with preselected and fixed exponents and centres, belongs to Peter Taylor. In collaboration with B. Joakim Persson he showed [59] that a linear combination of Gaussian-type correlation factors may be used to represent the linear r_{12} term, and while they originally intended to keep this linear combination fixed during the calculation, they ended up treating the coefficients as variational parameters in the proof of concept calculations that were made with the GEMINAL91 [64] program.

In early 1997, we started to develop a new integral program for the evaluation of integrals over combinations of orbitals and Gaussian-type geminals at the San Diego Supercomputer Center. This integral code was developed as a branch of Trygve Helgaker's ERI [82] (electron repulsion integrals) code, and the conventional two-electron repulsion integrals are, essentially, still calculated using his original code. The code for calculating geminal integrals, however, is today completely separated from the ERI program and is developed under the name GREMLIN [51].

The first equation solver was implemented by B. Joakim Persson in 1997, but this solver never got around to be used. Instead, it became a starting point for the equation solver later implemented by Dan Jonsson. In this implementation one of the challenges was to solve for the expansion coefficients of virtual orbitals and

the expansion coefficients of geminals separately. The final strategy to use a Schur decomposition was suggested by Trygve Helgaker.

The first pair energies were obtained in late 1998 after considerable effort had been made to identify and remove bugs from the integral code. Dan Jonsson played an important role in this work. Later, Robert Polly joined our efforts to keep the integral code as bug free as possible.

During 1999, we gradually realized that the original ansatz of Persson and Taylor to construct geminals as a linear combination of Gaussian-type correlation factors multiplied with a pair of occupied orbitals was deficient. This made us develop a set of new ansätze in which the pair of occupied orbitals is supplemented by more general orbital products, and by mid 2000, these had been implemented and tested. For the most flexible of them we sometimes get problems with linear dependencies and numerical stability. Knut Fægri has suggested a way to treat such singularities, but we have not been able to test it yet.

By the end of 2000, a lot of test calculations had been made and we were ready to make a systematic study of both one-electron and two-electron basis set effects. To be able to use a larger range of one-electron basis sets, general contraction had to be implemented in the integral code. This was done in the beginning of 2001 in close collaboration with Trygve Helgaker.

In chapter 6, we present formulas for prescreening of two- and three-electron integrals containing Gaussian-type geminals. These formulas have been developed in collaboration with Trygve Helgaker and Robert Polly. Robert Polly has also taken part in the development of expressions for reducing three-electron integrals to two-electron integrals by the use of the resolution of the identity.

The integral code has also been adapted for use in CASPT2 wave functions and with LMP2 methods. This work has been done in close collaboration with Robert Polly. No results from these projects are presented in this work however.

Acknowledgements

To those who gave me financial support . . .

As a doctoral student, I was not offered financial support by my local department to visit Peter Taylor and his research group at the San Diego Supercomputer Center. The collaboration with this group was therefore only possible due to the financial support I received from external sources.

The first stay in San Diego in the spring of 1997 was paid for by Peter Taylor who supported me with USD10.000 of his Grant No. CHE-9700627 from the National Science Foundation (United States). Later, he also paid for a travel to Lund where I stayed with Per-Åke Malmqvist and Robert Polly to work on the CASPT2 implementation, and for my travel to the "11$^{\text{th}}$ European Seminar on Computational Methods in Quantum Chemistry" which was held in Zakopane, Poland in 1999. The expenses covered by Peter Taylor for these two travels was NOK10.500.

The second stay in San Diego was supported by the Norwegian Research Council through Grant No. 125903/410 with the amount NOK77.000, but I also received several scholarships. From "Lise og Arnfinn Hejes fond" I received NOK20.000, from "Hans Henrik Maschmanns legat" I received NOK8.000, and from "Familien Stillesens stipendielegat" I received NOK6.000.

In 2000, I had a two-week stay in San Diego which was supported with NOK6.000 from "Familien Stillesens og professor S.A. Sexes legat", and a one-week stay in Stuttgart which was paid for by Hans-Joachim Werner with NOK7.000. In this stay I worked with Robert Polly on the LMP2 implementation.

In addition to the financial support received for travels, I have also received generous grants of computing time from the Norwegian Research Council through the Supercomputing Programme. Without these grants, the calculations presented in this work could not have been done.

Finally, I add that the Norwegian Computing Center gave me two weeks of paid leave to complete my thesis. These two weeks turned out to be invaluable to me.

I am deeply grateful for all the financial support I received for my research project; without this support I would never have been able to play an active part in the development of the GTG-MP2 theory.

To those who gave me personal support . . .

The years I have spent working on this project have been among the most stimulating and interesting of my life, and being privileged, I always looked forward to get to work. A major reason for this was probably the tea and coffee breaks at Café Erwin. This *ad hoc* Café was opened in 1993 and was always the natural meeting point for the theoretical chemistry group and cand.scient. students in environmental chemistry. I am very grateful to all the individuals who turned Café Erwin into the high-spirited meeting place it once was. As the list of Erwinists would count at least 50 people, I will not try and list any of them here. Along with the other chemistry students and employees, the Erwinists were also responsible for making the department of chemistry such a wonderful place to be a student.

A special thank goes to Trygve and Knut who always represented social and scientific backbones in the theoretical chemistry group. Along with Peter, Trygve also made valuable comments to this thesis.

Except for Trygve, all of my research associates were parts of Peter's research group in San Diego. In addition to Peter, these were Joakim, Dan, and Robert. I would like to thank all of you for your friendship and for making the stays in San Diego so memorable. How can I ever forget the lunch breaks at "The Grove" with chocolate-chip coffee cakes, the trips to "Spices" and "Thai house", the Penguin chocolates offered by Peter each time a new shipload had arrived from England, and the Friday at Porter's pub? A very special thank goes to Peter who made all of this possible. If it weren't for him and his research project, I would probably have left quantum chemistry in 1997.

I also thank my former wife Maria for making the stays in San Diego possible, and for giving me two precious children.

The last few years I have received a lot of personal support from my close friends Bent, Jon-Are, Jørund, and Rune. I highly appreciate your friendship and all the support you gave me when times were rough.

During my years as a student I also received support from my parents, brothers, and parents-in-law. Especially I appreciate the support I got from my mother when a middle-ear infection almost got me.

The final and biggest thank goes to my children, Gabriel and Linnea, who have seen less of their father the last couple of years than they should have, but without ever complaining. If nothing else, I hope that the persistence I have shown in this work may inspire you to reach the goals of your lives.

Oslo, May 2004

Pål Dahle

Contents

Chapter 1

Introduction

1.1 One-electron and N-electron expansions of the wave function

For nearly all systems of chemical interest, the Schrödinger equation can only be solved if approximations are introduced. Computational quantum chemistry has developed a set of models for the construction of approximate wave functions, which provide solutions of different accuracy to the Schrödinger equation. Common to these models is that they consist of linear combinations of Slater determinants, and the main difference between the methods is the computational procedure used to evaluate the expansion coefficients.

A Slater determinant is a linear combination of anti-symmetrised products of one-electron functions (orbitals), and the space in which the Slater determinant is expanded is referred to as the one-electron space or orbital space. The space distinguishing the different models, is spanned by all determinants that can be generated from the available orbitals, and is referred to as the N-electron space, or Fock space.

At the simplest level of approximation, the wave function is represented by a single Slater determinant. When the orbitals in this determinant are optimised with respect to the electronic energy, the Hartree–Fock (HF) determinant is obtained, and the optimised orbitals are referred to as the Hartree–Fock orbitals.

Beyond Hartree–Fock, there are methods like MP2, CCSD, CCSD(T), and FCI in which several (MP2) or all (CCSD, CCSD(T), FCI) Slater determinants are included in the expansion of the wave function. The expansion coefficients of these determinants are computed with gradually larger flexibility, and for the full CI method, which is the best wave function that can be constructed as a linear combination of Slater determinant in a given one-electron basis, all expansion coefficients are optimised variationally. In the following we will refer to methods using linear combinations of Slater determinants in the expansion of the wave function, as

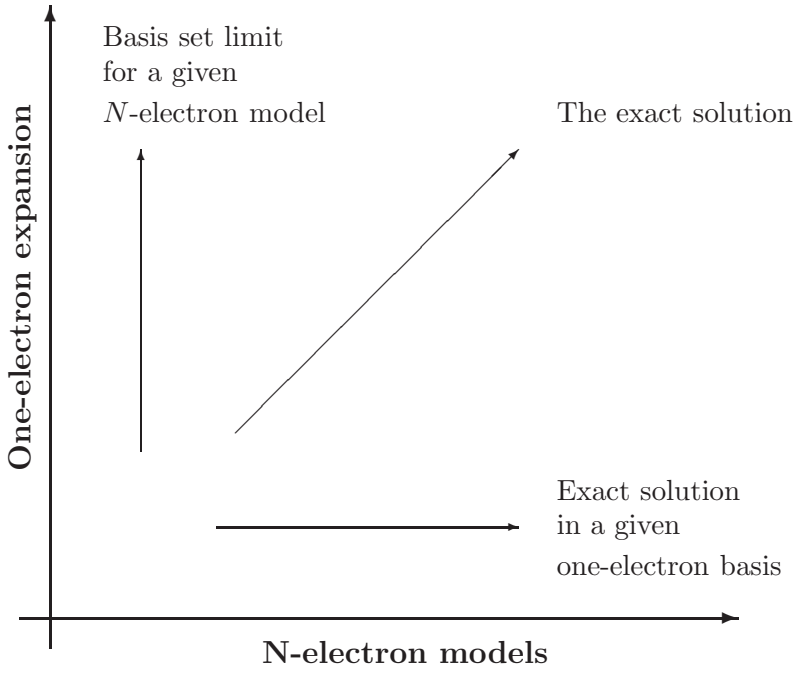

Figure 1.1: Approaching the exact solution by improving both the one-electron and the N-electron description [1].

configuration interaction (CI) methods.

An important point about the CI methods given above, is that they allow us to treat the errors in the Fock space systematically by using gradually better methods, that is, methods of higher levels of theory. This allows us to control the error in the computed molecular energies and molecular properties, and when better estimates are needed, higher levels of theory may be used.

If the orbitals in terms of which the determinants are expanded form a complete set in the orbital space and all determinants that can be generated from these orbitals are included in the expansion of the N-electron wave function, the exact wave function is obtained. If the orbital space is incomplete or determinants are left out, however, there will be an error in the wave function. Moreover, an improvement in the orbital space cannot compensate for errors in the Fock space and *vice versa*. It is therefore important to investigate both the one-electron space and the N-electron space independently, in order to understand what accuracy can be expected for a given calculation. The way a finite expansion of these spaces affect the quality of the wave function is illustrated in Figure 1.1.

In this work we present a new method which aims at reaching the one-electron basis set limit for the MP2 method. The MP2 method may be regarded as an approximation to the CCSD method, however, and conclusions made for the MP2 method will also be valid for the higher level methods.

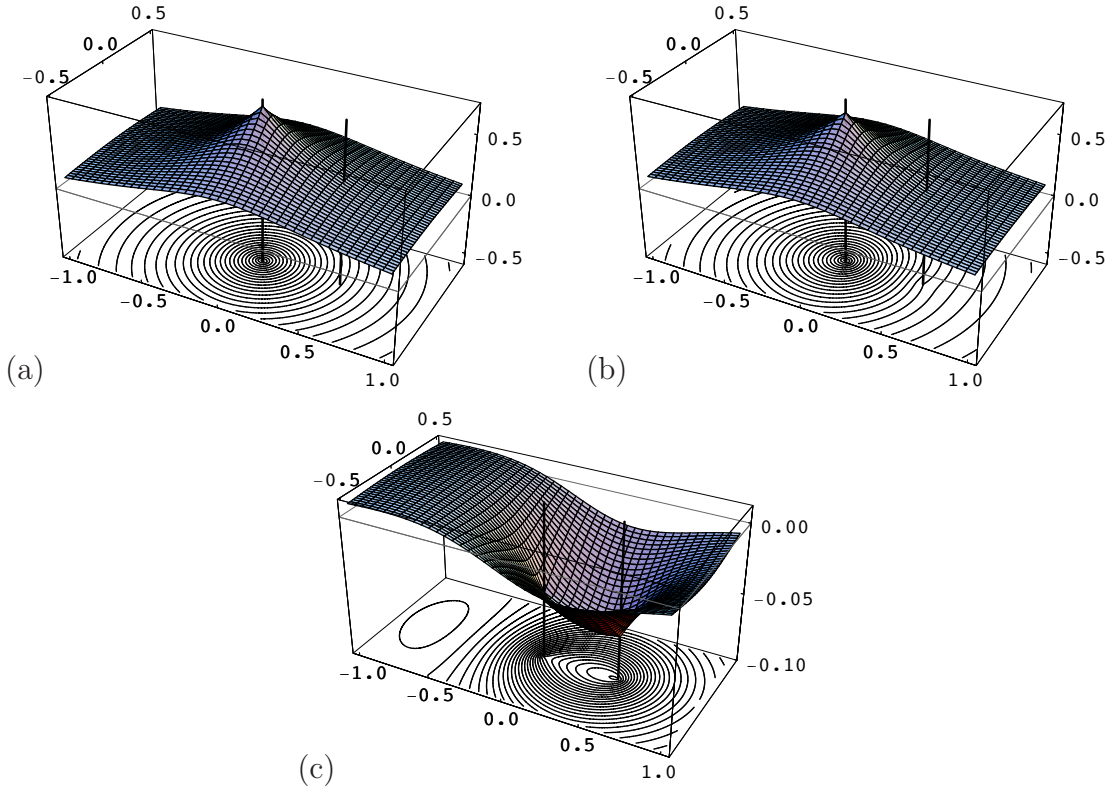

Figure 1.2: (a) The Hartree–Fock ground-state wave function and (b) the exact ground-state wave function of the helium atom with one electron fixed at a position $0.5a_0$ away from the nucleus. The wave functions are plotted in a plane containing the nucleus and the fixed electron, the positions of which are indicated by the vertical bars. (c) The Coulomb hole of the ground-state helium atom, calculated as the difference between the exact wave function and the Hartree–Fock wave function. Note that, the scale of Figure (c) differs from that of Figures (a) and (b). The illustration is taken from Ref. [1].

1.2 The Coulomb hole of the helium atom

In the Hartree–Fock approximation, the electrons move independently of each other in the average field of the other electrons, and the instantaneous position of the electrons does not affect the motion. This is illustrated in Figure 1.2 (a), where we have plotted the Hartree–Fock wave function of a helium atom in which one of the electrons have been fixed at a position $0.5a_0$ away from the nucleus. The concentric circles show that the wave function amplitude for the free electron only depends on the distance from the nucleus and not on the position of the fixed electron.

In Figure 1.2 (b), we have plotted the exact wave function for the same helium system. The contours in this plot are not perfect circles anymore, as small distortions

are seen close to the fixed electron. By comparing the plots for the exact wave function and the Hartree–Fock wave function, we see that the Hartree–Fock method overestimates the probability of finding two electrons near each other. This is seen more clearly in Figure 1.2 (c), where we have plotted the difference between the exact wave function and the Hartree–Fock wave function. The probability of finding the free electron is now shifted away from the fixed electron, leaving a hole called the *Coulomb hole* at the position of the fixed electron. The Coulomb hole is shallow but wide, and the amplitude removed from the hole is moved to the opposite side of the nucleus, creating a local maximum approximately $1.3a_0$ away from the fixed electron. Since the instantaneous position of one electron this way affects the movement of the other, the two electrons are said to be *correlated*.

Wave function models that go beyond Hartree–Fock, that is, include more than one Slater determinant in the expansion of the Fock space, gradually describes the Coulomb hole better as higher levels of theory are used. Within each of these models it is rather easy to obtain a crude approximation of the Coulomb hole using a superposition of antisymmetric orbital products, but it is very difficult to represent the hole accurately. And the shorter the electron-electron distance, the more difficult it is to describe the correlated movements of the electrons.

1.3 The Coulomb cusp of the helium atom

In the current section we investigate the analytical behaviour of the exact wave function for the helium atom when the two electrons coincide.

As the ground-state wave function of helium is totally symmetric we may express the Schrödinger equation in terms of radial coordinates as

$$H\Psi(r_1, r_2, r_{12}) = E\Psi(r_1, r_2, r_{12}) \tag{1.1}$$

where r_1 and r_2 are the distances between the electrons and the nucleus, and r_{12} is the inter-electronic distance. In terms of these coordinates the Hamiltonian is [2]

$$\begin{aligned} H = &-\frac{1}{2}\frac{\partial^2}{\partial r_1^2} - \frac{1}{r_1}\frac{\partial}{\partial r_1} - \frac{Z}{r_1} - \frac{1}{2}\frac{\partial^2}{\partial r_2^2} - \frac{1}{r_2}\frac{\partial}{\partial r_2} - \frac{Z}{r_2} \\ &- \frac{\partial^2}{\partial r_1 \partial r_{12}}\frac{r_1^2 - r_2^2 + r_{12}^2}{r_1 r_{12}} - \frac{\partial^2}{\partial r_2 \partial r_{12}}\frac{r_2^2 - r_1^2 + r_{12}^2}{r_2 r_{12}} \\ &- \frac{\partial^2}{\partial r_{12}^2} - \frac{2}{r_{12}}\frac{\partial}{\partial r_{12}} + \frac{1}{r_{12}} \end{aligned} \tag{1.2}$$

where Z is the charge of the helium nucleus. The exact solution to (1.1) should contain terms that balance the Coulomb singularities in the Hamiltonian. For electron one, for instance, the singularity at the nucleus is balanced if we impose the

condition

$$\left.\frac{\partial\Psi}{\partial r_1}\right|_{r_1=0} = -Z\Psi(0, r_2, r_{12}) \tag{1.3}$$

on the wave function, and for electron two there is a similar relationship. Likewise, there is a singularity in the Hamiltonian for $r_{12} = 0$, and this singularity can only be balanced, if we impose the additional condition

$$\left.\frac{\partial\Psi}{\partial r_{12}}\right|_{r_{12}=0} = \frac{1}{2}\Psi(r_c, r_c, 0) \tag{1.4}$$

on the wave function, for any point $\mathbf{r}_c$.

Equation (1.3) determines the behaviour of the exact wave function when the electrons are close to the nucleus, and is known as *nuclear cusp condition*. Similarly, Equation (1.4) determines the behaviour of the wave function when the two electrons are close in space, and is known as the *electronic cusp condition* [3, 4]. The latter condition implies, that for small electron-electron distances the wave function must scale linearly with r_{12}

$$\Psi(r_1, r_2, r_{12}) \propto 1 + \frac{1}{2}r_{12} + \mathcal{O}(r_{12}^2) \tag{1.5}$$

A CI expansion in pure orbital products cannot reproduce the electronic cusp condition. This was first realized by Hylleraas [2], who noted that the CI wave function, when expressed in terms of r_1, r_2, and r_{12} contains arbitrary powers of r_1 and r_2, but only even powers of r_{12}. This seemed unreasonable to Hylleraas as these coordinates are treated symmetrically in the Hamiltonian (1.2), and he decided to add terms of odd powers of r_{12} to the CI expansion. When doing this, Hylleraas managed to reduced the error in the calculated ionisation potential of helium from 0.12 eV to 0.01 eV relative to the value obtained from experiments. His final estimate of the ionisation potential was 24.58 eV.

1.4 Basis set truncation errors

The failure of the CI wave function to reproduce (1.5) is illustrated in Figure 1.3, where we have plotted partial-wave expansions of the inter-electronic distance, in which r_{12} is expressed in terms of r_1, r_2, and $\cos\theta_{12}$.

For the partial-wave expansion of the CI ground-state helium wave function, it has been shown [5, 6] that for high values of the angular momentum L, the energy increment $\varepsilon_L = E_L - E_{L-1}$ goes as

$$\varepsilon_L = e_4\left(L + \frac{1}{2}\right)^{-4} + e_5\left(L + \frac{1}{2}\right)^{-5} + \cdots \tag{1.6}$$

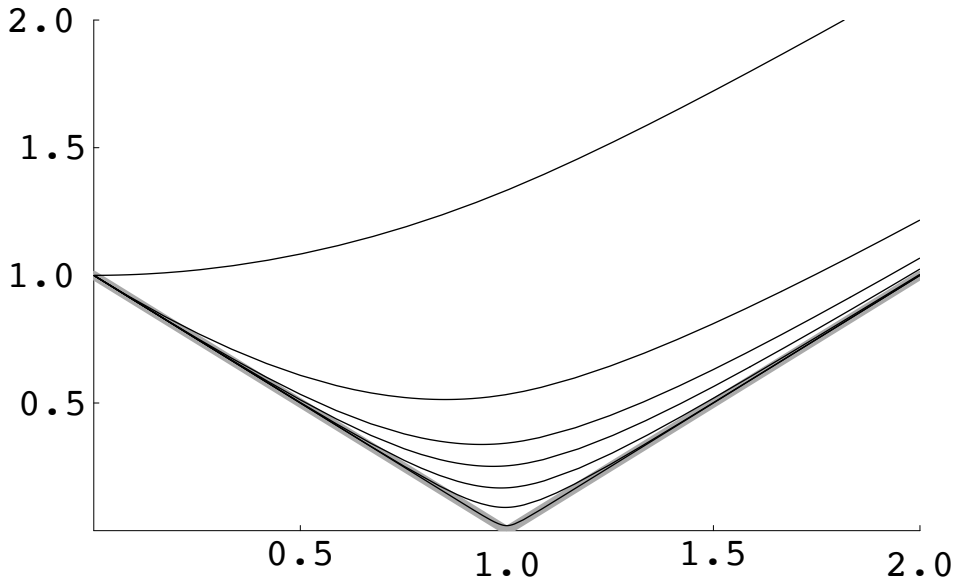

Figure 1.3: Partial-wave expansion of r_{12} in r_1, r_2 and θ_{12} for $r_2 = 1$ and $\theta_{12} = 0$. The orders of the expansions are $L = 0, 1, 2, 3, 5, 10$, and 50. The exact function r_{12} is represented by a thick grey line. The figure are taken from Ref. [1].

If the partial-wave expansion is truncated by including only terms less than or equal to L, the error in the ground-state energy becomes [1]

$$\Delta E_L \approx a\,(L+1)^{-3} \tag{1.7}$$

where the coefficient a is independent of L.

If we switch to the principal expansion, first studied by Helgaker *et al.* [1], a similar relationship is obtained. Letting N denote the maximum principal quantum number included in the expansion, the error in the energy is

$$\Delta E_N \approx cN^{-3} \tag{1.8}$$

This principal wave expansion and (1.8) has the advantage over the partial-wave expansion and (1.7), in that it allows us to predict the complete basis set limit of CI energies, by extrapolating energies obtained for small values of N.

1.5 First-order methods for many-electron systems

In the early 1960s, Sinanoğlu [7, 8] showed that the first-order many-body problem (e.g. MP2) may be reduced to a collection of uncoupled two-body equations for the first-order pair function. The MP2 many-electron wave function for atoms and

molecules could thereby be obtained from equations only slightly more complicated than those needed for two-electron systems like the helium atom.

Sinanoğlu [9] also showed how the second-order energy may be obtained variationally as a sum of pair contributions obtained by minimising a two-electron functional denoted the strong orthogonality (SO) functional. In contrast to solving first-order perturbation equations, this approach has the important consequence that it allows a large range of functions to be used in the expansion of pair functions, not just the product of virtual orbitals used in the orbital approximation. When the orbital approximation is used with Sinanoğlu's variational approach, however, the usual MP2 energy expression is obtained.

In search for the MP2 energy limit of atoms and molecules, Klopper and Kutzelnigg [6, 10, 11] have combined the SO functional of Sinanoğlu with basis functions linearly dependent of the inter-electronic distance r_{12}. This gives rise to expensive three- and four-electron integrals but these are avoided by the introduction of the resolution of the identity. The use of pair functions linearly dependent of r_{12}, allows for an accurate description of the inner part of the Coulomb hole.

An alternative approach for reaching the MP2 limit has been made by Szalewicz *et al.* [12–15]. Using the WO functional, which is a modification of the SO functional, these authors expand pair functions in Gaussian-type geminals, and optimise all non-linear parameters. The use of the WO functional removes the need for four-electron integrals, but three-electron integrals still have to be computed. The method of Szalewicz and co-workers is therefore computational more intensive than the method of Klopper and Kutzelnigg. An advantage, however, is that the computed pair energies are upper bounds to the true pair energies. Whereas Gaussian-type geminals do not describe the inner part of the Coulomb hole depicted in Figure 1.3 as well as basis functions linearly dependent of r_{12}, they are better suited for describing the overall shape depicted in Figure 1.2.

In this work, we shall investigate a new method for obtaining accurate second-order correlation energies using the WO functional and pair functions expanded in both the traditional pairs of virtual orbitals and a set of Gaussian-type geminals with preselected and fixed non-linear parameters.

Chapter 2

Time-independent perturbation theory

2.1 Rayleigh–Schrödinger perturbation theory

In bound-state, time-independent perturbation theory [16–19], we assume that the Hamiltonian may be partitioned as

$$H = H_0 + gH_1 \tag{2.1}$$

where gH_1 is a small correction to the zeroth-order Hamiltonian H_0. The perturbation parameter g is a real parameter, used for book keeping. Unless it may be identified with a physical quantity like an electric or magnetic field, the parameter is typically chosen as $g = 1$.

The eigenvalue problem we wish to solve is

$$H\left|\Psi_n\right\rangle = E_n\left|\Psi_n\right\rangle \tag{2.2}$$

and we assume that the unperturbed eigenvalue problem,

$$H_0\left|\Psi_n^{(0)}\right\rangle = E_n^{(0)}\left|\Psi_n^{(0)}\right\rangle \tag{2.3}$$

has already been solved and that no degeneracies are present. The fundamental idea of perturbation theory is to assume that both the exact wave functions Ψ_n and their corresponding eigenvalues E_n can be expanded in hopefully convergent power series of the perturbation parameter g

$$E_n = E_n^{(0)} + gE_n^{(1)} + g^2E_n^{(2)} + \cdots \tag{2.4}$$

$$\Psi_n = \Psi_n^{(0)} + g\Psi_n^{(1)} + g^2\Psi_n^{(2)} + \cdots \tag{2.5}$$

Substituting these expansions into (2.2) and comparing terms that are of the same order in g, we obtain the successive approximation equations

$$\begin{aligned} H_0 \left|\Psi_n^{(0)}\right\rangle &= E_n^{(0)} \left|\Psi_n^{(0)}\right\rangle && (2.6)\\ H_0 \left|\Psi_n^{(1)}\right\rangle + H_1 \left|\Psi_n^{(0)}\right\rangle &= E_n^{(0)} \left|\Psi_n^{(1)}\right\rangle + E_n^{(1)} \left|\Psi_n^{(0)}\right\rangle && (2.7)\\ H_0 \left|\Psi_n^{(2)}\right\rangle + H_1 \left|\Psi_n^{(1)}\right\rangle &= E_n^{(0)} \left|\Psi_n^{(2)}\right\rangle + E_n^{(1)} \left|\Psi_n^{(1)}\right\rangle + E_n^{(2)} \left|\Psi_n^{(0)}\right\rangle && (2.8)\\ H_0 \left|\Psi_n^{(k)}\right\rangle + H_1 \left|\Psi_n^{(k-1)}\right\rangle &= \sum_{l=0}^{k} E_n^{(l)} \left|\Psi_n^{(k-l)}\right\rangle && (2.9) \end{aligned}$$

The first of these, (2.6), is identical to (2.3) and gives nothing new. Equations (2.7) and (2.8) may be rewritten as

$$\begin{aligned} (H_0 - E_n^{(0)}) \left|\Psi_n^{(1)}\right\rangle &= (E_n^{(1)} - H_1) \left|\Psi_n^{(0)}\right\rangle && (2.10)\\ (H_0 - E_n^{(0)}) \left|\Psi_n^{(2)}\right\rangle &= (E_n^{(1)} - H_1) \left|\Psi_n^{(1)}\right\rangle + E_n^{(2)} \left|\Psi_n^{(0)}\right\rangle && (2.11) \end{aligned}$$

which are linear inhomogeneous equations for $\left|\Psi_n^{(1)}\right\rangle$ and $\left|\Psi_n^{(2)}\right\rangle$, respectively. Since these equations determine the wave function corrections only to within an arbitrary multiple of $\left|\Psi_n^{(0)}\right\rangle$, this multiple is chosen so that the relation

$$\left\langle \Psi_n | \Psi_n^{(0)} \right\rangle = 1 \qquad (2.12)$$

is fulfilled. This implies that the total wave function correction must be chosen orthogonal to the corresponding unperturbed state. Equations (2.10) and (2.11) are both associated with the homogeneous equation

$$(H_0 - E_n^{(0)}) \left|\Psi_n\right\rangle = 0 \qquad (2.13)$$

Since this equation has a nontrivial solution, namely the zeroth-order wave function, we cannot find the wave function corrections by direct inversion. However from linear algebra (see for instance [17]) we recall that a necessary and sufficient condition for inhomogeneous equations to have a solution is that the inhomogeneity has no components in the solution space of its associated homogeneous equation. In our case this translates to stating that the right hand sides of (2.10) and (2.11) must have no components in the null-space of the operator $H_0 - E_n^{(0)}$. That is, we must have

$$\begin{aligned} P_n^{(0)} (E_n^{(1)} - H_1) \left|\Psi_n^{(0)}\right\rangle &= 0 && (2.14)\\ P_n^{(0)} \left\{ (E_n^{(1)} - H_1) \left|\Psi_n^{(1)}\right\rangle + E_n^{(2)} \left|\Psi_n^{(0)}\right\rangle \right\} &= 0 && (2.15) \end{aligned}$$

where $P_n^{(0)}$ is a projection operator that projects onto the n'th component of the zeroth-order wave function

$$P_n^{(0)} = \left|\Psi_n^{(0)}\right\rangle \left\langle \Psi_n^{(0)}\right| \qquad (2.16)$$

Since $\left|\Psi_n^{(0)}\right\rangle$ cannot be a zero vector, the coefficients preceding this vector in equations (2.14) and (2.15) must add up to zero. Assuming that all zeroth-order wave functions have been normalised to unity, we get the expressions for the first- and second-order energy corrections

$$E_n^{(1)} = \left\langle \Psi_n^{(0)} \right| H_1 \left| \Psi_n^{(0)} \right\rangle \tag{2.17}$$

$$E_n^{(2)} = \left\langle \Psi_n^{(0)} \right| H_1 \left| \Psi_n^{(1)} \right\rangle \tag{2.18}$$

To find the energy correction to third order, a more subtle approach is required. We multiply (2.6) by $-\left\langle \Psi_n^{(3)} \right|$, (2.7) by $-\left\langle \Psi_n^{(2)} \right|$, (2.8) by $\left\langle \Psi_n^{(1)} \right|$, and the next successive approximation equation by $\left\langle \Psi_n^{(0)} \right|$, and add up. Using the Hermitticity of the operators H_0 and H_1, the resulting equation may be rearranged to

$$E_n^{(3)} = \left\langle \Psi_n^{(1)} \right| H_1 - E_n^{(1)} \left| \Psi_n^{(1)} \right\rangle \tag{2.19}$$

Thus, if the wave function is known to first order, we may calculate the energy to third order. More generally it may be shown [18] that, if we know the wave function to order n, we may calculate the energy to order $2n + 1$, a result often referred to as *Wigner's 2n+1 rule*. Accordingly, it would seem natural always to calculate perturbation energies to odd orders. This is supported by the fact that odd-order energies $E^{(0)} + E^{(1)} + \cdots + E^{(odd)}$ may be obtained directly from the variational principle and therefore must represent an upper bound to the exact energy (see section 2.3 of this text or Ref.[20]). The same is not true for even-order energies. However, as second-order energy corrections are known to give better estimates of molecular properties like bond angles and bond lengths [1], third-order energy corrections shall not be considered in this work.

In passing, we note that the first-order energy can be calculated with knowledge of the unperturbed wave function only. In fact, the first-order energy, which is the sum of the zeroth-order energy and the first-order energy correction, is equal to the expectation value of the exact Hamiltonian in the zeroth-order wave function. The first-order energy is therefore trivially an upper bound to the exact energy.

To get the second-order energy, we must first find $\left|\Psi_n^{(1)}\right\rangle$. In the conventional Rayleigh–Schrödinger perturbation theory, this is done by expanding the first-order wave function correction in the eigenfunctions of H_0

$$\left|\Psi_n^{(1)}\right\rangle = \sum_{k \neq n} C_{kn} \left|\Psi_k^{(0)}\right\rangle \tag{2.20}$$

Inserting this expression in (2.10), multiplying from the left with $\left\langle \Psi_n^{(0)} \right|$ and solving for the expansion coefficients, we get

$$\left|\Psi_n^{(1)}\right\rangle = \sum_{k \neq n} \left|\Psi_k^{(0)}\right\rangle \frac{\left\langle \Psi_k^{(0)} \right| H_1 \left| \Psi_n^{(0)} \right\rangle}{E_n^{(0)} - E_k^{(0)}} \tag{2.21}$$

which is an infinite summation. If we use this expression for $\left|\Psi_n^{(1)}\right\rangle$ in (2.10), we get an infinite sum in $E_n^{(2)}$ which is very difficult to evaluate. It may be shown (see for instance [21]) that the largest contributions to this summation often come from the continuum part of the orbital basis sets used.

2.2 Variational perturbation theory

To solve (2.10) for $\left|\Psi_n^{(1)}\right\rangle$ we are not restricted to use the Schrödinger method. Let us multiply (2.8) by $\left\langle\Psi_n^{(0)}\right|$, (2.7) by $\left\langle\Psi_n^{(1)}\right|$ and (2.6) by $-\left\langle\Psi_n^{(2)}\right|$ and add up. This gives an alternative expression for the second-order energy correction

$$E_n^{(2)} = 2\left\langle\Psi_n^{(1)}\right| H_1 - E^{(1)}\left|\Psi_n^{(0)}\right\rangle + \left\langle\Psi_n^{(1)}\right| H_0 - E^{(0)}\left|\Psi_n^{(1)}\right\rangle \tag{2.22}$$

If we regard (2.22) as a variational integral, that is

$$\tilde{E}_n^{(2)}[\Psi_{\text{trial}}^{(1)}] \equiv 2\left\langle\Psi_{\text{trial}}^{(1)}\right| H_1 - E_n^{(1)}\left|\Psi_n^{(0)}\right\rangle + \left\langle\Psi_{\text{trial}}^{(1)}\right| H_0 - E_n^{(0)}\left|\Psi_{\text{trial}}^{(1)}\right\rangle \tag{2.23}$$

then the trial function that makes this expression stationary

$$\delta\tilde{E}_n^{(2)}[\Psi_{\text{trial}}^{(1)}] = 2\left\{\left\langle\delta\Psi_{\text{trial}}^{(1)}\right| H_1 - E_n^{(1)}\left|\Psi_n^{(0)}\right\rangle + \left\langle\delta\Psi_{\text{trial}}^{(1)}\right| H_0 - E_n^{(0)}\left|\Psi_{\text{trial}}^{(1)}\right\rangle\right\} = 0 \tag{2.24}$$

is precisely the exact $\Psi_n^{(1)}$ for the nth state. This may be realized by identifying (2.10) as the Euler-Lagrange equation [22] for our variational integral (2.23). The first to use such a variational approach was Hylleraas [23], who used it to study two-electron systems. Because of this, functionals like (2.23) are often referred to as *Hylleraas functionals*. Even though (2.23) looks even more complicated than (2.10), it is much more practical as it allows us to use *any* acceptable wave function as an approximation to $\Psi_n^{(1)}$, as long as this trial wave function has some parameters left arbitrary. If the extremum $\tilde{E}_n^{(2)}[\Psi_n^{(1)}]$ is also a minimum then the trial function, $\Psi_{\text{trial}}^{(1)}$, may be varied until the lowest $\tilde{E}_n^{(2)}[\Psi_{\text{trial}}^{(1)}]$ is obtained. To find the states that correspond to such a minimum, we make the substitution $\Psi_{\text{trial}}^{(1)} = \Psi_n^{(1)} + \delta\Psi_n^{(1)}$ directly in the Hylleraas functional. This gives

$$\delta\tilde{E}_n^{(2)}[\Psi_{\text{trial}}^{(1)}] = E_n^{(2)}[\Psi_n^{(1)}] + \left\langle\delta\Psi_n^{(1)}\right| H_0 - E^{(0)}\left|\delta\Psi_n^{(1)}\right\rangle \tag{2.25}$$

where we have applied the stationary condition (2.24). Obviously, if a certain state n is to correspond to a minimum, the second term of (2.25) must be non-negative. Expanding $(H_0 - E^{(0)})\delta\Psi_n^{(1)}$ in the eigenfunctions of H_0, we get

$$\delta\tilde{E}_n^{(2)}[\Psi_{\text{trial}}^{(1)}] = E_n^{(2)}[\Psi_n^{(1)}] + \sum_{m=0}^{\infty}\left(E_m^{(0)} - E_n^{(0)}\right)\left\langle\delta\Psi_n^{(1)}|\Psi_m^{(0)}\right\rangle \tag{2.26}$$

For the ground state, the last term is trivially non-negative since $E_m^{(0)} > E_0^{(0)}$. Furthermore, the lowest state within each symmetry is also a minimum, since the variations $\delta\Psi_n^{(1)}$ must be kept within the irreducible representation of H and thus by symmetry be orthogonal to all states $\Psi_k^{(0)}$ lower than $\Psi_n^{(0)}$. Thus, as pointed out by Sinanoğlu [24], the (1s2s) ^{3}S, (1s2p) ^{1}P, and so on, states of helium can be treated like the ground state by minimising the functional $\tilde{E}[\Psi_{\text{trial}}^{(1)}]$ with suitable trial functions. If we try to find the second-order energy of the corresponding (1s2s) ^{1}S state by the same procedure we are going to fail, however, as the second term of (2.25) is not positive definite for this state and the minimum principle does therefore not apply. If we anyway manage to find a minimum, this can not be given a physical interpretation. Sinanoğlu however, showed that this problem is easily circumvented. He suggested that when varying the trial function for the nth state, the variations should be kept orthogonal to all states k for which $k < n$. Whenever this requirement is fulfilled the second term of (2.25) is positive definite and the variational approach discussed above applies. Note that this positive definiteness also implies that the trial function gives a second-order energy that is a true upper bound to the exact, that is

$$\tilde{E}_n^{(2)}[\Psi_{\text{trial}}^{(1)}] \geq E_n^{(2)} \tag{2.27}$$

The equality applies when the trial function equals the exact first-order wave function of the nth state. This is a very useful relationship since it means that the second-order energy converges to the exact energy in a well-behaved manner as the trial function is improved.

From (2.25) we see that the error in the second-order energy calculated using (2.23) is only quadratic in the error in the trial function. By contrast, when the second-order energy is calculated from (2.18), the error in the energy is linear in the error in the trial function.

2.3 First-order normalisation effects

So far we have established two different ways of obtaining the first-order wave functions. Before moving on, we show that a normalisation of the total first-order wave function, only affects energy corrections to fourth order or higher. To do this, we evaluate the expectation value of the Hamiltonian, H, in the first-order wave function for a given state n

$$E_n = \frac{\langle\Psi_n|\, H\, |\Psi_n\rangle}{\langle\Psi_n|\Psi_n\rangle} = E_n^{(0)} + E_n^{(1)} + \frac{E_n^{(2)} + E_n^{(3)}}{1 + \left\langle \Psi_n^{(1)} \middle| \Psi_n^{(1)} \right\rangle} \tag{2.28}$$

where we have applied (2.22) and (2.28) together with some algebraic manipulations. Equation (2.28) shows that normalising the first-order wave function only affects

energy corrections of fourth-order or higher. Also note that since the expectation value of the Hamiltonian always yields a higher energy than the exact, we have through (2.28) also shown that the third-order energy is an upper bound to the exact energy

$$E_n^{\text{exact}} \leq \frac{\langle \Psi_n | \, H \, | \Psi_n \rangle}{\langle \Psi_n | \Psi_n \rangle} \leq E_n^{(0)} + E_n^{(1)} + E_n^{(2)} + E_n^{(3)} \tag{2.29}$$

A similar but much more elaborate approach may be used to show that fifth-order energies also are upper bounds to the exact energy.

Chapter 3

Møller–Plesset perturbation theory

3.1 The Fock operator

Up to this point we have treated perturbation theory in general only, and have said nothing about the nature of either the zeroth-order Hamiltonian or the perturbation. Depending on the nature of the perturbation, the Rayleigh–Schrödinger approach presented in the previous chapter, may be used successfully. Whereas it often provides good results for isolated systems, for instance, it fails to describe weak inter-molecular interactions [25].

Consider a quantum chemical system consisting of one or more fixed nuclei surrounded by $2n$ electrons. For a field-free system, the non-relativistic, spin-free Hamiltonian is given by

$$H = \sum_{i=1}^{2n} h(i) + \sum_{i<j} g(i,j) + \sum_{A<B} \frac{Z_A Z_B}{R_{AB}} \tag{3.1}$$

where the summations i and j are over electrons and the summations A and B are over nuclei. The first term of this Hamiltonian is known as the *bare-nuclei Hamiltonian* and consists of one-particle operators $h(i)$, defined as

$$h(i) = -\frac{1}{2}\nabla_i^2 - \sum_A \frac{Z_A}{r_{iA}}, \tag{3.2}$$

where the first term gives the kinetic energy of an electron and the last term gives the attraction energy between the electron and all the nuclei. The second term of (3.1), represents the Coulomb repulsion between the electrons and consists of two-particle operators $g(i,j)$ defined as

$$g(i,j) = \frac{1}{r_{ij}}. \tag{3.3}$$

The last term of the Hamiltonian gives the repulsion energy between the nuclei in the system. This term shall not be encountered any further in this work, but it is always implicitly assumed to be a part of the total Hamiltonian.

The two-particle operators in the Hamiltonian (3.1) make the corresponding Schrödinger equation impossible to solve exactly. In the quest for an approximate solution, we ask ourselves whether perturbation theory may offer an adequate solution. The first step is to partition the Hamiltonian so that the zeroth-order part recovers most of the energy of the system and at the same time leads to a simpler Schrödinger equation. One fairly obvious approach is to exclude all electron-electron interactions from the zeroth-order Hamiltonian and instead treat these entirely as perturbations. This leads us to a simple zeroth-order Schrödinger equation that for a few special systems may be solved analytically. As a bonus, the perturbation series for the energy converges rapidly. This was demonstrated by Sanders and Scherr [26] who used perturbation theory based on the bare-nuclei Hamiltonian to calculate the energy of the helium atom. Their perturbation series for the energy converges oscillatory, but rapidly, towards the limit of $-2.9037\,\mathrm{E_h}$. Indeed, after adding up all energy correction terms to third order, the error in the energy is less than $1\,\mathrm{mE_h}$ and thus correct to within chemical precision.

Matcha and Byers Brown [27] reproduced these results for the hydrogen molecule. Their perturbation series for the energy oscillates just like the helium series of Sanders and Scherr, and their third-order energy is only $1.1\,\mathrm{mE_h}$ above the correct value of $-1.1745\,\mathrm{E_h}$.

Even though the bare-nuclei Hamiltonian leads to perturbation series for the energy that converges rapidly, it is not widely used in quantum chemistry. One reason for this is that the corresponding zeroth-order wave function is very different from the exact wave function. Although it is fairly well suited as a starting point for energy calculations, this zeroth-order wave function is a rather poor starting point for the calculation of molecular properties.

A more important reason for the limited use of the bare-nuclei Hamiltonian is the existence of another one-electron Hamiltonian that has better convergence properties for both energy calculations and the calculation of molecular properties. This is the *Fock operator*, which is the one-electron Hamiltonian that, to first order, gives the lowest energy for a quantum chemical system. For a closed shell system, which has an even number of electrons, the Fock operator is given by

$$H_0 = F = \sum_{i=1}^{2n} f(i), \qquad f = h + \sum_{k=1}^{n} (2J_k - K_k) \tag{3.4}$$

where spin has been integrated out. The one-particle operators J_k and K_k represents the average repulsion between the electrons and are described in detail below. In the meantime, we adopt the Fock operator as the new zeroth-order Hamiltonian and

summarise the solution to the zeroth-order problem (2.3) as

$$f\varphi_k = \varepsilon_k \varphi_k \tag{3.5}$$

$$\Psi^{(0)} = \Phi^{\mathrm{HF}} = \mathcal{A}\Pi_{k=1}^{2n}\psi_k(k) \tag{3.6}$$

$$E^{(0)} = 2\sum_{k=1}^{n}\varepsilon_k \tag{3.7}$$

where the operator $\mathcal{A}$ generates a normalised and antisymmetrised product of the spin orbitals ψ_k. The relation between these spin orbitals and the space orbitals, φ_k, is given below.

The Hartree–Fock energy, E^{HF}, which is the expectation value of the Hamiltonian in the Hartree–Fock wave function, Φ^{HF}, is

$$E^{\mathrm{HF}} = \left\langle \Phi^{\mathrm{HF}} \middle| H \middle| \Phi^{\mathrm{HF}} \right\rangle = E^{(0)} + E^{(1)} \tag{3.8}$$

The one-particle character of the Fock operator allows us to write its eigenfunctions as a product of orbitals. According to the Pauli principle, the wave function must be antisymmetric with respect to the interchanging of any two electrons. We comply with this demand by writing the Hartree–Fock (HF) wave function (3.6) as an antisymmetric product of spin orbitals ψ_k. The operator $\mathcal{A}$ takes care of anti-symmetrisation and normalisation. The antisymmetric product may also be written as a determinant and is often referred to as a Slater determinant. A wave function that may be written as a single determinant, or a linear combination of determinants, is symbolised by a Φ.

The spin orbitals needed to construct the HF wave function are obtained from the Hartree-Fock equation (3.5). Since spin has been integrated out from the Fock operator its eigenfunctions are spin-free space orbitals φ_k, and to obtain a spin orbital we must multiply a space orbital by a function giving either α or β spin.

$$\varphi_i \Rightarrow \begin{cases} \varphi_i\alpha = \psi_{2i-1} \\ \varphi_i\beta = \psi_{2i} \end{cases} \tag{3.9}$$

We now turn to the operators J_k and K_k which make the Fock operator different from the bare-nuclei Hamiltonian. These operators are integral operators, and their definitions are best understood by letting them act on an orbital

$$J_k\varphi_i(1) = \langle\varphi_k(2)|\, r_{12}^{-1}\, |\varphi_k(2)\rangle_2\, \varphi_i(1) \tag{3.10}$$

$$K_k\varphi_i(1) = \langle\varphi_k(2)|\, r_{12}^{-1}\, |\varphi_i(2)\rangle_2\, \varphi_k(1) \tag{3.11}$$

where $\langle\rangle_2$ denotes an integration with respect to electron 2. Inspecting the operator J_k we see that it represents the Coulomb potential set up by an electron present in orbital φ_k, and the operator is therefore called the *Coulomb operator*. The operator K_k, on the other hand, has no classical counterpart, but as it exchanges the

orbital it is acting on by one of the orbitals present in the integral, it is called the *exchange operator*. Through the Coulomb and exchange operators in the Hamiltonian (3.4), the electron-electron interaction is accounted for in some average sense, that is, rather than letting two electrons interact at their instantaneous positions, they interact through their probability amplitudes, the orbitals. Equations (3.10) and (3.11) show that the one-electron Hamiltonian, or Fock operator, is constructed from its own eigenfunctions, and the Hartree–Fock equations must therefore be solved iteratively.

Having established the Fock operator as our zeroth-order Hamiltonian, we make a new partitioning of the Hamiltonian.

$$H = F + (H - F) = \sum_{i=1}^{2n} f(i) + \sum_{i<j} g(i,j) - \sum_{i=1}^{2n} V^{\mathrm{HF}}(i) \tag{3.12}$$

where we have introduced the *Fock potential* V^{HF}

$$V^{\mathrm{HF}} = \sum_{k=1}^{n} (2J_k - K_k) \tag{3.13}$$

to simplify expressions. The difference between the true potential $g(i,j)$, and the Fock potential V^{HF}, is known as the fluctuation potential. Experience shows that the fluctuation potential is small, and the Hartree–Fock energy (3.8) typically recovers more than 99% of the total energy. Unfortunately, although small, the fluctuation potential is not negligible, and often the chemically most significant part of the energy is hidden in the last unrecovered percentage. This is especially evident for the helium dimer which is investigated in section 7.2.2. Nevertheless, the Hartree–Fock wave function represents a good starting point for more elaborate methods like, for instance, perturbation theory. This was first realized by Møller and Plesset [28] who in 1934 published a paper on what today is known as *Møller–Plesset* (MP) *perturbation theory*.

3.2 The MP2 energy expression

The energy not recovered by the Hartree–Fock wave function is referred to as the correlation energy. We shall in the following assume that most of the correlation energy is recovered by the second-order energy correction

$$E^{\mathrm{exact}} = E^{\mathrm{HF}} + E^{\mathrm{correlation}} \approx E^{\mathrm{HF}} + E^{(2)} \tag{3.14}$$

While the second-order energy correction accounts for some 90% of the correlation energy, an improvement is usually obtained if third-order energy corrections are

included. Several authors have shown (see for instance Ref. [29]), however, that for a wide range of small molecules, properties such as bond distances and bond angles are better described at the second-order level than at the third-order level, and third-order corrections shall therefore not be considered.

To obtain the second-order energy, from now on also referred to as the MP2 energy, it is sufficient to find the first-order wave function correction. Sinanoğlu [7, 8] showed that this correction, $\Phi^{(1)} = \Phi^{\mathrm{MP1}}$, only contains two-electron clusters, which in the language of second quantisation may be expressed as

$$\left|\Phi^{(1)}\right\rangle = T_2^{(1)} \left|\Phi^{\mathrm{HF}}\right\rangle = \frac{1}{2} \sum_{abij} t_{ij}^{ab(1)} E_{ai} E_{bj} \left|\Phi^{\mathrm{HF}}\right\rangle \tag{3.15}$$

where the operator $T_2^{(1)}$ is known as the *first-order cluster operator*. Through the excitation operators E_{ai} and E_{bj}

$$E_{ai} = a_{a\alpha}^\dagger a_{i\alpha} + a_{a\beta}^\dagger a_{i\beta} \qquad E_{bj} = a_{b\alpha}^\dagger a_{j\alpha} + a_{b\beta}^\dagger a_{j\beta} \tag{3.16}$$

the cluster operator moves a pair of electrons from the initially occupied orbitals i and j to the virtual orbitals a and b. The summations are over all occupied and all virtual orbitals so that any pair ij can be excited into any pair ab. The probability for one particular excitation to happen is given by the first-order cluster amplitudes $t_{ij}^{ab(1)}$. As the name suggests, the first-order cluster amplitudes are found by solving the first-order equation (2.10). Cluster amplitudes of the kind t_{ij}^{ab} may also be found by solving some other equation system, leading for instance, to the coupled cluster doubles (CCD) wave function.

$$\left|\Phi^{\mathrm{CCD}}\right\rangle = \exp(T_2) \left|\Phi^{\mathrm{HF}}\right\rangle \tag{3.17}$$

That being said, we drop from now on any further reference to the term first-order both for the cluster operator and its amplitudes.

Even though our Hartree–Fock problem is solved in basis of orbitals, the two-electron clusters referred to by Sinanoğlu are not restricted to products of virtual orbitals. Second quantisation, however, has not been designed to handle excitations between two-electron clusters, and to take advantage of both the framework offered by second quantisation and the flexibility offered by general two-electron clusters, we shall expand these clusters in an auxiliary basis assumed to be complete. To be able to distinguish orbitals belonging to this basis from orbitals belonging to the given basis we denote auxiliary orbitals by capital letters, leading to the following orbital notation

$i, j, k, \ldots$	occupied orbitals
$a, b, c, \ldots$	virtual orbitals contained in the given basis

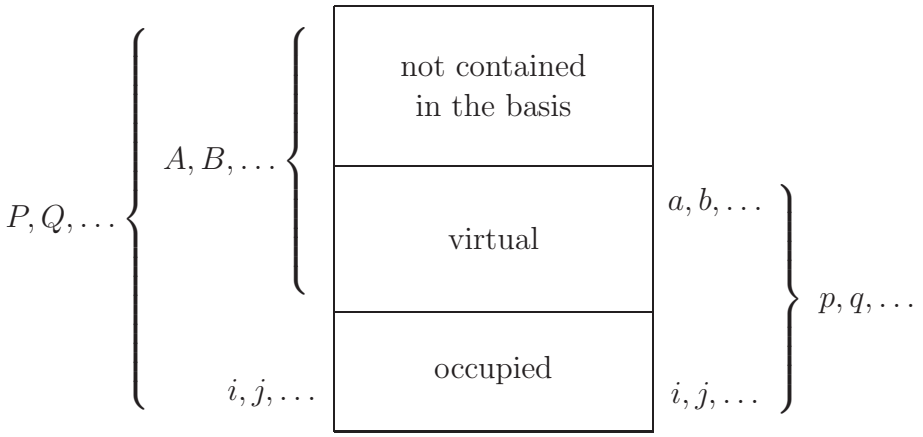

Figure 3.1: The spaces spanned by the given basis and the auxiliary basis assumed to be complete. See text for further details. The illustration is taken from Ref. [30]

$p, q, r, \ldots$	arbitrary orbitals contained in the given basis
$A, B, C, \ldots$	virtual orbitals contained in the complete basis
$P, Q, R, \ldots$	arbitrary orbitals contained in the complete basis

As illustrated in Figure 3.1, the occupied orbitals will be identical in the two basis sets. Furthermore, the virtual orbitals in the given set define a true subset of the virtual orbitals in the complete set.

The use of an auxiliary basis as a way of handling general two-electron functions in second quantisation has already been discussed by Kutzelnigg and Klopper [11], and we follow their approach in much the same spirit. In the complete basis, the *generalised cluster operator* may be written as

$$T_2 = \frac{1}{2} \sum_{ABij} u_{AB}^{ij} E_{Ai} E_{Bj} \tag{3.18}$$

where the matrix element u_{AB}^{ij} is defined as

$$u_{AB}^{ij} = \langle u_{ij}(1,2) | \varphi_A \varphi_B \rangle \tag{3.19}$$

The cluster operator (3.18) excites a pair of occupied orbitals ij into the virtual orbitals AB of the complete basis set. The overlap matrix u_{AB}^{ij} gives the amount of "AB" needed to produce the two-electron cluster $u_{ij}(1,2)$. The net effect, therefore, is that the pair of occupied orbitals is excited to this cluster. To avoid violating the Pauli principle, the two-electron function, or pair function, $u_{ij}(1,2)$, must exhibit the same symmetry with respect to interchanging of electrons 1 and 2 as the orbitals it replaces.

If we let the pair function be given as a sum of products of virtual orbitals

$$u_{ij}(1,2) = \sum_{ab} t_{ij}^{ab} \varphi_a(1)\varphi_b(2) \tag{3.20}$$

and insert this expression in (3.18), we obtain

$$\begin{aligned} T_2 &= \frac{1}{2} \sum_{ABij} \sum_{ab} t_{ij}^{ab} \langle \varphi_a \varphi_b | \varphi_A \varphi_B \rangle E_{Ai} E_{Bj} \\ &= \frac{1}{2} \sum_{ABij} \sum_{ab} t_{ij}^{ab} \delta_{aA} \delta_{bB} E_{Ai} E_{Bj} \\ &= \frac{1}{2} \sum_{abij} t_{ij}^{ab} E_{ai} E_{bj} \end{aligned} \tag{3.21}$$

which is the standard form of the cluster operator.

Since we have turned the cluster operator into a form that can handle all two-electron clusters, we shall now find an expression for the second-order energy in basis sets containing such clusters. Inserting the generalised cluster operator, as given in the first part of (3.15), into the expression for the second-order energy (2.18), we get

$$E^{(2)} = \left\langle \Phi^{\mathrm{HF}} \right| H_1 \left| \Phi^{(1)} \right\rangle = \left\langle \Phi^{\mathrm{HF}} \right| H_1 T_2 \left| \Phi^{\mathrm{HF}} \right\rangle \tag{3.22}$$

where the zeroth order wave function is the Hartree–Fock wave function, and the perturbation operator H_1 is the fluctuation potential given in (3.12). Since the cluster operator creates double excitations, the expectation value (3.22) can only survive if there is another two-electron operator present. The one-electron part of the fluctuation potential, the Fock potential, does therefore not contribute to the expectation value in (3.22), and the effect of the perturbation operator H_1 reduces to that of the two-electron operator $g(i,j)$. In spin-free second quantisation, this operator is given as

$$g = \frac{1}{2} \sum_{PQRS} g_{PQRS}(E_{PR}E_{QS} - \delta_{QR}E_{PS}) \tag{3.23}$$

where the transition probabilities g_{PQRS} are two-electron integrals,

$$g_{PQRS} = \langle \varphi_P \varphi_Q | \frac{1}{r_{12}} | \varphi_R \varphi_S \rangle \tag{3.24}$$

and where we have allowed the two-electron operator g to make excitations throughout the complete basis and not only in the given basis. In (3.23), we see that g also contains a single-excitation part that, as discussed above, cannot contribute to the expectation value (3.22).

On evaluating this expectation value, we take advantage of the fact that the cluster operator cannot make excitations to the left. This allows us to rewrite the operator gT_2 as a commutator $[g, T_2]$ which is readily evaluated by commutator techniques [1],

$$\begin{aligned} E^{(2)} &= \left\langle \Phi^{\mathrm{HF}} \right| [g, T_2] \left| \Phi^{\mathrm{HF}} \right\rangle \\ &= \frac{1}{4} \sum_{PQRS} \sum_{ABij} g_{PQRS} u_{AB}^{ij} \left\langle \Phi^{\mathrm{HF}} \right| [E_{PR}E_{QS}, E_{Ai}E_{Bj}] \left| \Phi^{\mathrm{HF}} \right\rangle \\ &= \sum_{ABij} (2g_{ijAB} - g_{jiAB})\, u_{AB}^{ij} \end{aligned} \tag{3.25}$$

This expression involves the infinite auxiliary basis, and to obtain an expression for the energy that only involves orbitals from the given basis or two-electron clusters, we introduce the resolution of the identity

$$1 = \sum_P |\varphi_P\rangle \langle\varphi_P| = \sum_i |\varphi_i\rangle \langle\varphi_i| + \sum_A |\varphi_A\rangle \langle\varphi_A| \tag{3.26}$$

Each of the terms given in (3.26) act as a projection operator, and as the term involving a summation over all occupied orbitals shall be encountered frequently in this text, we represent it by the operator P_{occ}

$$P_{\mathrm{occ}} = \sum_i |\varphi_i\rangle \langle\varphi_i| \tag{3.27}$$

To remove all auxiliary orbitals present in (3.25), we have to use the resolution of the identity twice

$$\sum_{AB} |\varphi_A\varphi_B\rangle \langle\varphi_A\varphi_B| = [1 - P_{\mathrm{occ}}(1)]\,[1 - P_{\mathrm{occ}}(2)] \equiv Q_{\mathrm{occ}}(1,2) \tag{3.28}$$

Inserting (3.28) into the last equality of (3.25), and using the definition of u_{AB}^{ij} given in (3.19), we get the final expression for the second-order energy

$$E^{(2)} = \sum_{ij} \left(2 \langle Q_{\mathrm{occ}} u_{ij}| \, r_{12}^{-1} \, |\varphi_i\varphi_j\rangle - \langle Q_{\mathrm{occ}} u_{ij}| \, r_{12}^{-1} \, |\varphi_j\varphi_i\rangle \right) \tag{3.29}$$

In this expression there is no limitation to which part of the two-electron space the pair function u_{ij} can belong. Any components lying in the space spanned by occupied orbitals are projected out by Q_{occ}.

Equation (3.29) could very well have been used throughout the rest of this text, but we shall develop it a bit further. As shown in (3.9), a single space orbital φ_i may be combined with a function for either α or β spin to produce two different

electron states. Likewise, the product of two space orbitals φ_i and φ_j, gives rise to four different electron states since each electron may have either α or β spin

$$\{\varphi_i\varphi_j\alpha\alpha, \quad \varphi_i\varphi_j\alpha\beta, \quad \varphi_i\varphi_j\beta\alpha, \quad \varphi_i\varphi_j\beta\beta\} \tag{3.30}$$

In (3.30), we have implicitly assumed that the first space orbital and first spin function belong to electron one, that is, $\varphi_i\varphi_j\alpha\alpha \equiv \varphi_i(1)\varphi_j(2)\alpha(1)\alpha(2)$.

Each spin function is an eigenfunction of both the operator for total spin, $\hat{S}$, and spin projection $\hat{S}_z$. Through a simple unitary transformation, the four states in (3.30) may also be turned into eigenfunctions $\varphi_i\varphi_j\vartheta[S, M_s]$ of $\hat{S}$ and $\hat{S}_z$ characterised by quantum numbers S and M_s. As we see shortly, these four eigenfunctions consist of one singlet which has a spin part that is antisymmetric with respect to the interchanging of electrons 1 and 2, and three triplets which have symmetric spin parts. The orbital part, $\varphi_i\varphi_j$, may also be written in terms of a symmetric ($\mathcal{S}$) and an antisymmetric ($\mathcal{A}$) component

$$\varphi_i\varphi_j = 1/2[\varphi_i\varphi_j + \varphi_j\varphi_i] + 1/2[\varphi_i\varphi_j - \varphi_j\varphi_i] = 1/\sqrt{2}\phi_{ij}^{\mathcal{S}} + 1/\sqrt{2}\phi_{ij}^{\mathcal{A}} \tag{3.31}$$

According to the Pauli principle, a proper two-electron state must be overall antisymmetric. For this principle to be fulfilled only the spatial part component having a symmetry opposite to the spin part can contribute. This gives us the following normalised two-electron states which both fulfil the Pauli principle and have well-defined spin quantum numbers

$$\phi_{ij}^{\mathcal{S}}\vartheta(0,0) = \frac{1}{\sqrt{2}}(\varphi_i\varphi_j + \varphi_j\varphi_i)\frac{1}{\sqrt{2}}(\alpha\beta - \beta\alpha) \tag{3.32}$$

$$\phi_{ij}^{\mathcal{A}}\vartheta(1,M_s) = \frac{1}{\sqrt{2}}(\varphi_i\varphi_j - \varphi_j\varphi_i)\begin{cases} \alpha\alpha & M_s = 1 \\ \frac{1}{\sqrt{2}}(\alpha\beta + \beta\alpha) & M_s = 0 \\ \beta\beta & M_s = -1 \end{cases} \tag{3.33}$$

Since two interacting electrons form spectroscopically distinguishable singlet and triplet states [31], we shall from now on assume that all two-electron states are spin adapted according to either (3.32) or (3.33). We have chosen to work in a formalism where spin has been integrated out, however, and shall therefore only refer to the symmetric and antisymmetric spatial parts. We keep in mind though, that the symmetric spatial part comes with the singlet and that the antisymmetric spatial part comes with each of the three triplets. Using this new terminology, we give the second-order energy in parity-adapted (spin-adapted) form

$$E^{(2)} = \sum_{i=1}^{n}\epsilon_{ii}^{\mathcal{S}} + \sum_{i<j}(\epsilon_{ij}^{\mathcal{S}} + \epsilon_{ij}^{\mathcal{A}}) \tag{3.34}$$

where the pair energy $\epsilon_{ij}^{\mathcal{P}}$ for electron i and j having orbital parity $\mathcal{P}$ is

$$\epsilon_{ij}^{\mathcal{P}} = \Lambda_{ij}^{\mathcal{P}}\left\langle Q_{\mathrm{occ}}u_{ij}^{\mathcal{P}}\right| r_{12}^{-1}\left|\phi_{ij}^{\mathcal{P}}\right\rangle, \qquad \Lambda_{ij}^{\mathcal{P}} = \frac{2\delta_{\mathcal{A}\mathcal{P}} + 1}{1 + \delta_{ij}} \tag{3.35}$$

Equation (3.34) is easily verified to be equivalent to (3.29) by inserting (3.35) in (3.34) and replacing the parity-adapted functions $\phi_{ij}^{\mathcal{P}}$ and $u_{ij}^{\mathcal{P}}$ by non-adapted functions. Note that the pair function must have exactly the same parity as the pair of orbitals it replaces. For antisymmetric pairs for which $\mathcal{P} = \mathcal{A}$, the factor $\Lambda_{ij}^{\mathcal{P}}$ is identical to 3, thus accounting for the three triplet states. For a singlet state for which $i \neq j$ the factor reduces to 1, and when $i = j$ the factor is $1/2$. In the latter case, there is also a factor 2 coming from the integral as the combined space orbital, $\phi_{ii}^{\mathcal{S}}$, is given as $\sqrt{2}\varphi_i\varphi_i$ rather than $\varphi_i\varphi_i$. This convention is adopted from Shibuya and Sinanoğlu [32, 33].

We opened this section with Sinanoğlu's observation that the first-order wave function correction $\Phi^{(1)}$ contains only two-electron clusters. These two-electron clusters are pairs of interacting electrons, the interaction in one pair being completely independent of the interaction in all other pairs. The first-order wave function correction may therefore be written as a linear combination of all Slater determinants that can be constructed by replacing one pair of orbitals at the time by a pair function. This is most easily expressed using second quantisation formalism and a cluster operator of the form (3.18). As is evident from (3.34) and (3.35), the decoupling of the wave function correction into pair contributions has the important consequence that the second-order energy may be written as a sum of pair energies. In the case of the beryllium atom for instance, there are four symmetry-adapted pairs

$$^1(1s1s), \quad ^1(1s2s), \quad ^3(1s2s) \quad \text{and} \quad ^1(2s2s). \tag{3.36}$$

The electron-electron interaction in each of these pairs may be represented by a pair function. When we have obtained one pair function for each pair, the second-order energy is given by

$$E^{(2)}_{\text{Beryllium}} = \epsilon^1_{1s1s} + \epsilon^1_{1s2s} + \epsilon^3_{1s2s} + \epsilon^1_{2s2s} \tag{3.37}$$

where we have used 1 instead of $\mathcal{S}$ and 3 instead of $\mathcal{A}$ to symbolise singlet and triplet energies, respectively. When we later look at applications in chapter 7, this convention is fully adopted.

Sinanoğly [7] showed that for the simple additivity displayed in (3.34) and (3.37) to be true, we must require that the pair functions are orthogonal to all occupied orbitals. In (3.35) this is taken care of by the *strong orthogonality operator* Q_{occ} which, apparent from its definition (3.28), projects out all components of occupied orbitals from the function it operates on. Using the definition, the strong orthogonality (SO) operator may be shown to be both idempotent and Hermitian

$$Q_{\text{occ}}^2 = Q_{\text{occ}}, \qquad Q_{\text{occ}}^\dagger = Q_{\text{occ}}. \tag{3.38}$$

Since our second quantisation approach is based on orthogonal Hartree–Fock orbitals, all excited states are orthogonal to the reference (HF) state. As we have seen in (3.35) and shall see more of in the following, this implies that pair functions are always accompanied by the strong orthogonality operator.

3.3 Variational formulation of the MP2 energy

In the previous section we showed that the second-order energy may be expressed in terms of independent pair energies, expressed in terms of independent pair functions. The first to realize this was Sinanoğlu [9, 34] who showed that the first-order equation (2.10) may be decoupled into n^2 independent first-order equations, one for each parity-adapted pair. Even though this decoupling represents a major simplification, the decoupled pair-equations are still to complex to be solved analytically. Sinanoğlu solved this problem by showing that pair functions may also be obtained by minimising a certain pair functional. Using second quantisation, we find the form of this functional below.

In section 2.2, we found an alternative expression for the second-order energy. In terms of Hartree–Fock ground-state corrections, this alternative expression is

$$E^{(2)} = 2\left\langle \Phi^{(1)} \right| H_1 - E^{(1)} \left| \Phi^{\mathrm{HF}} \right\rangle + \left\langle \Phi^{(1)} \right| H_0 - E^{(0)} \left| \Phi^{(1)} \right\rangle \tag{3.39}$$

The functional form of (3.39) makes it suitable for a variational treatment, as the corresponding stationary condition is exactly the first-order equation. Since the normalisation condition for the exact wave function (2.12) requires the first-order wave function correction to be orthogonal to the Hartree–Fock state

$$\left\langle \Phi^{(1)} | \Phi^{\mathrm{HF}} \right\rangle = 0 \tag{3.40}$$

we may remove $E^{(1)}$ from (3.39) and identify the first term of this equation as twice the second-order energy. The second term of (3.39) must therefore also be related to the second order energy, namely by

$$\left\langle \Phi^{(1)} \right| H_0 - E^{(0)} \left| \Phi^{(1)} \right\rangle = -E^{(2)} \tag{3.41}$$

The first term of (3.39) was decoupled into pair-function form in the previous section. For the second term, the decoupling is somewhat more elaborate. We start by replacing the first-order corrections $\Phi^{(1)}$ by cluster operators operating on the Hartree–Fock state

$$\begin{aligned} &\left\langle \Phi^{(1)} \right| H_0 - E^{(0)} \left| \Phi^{(1)} \right\rangle \\ &\quad = \left\langle \Phi^{\mathrm{HF}} \right| T_2^\dagger H_0 T_2 \left| \Phi^{\mathrm{HF}} \right\rangle - \left\langle \Phi^{\mathrm{HF}} \right| T_2^\dagger T_2 \left| \Phi^{\mathrm{HF}} \right\rangle \left\langle \Phi^{\mathrm{HF}} \right| H_0 \left| \Phi^{\mathrm{HF}} \right\rangle \end{aligned} \tag{3.42}$$

Next, invoking the resolution of the identity, we find that

$$\left\langle \Phi^{\mathrm{HF}} \right| T_2^\dagger T_2 H_0 \left| \Phi^{\mathrm{HF}} \right\rangle = \left\langle \Phi^{\mathrm{HF}} \right| T_2^\dagger T_2 \left| \Phi^{\mathrm{HF}} \right\rangle \left\langle \Phi^{\mathrm{HF}} \right| H_0 \left| \Phi^{\mathrm{HF}} \right\rangle \tag{3.43}$$

since only the Hartree–Fock state has a nonzero overlap with $\left\langle \Phi^{\mathrm{HF}} \right| T_2^\dagger T_2$. The expectation value of (3.42) may therefore be written in the form

$$\left\langle \Phi^{(1)} \right| H_0 - E^{(0)} \left| \Phi^{(1)} \right\rangle = \left\langle \Phi^{\mathrm{HF}} \right| T_2^\dagger H_0 T_2 - T_2^\dagger T_2 H_0 \left| \Phi^{\mathrm{HF}} \right\rangle \tag{3.44}$$

which may be expressed in terms of commutators

$$\left\langle \Phi^{(1)} \right| H_0 - E^{(0)} \left| \Phi^{(1)} \right\rangle = \left\langle \Phi^{\mathrm{HF}} \right| \left[T_2^\dagger, [H_0, T_2] \right] \left| \Phi^{\mathrm{HF}} \right\rangle \tag{3.45}$$

The introduction of the outer commutator is justified by the fact that $T_2^\dagger$ annihilates $\left|\Phi^{\mathrm{HF}}\right\rangle$. The zeroth order Hamiltonian in (3.45), is the Fock operator. Assuming that the Fock operator is given in the canonical representation (diagonal Fock matrix), its second quantisation form is

$$H_0 = \sum_{PQ} f_{PQ} E_{PQ} = \sum_{PQ} \varepsilon_P \delta_{PQ} E_{PQ} = \sum_P \varepsilon_P E_{PP} \tag{3.46}$$

where the ε_P is the orbital energy of the canonical orbital φ_P. In this canonical representation, the commutator between H_0 and T_2 is easily evaluated

$$\begin{aligned} [H_0, T_2] &= \frac{1}{2} \sum_{ijAB} u_{AB}^{ij} \sum_P \varepsilon_P \left[E_{PP}, E_{Ai} E_{Bj} \right] \\ &= \frac{1}{2} \sum_{ijAB} u_{AB}^{ij} \left(\varepsilon_A + \varepsilon_B - \varepsilon_i - \varepsilon_j \right) E_{Ai} E_{Bj} \end{aligned} \tag{3.47}$$

Inserting this commutator in (3.45) along with an explicit form for $T_2^\dagger$ we get

$$\begin{aligned} &\left\langle \Phi^{(1)} \right| H_0 - E^{(0)} \left| \Phi^{(1)} \right\rangle \\ &\quad = \frac{1}{4} \sum_{klCD} \sum_{ijAB} u_{AB}^{ij} \left(\varepsilon_A + \varepsilon_B - \varepsilon_i - \varepsilon_j \right) u_{kl}^{CD} \left\langle \Phi^{\mathrm{HF}} \right| \left[E_{lD} E_{kC}, E_{Ai} E_{Bj} \right] \left| \Phi^{\mathrm{HF}} \right\rangle \\ &\quad = \sum_{ijAB} \left(2 u_{AB}^{ij} - u_{AB}^{ji} \right) \left(\varepsilon_A + \varepsilon_B - \varepsilon_i - \varepsilon_j \right) u_{ij}^{AB} \end{aligned} \tag{3.48}$$

where we once again have used commutator techniques to evaluate the expectation value. Note that the final form of (3.48) is expressed in terms of auxiliary basis functions φ_A and φ_B. Just as for (3.25), an infinite summation over two such functions may be replaced by the strong orthogonality operator

$$\begin{aligned} &\sum_{AB} u_{AB}^{ij} \left(\varepsilon_A + \varepsilon_B - \varepsilon_i - \varepsilon_j \right) u_{ij}^{AB} \\ &\quad = \sum_{AB} \left\langle u_{ij} | \varphi_A \varphi_B \right\rangle \left(\left\langle \varphi_A \varphi_B \right| f(1) + f(2) \left| \varphi_A \varphi_B \right\rangle - \varepsilon_i - \varepsilon_j \right) \left\langle \varphi_A \varphi_B | u_{ij} \right\rangle \\ &\quad = \left\langle u_{ij} \right| Q_{\mathrm{occ}} \left[f(1) + f(2) \right] Q_{\mathrm{occ}} \left| u_{ij} \right\rangle - \left(\varepsilon_i + \varepsilon_j \right) \left\langle u_{ij} \right| Q_{\mathrm{occ}} \left| u_{ij} \right\rangle \end{aligned} \tag{3.49}$$

Using the idempotency and Hermitticity of the strong orthogonality operator, we may gather the two terms in (3.49) into one. This allows us to write the expectation value (3.48) as

$$\begin{aligned} \left\langle \Phi^{(1)} \right| H_0 - E^{(0)} \left| \Phi^{(1)} \right\rangle = \sum_{ij} \big(& 2 \left\langle Q_{\mathrm{occ}} u_{ij} \right| f(1) + f(2) - \varepsilon_i - \varepsilon_j \left| Q_{\mathrm{occ}} u_{ij} \right\rangle \\ & - \left\langle Q_{\mathrm{occ}} u_{ji} \right| f(1) + f(2) - \varepsilon_i - \varepsilon_j \left| Q_{\mathrm{occ}} u_{ij} \right\rangle \big) \end{aligned} \tag{3.50}$$

Finally, comparing (3.50) with (3.29), we conclude that the second-order energy as given by (3.39), may be written in the separated form

$$E^{(2)} = \sum_{i=1}^{n} \epsilon_{ii}^{\mathcal{S}} + \sum_{i<j} (\epsilon_{ij}^{\mathcal{S}} + \epsilon_{ij}^{\mathcal{A}}) \tag{3.51}$$

which is identical to the original expression (3.34) but with pair energies $\epsilon_{ij}^{\mathcal{P}}$ given by the alternative expression

$$\epsilon_{ij}^{\mathcal{P}} = \Lambda_{ij}^{\mathcal{P}} \left(2 \left\langle \hat{u}_{ij}^{\mathcal{P}} \right| r_{12}^{-1} \left| \phi_{ij}^{\mathcal{P}} \right\rangle + \left\langle \hat{u}_{ij}^{\mathcal{P}} \right| f(1) + f(2) - \varepsilon_i - \varepsilon_j \left| \hat{u}_{ij}^{\mathcal{P}} \right\rangle \right) \tag{3.52}$$

where the "hat" denote a pair function with all occupied components projected out

$$\hat{u}_{ij}^{\mathcal{P}} = Q_{\text{occ}} u_{ij}^{\mathcal{P}} \tag{3.53}$$

To summarise, we have managed to write the second-order energy correction $E^{(2)}$ in a variational form and as a function of n^2 independent pair functions

$$E^{(2)} = E^{(2)} \left[u_{11}^{\mathcal{S}}, u_{12}^{\mathcal{S}}, u_{12}^{\mathcal{A}}, \ldots, u_{nn}^{\mathcal{S}} \right] \tag{3.54}$$

The independence of these pair functions implies that the differentiation of $E^{(2)}$ with respect $u_{ij}^{\mathcal{P}}$ reduces to the differentiation of $\epsilon_{ij}^{\mathcal{P}}$ with respect $u_{ij}^{\mathcal{P}}$

$$\frac{\partial E^{(2)}}{\partial u_{ij}^{\mathcal{P}}} = \frac{\partial \epsilon_{ij}^{\mathcal{P}}}{\partial u_{ij}^{\mathcal{P}}} \tag{3.55}$$

thus leading us to n^2 independent equations, exactly as shown by Sinanoğlu.

3.4 Optimisation of pair functions

3.4.1 The strong orthogonality functional

Setting the derivative (3.55) equal to zero and solving for $u_{ij}^{\mathcal{P}}$, we find the pair function that within our variational space minimises $\epsilon_{ij}^{\mathcal{P}}$. The minimum value however, is only an approximation to the exact pair energy. To distinguish this approximate value from the exact given in (3.52), we denote the functional to be minimised with the letter F. We also add a tilde to our approximate trial functions to distinguish them from the exact pair functions. Thus we write

$$\begin{aligned} F_{ij}^{\mathcal{P}}[\tilde{u}_{ij}^{\mathcal{P}}] = \Lambda_{ij}^{\mathcal{P}} \big(& 2 \left\langle \tilde{u}_{ij}^{\mathcal{P}} \right| Q_{\text{occ}} r_{12}^{-1} \left| \phi_{ij}^{\mathcal{P}} \right\rangle \\ & + \left\langle \tilde{u}_{ij}^{\mathcal{P}} \right| Q_{\text{occ}} \left(f(1) + f(2) - \varepsilon_i - \varepsilon_j \right) Q_{\text{occ}} \left| \tilde{u}_{ij}^{\mathcal{P}} \right\rangle \big) \end{aligned} \tag{3.56}$$

Sinanoğlu [24] showed that the minimum value of $F_{ij}^{\mathcal{P}}$ is equal to the exact pair energy $\epsilon_{ij}^{\mathcal{P}}$ if the pair function $\tilde{u}_{ij}^{\mathcal{P}}$ is expanded in a complete basis. Moreover, he

pointed out that, for the minimum principle to apply to (3.56), the pair function must be kept orthogonal to all two-electron states $\phi_{kl}^{\mathcal{P}'}$ equal to or lower than $\phi_{ij}^{\mathcal{P}}$ in energy. Since a two-electron state is just a special case of an N-electron state, this also follows directly from the discussion of first-order wave functions made in section 2.2. Acknowledging Sinanoğlu's contribution to the description of many electron systems, we refer to (3.56) as *Sinanoğlu's strong orthogonality functional*, or just the SO functional.

When the MP2 energy expressions (3.35) and (3.52) are deduced using second quantisation, the orthogonality requirements put on pair functions are automatically provided by the operator Q_{occ}, and this makes it easy to miss the fundamental importance of such orthogonality. Obtaining (3.56) by other means than second quantisation, orthogonality may not be automatically provided, and the SO operator have to be introduced "by hand".

Assuming that the Hartree–Fock equations have been solved exactly, the operator $Q_{\text{occ}}(f(1)+f(2)-\varepsilon_i-\varepsilon_j)Q_{\text{occ}}$ becomes positive definite. From the discussion in section 2.2, we know that this makes the SO functional (3.56) a true upper bound to the exact pair energy

$$F_{ij}^{\mathcal{P}}[\tilde{u}_{ij}^{\mathcal{P}}] \geq \epsilon_{ij}^{\mathcal{P}} \tag{3.57}$$

In practice however, Fock operators are never exact but expanded in some finite basis. This makes the orbital energies ε_i and ε_j also approximate, and by the variational principle, higher than the exact. The positive definiteness needed for (3.57) to be valid is then no longer ensured since the expectation value of $f(1)+f(2)$ *may* be lower than $\varepsilon_i+\varepsilon_j$. In some cases, this may produce pair energies that are lower than the exact ones. However, all but a very few calculations done in this work obey (3.57) and pair energies converge nicely against the exact limit as trials functions are improved. For the hydrogen molecule (see Table 7.14) the boundedness is broken in two calculations, but only when the Fock operator is poorly approximated using s-orbitals only.

Far more worrying is the existence of three- and especially four-electron integrals in the SO functional. Let us, for simplicity, assume that the Fock operator is known exactly. Since the SO operator Q_{occ} then is constructed from eigenfunctions of the Fock operator, these two operators commute, allowing us to write

$$Q_{\text{occ}}\left[f(1)+f(2)\right]Q_{\text{occ}} = Q_{\text{occ}}\left[f(1)+f(2)\right] \tag{3.58}$$

where we have also exploited the idempotency of Q_{occ}. Writing this operator in terms of the projection operators P_{occ} we obtain

$$Q_{\text{occ}}(1,2) = 1 - P_{\text{occ}}(1) - P_{\text{occ}}(2) + P_{\text{occ}}(1)P_{\text{occ}}(2) \tag{3.59}$$

The combination of Q_{occ} and Fock operators turns the last term of (3.56), that is the expectation value, into several three- and four-electron integrals. The latter arises

when a projection operator P_{occ} is combined with either a Coulomb or an exchange operator. Using the Coulomb part of the $f(1)$ operator, we shall write the three kinds of integrals coming out of the $Q_{\text{occ}}(1,2)J(1)$ operator in explicit form.

Without the company of a projection operator P_{occ}, the Coulomb operator from (3.10) turns the expectation value into a sum over three-electron integrals.

$$\begin{aligned}
&\langle u_{ij}(1,2)|\, J(1)\, |u_{ij}(1,2)\rangle \\
&\quad = \sum_k \langle u_{ij}(1,2)|\, \langle \varphi_k(3)|\, r_{13}^{-1}\, |\varphi_k(3)\rangle\, |u_{ij}(1,2)\rangle \\
&\quad = \sum_k \langle u_{ij}(1,2)\varphi_k(3)|\, r_{13}^{-1}\, |\varphi_k(3) u_{ij}(1,2)\rangle
\end{aligned} \tag{3.60}$$

Since this integral has the same form for any pair function, also the exact, we have omitted the tilde. To further simplify expressions, pair functions are given in non-parity-adopted form.

With one projection operator present, the expectation value is turned into a double sum of four-electron integrals

$$\begin{aligned}
&\langle u_{ij}(1,2)|\, P_{\text{occ}}(1) J(1)\, |u_{ij}(1,2)\rangle \\
&\quad = \sum_{mk} \langle u_{ij}(1,2)|\varphi_m(1)\rangle\, \langle \varphi_m(1)|\, \langle \varphi_k(3)|\, r_{13}^{-1}\, |\varphi_k(3)\rangle\, |u_{ij}(1,2)\rangle \\
&\quad = \sum_{mk} \langle u_{ij}(1,2)\varphi_k(3)\varphi_m(4)|\, r_{34}^{-1}\, |\varphi_m(1)\varphi_k(3) u_{ij}(4,2)\rangle
\end{aligned} \tag{3.61}$$

Naively, one might expect the combination $P_{\text{occ}}(1)P_{\text{occ}}(2)J(1)$ to produce a triple sum over five-electron integrals, but this is only partly true. Since we project against occupied orbitals for both electron 1 and electron 2, each five-electron integral decouples into a product of a two-electron and a three-electron integral.

$$\begin{aligned}
&\langle u_{ij}(1,2)|\, P_{\text{occ}}(1) P_{\text{occ}}(2) J(1)\, |u_{ij}(1,2)\rangle \\
&\quad = \sum_{mnk} \langle u_{ij}(1,2)|\varphi_m(1)\rangle\, \langle \varphi_m(1)|\, |\varphi_n(2)\rangle\, \langle \varphi_n(2)|\, \langle \varphi_k(3)|\, r_{13}^{-1}\, |\varphi_k(3)\rangle\, |u_{ij}(1,2)\rangle \\
&\quad = \sum_{mnk} \langle u_{ij}(1,2)|\varphi_m(1)\varphi_n(2)\rangle\, \langle \varphi_m(1)\varphi_n(2)\varphi_k(3)|\, r_{13}^{-1}\, |\varphi_k(3) u_{ij}(1,2)\rangle
\end{aligned} \tag{3.62}$$

If the Fock operator is only approximate, the simplification used in (3.58) cannot be justified. This complicates things further, and integrals coming from operators like $P_{\text{occ}}(1)f(1)P_{\text{occ}}(2)$, for instance, turn out to be true five-electron integrals. As such many-electron integrals are very time consuming to compute, they are highly undesirable.

From discussion made above we see that four-electron integrals and higher may be avoided if we do either of the following

- Use trial functions that are in nature orthogonal to the occupied orbitals
- Approximate the Q_{occ} operator
- Approximate the entire $Q_{\text{occ}}\left[f(1)+f(2)\right]Q_{\text{occ}}$ operator

As we shall see below, the first of these approximations also removes the need for three-electron integrals. For the other two approximations, the only way to avoid calculating three-electron integrals, is to approximate them using the *resolution of the identity* (RI). This is covered in section 3.5.

3.4.2 The orbital approximation

If we require our trial functions $\tilde{u}_{ij}$ to be constructed from a basis orthogonal to the occupied orbitals, the effect of the strong orthogonality operator reduces to that of the identity operation. This may be obtained, for instance, by expanding the pair functions in pairs of virtual orbitals.

$$\tilde{u}_{ij}^{\mathcal{P}}(1,2)=\sum_{a\geq b}c_{ij,\mathcal{P}}^{ab,\mathcal{P}}\,\phi_{ab}^{\mathcal{P}}(1,2) \tag{3.63}$$

This is referred to as *the orbital approximation* and is the traditional way to approximate pair-functions within MP2 theory. The orbital approximation reduces the SO functional (3.56) to a function of the parameters $c_{ij,\mathcal{P}}^{ab,\mathcal{P}}$. These parameters may be arranged in a matrix where pairs $(ab,\mathcal{P})$ specify a certain row and pairs $(ij,\mathcal{P})$ specify a certain column. Denoting this matrix $\mathbf{C}_{\text{o}}$, the column denoted $[\mathbf{C}_{\text{o}}]_{ij}^{\mathcal{P}}$ is the solution vector for pair $(ij,\mathcal{P})$ once the elements of $\mathbf{C}_{\text{o}}$ have been optimised. Keeping in mind that $Q_{\text{occ}}\phi_{ab}=\phi_{ab}$, we may now write the SO functional as

$$\begin{aligned}F_{ij}^{\mathcal{P}}[\mathbf{C}_{\text{o}}]=\Lambda_{ij}^{\mathcal{P}}\Bigg(&\sum_{a\geq b}\sum_{c\geq d}c_{ij,\mathcal{P}}^{ab,\mathcal{P}}\left\langle\phi_{ab}^{\mathcal{P}}\right|f(1)+f(2)-\varepsilon_i-\varepsilon_j\left|\phi_{cd}^{\mathcal{P}}\right\rangle c_{ij,\mathcal{P}}^{cd,\mathcal{P}}\\&+2\sum_{a\geq b}c_{ij,\mathcal{P}}^{ab,\mathcal{P}}\left\langle\phi_{ab}^{\mathcal{P}}\right|r_{12}^{-1}\left|\phi_{ij}^{\mathcal{P}}\right\rangle\Bigg)\\=\Lambda_{ij}^{\mathcal{P}}&\left([\mathbf{C}_{\text{o}}]_{ij}^{\mathcal{P}\dagger}\mathbf{H}_{\text{oo}}[\mathbf{C}_{\text{o}}]_{ij}^{\mathcal{P}}+2[\mathbf{C}_{\text{o}}]_{ij}^{\mathcal{P}\dagger}[\mathbf{R}_{\text{o}}]_{ij}^{\mathcal{P}}\right)\end{aligned} \tag{3.64}$$

where we have introduced the matrices $\mathbf{H}_{\text{oo}}$ and $\mathbf{R}_{\text{o}}$ with elements

$$\mathrm{H}_{\text{oo}}=\left\langle\phi_{ab}^{\mathcal{P}}\right|f(1)+f(2)-\varepsilon_i-\varepsilon_j\left|\phi_{cd}^{\mathcal{P}}\right\rangle=(\varepsilon_a+\varepsilon_b-\varepsilon_i-\varepsilon_j)\,\delta_{ac}\delta_{bd} \tag{3.65}$$

$$\mathrm{R}_{\text{o}}=\left\langle\phi_{ab}^{\mathcal{P}}\right|Q_{\text{occ}}r_{12}^{-1}\left|\phi_{ij}^{\mathcal{P}}\right\rangle=\left\langle\phi_{ab}^{\mathcal{P}}\right|r_{12}^{-1}\left|\phi_{ij}^{\mathcal{P}}\right\rangle \tag{3.66}$$

As usual, the indices in the bra give the row number of the matrix while the indices in the ket give the column number. The one or two o's indexed on matrices or matrix

elements refers to the orbital approximation only and should not be confused with matrix dimensions. Neither is their number used to distinguish between matrices and vectors. Since the notation becomes apparent in the next section, it is not discussed any further here.

To optimise the parameters $[\mathbf{C}_\mathrm{o}]_{ij}^{\mathcal{P}}$ we differentiate the SO functional with respect to these parameters and put the derivative equal to zero

$$\frac{\partial F_{ij}^{\mathcal{P}}}{\partial \mathbf{C}_\mathrm{o}} = 2\Lambda_{ij}^{\mathcal{P}} \left(\mathbf{H}_\mathrm{oo} [\mathbf{C}_\mathrm{o}]_{ij}^{\mathcal{P}} + [\mathbf{R}_\mathrm{o}]_{ij}^{\mathcal{P}} \right) = \mathbf{0} \tag{3.67}$$

Solving this equation for the expansion coefficients, we get

$$[\mathbf{C}_\mathrm{o}]_{ij}^{\mathcal{P}} = -\mathbf{H}_\mathrm{oo}^{-1} [\mathbf{R}_\mathrm{o}]_{ij}^{\mathcal{P}} \tag{3.68}$$

Equation (3.68) gives the solution vector for one parity adapted pair of electrons. Clearly, the solution vector for the other pairs is given in an identical form. Therefore, removing the square brackets in equation (3.68), we get an equation for the total solution matrix $\mathbf{C}_\mathrm{o}$

$$\mathbf{C}_\mathrm{o} = -\mathbf{H}_\mathrm{oo}^{-1} \mathbf{R}_\mathrm{o} \tag{3.69}$$

Finally, using the definitions of $\mathbf{H}_\mathrm{oo}$ and $\mathbf{R}_\mathrm{o}$ given in (3.65) and (3.66) we obtain the well-known expression for $c_{ij,\mathcal{P}}^{ab,\mathcal{P}}$

$$c_{ij,\mathcal{P}}^{ab,\mathcal{P}} = -\frac{\left\langle \phi_{ab}^{\mathcal{P}} \right| r_{12}^{-1} \left| \phi_{ij}^{\mathcal{P}} \right\rangle}{\varepsilon_a + \varepsilon_b - \varepsilon_i - \varepsilon_j} \tag{3.70}$$

If we insert this expression for the expansion coefficients into (3.63), the pair energy (3.35) may be written

$$\epsilon_{ij}^{\mathcal{P}} = \Lambda_{ij}^{\mathcal{P}} \sum_{a \geq b} c_{ij,\mathcal{P}}^{ab,\mathcal{P}} \left\langle \phi_{ab}^{\mathcal{P}} \right| r_{12}^{-1} \left| \phi_{ij}^{\mathcal{P}} \right\rangle = -\Lambda_{ij}^{\mathcal{P}} \sum_{a \geq b} \frac{\left| \left\langle \phi_{ab}^{\mathcal{P}} \right| r_{12}^{-1} \left| \phi_{ij}^{\mathcal{P}} \right\rangle \right|^2}{\varepsilon_a + \varepsilon_b - \varepsilon_i - \varepsilon_j} \tag{3.71}$$

Alternatively, we may choose to express the pair energy in term of matrices $\mathbf{H}_\mathrm{oo}$ and $\mathbf{R}_\mathrm{o}$ giving

$$\epsilon_{ij}^{\mathcal{P}} = \sum_{a \geq b} c_{ij,\mathcal{P}}^{ab,\mathcal{P}} \left\langle \phi_{ab}^{\mathcal{P}} \right| r_{12}^{-1} \left| \phi_{ij}^{\mathcal{P}} \right\rangle \Lambda_{ij}^{\mathcal{P}} = [\mathbf{C}_\mathrm{o}]_{ij}^{\mathcal{P}\dagger} [\overline{\mathbf{R}}_\mathrm{o}]_{ij}^{\mathcal{P}} \tag{3.72}$$

where we have introduced a parity-weighed version of the right hand side matrix $\mathbf{R}_\mathrm{o}$ defined as

$$[\overline{\mathbf{R}}_\mathrm{o}]_{ij}^{\mathcal{P}} = \Lambda_{ij}^{\mathcal{P}} [\mathbf{R}_\mathrm{o}]_{ij}^{\mathcal{P}} \tag{3.73}$$

The total second-order energy $E^{(2)}$ is the sum over all pair energies. Using matrices, this sum may conveniently be written as a trace

$$E^{(2)} = \mathrm{tr}(\mathbf{C}_\mathrm{o}^\dagger \overline{\mathbf{R}}_\mathrm{o}) = -\mathrm{tr}(\mathbf{R}_\mathrm{o}^\dagger \mathbf{H}_\mathrm{oo}^{-1} \overline{\mathbf{R}}_\mathrm{o}) \tag{3.74}$$

The orbital approximation removes the need for many-electron integrals completely and leaves us with the usual two-electron AO integrals. These integrals are also used to obtain the Hartree–Fock energy for some system. In this case they are combined with the AO density matrix to form a Fock matrix. Using some iterative approach in which the Fock matrix in each iteration is transformed to MO basis, the Hartree–Fock energy may be obtained. Even though we do the MO transformation several times it is not considered a time-critical step.

At the MP2 level, the two-electron integrals must undergo a full MO transformation of type $T : g_{\mu\nu\sigma\tau} \rightarrow g_{abij}$. For calculations employing large basis sets this four-index transformation turns out to be the major bottle-neck. Dynamic electron correlation in nonmetallic systems is a short-range effect, however, with an asymptotic distance dependency of $\propto r^{-6}$ (dispersion energy). Using MOs from all parts of a molecule to describe the dynamic correlation in one particular part, therefore, is not physically justified. Pulay [35] realized this and developed a *local method for dynamic electron correlation*, which he later implemented for MP2 together with Sæbø [36, 37]. This method and other local methods (see Ref. [38] for a review) efficiently removes the MO transformation bottle-neck. And combined with schemes for prescreening or approximating two-electron AO integrals, MP2 methods that scale linear with the system size have been obtained [39, 40].

However, no matter how efficient such methods become, they can do nothing to improve the orbital approximation itself. As discussed in the introduction, the error in the energy is of order N^{-3} when we include virtual orbitals having N as the largest principal quantum number in our expansions. To get second-order energies converged to within the "thermo-chemical accuracy" of approximately $1\,\mathrm{mE_h}$ we are therefore required to use principal expansions with $N = 9$ or even $N = 10$. While this may be achieved for small molecular systems, it is clearly an impossible task for large molecules. When employing the orbital approximation to obtain bonding energies, for instance, we therefore always have to rely on cancellation of errors.

3.4.3 The weak orthogonality functional

The orbital approximation has an inherent deficiency in its ability to describe pair functions correctly. To remove, or at least reduce this deficiency, we have to include basis functions that are explicitly dependent of the inter-electronic distance r_{12} in the expansion of the pair function. Such explicitly r_{12}-dependent functions are often referred to as *geminals*. For geminals to be useful they must be able to describe the Coulomb hole properly, and equally important, there must be methods available for evaluating integrals containing these two-electron functions. These two requirements put restrictions on how geminals may be constructed. In section 6.1, we shall see that if we construct geminals from a product of orbitals multiplied by a *correlation factor* $f_v(r_{12})$

$$g^{\mathcal{P}}_{pq,v}(\mathbf{r}_1, \mathbf{r}_2, r_{12}) = f_v(r_{12})\phi^{\mathcal{P}}_{pq}(\mathbf{r}_1, \mathbf{r}_2) \tag{3.75}$$

both requirements may be fulfilled, provided that the right functional form is chosen for the correlation factor. Note that, we allow the geminals to be constructed from any pair of orbitals and not only, for instance, occupied orbitals.

Even though geminals are better suited for describing the Coulomb hole than the virtual orbitals expansion, there is no reason to exclude the latter. After all, it represents an efficient way to retrieve a large proportion of the correlation energy. We propose, therefore, to expand pair functions in a basis consisting of both geminals and products of virtual orbitals

$$\tilde{u}_{ij}^{\mathcal{P}}(1,2) = \sum_{a \geq b} c_{ij,\mathcal{P}}^{ab,\mathcal{P}} \phi_{ab}^{\mathcal{P}}(1,2) + \sum_{p \geq q,v} c_{ij,\mathcal{P}}^{pq,v,\mathcal{P}} g_{pq,v}^{\mathcal{P}}(1,2) \tag{3.76}$$

In (3.76) we have omitted explicit reference to the electronic position vectors $\mathbf{r}_1$ and $\mathbf{r}_2$ and the inter-electronic distance r_{12}, and we have introduced the indices 1 and 2 merely to emphasise that these functions are two-electron functions.

Having introduced geminals in our pair functions, they are no longer automatically orthogonal to the occupied orbitals. When pair functions are to be optimised by means of the SO functional (3.56), we therefore have to face the strong orthogonality operator. From the discussion above, we know that this implies the appearance of four-electron integrals and even five-electron integrals if the Fock operator and Q_{occ} do not commute. These many-electron integrals are especially unfortunate since we only need three-electron integrals to calculate the pair-energy from (3.35). This makes it natural to search for an approximate way to optimise pair functions.

Integrals over many electrons arise from expectation values of operators like $P_{\text{occ}}(1)f(1)$, while apparently more complicated operators like $P_{\text{occ}}(1)P_{\text{occ}}(2)f(1)$ gives rise to three-electron integrals only. We may therefore suggest to approximate or modify the SO operator in a way that maintains the strong orthogonality property but removes the operators producing many-electron integrals. This is indeed possible, but first, we discuss an approach proposed by Szalewicz *et al.* [12, 13], in which the the entire SO functional is modified rather than just the Q_{occ} operator. As an alternative to the complicated SO functional, Szalewicz an co-workers suggested the following functional

$$\begin{aligned} J_{ij}^{\mathcal{P}}[\tilde{u}_{ij}^{\mathcal{P}}] = \Lambda_{ij}^{\mathcal{P}} \big(& \langle \tilde{u}_{ij}^{\mathcal{P}} | \, f(1) + f(2) - \varepsilon_i - \varepsilon_j \, | \tilde{u}_{ij}^{\mathcal{P}} \rangle \\ & + \Delta_{ij} \langle \tilde{u}_{ij}^{\mathcal{P}} | \, P_{\text{occ}}(1) + P_{\text{occ}}(2) \, | \tilde{u}_{ij}^{\mathcal{P}} \rangle + 2 \langle \tilde{u}_{ij}^{\mathcal{P}} | \, Q_{\text{occ}} r_{12}^{-1} \, | \phi_{ij}^{\mathcal{P}} \rangle \big) \end{aligned} \tag{3.77}$$

where Δ_{ij} is a level-shift defined as

$$\Delta_{ij} = \frac{1}{2} (\varepsilon_i + \varepsilon_j - 2\varepsilon_1) + \eta \tag{3.78}$$

where ε_1 is the orbital energy of the lowest occupied energy and η is some arbitrary, nonnegative parameter with the dimension of energy. The functional (3.77), which

is called the *weak orthogonality functional* or just the WO functional, may be written in the alternative form

$$J_{ij}^{\mathcal{P}}[\tilde{u}_{ij}^{\mathcal{P}}] = \Lambda_{ij}^{\mathcal{P}} \left(\left\langle \tilde{u}_{ij}^{\mathcal{P}} \right| \tilde{f}(1) + \tilde{f}(2) - \varepsilon_i - \varepsilon_j \left| \tilde{u}_{ij}^{\mathcal{P}} \right\rangle + 2 \left\langle \tilde{u}_{ij}^{\mathcal{P}} \right| Q_{\mathrm{occ}} r_{12}^{-1} \left| \phi_{ij}^{\mathcal{P}} \right\rangle \right) \tag{3.79}$$

where $\tilde{f}$ is a modified Fock operator given as

$$\tilde{f} = f + \Delta_{ij} P_{\mathrm{occ}} \tag{3.80}$$

The presence of $\Delta_{ij} P_{\mathrm{occ}}$ in the $\tilde{f}$-operators makes the $\tilde{f}(1) + \tilde{f}(2)$ expectation value smaller than the corresponding $-(\varepsilon_i + \varepsilon_j)$ expectation value, for all $\tilde{u}_{ij}^{\mathcal{P}}$. The second-order term in (3.79) is therefore positive definite, and we may apply the minimum principle to the WO functional. In appendix A we discuss different aspects of this functional and we also justify its usefulness. In particular, we show that the minimum value of the WO functional is an upper bound to the minimum value of the SO functional, that is

$$J_{ij}^{\mathcal{P}}[\tilde{u}_{ij}^{\mathcal{P}}] \geq F_{ij}^{\mathcal{P}}[\tilde{u}_{ij}^{\mathcal{P}}] \geq \epsilon_{ij}^{\mathcal{P}} \tag{3.81}$$

provided that the Hartree–Fock equations have been solved exactly. To justify the WO functional is a rather comprehensive task, however, and having it here will only makes us lose focus. Therefore, we apply the results of appendix A directly and assume that the WO functional may be used to optimised pair functions.

Expanding pair functions in pairs of virtual orbitals and geminals as in (3.76), the WO functional may be written as

$$J_{ij}^{\mathcal{P}}[\tilde{u}_{ij}^{\mathcal{P}}] = J_{ij}^{\mathcal{P}}[\mathbf{C}_{\mathrm{o}}, \mathbf{C}_{\mathrm{g}}] \tag{3.82}$$

where $\mathbf{C}_{\mathrm{o}}$ is the matrix holding orbital expansion coefficients $c_{ij,\mathcal{P}}^{ab,\mathcal{P}}$ and $\mathbf{C}_{\mathrm{g}}$ is the matrix holding geminal expansion coefficients $c_{ij,\mathcal{P}}^{pq,v,\mathcal{P}}$. Note that the WO functional for the pair of electrons $(ij, \mathcal{P})$ do not depend on all matrix elements, but only those belonging to the proper column. Writing $J_{ij}^{\mathcal{P}}$ as a function of the full matrices is therefore just a matter of convenience. Applying the minimum principle to the WO functional for each pair of electrons, and collecting the resulting equations into one extended matrix equation we get

$$\begin{pmatrix} \mathbf{H}_{\mathrm{oo}} & \mathbf{H}_{\mathrm{og}} \\ \mathbf{H}_{\mathrm{go}} & \tilde{\mathbf{H}}_{\mathrm{gg}} \end{pmatrix} \begin{pmatrix} \mathbf{C}_{\mathrm{o}} \\ \mathbf{C}_{\mathrm{g}} \end{pmatrix} = - \begin{pmatrix} \mathbf{R}_{\mathrm{o}} \\ \mathbf{R}_{\mathrm{g}} \end{pmatrix} \tag{3.83}$$

where the four blocks of the left-hand-side matrix, $\mathbf{H}$, have elements given by

$$\mathrm{H}_{\mathrm{oo}} = (\varepsilon_a + \varepsilon_b - \varepsilon_i - \varepsilon_j)\, \delta_{ac} \delta_{bd} \tag{3.84}$$

$$\mathrm{H}_{\mathrm{go}} = \left\langle g_{pq,v}^{\mathcal{P}} \right| f(1) + f(2) - \varepsilon_i - \varepsilon_j \left| \phi_{cd}^{\mathcal{P}} \right\rangle \tag{3.85}$$

$$\tilde{\mathrm{H}}_{\mathrm{gg}} = \left\langle g_{pq,v}^{\mathcal{P}} \right| \tilde{f}(1) + \tilde{f}(2) - \varepsilon_i - \varepsilon_j \left| g_{rs,w}^{\mathcal{P}} \right\rangle \tag{3.86}$$

and the two blocks of the right-hand-side matrix, $\mathbf{R}$, have elements given by

$$\mathrm{R_o} = \left\langle \phi_{ab}^{\mathcal{P}} \right| r_{12}^{-1} \left| \phi_{ij}^{\mathcal{P}} \right\rangle \tag{3.87}$$

$$\mathrm{R_g} = \left\langle g_{pq,v}^{\mathcal{P}} \right| Q_{\mathrm{occ}} r_{12}^{-1} \left| \phi_{ij}^{\mathcal{P}} \right\rangle \tag{3.88}$$

Since $\mathbf{H}$ is Hermitian $\mathbf{H}_{\mathrm{og}} = \mathbf{H}_{\mathrm{go}}^{\dagger}$, and it is sufficient to give the matrix elements for one of these blocks. Note also that the modified Fock operator, $\tilde{f}$, only appears in the geminal-geminal block. Since virtual orbitals are projected away by P_{occ}, $\tilde{f}$ reduces to the normal Fock operator if we have an expansion of virtual orbitals in either the bra or the ket. For the orbital approximation, the diagonal nature of $\mathbf{H}_{\mathrm{oo}}$ makes it easy to compute the amplitudes $\mathbf{C}_{\mathrm{o}}$ by direct inversion. This is not possible here, however, as the matrix $\mathbf{H}$ is not diagonal. The equation system (3.83) must therefore be solved by some iterative process.

Having converged the amplitudes $\mathbf{C}_{\mathrm{o}}$ and $\mathbf{C}_{\mathrm{g}}$, the second-order energy may be obtained from the expression

$$E^{(2)} = \mathrm{tr}(\mathbf{C}_{\mathrm{o}}^{\dagger}\overline{\mathbf{R}}_{\mathrm{o}}) + \mathrm{tr}(\mathbf{C}_{\mathrm{g}}^{\dagger}\overline{\mathbf{R}}_{\mathrm{g}}) \tag{3.89}$$

where the amplitudes for the virtual orbital expansion are different from those obtained in equation (3.69), due to the coupling to geminals through $\mathbf{H}_{\mathrm{og}}$.

The fact that $\mathbf{H}$ is both Hermitian and positive definite, allows us to reformulate the extended matrix problem using a *Schur-like decomposition*[1]

$$\begin{pmatrix} \mathbf{H}_{\mathrm{oo}} & \mathbf{H}_{\mathrm{og}} \\ \mathbf{H}_{\mathrm{go}} & \tilde{\mathbf{H}}_{\mathrm{gg}} \end{pmatrix} = \begin{pmatrix} \mathbf{1} & \mathbf{0} \\ \mathbf{Z} & \mathbf{1} \end{pmatrix} \begin{pmatrix} \mathbf{H}_{\mathrm{oo}} & \mathbf{0} \\ \mathbf{0} & \tilde{\mathbf{G}}_{\mathrm{gg}} \end{pmatrix} \begin{pmatrix} \mathbf{1} & \mathbf{Z}^{\dagger} \\ \mathbf{0} & \mathbf{1} \end{pmatrix} \tag{3.90}$$

where the matrices $\mathbf{Z}$ and $\tilde{\mathbf{G}}_{\mathrm{gg}}$ are defined as

$$\mathbf{Z} = \mathbf{H}_{\mathrm{go}}\mathbf{H}_{\mathrm{oo}}^{-1} \tag{3.91}$$

$$\tilde{\mathbf{G}}_{\mathrm{gg}} = \tilde{\mathbf{H}}_{\mathrm{gg}} - \mathbf{H}_{\mathrm{go}}\mathbf{H}_{\mathrm{oo}}^{-1}\mathbf{H}_{\mathrm{og}} \tag{3.92}$$

Since $\mathbf{H}_{\mathrm{oo}}$ is diagonal, the inverse is easily formed by replacing all diagonal elements $\mathrm{H_{oo}}$ by $1/\mathrm{H_{oo}}$. The decomposition (3.90) is therefore not only feasible but straight forward. Inserting the decomposed $\mathbf{H}$ in (3.83) and rearranging we obtain

$$\begin{pmatrix} \mathbf{H}_{\mathrm{oo}} & \mathbf{H}_{\mathrm{og}} \\ \mathbf{0} & \tilde{\mathbf{G}}_{\mathrm{gg}} \end{pmatrix} \begin{pmatrix} \mathbf{C}_{\mathrm{o}} \\ \mathbf{C}_{\mathrm{g}} \end{pmatrix} = - \begin{pmatrix} \mathbf{R}_{\mathrm{o}} \\ \mathbf{S}_{\mathrm{g}} \end{pmatrix} \tag{3.93}$$

where the transformed right-hand-side matrix $\mathbf{S}_{\mathrm{g}}$ is defined as

$$\mathbf{S}_{\mathrm{g}} = \mathbf{R}_{\mathrm{g}} - \mathbf{Z}\mathbf{R}_{\mathrm{o}} \tag{3.94}$$

[1] A true Schur decomposition requires the decomposed matrix to be strictly upper triangular. This is not the case with $\tilde{\mathbf{G}}_{\mathrm{gg}}$.

The blocked form of the transformed equation system (3.93), allows us to first solve for $\mathbf{C}_\mathrm{g}$ and then next use this solution to obtain $\mathbf{C}_\mathrm{o}$. $\mathbf{C}_\mathrm{g}$ may be found by solving the equation

$$\tilde{\mathbf{G}}_\mathrm{gg}\mathbf{C}_\mathrm{g} = -\mathbf{S}_\mathrm{g} \tag{3.95}$$

by some iterative method. Next, solving (3.93) for $\mathbf{C}_\mathrm{o}$ we get

$$\mathbf{C}_\mathrm{o} = -\mathbf{H}_\mathrm{oo}^{-1}\mathbf{R}_\mathrm{o} - \mathbf{Z}\mathbf{C}_\mathrm{g} \tag{3.96}$$

which means that these amplitudes can be retrieved with a few matrix operations only and without having to solve any more equations.

Using the decomposition method, we have reduced the size of the equation system from $N_\mathrm{voe} + N_\mathrm{gem}$ in (3.83) to N_gem in (3.95), where N_voe is the number of functions in the virtual orbital expansion and N_gem is the number of geminals. Another interesting feature about the decomposition, is that it allows us to rewrite the energy as

$$E^{(2)} = -\mathrm{tr}(\mathbf{R}_\mathrm{o}^\dagger\mathbf{H}_\mathrm{oo}^{-1}\overline{\mathbf{R}}_\mathrm{o}) + \mathrm{tr}(\mathbf{C}_\mathrm{g}^\dagger\overline{\mathbf{S}}_\mathrm{g}) \tag{3.97}$$

Comparing this expression with (3.74), we identify the first term as the second-order energy correction due to the virtual orbitals alone. The second term therefore, represents the portion of the second-order energy recovered by geminals and which is not already recovered by the virtual orbital expansion. This picture is justified by the fact that

$$\mathbf{S}_\mathrm{g} \to \mathbf{0} \quad \text{when} \quad \sum |\varphi_p\rangle \langle\varphi_p| \to 1 \tag{3.98}$$

since $\mathbf{R}_\mathrm{o}$ in a complete one-particle basis is transformed into $\mathbf{R}_\mathrm{g}$ by $\mathbf{Z}$. By symmetry it is also possible to view the virtual orbital expansion as a correction to the geminal basis. Depending on how geminals are constructed, they may recover a much larger proportion of the second-order energy alone, than do the virtual orbitals alone. This supports viewing the virtual orbital expansion as a correction to the geminals. On the other hand, the virtual orbitals are the ones used in conventional MP2 calculations, and it is not unreasonable, therefore, to consider the geminals as representing a correction to such calculations. In the bottom line, this is a matter of personal preference only.

3.4.4 Approximating the strong orthogonality operator

Modifying the whole SO functional in order to avoid many-electron integrals may seem unnecessarily comprehensive, and it is tempting to search for modest approximations to the strong orthogonality operator that allows us to maintain the SO functional in its original form. Since the many-electron integrals are generated by the single-projection operators $P_\mathrm{occ}(1)$ and $P_\mathrm{occ}(2)$, these are the ones we need to modify. One possible modification, is to transform them into relatively "harmless"

double-projection operators, using the resolution of the identity (RI)

$$\sum_p |\varphi_p\rangle \langle\varphi_p| = 1 \tag{3.99}$$

In principle, the resolution of the identity is valid only when the one-particle basis is complete. It has been argued [41], however, that the resolution of the identity in some contexts hold, even when the expansion (3.99) is truncated after angular momentum $l = 3l_{\text{occ}}$, where l_{occ} is the highest angular momentum used in the occupied orbitals. This is, of course, of no importance for the theoretical discussion made here, but may be crucial from an implementational point of view. We should also keep in mind, that a one-particle basis that is nearly complete, gives a two-particle basis encumbered with linear dependencies. When using the resolution of the identity one should therefore consider introducing a second, near complete, basis set reserved for the RI. Projection operators expressed in near complete basis sets, are in the rest of this section assigned with a tilde. Note that the use of a second basis set also separates the effect of the RI approximation from all other approximations done. This in turn, allows us to keep track of the error introduced by using a specific RI expansion.

Inserting the resolution of the identity in the strong orthogonality operator given in (3.59), we get

$$\begin{aligned} Q_{\text{occ}}(1,2) &= 1 - O(1) - O(2) + O(1)O(2) \\ &\approx 1 - O(1)\tilde{P}(2) - \tilde{P}(1)O(2) + O(1)O(2) \end{aligned} \tag{3.100}$$

where we have introduced the operator $O(i)$ and $P(i)$ to make equations more readable. These operators are defined as

$$O(i) = P_{\text{occ}}(i) = \text{projection onto occupied orbitals,} \tag{3.101}$$

$$\tilde{P}(i) = \tilde{P}_{\text{all}}(i) \ = \text{projection on all orbitals} \tag{3.102}$$

where i refers to electron 1 or 2 and the tilde denotes a projection onto a near complete basis set.

Since all single-projection operator have disappeared in the final expression of (3.100), there is no longer need for integrals higher than three-electron ones. Remember, however, that terms containing constructions like $O(1)\tilde{P}(2)$, give rise to three-electron integrals (cf. equation (3.62)). The use of the resolution of the identity, therefore requires us to calculate three-electron integrals over basis functions with high angular momentum. For the approximation (3.100) to be useful, we will most likely have to introduce the RI in these three-electron integrals as well. As we shall see in the next section, this reduces each three-electron integral to a sum over two-electron integrals.

The need for two different basis sets is a complicating factor from an implementational point of view, and Klopper and Samson [42] were recently the first to report an implementation of the Q_{occ} approximation given in (3.100). If only one basis set is available, the approximation (3.100) may still be used, but all operators have to be given in a basis set that is nearly complete. In this case, it turns out that a slightly different approximation is more useful.

Instead of restricting the strong orthogonality operator to project out occupied orbitals only, it may be extended to also project out virtual orbitals. This new SO operator, which we denote $Q_{\text{all}}(1,2)$, is given by

$$Q_{\text{all}}(1,2) = 1 - \tilde{P}(1) - \tilde{P}(2) + \tilde{P}(1)\tilde{P}(2) \tag{3.103}$$

Once again, we introduce the resolution of the identity to transform single-projection operators, and get

$$\begin{aligned} Q_{\text{all}}(1,2) &\approx 1 - \tilde{P}(1)\tilde{P}(2) - \tilde{P}(1)\tilde{P}(2) + \tilde{P}(1)\tilde{P}(2) \\ &= 1 - \tilde{P}(1)\tilde{P}(2) \end{aligned} \tag{3.104}$$

which in form is simpler than the SO operator given in (3.100). To optimise pair functions using the SO functional with this new SO operator, we proceed exactly as with the WO functional. This leads us to an equation system similar to that of (3.83) but with some of the matrix blocks redefined

$$\begin{pmatrix} \mathbf{H}_{\text{oo}} & \bar{\mathbf{H}}_{\text{og}} \\ \bar{\mathbf{H}}_{\text{go}} & \bar{\mathbf{H}}_{\text{gg}} \end{pmatrix} \begin{pmatrix} \mathbf{C}_{\text{o}} \\ \mathbf{C}_{\text{g}} \end{pmatrix} = - \begin{pmatrix} \mathbf{R}_{\text{o}} \\ \mathbf{R}_{\text{g}} \end{pmatrix} \tag{3.105}$$

The redefined matrix blocks are assigned with a "bar" and are

$$\bar{\mathbf{H}}_{\text{go}} = \mathbf{H}_{\text{go}} - \mathbf{S}_{\text{go}}\mathbf{H}_{\text{oo}} \tag{3.106}$$

$$\bar{\mathbf{H}}_{\text{gg}} = \mathbf{H}_{\text{gg}} - \mathbf{S}_{\text{gc}}\mathbf{H}_{\text{cg}} - \mathbf{H}_{\text{gc}}\mathbf{S}_{\text{cg}} + \mathbf{S}_{\text{gc}}\mathbf{H}_{\text{cc}}\mathbf{S}_{\text{cg}} \tag{3.107}$$

where $\mathbf{S}_{\text{gc}}$ is the overlap matrix between the geminal basis and the orbital basis

$$\mathrm{S}_{\text{gc}} = \left\langle g^{\mathcal{P}}_{pq,v} | \tilde{\phi}^{\mathcal{P}}_{rs} \right\rangle . \tag{3.108}$$

This matrix should not be confused with $\mathbf{S}_{\text{g}}$ defined in (3.94). Note also, that the Fock operators used in $\bar{\mathbf{H}}_{\text{gg}}$ are the normal Fock operators and not the modified operators given in (3.80).

For a basis set that is near complete, $\bar{\mathbf{H}}_{\text{go}} \approx \mathbf{0}$, and the orbital part and geminal part of the equation system become decoupled. A basis set can never be mathematical complete, however, and whenever a decoupling is enforced, the pair energies become too low. This implies that the boundedness given in (3.57), which is a valuable property when energy limits are pursued, can no longer be assumed. Since a

decoupling has no major cost saving effects from a computational point of view, the $\bar{\mathbf{H}}_{\mathrm{go}}$ block should therefore be kept in the equation system.

If we use the RI-approximated Q_{occ} operator given in (3.100) in the SO functional, the corresponding equation system is analogues to (3.105), but the matrix elements needed to construct the $\bar{\mathbf{H}}_{\mathrm{go}}$ and $\bar{\mathbf{H}}_{\mathrm{gg}}$ blocks are different.

3.5 Avoiding three-electron integrals

As we have seen in the previous section, three-electron integrals are required when pair functions are optimised with the WO functional. These integrals are time-consuming to compute and their number grows as N^6, where N is the number of basis functions in the one-electron basis. Due to this scaling, it may turn out to be important to approximate three-electron integrals. Kutzelnigg and Klopper [11] have shown how this may be done by introducing the resolution of the identity into the integrals. In this section we shall use their approach to approximate the three-electron integrals that arise when the WO functional is used.

Three-electron integrals are encountered in the $\mathbf{H}_{\mathrm{og}}$, $\mathbf{H}_{\mathrm{gg}}$, and $\mathbf{R}_{\mathrm{g}}$ matrix blocks, where they are generated by the Coulomb, the exchange, and the projection operators. If we drop parity-adaption, the matrix elements containing three-electron integrals, may be written

$$h_{\mathrm{og}} = \langle \phi_{ab}(1,2)| \, f(1) + f(2) \, |g_{pq,v}(1,2)\rangle \tag{3.109}$$

$$h_{\mathrm{gg}} = \langle g_{pq,v}(1,2)| \, f(1) + f(2) \, |g_{rs,w}(1,2)\rangle \tag{3.110}$$

$$p_{\mathrm{gg}} = \langle g_{pq,v}(1,2)| \, P_{\mathrm{occ}}(1) + P_{\mathrm{occ}}(2) \, |g_{rs,w}(1,2)\rangle \tag{3.111}$$

$$r_{\mathrm{g}} = \langle g_{pq,v}(1,2)| \, Q_{\mathrm{occ}} r_{12}^{-1} \, |\phi_{ij}(1,2)\rangle \tag{3.112}$$

Since these matrix elements are symmetric in electrons 1 and 2, it is sufficient to treat integrals with only half the operator. Choosing operators with respect to electron 1, the RI modified h_{og} integral becomes

$$\begin{aligned}
&\langle \phi_{ab}(1,2)| \, f(1) \, |g_{pq,v}(1,2)\rangle \\
&\quad \approx \sum_{\tilde{t}} \langle \phi_{ab}(1,2)| \, f(1) \, |\tilde{\varphi}_t(1)\rangle_1 \, \langle \tilde{\varphi}_t(1)|g_{pq,v}(1,2)\rangle_1 \\
&\quad = \sum_{\tilde{t}} \langle \varphi_a(1)| \, f(1) \, |\tilde{\varphi}_t(1)\rangle \, \langle \phi_{\tilde{t}b}(1,2)|g_{pq,v}(1,2)\rangle \\
&\quad = \sum_{\tilde{t}} f_{a\tilde{t}} \, \langle \phi_{\tilde{t}b}|g_{pq,v}\rangle
\end{aligned} \tag{3.113}$$

and we see that the three-electron integral reduces to a summation over one-electron Fock matrix elements multiplied by two-electron overlap matrix elements. In general, the Fock matrix element $f_{a\tilde{t}}$ represents a transition between different basis sets and

cannot be replaced by, say, ε_a. As in the previous section, a summation index given a tilde, as in $\tilde{t}$, indicates a basis set that is near complete.

It is essential that the RI expansion is inserted between the Fock operator and the two-electron function (geminal). As a consequence, we have to insert four RI expansions (two for each electrons) into h_{gg} to be able to decompose it

$$\begin{aligned}
&\langle g_{pq,v}(1,2)|\, f(1)\, |g_{rs,w}(1,2)\rangle \\
&\quad\approx \sum_{\tilde{t},\tilde{u}} \sum_{\tilde{t}',\tilde{u}'} \langle g_{pq,v}(1,2)|\tilde{\varphi}_t(1)\tilde{\varphi}_u(2)\rangle \\
&\qquad\times \langle \tilde{\varphi}_t(1)\tilde{\varphi}_u(2)|\, f(1)\, |\tilde{\varphi}_{t'}(1)\tilde{\varphi}_{u'}(2)\rangle \, \langle \tilde{\varphi}_{t'}(1)\tilde{\varphi}_{u'}(2)|g_{rs,w}(1,2)\rangle \\
&\quad= \sum_{\tilde{t},\tilde{u},\tilde{t}'} \langle g_{pq,v}|\phi_{\tilde{t}\tilde{u}}\rangle \, f_{\tilde{t}\tilde{t}'} \, \langle \phi_{\tilde{t}'\tilde{u}}|g_{rs,w}\rangle
\end{aligned} \tag{3.114}$$

Again, the three-electron integrals are decomposed into products of one-electron and two-electron matrix elements. Note that, we arrive at a simpler expression, if the Fock operator is diagonal in the complete basis.

For the matrix elements p_{gg}, it is sufficient to use one RI expansion. This gives

$$\begin{aligned}
&\langle g_{pq,v}(1,2)|\, P_{\mathrm{occ}}(1)\, |g_{rs,w}(1,2)\rangle \\
&\quad\approx \sum_{k,\tilde{t}} \langle g_{pq,v}(1,2)|\varphi_k(1)\tilde{\varphi}_t(2)\rangle \, \langle \varphi_k(1)\tilde{\varphi}_t(2)|g_{rs,w}(1,2)\rangle \\
&\quad= \sum_{k,\tilde{t}} \langle g_{pq,v}|\phi_{k\tilde{t}}\rangle \, \langle \phi_{k\tilde{t}}|g_{rs,w}\rangle
\end{aligned} \tag{3.115}$$

The RHS matrix element r_{g} consists of four different terms. The only of these terms that are three-electron integrals, are the terms containing single-projection operators. Inserting an RI expansion in one of these gives

$$\begin{aligned}
&\langle g_{pq,v}(1,2)|\, P_{\mathrm{occ}}(1) r_{12}^{-1}\, |\phi_{ij}(1,2)\rangle \\
&\quad\approx \sum_{k,\tilde{t}} \langle g_{pq,v}(1,2)|\varphi_k(1)\tilde{\varphi}_t(2)\rangle \, \langle \varphi_k(1)\tilde{\varphi}_t(2)|\, r_{12}^{-1}\, |\phi_{ij}(1,2)\rangle \\
&\quad= \sum_{k,\tilde{t}} \langle g_{pq,v}|\phi_{k\tilde{t}}\rangle \, \langle \phi_{k\tilde{t}}|\, r_{12}^{-1}\, |\phi_{ij}\rangle
\end{aligned} \tag{3.116}$$

Strictly speaking, we do not have to approximate matrix elements of the entire Fock operator as we have done in (3.113) and (3.114). Both the kinetic energy part and the nuclear attraction part may be calculated as two-electron integrals without any use of the resolution of the identity. The effect of introducing the RI expansion in such integrals is in fact to reduce them to summations over one-electron integrals multiplied by two-electron overlap integrals, an approach which is less accurate and probably less effective as well. For the Coulomb and exchange parts things are

different, however, and the approach taken in (3.113) and (3.114) may turn out to be both fast and sufficiently accurate ways to approximate such integrals.

In the case of the Coulomb operator, the final expression of (3.114) is more complicated than necessary. If we use the Coulomb operator from the start, we get

$$\begin{aligned}
&\langle g_{pq,v}(1,2)|\, J(1)\, |g_{rs,w}(1,2)\rangle \\
&\quad = \langle g_{pq,v}(1,2)|\, J(1)\, |f_w(r_{12})\phi_{rs}(1,2)\rangle \\
&\quad \approx \sum_{\tilde{t}} \langle g_{pq,v}(1,2)|\, f_w(r_{12})\, |\tilde{\varphi}_t(1)\rangle_1\, \langle \tilde{\varphi}_t(1)|\, J(1)\, |\phi_{rs}(1,2)\rangle_1 \\
&\quad = \sum_{\tilde{t}} \left\langle g_{pq,v}(1,2)|g_{\tilde{t}s,v}(1,2)\right\rangle \langle \tilde{\varphi}_t(1)|\, J(1)\, |\varphi_r(1)\rangle \\
&\quad = \sum_{\tilde{t}} \left\langle g_{pq,v}|g_{\tilde{t}s,v}\right\rangle J_{\tilde{t}r}
\end{aligned} \tag{3.117}$$

and the integral may be evaluated with the use of only one RI expansion. For the exchange part this is not possible, and the integral must be evaluated as in (3.114) with the summation running over three general indices in the complete basis set.

3.6 A hierarchy of approximations

In the previous sections we have discussed different ways to obtain MP2 energies. First we have to determine what kind of basis set the pair functions are to be expanded in. Next, we must decide what functional to use in optimising these functions, and finally, we must calculate the pair energies. In both the optimisation and the energy calculation, we may introduce various approximations. These approximations affect the accuracy of the calculated energy to different degrees and the approximations should therefore be arranged in a hierarchy. At the first level of this hierarchy, we introduce approximations that affect the energy only to a small extent. Then, as we go to higher levels, the approximations have larger and larger impact on the accuracy. Consequently, there is no reason to introduce an approximation at a certain level if all earlier levels have been treated exactly. This is illustrated in Figure 3.2, where each complete path outlines a possible method. The boxes show whether or not an approximation is introduced at a certain level. There are altogether five different paths we may take to obtain MP2 energies and this gives us a total of six different methods. The sixth method corresponds to introducing no approximations at all and is not represented with path in the figure.

3.6.1 No approximations

In the current context, no approximations, means that the SO functional is used to optimise pair functions, and that all integrals are calculated exactly. As already

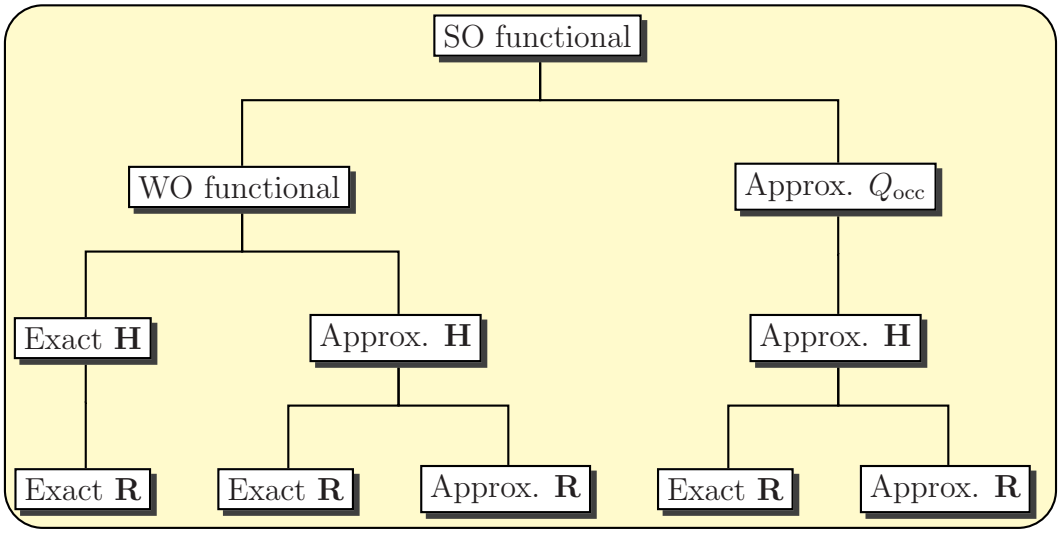

Figure 3.2: Approximations derived from the SO functional. Each path outlines a possible method for optimising pair functions and calculating energies. **H** and **R** are taken from (3.83) or (3.105). Both may be simplified using the RI to approximate three-electron integrals.

discussed, this approach is only possible if the pair functions are expanded in products of virtual orbitals (VOE). This is often referred to as the orbital approximation and represents the conventional way to do MP2. It has not always been recognised though [43, 44], that this is just a special case of the variational approach outlined by Sinanoğlu.

3.6.2 First level of approximation

If pair functions are constructed from true two-electron functions, the SO functional becomes prohibitively expensive to use. Depending on the quality of the Fock operator, up to four-electron or even five-electron integrals, are encountered. At the first level of approximation, these many-electron integrals should be avoided. As already discussed, this can be accomplished in two different ways. Either by approximating the Q_{occ} operator using the resolution of the identity, or by approximating the entire functional. The first of these approaches goes along the main right branch of the decision tree of Figure 3.2. The second goes along the main left branch. Note that the WO functional does not represent the only "left branch alternative" (see for instance Ref.[45]), but it is the only one treated in this work. Also, when we later turn to applications in chapter 7, we shall see that this functional is a good one.

3.6.3 Second level of approximation

No longer in need for four-electron integrals or higher, we are left with three-electron integrals as the most time consuming step of a calculation. As discussed in section 3.5, such integrals may be approximated using the resolution of the identity. This is the second level of approximation. However, we do not approximate all three-electron integrals at the same level. Comparing (3.79) with (3.83)–(3.88), we see that while matrix elements of $\mathbf{R}$ affect the WO functional to first order in $\tilde{u}_{ij}^{\mathcal{P}}$, the matrix elements of $\mathbf{H}$ affect the functional only to second order. Therefore, only the three-electron integrals present in $\mathbf{H}$ are approximated at this level. This has the important implication that only the optimisation of pair functions is affected, while the energy evaluation still employs exact expressions. The computational cost, however, may decrease considerably. All calculations presented in this work have employed exact three-electron integrals, and the cost of evaluating these integrals is $T_{\text{cpu}} \sim N_{\text{GCF}}(3N_{\text{GCF}} + 7)/2$, where N_{GCF} is the number of Gaussian-type correlation factors[2] (GCFs) used in the expansion of a geminal. Assuming that an RI-approximated three-electron integral may be calculated at no cost compared to the exact integral, the computational cost decreases to $T_{\text{cpu}} \sim N_{\text{GCF}}$ at the current level of approximation. For the calculations presented later, for which N_{GCF} is 9, this would imply a decrease in calculation time by a factor of 17.

3.6.4 Third level of approximation

At the third level of approximation we also use the RI to approximate three-electron integrals in the matrix elements of $\mathbf{R}$. By doing this, the energy expression also becomes approximate.

[2]Gaussian correlation factors are discussion in section 6.1.

Chapter 4

Many-electron integrals over Gaussian-type geminals

4.1 MO transformations

As we shall see in chapter 6, the two orbitals present in a Gaussian-type geminal of kind (3.75) may either both be chosen from all MOs, both from occupied MOs, or one from each of these groups. Moreover, if one of the orbitals are chosen general, we may use the AO basis as well as the MO basis. Independent of this choice, however, all integrals are calculated in the AO basis and then, possibly, the integral indices are transformed to the full MO basis or the occupied orbitals.

The different matrix blocks of the equation system (3.83) have all different MO structures. This, combined with the flexibility we have allowed in the orbital part of a GTG, gives us a large number of different MO transformations that have to be handled. It is not tractable to give a detailed discussion of each of these transformations here. However, since the different MO transformations are closely related, it is sufficient to study the transformation of one particular integral. Any candidate will in principle do, and we choose the integral

$$I^{\mathcal{P}}_{abpq} = \left\langle \phi^{\mathcal{P}}_{ab}(1,2) \right| f(1) + f(2) \left| g^{\mathcal{P}}_{pq,v}(1,2) \right\rangle \tag{4.1}$$

which was also listed in (3.109) but then in non parity-adapted form. Note that, the index v is unaffected by an MO transformation and is therefore left out of $I^{\mathcal{P}}_{abpq}$. Also note, that there is no overlap integral in this matrix element. Since overlap integrals are to be multiplied with MO energies, they cannot be transformed along with integrals over the Fock operator.

Using the definitions of symmetric and antisymmetric pairs given in (3.32) and (3.33), we write the integral (4.1) as

$$I^{\mathcal{P}}_{abpq} = B_{abpq} \pm B_{abqp} \tag{4.2}$$

where the positive sign is used for symmetric pairs ($\mathcal{P} = \mathcal{S}$) and the negative sign is used for antisymmetric pairs ($\mathcal{P} = \mathcal{A}$). The integral B_{abpq} is given by

$$B_{abpq} = \langle \phi_{ab} | \, f(1) + f(2) \, | g_{pq,v} \rangle \tag{4.3}$$

While the parity-adapted integral $I^{\mathcal{P}}_{abpq}$ is triangular in both index pairs, that is $a \leq b$ and $p \leq q$, the integrals (4.3) are triangular in ab but not in pq.

The B_{abpq} integrals may in principle be MO transformed straightforwardly as

$$B_{abpq} = \sum_{\mu\nu\tilde{\sigma}\tilde{\tau}} B_{\mu\nu\tilde{\sigma}\tilde{\tau}} C_{\mu a} C_{\nu b} C_{\tilde{\sigma} p} C_{\tilde{\tau} q} \tag{4.4}$$

where

$$B_{\mu\nu\tilde{\sigma}\tilde{\tau}} = \langle \chi_{\mu\nu} | \, f(1) + f(2) \, | g_{\sigma\tau,v} \rangle \, . \tag{4.5}$$

The operator $f(1)+f(2)$ is symmetric in electrons 1 and 2 and this symmetry is also exhibited in the AO integrals (4.5). We may therefore limit the integral evaluation to those integrals for which $\mu\tilde{\sigma} \leq \nu\tilde{\tau}$. Although there are certain advantages by using a symmetric operator, we are not restricted to use one. Instead, we may decompose the B_{abpq} integrals as

$$B_{abpq} = A_{abpq} + A_{baqp} \tag{4.6}$$

where A_{abpq} is

$$A_{abpq} = \langle \phi_{ab} | \, f(2) \, | g_{pq,v} \rangle \tag{4.7}$$

In this integral, there is no triangularity left in the indices. Assuming that the implementation has loops for electron 1 outermost, we use the operator $f(2)$ in (4.7) rather than $f(1)$. This prevents the exchange operator from mixing indices for electron 1 with indices for electron 3, implying that we may transform a large number of AO integrals simultaneously to MO basis rather than just a few at a time. This is achieved by calculating all integrals corresponding to indices $\nu\tilde{\tau}$ (electron 2) for a particular choice of indices $\mu\tilde{\sigma}$ (electron 1). Storing these integrals in an AO matrix $T_{\nu\tilde{\tau}}$, we may MO transform indices $\nu\tilde{\tau}$ using efficient library routines for matrix multiplication. The MO transformation for A_{abpq} thus becomes

$$A_{abpq} = \sum_{\mu\tilde{\sigma}} T^{\mu\tilde{\sigma}}_{bq} C_{\mu a} C_{\tilde{\sigma} p} = \sum_{\mu\tilde{\sigma}} \left\{ \sum_{\nu\tilde{\tau}} T^{\mu\tilde{\sigma}}_{\nu\tilde{\tau}} C_{\nu b} C_{\tilde{\tau} q} \right\} C_{\mu a} C_{\tilde{\sigma} p} \tag{4.8}$$

where the matrix $T_{\nu\tilde{\tau}}$ is labelled with indices $\mu\tilde{\sigma}$ for electron 1. In Table 4.1 we have outlined a pseudo-code for this MO transformation and we have also included the transformations needed to obtain parity-adapted integrals.

When we transform $T^{\mu\tilde{\sigma}}_{\nu\tilde{\tau}}$ integrals into A_{pqrs} integrals we cannot use the symmetry relation $\mu\tilde{\sigma} \leq \nu\tilde{\tau}$ as the AO integrals are not symmetric in electrons 1 and 2. This, in turn, means that we must calculate twice as many integrals (roughly),

Table 4.1: Pseudo code for a sample integral calculation

Allocate $I^{\mathcal{P}}_{abpq}$, B_{abpq} and A_{abpq}
do v
  do $\mu\tilde{\sigma}$

    Calculate all integrals for indices $\nu\tilde{\tau}$

    Allocate $T^{\mu\tilde{\sigma}}_{\nu\tilde{\tau}}$
    for $\mathcal{O}$ **in** {kinetic energy, nuclear attraction, Coulomb, exchange}
      do $\nu\tilde{\tau}$
        $T^{\mu\tilde{\sigma}}_{\nu\tilde{\tau}} = T^{\mu\tilde{\sigma}}_{\nu\tilde{\tau}} + \langle\mu\nu|\,\mathcal{O}\,|\tilde{\sigma}\tilde{\tau}\rangle$
      end do
    end for

    Transform electron 2 using matrix multiplications

    Allocate $T^{\mu\tilde{\sigma}}_{bq}$
    do bq, $\nu\tilde{\tau}$
      $T^{\mu\tilde{\sigma}}_{bq} = T^{\mu\tilde{\sigma}}_{bq} + T^{\mu\tilde{\sigma}}_{\nu\tilde{\tau}} C_{\nu b} C_{\tilde{\tau} q}$
    end do

    Transform electron 1

    do ap
      $A_{abpq} = A_{abpq} + T^{\mu\tilde{\sigma}}_{bq} C_{\mu a} C_{\tilde{\sigma} p}$
    end do
  end do

  Symmetries operator

  do $a \leq b, pq$
    $B_{abpq} = A_{abpq} + A_{baqp}$
  end do

  Parity-adapt integrals

  do $a \leq b, p \leq q$
    $I^{\mathcal{S}}_{abpq} = B_{abpq} + B_{abqp}$
    $I^{\mathcal{A}}_{abpq} = B_{abpq} - B_{qbqp}$
  end do
end do

as needed with the B_{pqrs} approach. Integrals over the $f(1) + f(2)$ operator are more time consuming to calculate than integrals over the $f(2)$ operator, however, and even though the difference lies only in the calculation of an additional Hermite integral (see section 4.2), for three-electron integrals, such Hermite integrals typically consume 70–80% of the total calculation time (see section 6.5). Since the A_{pqrs} and B_{pqrs} approaches have almost the same computational performance, we shall choose the former as it is simpler to implement.

4.2 One-electron basis sets of GTOs

In section 6.1, we shall discuss different forms for the GTGs constituting the two-electron basis. In the current section, we briefly review some properties of the Gaussian-type orbitals (GTOs) used for the one-electron basis[1]. When we later develop formulas for many-electron integrals over Gaussian-type orbitals, the conventions adopted here are used.

In quantum chemical calculations, a class of orbitals known as solid-harmonic Gaussian-type orbitals are frequently used. A primitive solid-harmonic GTO may be written

$$\chi_{lm}(r, \varphi, \vartheta, a, \mathbf{A}) = N_{lm} Y_{lm}(\vartheta, \varphi)\, r^l \exp\left(-a r_A^2\right) \tag{4.9}$$

where N_{lm} is a normalisation constant, $Y_{lm}(\vartheta, \varphi)$ is the spherical harmonic for quantum numbers l and m, and $\mathbf{A}$ is the centre of the orbital. For technical reasons, integrals are usually not calculated directly in the spherical basis. Rather, they are calculated in a Cartesian basis and then transformed to the spherical basis. A Cartesian GTO may be written

$$G_{ijk}(\mathbf{r}, a, \mathbf{A}) = x_A^i y_A^j z_A^k \exp(-a r_A^2) \tag{4.10}$$

where $\mathbf{r}_a = (x - A_x, y - A_y, z - A_z)$. A solid-harmonic, χ_{lm}, is obtained by taking some linear combination of Cartesian Gaussians satisfying $i + j + k = l + 1$.

An important property of the Cartesian Gaussians is that they may be factorised in the three Cartesian directions

$$G_{ijk}(\mathbf{r}, a, \mathbf{A}) = G_i(x, a, A_x) G_j(y, a, A_y) G_k(z, a, A_z) \tag{4.11}$$

where, for instance, $G_i(x, a, A_x) = x_A^i \exp(-a x_A^2), x_A = x - A_x$.

Another important property of the Cartesian Gaussians, is that GTOs belonging to the same electron may be combined into an *overlap distribution*. This is obtained by applying the *Gaussian product rule*

$$\exp(-a\mathbf{r}_A^2) \exp(-b\mathbf{r}_B^2) = \exp(-qQ^2) \exp(-p r_P^2) \tag{4.12}$$

[1]Confer Ref. [1], for instance, for a review of Gaussian basis sets

where

$$p = a + b, \qquad p\mathbf{P} = a\mathbf{A} + b\mathbf{B} \tag{4.13}$$

$$q = \frac{ab}{a+b}, \qquad \mathbf{Q} = \mathbf{A} - \mathbf{B} \tag{4.14}$$

Here $\mathbf{P}$ is the centre of the overlap distribution and corresponds to the "centre of mass" of the two Gaussians. The factor $K_{AB} = \exp(-qQ_x^2)$, also known as the "prefactor", is the overlap amplitude. For two Gaussians that share a common centre, the overlap amplitude is one, and for Gaussians that are infinitely far apart, it is zero.

Applying the product rule on the x-component of $G_{ijk}(\mathbf{r}, a, \mathbf{A})G_{i'j'k'}(\mathbf{r}, b, \mathbf{B})$, for instance, we get

$$\begin{aligned} \Omega_{ii'}(x, a, b, A_x, B_x) &= G_i(x, a, A_x)G_{i'}(x, b, B_x) \\ &= x_A^i x_B^{i'} \exp(-qQ_x^2) \exp(-px_P^2) \end{aligned} \tag{4.15}$$

where $\Omega_{ii'}$ is the overlap distribution (OD) of Gaussians G_i and $G_{i'}$.

The overlap distribution given in (4.15) cannot be integrated directly because of the product $x_A^i x_B^{i'}$. We could rewrite this product as a polynomial in x_P using the binomial theorem, but this is not the most efficient way to proceed. Instead, we introduce the *Hermite Gaussian functions* Λ_t defined by

$$\Lambda_t(x, p, P_x) = \left(\frac{\partial}{\partial P_x}\right)^t \exp(-px_P^2) \tag{4.16}$$

The Hermite Gaussians differ from the overlap distribution given in (4.15) only in the polynomial factors which for Hermite Gaussians are generated by differentiation. Moreover, since the overlap distribution may be written as a polynomial of degree $i + i'$ in x_P, it may be expanded exactly in Hermite Gaussians of degree $t \leq i + i'$. We may therefore write

$$\Omega_{ii'} = \sum_{t=0}^{i+i'} E_t^{i,i'} \Lambda_t \tag{4.17}$$

The expansion coefficients $E_t^{i,i'}$ may be from the basic $E_0^{00} = K_{AB}$ using the recurrence relations

$$E_t^{i+1,i'} = \frac{1}{2p} E_{t-1}^{i,i'} - \frac{qQ_x}{a} E_t^{i,i'} + (t+1)E_{t+1}^{i,i'} \tag{4.18}$$

and

$$E_t^{i,i'+1} = \frac{1}{2p} E_{t-1}^{i,i'} - \frac{qQ_x}{b} E_t^{i,i'} + (t+1)E_{t+1}^{i,i'} \tag{4.19}$$

While the Λ_t in (4.18) is a function of P_x but not Q_x, we see from (4.18) and (4.19) that the opposite is true for the expansion coefficients.

The reason the Hermite Gaussians are so useful is the fact that they are defined by differentiation, and when we calculate molecular integrals, this leads to many simplifications. In three dimensions a Hermite Gaussian may be written

$$\Lambda_{tuv}(\mathbf{r}, p, \mathbf{P}) = \left(\frac{\partial}{\partial P_x}\right)^t \left(\frac{\partial}{\partial P_y}\right)^u \left(\frac{\partial}{\partial P_z}\right)^v \exp\left(-pr_P^2\right) \tag{4.20}$$

The operators for differentiation are used extensively below, and in order to get a more compact notation we shall write them as

$$\partial_P^t = \left(\frac{\partial}{\partial P_x}\right)^t \tag{4.21}$$

and, in the three dimensional case,

$$\partial_P^{tuv} = \left(\frac{\partial}{\partial P_x}\right)^t \left(\frac{\partial}{\partial P_y}\right)^u \left(\frac{\partial}{\partial P_z}\right)^v \tag{4.22}$$

In terms of the Hermite Gaussian given in (4.20), we may write an overlap distribution of two GTOs as

$$\begin{aligned} \Omega_{\mu\nu} &= \Omega_{ii'}\Omega_{jj'}\Omega_{kk'} \\ &= \sum_{t=0}^{i+i'} \sum_{u=0}^{j+j'} \sum_{v=0}^{k+k'} E_t^{i,i'} E_u^{j,j'} E_v^{k,k'} \Lambda_t \Lambda_u \Lambda_v \\ &= \sum_{tuv} E_{tuv}^{\mu\nu} \Lambda_{tuv} \end{aligned} \tag{4.23}$$

a relationship that is frequently encountered below.

4.3 Exploiting translational invariance

Since a molecular integral is a scalar, it cannot depend on the orientation of the molecule or where it is centred. Thus, rotating the molecule or displacing it in space cannot change the magnitude of the corresponding integral. The integral is therefore said to be *rotational* and *translational invariant*.

Consider a molecular three-electron integral $I = I_{abcdef}$ having six orbitals centred at $\mathbf{A}, \mathbf{B}, \mathbf{C}, \mathbf{D}, \mathbf{E}$, and $\mathbf{F}$. Moving the molecule by a small amount δ_x in the x-direction cannot change the integral, so that

$$\delta_x I = \left(\frac{\partial I}{\partial A_x} + \frac{\partial I}{\partial B_x} + \frac{\partial I}{\partial C_x} + \frac{\partial I}{\partial D_x} + \frac{\partial I}{\partial E_x} + \frac{\partial I}{\partial F_x}\right) \delta x = 0 \tag{4.24}$$

due to the translational invariance requirement. Of course, this requirement is independent of the size of the displacement, giving

$$\frac{\partial I}{\partial A_x} + \frac{\partial I}{\partial B_x} + \frac{\partial I}{\partial C_x} + \frac{\partial I}{\partial D_x} + \frac{\partial I}{\partial E_x} + \frac{\partial I}{\partial F_x} = 0 \tag{4.25}$$

Similar relationships holds for the other Cartesian directions.

As discussed in the previous section, an overlap distributions Ω_{ab} is expanded in Hermite Gaussians. An molecular integral over Cartesian GTOs is therefore expressed as a linear combination of integrals over Hermite Gaussians. These *Hermite integrals* are functions of the three centres $\mathbf{P}$, $\mathbf{P}'$, and $\mathbf{P}''$, rather than the six orbital centres. Using the definition of $\mathbf{P}$ given in (4.13), we define $\mathbf{P}'$ and $\mathbf{P}''$ to be constellations of centres $(\mathbf{C}, \mathbf{D})$ and $(\mathbf{E}, \mathbf{F})$, respectively. From the translational invariance of integrals over Cartesian GTOs, we deduce that integrals over Hermite Gaussians must also be translational invariant. If we denote a Hermite integral V, this gives

$$\frac{\partial V}{\partial P_x} + \frac{\partial V}{\partial P'_x} + \frac{\partial V}{\partial P''_x} = 0 \tag{4.26}$$

which has the important consequence that partial derivatives with respect to, say, P''_x may be replaced by partial derivatives with respect to P_x and P'_x

$$\frac{\partial}{\partial P''_x} = -\left(\frac{\partial}{\partial P_x} + \frac{\partial}{\partial P'_x}\right) \tag{4.27}$$

If more than one partial derivative with respect to P''_x is present, we invoke the binomial theorem and get

$$\left(\frac{\partial}{\partial P''_x}\right)^{t''} = (-1)^{t''} \sum_{\overline{x}''} \binom{t''}{\overline{x}''} \left(\frac{\partial}{\partial P_x}\right)^{\overline{x}''} \left(\frac{\partial}{\partial P'_x}\right)^{t''-\overline{x}''} \tag{4.28}$$

where $\binom{t''}{\overline{x}''}$ is a binomial coefficient. Similar relationships hold for the y- and z-directions.

Using the definition (4.20) of a Hermite Gaussian, we write a general three-electron Hermite integral as

$$\begin{aligned} &V_{tuv;t'u'v';t''u''v''} \\ &\quad = \iiint \mathcal{O}(r_1, r_2, r_3) \Lambda_{tuv}(\mathbf{r}_1, p, \mathbf{P}) \Lambda_{t'u'v'}(\mathbf{r}_2, p', \mathbf{P}') \Lambda_{t''u''v''}(\mathbf{r}_3, p'', \mathbf{P}'') \mathrm{d}r_1 \mathrm{d}r_2 \mathrm{d}r_3 \\ &\quad = \partial_P^{tuv} \partial_{P'}^{t'u'v'} \partial_{P''}^{t''u''v''} V_{000;000;000} \end{aligned} \tag{4.29}$$

where $V_{000;000;000}$ is the basic spherical integral

$$\begin{aligned} &V_{000;000;000} \\ &\quad = \iiint \mathcal{O}(r_1, r_2, r_3) \exp(-p r_P^2) \exp(-p' r_{P'}^2) \exp(-p'' r_{P''}^2) \mathrm{d}r_1 \mathrm{d}r_2 \mathrm{d}r_3 \end{aligned} \tag{4.30}$$

and $\mathcal{O}(r_1, r_2, r_3)$ is some one-, two-, or three-electron operator, or the unit operator.

Using relationships like (4.28), we may express the Hermite integral in (4.29) as

$$V_{tuv;t'u'v';t''u''v''} = \sum_{\overline{x}''=0}^{t''} \sum_{\overline{y}''=0}^{u''} \sum_{\overline{z}''=0}^{v''} \binom{t''}{\overline{x}''} \binom{u''}{\overline{y}''} \binom{v''}{\overline{z}''} V_{t+\overline{x}'',u+\overline{y}'',v+\overline{z}'';t'+t''-\overline{x}'',u'+u''-\overline{y}'',v'+v''-\overline{z}'';000} \tag{4.31}$$

Although it is possible to calculate Hermite integrals using (4.31), it is much more efficient to gradually build them up using the simpler relations

$$\begin{aligned} V_{tuv;t'u'v';(t''+1)u''v''} &= -(V_{(t+1)uv;t'u'v';t''u''v''} + V_{tuv;(t'+1)u'v';t''u''v''}) \\ V_{tuv;t'u'v';t''(u''+1)v''} &= -(V_{t(u+1)v;t'u'v';t''u''v''} + V_{tuv;t'(u'+1)v';t''u''v''}) \\ V_{tuv;t'u'v';t''u''(v''+1)} &= -(V_{tu(v+1);t'u'v';t''u''v''} + V_{tuv;t'u'(v'+1);t''u''v''}) \end{aligned} \tag{4.32}$$

which is based directly on (4.27). Before the recurrence relations (4.32) may be applied, however, all Hermite integrals $V_{\overline{x}\,\overline{y}\,\overline{z};\overline{x}'\overline{y}'\overline{z}';000}$ satisfying

$$\begin{aligned} &\overline{x} \le t + t'', \qquad &&\overline{x}' \le t' + t'', \qquad &&\overline{x} + \overline{x}' \le t + t' + t'' \\ &\overline{y} \le u + u'', \qquad &&\overline{y}' \le u' + u'', \qquad &&\overline{y} + \overline{y}' \le u + u' + u'' \\ &\overline{z} \le v + v'', \qquad &&\overline{z}' \le v' + v'', \qquad &&\overline{z} + \overline{z}' \le v + v' + v'' \end{aligned} \tag{4.33}$$

must be calculated. A favourable aspect with recurrence relations like that in (4.32) is that as we recur forward to get some Hermite integral $V_{tuv;t'u'v';t''u''v''}$, we usually generate other Hermite integrals that are also needed.

From the above equation, one might get the impression that it is always the Hermite Gaussian corresponding to electron 3 that is generated by recurrence, but this is not the case. Rather we generate by recurrence the Hermite Gaussian having the lowest angular momentum.

4.4 The integrals: An overview

Having discussed basis sets and MO transformations, we now work out explicit formulas for the AO integrals needed in GTG-MP2 theory. The formulas developed in the sections below are similar to those developed by Persson and Taylor [46], but are discussed in some more detail.

In order to calculate the second-order energy using the GTG-MP2 theory, we have to calculate a total of 15 different integrals, If we collect these integrals in groups of exchange integrals, Coulomb integrals, nuclear attraction integrals, kinetic

energy integrals, and overlap integrals, we may write

$$\text{Exchange}: \begin{cases} \mathsf{INT3E2}: \langle g_{\mu\nu,v}| \, K_2 \, |g_{\sigma\tau,w}\rangle \\ \mathsf{INT3E1}: \langle g_{\mu\nu,v}| \, K_2 \, |\chi_{\sigma\tau}\rangle \\ \mathsf{INT3P1}: \langle g_{\mu\nu,v}| \, P_2 r_{12}^{-1} \, |\chi_{\sigma\tau}\rangle \end{cases}$$

$$\text{Coulomb}: \begin{cases} \mathsf{INT3C1}: \langle g_{\mu\nu,v}| \, J_2 \, |\chi_{\sigma\tau}\rangle \\ \mathsf{INT3C2}: \langle g_{\mu\nu,v}| \, J_2 \, |g_{\sigma\tau,w}\rangle \\ \mathsf{INT2C0}: \langle \chi_{\mu\nu}| \, r_{12}^{-1} \, |\chi_{\sigma\tau}\rangle \\ \mathsf{INT2C1}: \langle g_{\mu\nu,v}| \, r_{12}^{-1} \, |\chi_{\sigma\tau}\rangle \\ \mathsf{INT4C1}: \langle g_{\mu\nu,v}| \, P_1 P_2 r_{12}^{-1} \, |\chi_{\sigma\tau}\rangle \end{cases}$$

$$\text{Nuclear attraction}: \begin{cases} \mathsf{INT2V1}: \langle g_{\mu\nu,v}| \, V_{2C} \, |\chi_{\sigma\tau}\rangle \\ \mathsf{INT2V2}: \langle g_{\mu\nu,v}| \, V_{2C} \, |g_{\sigma\tau,w}\rangle \end{cases}$$

$$\text{Kinetic energy}: \begin{cases} \mathsf{INT2K1}: \langle g_{\mu\nu,v}| \, \nabla_1^2 \, |\chi_{\sigma\tau}\rangle \text{ and } -\langle \nabla_1 g_{\mu\nu,v}|\nabla_1 \chi_{\sigma\tau}\rangle \\ \mathsf{INT2K2}: \langle g_{\mu\nu,v}| \, \nabla_1^2 \, |g_{\sigma\tau,w}\rangle \text{ and } -\langle \nabla_1 g_{\mu\nu,v}|\nabla_1 g_{\sigma\tau,w}\rangle \end{cases}$$

$$\text{Overlap}: \begin{cases} \mathsf{INT21}: \langle g_{\mu\nu,v}|\chi_{\sigma\tau}\rangle \\ \mathsf{INT22}: \langle g_{\mu\nu,v}|g_{\sigma\tau,w}\rangle \\ \mathsf{INT32}: \langle g_{\mu\nu,v}| \, P_2 \, |g_{\sigma\tau,w}\rangle \end{cases}$$

where we have associated a unique keyword with each AO integral. These keywords, which have the general form INTXYZ, are very useful whenever we shall refer to one of the integrals. Each keyword has the following logical structure: INT is short for integral, X specifies whether it is a two- or three-electron integral (there are no one-electron integrals involved), Y is a letter specifying the operator involved (if any), and Z gives the number of geminal involved. The number of geminals may be 2 (geminals in both the bra and the ket), 1 or 0. Note that, the integral INT4C1 is not a true four-electron integral, but a sum of products of two-electron integrals.

4.5 Exchange integrals

We start studying the exchange integrals which are all of three-electron type. Moreover, we shall study the most complicated three-electron integral first, the *cyclic three-electron integral*. Even though the formulas for this integral are the most com-

prehensive, they provide a convenient starting point, as many of the them are needed in the construction of other integrals.

4.5.1 INT3E2: $\langle g_{\mu\nu,v}| K_2 |g_{\sigma\tau,w}\rangle$

The cyclic three-electron integrals is an exchange integral between two geminals. It may be expressed in terms of Hermite integrals as

$$\begin{aligned}
&\left\langle \exp(-\gamma_v r_{12}^2)\tilde{\chi}_{\mu\nu}\right| K_2 \left|\exp(-\gamma_w r_{12}^2)\tilde{\chi}_{\sigma\tau}\right\rangle \\
&\quad = \iiint \exp(-\gamma_v r_{12}^2)\tilde{\chi}_{\mu\nu} \left(\sum_k \phi_k(3) r_{23}^{-1} P_{23}\phi_k(3)\right) \exp(-\gamma_w r_{12}^2)\tilde{\chi}_{\sigma\tau} \mathrm{d}r_1\mathrm{d}r_2\mathrm{d}r_3 \\
&\quad = \sum_{\eta\xi} D_{\eta\xi} \iiint \Omega_{\tilde{\mu}\tilde{\sigma}}(1)\,\Omega_{\tilde{\nu}\xi}(2)\,\Omega_{\tilde{\tau}\eta}(3)\, r_{23}^{-1} \exp(-\gamma_v r_{12}^2) \exp(-\gamma_w r_{13}^2)\mathrm{d}r_1\mathrm{d}r_2\mathrm{d}r_3 \\
&\quad = \sum_{tuv} E_{tuv}^{\tilde{\mu}\tilde{\sigma}} \sum_{\eta\xi} D_{\eta\xi} \left(\sum_{t'u'v'} E_{t'u'v'}^{\tilde{\nu}\xi} \sum_{t''u''v''} E_{t''u''v''}^{\tilde{\tau}\eta} V_{tuv;t'u'v';t''u''v''}\right)
\end{aligned} \tag{4.34}$$

In the last equality of (4.34), density matrix elements are multiplied with integrals that have only been half-transformed from Hermite Gaussians to spherical (or Cartesian) GTOs. In practice, however, we transform the integrals completely to GTO basis before we multiply them with density matrix elements. This generates simpler code and the loss of performance is marginal.

Hermite integrals

To work out formulas for the Hermite integrals in (4.34), we first express them in terms of an undifferentiated Hermite integral

$$\begin{aligned}
&V_{tuv;t'u'v';t''u''v''} \\
&\quad = \iiint \Lambda_{tuv}(\mathbf{r}_1, p, \mathbf{P})\Lambda_{t'u'v'}(\mathbf{r}_2, p', \mathbf{P}')\Lambda_{t''u''v''}(\mathbf{r}_3, p'', \mathbf{P}'') \\
&\qquad\qquad \times r_{23}^{-1} \exp(-\gamma_v r_{12}^2) \exp(-\gamma_w r_{13}^2)\mathrm{d}r_1\mathrm{d}r_2\mathrm{d}r_3 \\
&\quad = \partial_P^{tuv}\partial_{P'}^{t'u'v'}\partial_{P''}^{t''u''v''} \iiint \exp(-p r_{1P}^2) \exp(-p' r_{2P'}^2) \exp(-p'' r_{3P''}^2) \\
&\qquad\qquad\qquad\qquad \times r_{23}^{-1} \exp(-\gamma_v r_{12}^2) \exp(-\gamma_w r_{13}^2)\mathrm{d}r_1\mathrm{d}r_2\mathrm{d}r_3 \\
&\quad = \partial_P^{tuv}\partial_{P'}^{t'u'v'}\partial_{P''}^{t''u''v''} V_{000;000;000}
\end{aligned} \tag{4.35}$$

where we have used the compact notation ∂_P^{tuv} for partial derivatives. Undifferentiated Hermite integrals are often referred to as *spherical Hermite integrals*. In (4.35),

$V_{000;000;000}$ is a spherical Hermite integral. It may be evaluated as

$$\begin{aligned}
&V_{000;000;000} \\
&\quad = \left(\frac{\pi}{p+\gamma_v+\gamma_w}\right)^{\frac{3}{2}} \iint \exp(-q' r_{2P}^2)\exp(-p' r_{2P'}^2)\exp(-q'' r_{3P}^2) \\
&\qquad\qquad \times \exp(-p'' r_{3P''}^2)\exp(-q r_{23}^2) r_{23}^{-1} \mathrm{d}r_2 \mathrm{d}r_3 \\
&\quad = \left(\frac{\pi}{p+\gamma_v+\gamma_w}\right)^{\frac{3}{2}} K_{PP'} K_{PP''} \iint \exp(-s r_{2S}^2)\exp(-s' r_{3S'}^2) \\
&\qquad\qquad \times \exp(-q r_{23}^2) r_{23}^{-1} \mathrm{d}r_2 \mathrm{d}r_3 \\
&\quad = \left(\frac{\pi}{p+\gamma_v+\gamma_w}\right)^{\frac{3}{2}} K_{PP'} K_{PP''} \frac{2\pi^{\frac{5}{2}}}{(u+q)(s+s')^{\frac{3}{2}}} K_{SS'} F_0
\end{aligned} \tag{4.36}$$

where we have used the relations

$$\begin{aligned}
q &= \gamma_v\gamma_w \left(p+\gamma_v+\gamma_w\right)^{-1} \\
q' &= p\gamma_v \left(p+\gamma_v+\gamma_w\right)^{-1} \\
q'' &= p\gamma_w \left(p+\gamma_v+\gamma_w\right)^{-1} \\
s &= q'+p' \\
s' &= q''+p'' \\
s\mathbf{S} &= q'\mathbf{P}+p'\mathbf{P'} \\
s'\mathbf{S'} &= q''\mathbf{P}+p''\mathbf{P''} \\
u &= ss' \left(s+s'\right)^{-1}
\end{aligned} \tag{4.37}$$

and

$$\begin{aligned}
K_{PP'} &= \exp(-\beta_1 R_{PP'}^2) = \exp\left(-\frac{q'p'}{q'+p'} R_{PP'}^2\right) \\
K_{PP''} &= \exp(-\beta_2 R_{PP''}^2) = \exp\left(-\frac{q''p''}{q''+p''} R_{PP''}^2\right) \\
K_{SS'} &= \exp(-\beta_3 R_{SS'}^2) = \exp\left(-\frac{uq}{u+q} R_{SS'}^2\right) \\
F_0 &= F_0\left(\alpha R_{SS'}^2\right) = F_0\left(\frac{u^2}{u+q} R_{SS'}^2\right)
\end{aligned} \tag{4.38}$$

The function F_0 is in the literature both referred to as a zeroth order *incomplete gamma function* and as the zeroth order *Boys function*. It is defined as

$$F_n(x) = \int_0^1 \exp(-xt^2) t^{2n} \mathrm{d}t \tag{4.39}$$

The properties of the Boys functions have been exhaustively discussed elsewhere [1] and shall not be pursued here. We note, however, that through (4.36) we have managed to reduce an originally nine dimensional integral to a one dimensional integral that may be evaluated by a functional approximation or a numerical integration.

Using the results of (4.36), we may express the Hermite integral in (4.35) as

$$\begin{aligned} V_{tuv;t'u'v';t''u''v''} = & \frac{2\pi^4}{(p+\gamma_v+\gamma_w)^{\frac{3}{2}}(u+q)(s+s')^{\frac{3}{2}}} \\ & \times \partial_P^{tuv}\partial_{P'}^{t'u'v'}\partial_{P''}^{t''u''v''}\left(K_{PP'}K_{PP''}K_{SS'}F_0\right) \end{aligned} \tag{4.40}$$

Let $f = K_{PP'}K_{PP''}K_{SS'}$ and $g = F_0$. By invoking the binomial formula

$$D^n\left(f\cdot g\right) = \sum_{k=0}^{n}\binom{n}{k} f^{(n-k)}g^{(k)} \tag{4.41}$$

for each of the differential operators in (4.40), we arrive at the following expression

$$\begin{aligned} & \partial_P^{tuv}\partial_{P'}^{t'u'v'}\partial_{P''}^{t''u''v''}\left(K_{PP'}K_{PP''}K_{SS'}\right)F_0 \\ & = \sum_{\overline{x}=0}^{t}\sum_{\overline{y}=0}^{u}\sum_{\overline{z}=0}^{v}\sum_{\overline{x}'=0}^{t'}\sum_{\overline{y}'=0}^{u'}\sum_{\overline{z}'=0}^{v'}\sum_{\overline{x}''=0}^{t''}\sum_{\overline{y}''=0}^{u''}\sum_{\overline{z}''=0}^{v''} \\ & \qquad \binom{t}{\overline{x}}\binom{u}{\overline{y}}\binom{v}{\overline{z}}\binom{t'}{\overline{x}'}\binom{u'}{\overline{y}'}\binom{v'}{\overline{z}'}\binom{t''}{\overline{x}''}\binom{u''}{\overline{y}''}\binom{v''}{\overline{z}''} \\ & \qquad \times\left(\partial_P^{t-\overline{x},u-\overline{y},v-\overline{z}}\partial_{P'}^{t'-\overline{x}',u'-\overline{y}',v'-\overline{z}'}\partial_{P''}^{t''-\overline{x}'',u''-\overline{y}'',v''-\overline{z}''}K_{PP'}K_{PP''}K_{SS'}\right) \\ & \qquad \times\left(\partial_P^{\overline{xyz}}\partial_{P'}^{\overline{x}'\overline{y}'\overline{z}'}\partial_{P''}^{\overline{x}''\overline{y}''\overline{z}''}F_0\right) \end{aligned} \tag{4.42}$$

Note that, these loops are connected in triples and the sum $t+u+v$, for instance, must be equal to or less than the total angular momentum of the overlap distribution $\Omega_{\tilde{\mu}\tilde{\sigma}}$ present in (4.34). Similar relationships applies for the primed and doubly primed summation indices.

The differentiated Boys functions may be obtained from a set of recurrence relations similar to the usual McMurchie–Davidson ones. For the derivatives of the product $K_{PP'}K_{PP''}K_{SS'}$, which we shall refer to as KKK functions, a recurrence scheme that exploits separability into Cartesian directions has been developed by Persson and Taylor [46].

In both the McMurchie–Davidson and the Persson–Taylor recurrence schemes, the derivatives of $\mathbf{R}_{SS'} = (X_{SS'}, Y_{SS'}, Z_{SS'})$ with respect to unprimed, primed and doubly primed centres are frequently encountered. For the $X_{SS'}$ component, these

derivatives are

$$\begin{aligned} r_1 &= \frac{\partial X_{SS'}}{\partial P_x} = \frac{q's' - q''s}{ss'} \\ r_2 &= \frac{\partial X_{SS'}}{\partial P'_x} = \frac{p'}{s} \\ r_3 &= \frac{\partial X_{SS'}}{\partial P''_x} = -\frac{p''}{s'} \end{aligned} \tag{4.43}$$

and the derivatives of the $Y_{SS'}$ and $Z_{SS'}$ components are identical.

KKK functions

To find recurrence relations for derivatives of the product $K_{PP'}K_{PP''}K_{SS'}$, it is convenient to introduce a new set of functions. For the x-component, these are

$$\begin{aligned} K^i_{PP'} &= X^i_{PP'} \exp(-\beta_1 X^2_{PP'}) \\ K^j_{PP''} &= X^j_{PP''} \exp(-\beta_2 X^2_{PP''}) \\ K^k_{SS'} &= X^k_{SS'} \exp(-\beta_3 X^2_{SS'}) \end{aligned} \tag{4.44}$$

where the exponents β_1, β_2 and β_3 are defined in (4.38). The functions defined in (4.44) have counterparts for the y- and z-directions that are similarly defined.

Differentiating the product $K^i_{PP'}K^j_{PP''}K^k_{SS'}$ with respect to each of the centres P_x, P'_x and P''_x, we get

$$\begin{aligned} \partial^{q+1}_{P_x} K^i_{PP'}K^j_{PP''}K^k_{SS'} &= \partial^q_{P_x}\left(iK^{i-1}_{PP'} - 2\beta_1 K^{i+1}_{PP'}\right) K^j_{PP''}K^k_{SS'} \\ &\quad + \partial^q_{P_x}\left(jK^{j-1}_{PP''} - 2\beta_2 K^{j+1}_{PP''}\right) K^i_{PP'}K^k_{SS'} \\ &\quad + \partial^q_{P_x}\left(r_1 kK^{k-1}_{SS'} - 2\beta_3 r_1 K^{k+1}_{SS'}\right) K^i_{PP'}K^j_{PP''} \\ \\ \partial^{r+1}_{P'_x} K^i_{PP'}K^j_{PP''}K^k_{SS'} &= \partial^r_{P'_x}\left(-iK^{i-1}_{PP'} + 2\beta_1 K^{i+1}_{PP'}\right) K^j_{PP''}K^k_{SS'} \\ &\quad + \partial^r_{P'_x}\left(r_2 kK^{k-1}_{SS'} - 2\beta_3 r_2 K^{k+1}_{SS'}\right) K^i_{PP'}K^j_{PP''} \\ \\ \partial^{s+1}_{P''_x} K^i_{PP'}K^j_{PP''}K^k_{SS'} &= \partial^s_{P''_x}\left(-jK^{j-1}_{PP''} + 2\beta_2 K^{j+1}_{PP'}\right) \\ &\quad + \partial^s_{P''_x}\left(r_3 kK^{k-1}_{SS'} - 2\beta_3 r_3 K^{k+1}_{SS'}\right) K^i_{PP'}K^j_{PP''} \end{aligned} \tag{4.45}$$

Generally, the differentiation operators in (4.45) appear in combination. Consider, therefore, some functions $\mathcal{S}^{qrs}_{ijk}$ given by $\mathcal{S}^{qrs}_{ijk} = \partial^q_{P_x}\partial^r_{P'_x}\partial^s_{P''_x}K^i_{PP'}K^j_{PP''}K^k_{SS'}$. To be able to construct the Hermite integrals of (4.42) we only need the subset $\mathcal{S}^{qrs} \equiv \mathcal{S}^{qrs}_{000}$ of these functions. According to (4.45), this subset may be obtained by taking a linear combination of another subset $\mathcal{S}_{ijk} \equiv \mathcal{S}^{000}_{ijk}$. To see this more clearly, let $\theta_1 = -2\beta_1$,

$\theta_2 = -2\beta_2$ and $\theta_3 = -2\beta_3$. Using these definitions, we may turn (4.45) into the following recurrence relations

$$\begin{aligned}
\mathcal{S}_{ijk}^{(q+1)rs} = \quad & i\mathcal{S}_{(i-1)jk}^{qrs} + \theta_1\mathcal{S}_{(i+1)jk}^{qrs} + j\mathcal{S}_{i(j-1)k}^{qrs} + \theta_2\mathcal{S}_{i(j+1)k}^{qrs} + r_1 k\mathcal{S}_{ij(k-1)}^{qrs} + r_1\theta_3\mathcal{S}_{ij(k+1)}^{qrs} \\
\mathcal{S}_{ijk}^{q(r+1)s} = & -i\mathcal{S}_{(i-1)jk}^{qrs} - \theta_1\mathcal{S}_{(i+1)jk}^{qrs} + r_2 k\mathcal{S}_{ij(k-1)}^{qrs} + r_2\theta_3\mathcal{S}_{ij(k+1)}^{qrs} \\
\mathcal{S}_{ijk}^{qr(s+1)} = & -j\mathcal{S}_{i(j-1)k}^{qrs} - \theta_2\mathcal{S}_{i(j+1)k}^{qrs} + r_3 k\mathcal{S}_{ij(k-1)}^{qrs} + r_3\theta_3\mathcal{S}_{ij(k+1)}^{qrs}
\end{aligned} \tag{4.46}$$

These relations may be used to evaluate $\mathcal{S}^{qrs}$, once all functions $\mathcal{S}_{ijk}$ for which

$$i \le q + r, \qquad j \le q + s, \qquad k \le q + r + s, \qquad i + j + k \le q + r + s \tag{4.47}$$

have been evaluated. The recurrence relations (4.46) are then used to build up all singly differentiated functions, that is, $\mathcal{S}_{ijk}^{100}$, $\mathcal{S}_{ijk}^{010}$ and $\mathcal{S}_{ijk}^{001}$, which in turn are used to construct the doubly differentiated functions and so on.

Boys functions

The recurrence relations for the Boys functions may be simplified by establishing relationships between the different derivatives of F_n. Differentiating the nth order Boys function with respect to P_x, P'_x and P''_x, we get

$$\begin{aligned}
\frac{\partial F_n}{\partial P_x} &= -2\alpha X_{SS'} r_1 F_{n+1} \\
\frac{\partial F_n}{\partial P'_x} &= -2\alpha X_{SS'} r_2 F_{n+1} \\
\frac{\partial F_n}{\partial P''_x} &= -2\alpha X_{SS'} r_3 F_{n+1}
\end{aligned} \tag{4.48}$$

where we have used the results from (4.43). The derivatives for the y- and z-directions are similar and are not given.

The relations (4.48) imply that we only have to differentiate the Boys function with respect to one of the centres, for instance the unprimed, as the derivatives for the other directions may be expressed in terms of this

$$\begin{aligned}
\partial_{P'}^{t'u'v'} F_n &= \left(\frac{r_2}{r_1}\right)^{t'+u'+v'} \partial_P^{t'u'v'} F_n \\
\partial_{P''}^{t''u''v''} F_n &= \left(\frac{r_3}{r_1}\right)^{t''+u''+v''} \partial_P^{t''u''v''} F_n
\end{aligned} \tag{4.49}$$

By means of the functions $\mathcal{R}_{tuv}^n$ defined as

$$\mathcal{R}_{tuv}^n = (-2\alpha r_1)^n \, \partial_P^{tuv} F_n \tag{4.50}$$

we may generate by recurrence the differentiated Boys functions $\mathcal{R}_{tuv} \equiv \mathcal{R}^0_{tuv}$ needed for (4.42). These functions may be constructed from a subset $\mathcal{R}^n \equiv \mathcal{R}^n_{000}$ using the McMurchie–Davidson-type recurrence relations

$$\begin{aligned}
\mathcal{R}^n_{(t+1)uv} &= r_1 t \mathcal{R}^{n+1}_{(t-1)uv} + X_{SS'} \mathcal{R}^{n+1}_{tuv} \\
\mathcal{R}^n_{t(u+1)v} &= r_1 u \mathcal{R}^{n+1}_{t(u-1)v} + Y_{SS'} \mathcal{R}^{n+1}_{tuv} \\
\mathcal{R}^n_{tu(v+1)} &= r_1 v \mathcal{R}^{n+1}_{tu(v-1)} + Z_{SS'} \mathcal{R}^{n+1}_{tuv}
\end{aligned} \tag{4.51}$$

allowing us, finally, to write the Hermite integral in (4.40) as

$$\begin{aligned}
V_{tuv;t'u'v';t''u''v''} = {} & \frac{2\pi^4}{(p+\gamma_v+\gamma_w)^{\frac{3}{2}}(u+q)(s+s')^{\frac{3}{2}}} \\
& \times \sum_{\overline{x}=0}^{t} \sum_{\overline{x}'=0}^{t'} \sum_{\overline{x}''=0}^{t''} \binom{t}{\overline{x}} \binom{t'}{\overline{x}'} \binom{t''}{\overline{x}''} \left(\frac{r_2}{r_1}\right)^{\overline{x}'} \left(\frac{r_3}{r_1}\right)^{\overline{x}''} \mathcal{S}^{t-\overline{x},t'-\overline{x}',t''-\overline{x}''} \\
& \quad \sum_{\overline{y}=0}^{u} \sum_{\overline{y}'=0}^{u'} \sum_{\overline{y}''=0}^{u''} \binom{u}{\overline{y}} \binom{u'}{\overline{y}'} \binom{u''}{\overline{y}''} \left(\frac{r_2}{r_1}\right)^{\overline{y}'} \left(\frac{r_3}{r_1}\right)^{\overline{y}''} \mathcal{T}^{u-\overline{y},u'-\overline{y}',u''-\overline{y}''} \\
& \quad\quad \sum_{\overline{z}=0}^{v} \sum_{\overline{z}'=0}^{v'} \sum_{\overline{z}''=0}^{v''} \binom{v}{\overline{z}} \binom{v'}{\overline{z}'} \binom{v''}{\overline{z}''} \left(\frac{r_2}{r_1}\right)^{\overline{z}'} \left(\frac{r_3}{r_1}\right)^{\overline{z}''} \mathcal{U}^{v-\overline{z},v'-\overline{z}',v''-\overline{z}''} \\
& \quad\quad\quad \times \mathcal{R}_{\overline{x}+\overline{x}'+\overline{x}'',\overline{y}+\overline{y}'+\overline{y}'',\overline{z}+\overline{z}'+\overline{z}''}
\end{aligned} \tag{4.52}$$

where $\mathcal{T}^{qrs}$ and $\mathcal{U}^{qrs}$ are equivalents of $\mathcal{S}^{qrs}$ for the y- and z-directions, respectively.

Equation (4.52) may be reduced further if we make use of the translational invariance discussed in section 4.3, but this is not pursued here.

4.5.2 INT3E1: $\langle g_{\mu\nu,v}| \, K_2 \, |\chi_{\sigma\tau}\rangle$

The second exchange integral we need is the one between a geminal and an orbital product. This integral is given by

$$\begin{aligned}
& \left\langle \exp(-\gamma_v r_{12}^2)\tilde{\chi}_{\mu\nu} \right| K_2 \left| \chi_{\sigma\tau} \right\rangle \\
& \quad = \iiint \exp(-\gamma_v r_{12}^2)\tilde{\chi}_{\mu\nu} \left(\sum_k \phi_k(3) r_{23}^{-1} P_{23} \phi_k(3) \right) \chi_{\sigma\tau} \mathrm{d}r_1 \mathrm{d}r_2 \mathrm{d}r_3 \\
& \quad = \sum_{\eta\xi} D_{\eta\xi} \iiint \Omega_{\tilde{\mu}\sigma}(1) \, \Omega_{\tilde{\nu}\xi}(2) \, \Omega_{\tau\eta}(3) \, r_{23}^{-1} \exp(-\gamma_v r_{12}^2) \mathrm{d}r_1 \mathrm{d}r_2 \mathrm{d}r_3 \\
& \quad = \sum_{tuv} E^{\tilde{\mu}\sigma}_{tuv} \sum_{\eta\xi} D_{\eta\xi} \left(\sum_{t'u'v'} E^{\tilde{\nu}\xi}_{t'u'v'} \sum_{t''u''v''} E^{\tau\eta}_{t''u''v''} V_{tuv;t'u'v';t''u''v''} \right)
\end{aligned} \tag{4.53}$$

If geminals and virtual orbitals are expanded in the same AO basis, we may use the expression for the cyclic three-electron integral (4.34) to evaluate it by setting $\gamma_w = 0$. This gives us an invaluable opportunity to check both integrals.

Hermite integrals

As with the cyclic three-electron integrals, the Hermite integral of (4.53) may be expressed in terms of a spherical Hermite integral

$$\begin{aligned}
&V_{tuv;t'u'v';t''u''v''} \\
&\quad = \iiint \Lambda_{tuv}(\mathbf{r}_1, p, \mathbf{P})\Lambda_{t'u'v'}(\mathbf{r}_2, p', \mathbf{P}')\Lambda_{t''u''v''}(\mathbf{r}_3, p'', \mathbf{P}'') \\
&\qquad\qquad \times r_{23}^{-1}\exp(-\gamma_v r_{12}^2)\mathrm{d}r_1\mathrm{d}r_2\mathrm{d}r_3 \\
&\quad = \partial_P^{tuv}\partial_{P'}^{t'u'v'}\partial_{P''}^{t''u''v''} \iiint \exp(-pr_{1P}^2)\exp(-p'r_{2P'}^2)\exp(-p''r_{3P''}^2) \\
&\qquad\qquad\qquad\qquad \times r_{23}^{-1}\exp(-\gamma_v r_{12}^2)\mathrm{d}r_1\mathrm{d}r_2\mathrm{d}r_3 \\
&\quad = \partial_P^{tuv}\partial_{P'}^{t'u'v'}\partial_{P''}^{t''u''v''} V_{000;000;000}
\end{aligned} \tag{4.54}$$

The spherical Hermite integral is evaluated as

$$\begin{aligned}
&V_{000;000;000} \\
&\quad = \left(\frac{\pi}{p+\gamma_v}\right)^{\frac{3}{2}} \iint \exp(-qr_{2P}^2)\exp(-p'r_{2P'}^2)\exp(-p''r_{3P''}^2)r_{23}^{-1}\mathrm{d}r_2\mathrm{d}r_3 \\
&\quad = \left(\frac{\pi}{p+\gamma_v}\right)^{\frac{3}{2}} K_{PP'} \iint \exp(-sr_{2S}^2)\exp(-p''r_{3P''}^2)r_{23}^{-1}\mathrm{d}r_2\mathrm{d}r_3 \\
&\quad = \left(\frac{\pi}{p+\gamma_v}\right)^{\frac{3}{2}} K_{PP'}\frac{2\pi^{\frac{5}{2}}}{sp''\sqrt{s+p''}}F_0
\end{aligned} \tag{4.55}$$

where we have used the relations

$$\begin{aligned}
q &= \frac{p\gamma_v}{p+\gamma_v} \\
s &= q + p' \\
s\mathbf{S} &= q\mathbf{P} + p'\mathbf{P}'
\end{aligned} \tag{4.56}$$

and

$$\begin{aligned}
K_{PP'} &= \exp(-\beta R_{PP'}^2) = \exp\left(-\frac{qp'}{q+p'}R_{PP'}^2\right) \\
F_0 &= F_0(\alpha R_{SP''}^2) = F_0\left(\frac{sp''}{s+p''}R_{SP''}^2\right)
\end{aligned} \tag{4.57}$$

The Hermite integral (4.54) may now be written

$$V_{tuv;t'u'v';t''u''v''} = \left(\frac{\pi}{p+\gamma_v}\right)^{\frac{3}{2}} \frac{2\pi^{\frac{5}{2}}}{sp''\sqrt{s+p''}}\partial_P^{tuv}\partial_{P'}^{t'u'v'}\left(K_{PP'}\left(\partial_{P''}^{t''u''v''}F_0\right)\right) \tag{4.58}$$

As with the cyclic three-electron integrals, the multiple derivatives are resolved by invoking the binomial formula (4.41). This gives

$$\begin{aligned}
&\partial_P^{tuv}\partial_{P'}^{t'u'v'}\left(K_{PP'}\left(\partial_{P''}^{t''u''v''}F_0\right)\right) \\
&\quad=\sum_{\overline{x}=0}^{t}\sum_{\overline{y}=0}^{u}\sum_{\overline{z}=0}^{v}\sum_{\overline{x}'=0}^{t'}\sum_{\overline{y}'=0}^{u'}\sum_{\overline{z}'=0}^{v'} \\
&\qquad\qquad\binom{t}{\overline{x}}\binom{u}{\overline{y}}\binom{v}{\overline{z}}\binom{t'}{\overline{x}'}\binom{u'}{\overline{y}'}\binom{v'}{\overline{z}'} \\
&\qquad\qquad\quad\times\left(\partial_P^{t-\overline{x},u-\overline{y},v-\overline{z}}\partial_{P'}^{t'-\overline{x}',u'-\overline{y}',v'-\overline{z}'}K_{PP'}\right) \\
&\qquad\qquad\quad\times\left(\partial_P^{\overline{xyz}}\partial_{P'}^{\overline{x}'\overline{y}'\overline{z}'}\partial_{P''}^{t''u''v''}F_0\right)
\end{aligned} \tag{4.59}$$

which may be compared to (4.42). Each of the two derivatives of (4.59) is evaluated by recurrence.

K functions

The differentiated $K_{PP'}$ functions (K functions) may be evaluated in much the same way as the more complicated KKK functions. However, due to the simple form of the K functions we may use the relationship

$$\frac{\partial K_{PP'}}{\partial P'_x}=-\frac{\partial K_{PP'}}{\partial P_x} \tag{4.60}$$

to replace all derivatives with respect to primed centres by derivatives with respect to unprimed centres

$$\partial_{P'_x}^{t'}K_{PP'}=(-1)^{t'}\partial_{P_x}^{t'}K_{PP'} \tag{4.61}$$

Derivatives with respect to unprimed centres may be recurred from functions

$$K_{PP'}^{i}=X_{PP'}^{i}\exp(-\beta X_{PP'}^{2}) \tag{4.62}$$

through the recurrence relation

$$\mathcal{S}_i^{q+1}=i\mathcal{S}_{i-1}^{q}-2\beta\mathcal{S}_{i+1}^{q} \tag{4.63}$$

where $\mathcal{S}_i^q=\partial_{P_x}^q K_{PP'}^i$. Using this relation, we may generate the K functions $\mathcal{S}^q\equiv\mathcal{S}_0^q$ from the functions $\mathcal{S}_i\equiv\mathcal{S}_i^0$ which are easily evaluated.

Keeping this in mind, we switch to the notation $\mathcal{S}_i^{q,r}=(-1)^r\mathcal{S}_i^{q+r}$ in all formulas below, as this makes most of them appear in a simpler form.

Boys functions

For the recurrence relations of the Boys functions, we need the derivatives of $\mathbf{R}_{SP''} = (X_{SP''}, Y_{SP''}, Z_{SP''})$ with respect to the unprimed, primed and doubly primed centres. Again, the derivative is independent of the Cartesian direction, and if we choose the x-direction, out of habit, we get

$$\begin{aligned} r_1 &= \frac{\partial X_{SP''}}{\partial P_x} = \frac{q}{s} \\ r_2 &= \frac{\partial X_{SP''}}{\partial P'_x} = \frac{p'}{s} \\ r_3 &= \frac{\partial X_{SP''}}{\partial P''_x} = -1 \end{aligned} \tag{4.64}$$

The Boys functions needed in (4.59) may be generated using the relations (4.49)–(4.51) developed for the cyclic three-electron integrals. We definitions of r_1, r_2 and r_3 must be altered, however, and we must also replace $X_{SS'}$ in (4.51) by $X_{SP''}$, and so forth. If we make these changes, we may write the Hermite integrals (4.58) in the final form

$$\begin{aligned} V_{tuv;t'u'v';t''u''v''} = &\left(\frac{\pi}{p+\gamma_v}\right)^{\frac{3}{2}} \frac{2\pi^{\frac{5}{2}}}{sp''\sqrt{s+p''}} \left(\frac{r_3}{r_1}\right)^{t''+u''+v''} \\ &\times \sum_{\overline{x}=0}^{t}\sum_{\overline{x}'=0}^{t'} \binom{t}{\overline{x}}\binom{t'}{\overline{x}'} \left(\frac{r_2}{r_1}\right)^{\overline{x}'} \mathcal{S}^{t-\overline{x},t'-\overline{x}'} \\ &\sum_{\overline{y}=0}^{u}\sum_{\overline{y}'=0}^{u'} \binom{u}{\overline{y}}\binom{u'}{\overline{y}'} \left(\frac{r_2}{r_1}\right)^{\overline{y}'} \mathcal{T}^{u-\overline{y},u'-\overline{y}'} \\ &\sum_{\overline{z}=0}^{v}\sum_{\overline{z}'=0}^{v'} \binom{v}{\overline{z}}\binom{v'}{\overline{z}'} \left(\frac{r_2}{r_1}\right)^{\overline{z}'} \mathcal{U}^{v-\overline{z},v'-\overline{z}'} \mathcal{R}_{\overline{x}+\overline{x}'+t'',\overline{y}+\overline{y}'+u'',\overline{z}+\overline{z}'+v''} \end{aligned} \tag{4.65}$$

which may be compared with (4.52).

4.5.3 INT3P1: $\langle g_{\mu\nu,v}|\, P_2 r_{12}^{-1}\, |\chi_{\sigma\tau}\rangle$

Even though this projection integral does not correspond to an exchange operator matrix element like the INT3E2 and INT3E1 integrals, it is best characterised as an

exchange-type integral. It may be expanded in Hermite integrals as

$$\begin{aligned}
&\left\langle \exp(-\gamma_v r_{12}^2)\tilde{\chi}_{\mu\nu}\right| P_2 r_{12}^{-1} \left|\chi_{\sigma\tau}\right\rangle \\
&\quad = \sum_k \iiint \exp(-\gamma_v r_{12}^2)\tilde{\chi}_{\mu\nu}(1,2)\,\phi_k(2)\,\phi_k(3)\,r_{13}^{-1}\chi_{\sigma\tau}(1,3)\,\mathrm{d}r_1\mathrm{d}r_2\mathrm{d}r_3 \\
&\quad = \sum_{\eta\xi} D_{\eta\xi} \iiint \Omega_{\tilde{\mu}\sigma}(1)\,\Omega_{\tilde{\nu}\xi}(2)\,\Omega_{\tau\eta}(3)\,r_{13}^{-1}\exp(-\gamma_v r_{12}^2)\mathrm{d}r_1\mathrm{d}r_2\mathrm{d}r_3 \\
&\quad = \sum_{tuv} E_{tuv}^{\tilde{\mu}\sigma} \sum_{\eta\xi} D_{\eta\xi} \left(\sum_{t'u'v'} E_{t'u'v'}^{\tilde{\nu}\xi} \sum_{t''u''v''} E_{t''u''v''}^{\tau\eta} V_{tuv;t'u'v';t''u''v''} \right)
\end{aligned} \tag{4.66}$$

The expansion (4.66) is seen to exhibit the characteristic of an exchange-type integral which is a coupling of two overlap distributions through a density matrix element.

Hermite integrals

The Hermite integrals in (4.66) are calculated as

$$\begin{aligned}
&V_{tuv;t'u'v';t''u''v''} \\
&\quad = \iiint \Lambda_{tuv}(\mathbf{r}_1, p, \mathbf{P})\Lambda_{t'u'v'}(\mathbf{r}_2, p', \mathbf{P}')\Lambda_{t''u''v''}(\mathbf{r}_3, p'', \mathbf{P}'') \\
&\qquad\qquad \times r_{13}^{-1}\exp(-\gamma_v r_{12}^2)\mathrm{d}r_1\mathrm{d}r_2\mathrm{d}r_3 \\
&\quad = \partial_P^{tuv}\partial_{P'}^{t'u'v'}\partial_{P''}^{t''u''v''} \iiint \exp(-pr_{1P}^2)\exp(-p'r_{2P'}^2)\exp(-p''r_{3P''}^2) \\
&\qquad\qquad\qquad\qquad \times r_{13}^{-1}\exp(-\gamma_v r_{12}^2)\mathrm{d}r_1\mathrm{d}r_2\mathrm{d}r_3 \\
&\quad = \partial_P^{tuv}\partial_{P'}^{t'u'v'}\partial_{P''}^{t''u''v''} V_{000;000;000}
\end{aligned} \tag{4.67}$$

and up to this point, the expressions look *exactly* like those of the INT3E1 integral. The spherical Hermite integrals are different, however, and are given by

$$\begin{aligned}
&V_{000;000;000} \\
&\quad = \left(\frac{\pi}{p'+\gamma_v}\right)^{\frac{3}{2}} \iint \exp(-pr_{1P}^2)\exp(-q'r_{1P'}^2)\exp(-p''r_{3P''}^2)r_{13}^{-1}\mathrm{d}r_2\mathrm{d}r_3 \\
&\quad = \left(\frac{\pi}{p'+\gamma_v}\right)^{\frac{3}{2}} K_{PP'} \iint \exp(-s'r_{1S'}^2)\exp(-p''r_{3P''}^2)r_{13}^{-1}\mathrm{d}r_2\mathrm{d}r_3 \\
&\quad = \left(\frac{\pi}{p'+\gamma_v}\right)^{\frac{3}{2}} K_{PP'} \frac{2\pi^{\frac{5}{2}}}{s'p''\sqrt{s'+p''}} F_0
\end{aligned} \tag{4.68}$$

where we have used the relations

$$\begin{aligned} q' &= \frac{p'\gamma_v}{p'+\gamma_v} \\ s' &= p + q' \\ s'\mathbf{S}' &= p\mathbf{P} + q'\mathbf{P}' \end{aligned} \tag{4.69}$$

and

$$\begin{aligned} K_{PP'} &= \exp(-\beta R^2_{PP'}) = \exp(-\frac{pq'}{p+q'}R^2_{PP'}) \\ F_0 &= F_0\left(\alpha R^2_{S'P''}\right) = F_0\left(\frac{s'p''}{s'+p''}R^2_{S'P''}\right) \end{aligned} \tag{4.70}$$

The Hermite integral (4.67), may now be written as

$$V_{tuv;t'u'v';t''u''v''} = \left(\frac{\pi}{p'+\gamma_v}\right)^{\frac{3}{2}} \frac{2\pi^{\frac{5}{2}}}{s'p''\sqrt{s'+p''}} \partial_P^{tuv} \partial_{P'}^{t'u'v'} \left(K_{PP'}\left(\partial_{P''}^{t''u''v''} F_0\right)\right) \tag{4.71}$$

Since the difference between the INT3P1 and the INT3E1 integrals lies only in the spherical Hermite integrals, they may use the same implementation, and in practice, only a few tens of lines of code differ for the two integrals.

4.6 Coulomb integrals

While the exchange integrals were all three-electron integrals, the Coulomb integrals appear in two-electron, three-electron and even a (quasi) four-electron form. We start, however, by considering the three-electron integrals.

4.6.1 INT3C1: $\langle g_{\mu\nu,v}| J_2 |\chi_{\sigma\tau}\rangle$

The matrix element of the Coulomb operator between a geminal and an orbital product may be expressed as

$$\begin{aligned} &\left\langle \exp(-\gamma_v r_{12}^2)\tilde{\chi}_{\mu\nu}\right| J_2 \left|\chi_{\sigma\tau}\right\rangle \\ &\quad = \iiint \exp(-\gamma_v r_{12}^2)\tilde{\chi}_{\mu\nu}\left(\sum_k \phi_k(3)\, r_{23}^{-1}\phi_k(3)\right)\chi_{\sigma\tau}\mathrm{d}r_1\mathrm{d}r_2\mathrm{d}r_3 \\ &\quad = \sum_{\eta\xi} D_{\eta\xi} \iiint \Omega_{\tilde{\mu}\sigma}(1)\,\Omega_{\tilde{\nu}\tau}(2)\,\Omega_{\eta\xi}(3)\, r_{23}^{-1}\exp(-\gamma_v r_{12}^2)\mathrm{d}r_1\mathrm{d}r_2\mathrm{d}r_3 \\ &\quad = \sum_{tuv} E^{\tilde{\mu}\sigma}_{tuv} \sum_{t'u'v'} E^{\tilde{\nu}\tau}_{t'u'v'} \sum_{\eta\xi} D_{\eta\xi}\left(\sum_{t''u''v''} E^{\eta\xi}_{t''u''v''} V_{tuv;t'u'v';t''u''v''}\right) \end{aligned} \tag{4.72}$$

Note that, the density matrix in this case does not couple different overlap distributions. This is characteristic of the Coulomb integrals arising from the Coulomb operator given in (3.10).

We shall not discuss the Hermite integrals in (4.72) here, as they are identical to those for the INT3E1 integral.

4.6.2 INT3C2: $\langle g_{\mu\nu,v}|\, J_2\, |g_{\sigma\tau,w}\rangle$

The matrix elements of the Coulomb operator between two geminals are given by

$$\begin{aligned}
&\left\langle \exp(-\gamma_v r_{12}^2)\tilde{\chi}_{\mu\nu}\right|\, J_2\, \left|\exp(-\gamma_v r_{12}^2)\tilde{\chi}_{\sigma\tau}\right\rangle \\
&\quad = \iiint \exp(-\gamma_v r_{12}^2)\tilde{\chi}_{\mu\nu} \left(\sum_k \phi_k\left(3\right) r_{23}^{-1}\phi_k\left(3\right)\right) \exp(-\gamma_w r_{12}^2)\tilde{\chi}_{\sigma\tau}\mathrm{d}r_1\mathrm{d}r_2\mathrm{d}r_3 \\
&\quad = \sum_{\eta\xi} D_{\eta\xi} \iiint \Omega_{\tilde{\mu}\tilde{\sigma}}\left(1\right)\Omega_{\tilde{\nu}\tilde{\tau}}\left(2\right)\Omega_{\eta\xi}\left(3\right) r_{23}^{-1} \exp\left(-(\gamma_v+\gamma_w)r_{12}^2\right)\mathrm{d}r_1\mathrm{d}r_2\mathrm{d}r_3 \\
&\quad = \sum_{tuv} E_{tuv}^{\tilde{\mu}\tilde{\sigma}} \sum_{t'u'v'} E_{t'u'v'}^{\tilde{\nu}\tilde{\tau}} \sum_{\eta\xi} D_{\eta\xi} \left(\sum_{t''u''v''} E_{t''u''v''}^{\eta\xi} V_{tuv;t'u'v';t''u''v''}\right)
\end{aligned} \tag{4.73}$$

If geminals and virtual orbitals are expanded in the same basis set, (4.73) becomes identical in form to (4.72). The only difference is the GCF exponent which has to be updated from γ_v to $\gamma_v + \gamma_w$. This implies that these integrals share a common implementation.

4.6.3 INT2C0: $\langle \chi_{\mu\nu}|\, r_{12}^{-1}\, |\chi_{\sigma\tau}\rangle$

The simplest two-electron Coulomb integral, is the electrostatic repulsion integral between two spherical charge distributions. It is given by

$$\begin{aligned}
\langle \chi_{\mu\nu}|\, r_{12}^{-1}\, |\chi_{\sigma\tau}\rangle &= \iint \chi_{\mu\nu} r_{12}^{-1} \chi_{\sigma\tau}\mathrm{d}r_1\mathrm{d}r_2 \\
&= \iint \Omega_{\mu\sigma}\left(1\right)\Omega_{\nu\tau}\left(2\right) r_{12}^{-1}\mathrm{d}r_1\mathrm{d}r_2 \\
&= \sum_{tuv} E_{tuv}^{\mu\sigma} \sum_{t'u'v'} E_{t'u'v'}^{\nu\tau} V_{tuv;t'u'v'}
\end{aligned} \tag{4.74}$$

This integral is needed for the conventional MP2 part but also for the quasi four-electron integral discussed in section 4.6.5.

Hermite integrals

The Hermite integral in (4.74) is well-known and reads

$$\begin{aligned} V_{tuv;t'u'v'} &= \iint \Lambda_{tuv}(\mathbf{r}_1, p, \mathbf{P})\Lambda_{t'u'v'}(\mathbf{r}_2, p', \mathbf{P}')r_{12}^{-1}\mathrm{d}r_1\mathrm{d}r_2 \\ &= \partial_P^{tuv}\partial_{P'}^{t'u'v'} \iint \exp(-pr_{1P}^2)\exp(-p'r_{2P'}^2)r_{12}^{-1}\mathrm{d}r_1\mathrm{d}r_2 \\ &= \frac{2\pi^{\frac{5}{2}}}{pp'\sqrt{(p+p')}}\partial_P^{tuv}\partial_{P'}^{t'u'v'}F_0 \end{aligned} \tag{4.75}$$

where

$$F_0 = F_0\left(\alpha R_{PP'}^2\right) = F_0\left(\frac{pp'}{p+p'}R_{PP'}^2\right) \tag{4.76}$$

Again, differentiation of the Boys function with respect to primed centres may be replaced by differentiation with respect to unprimed centres

$$\partial_{P'}^{t'u'v'}F_n = (-1)^{t'+u'+v'}\partial_P^{t'u'v'}F_n \tag{4.77}$$

The Boys function differentiated with respect to unprimed centres may be recurred from functions $\mathcal{R}_{tuv}^n$ defined as

$$\mathcal{R}_{tuv}^n = (-2\alpha)^n\,\partial_P^{tuv}F_n \tag{4.78}$$

which differ slightly from those of (4.50). The corresponding recurrence relations become

$$\begin{aligned} \mathcal{R}_{(t+1)uv}^n &= t\mathcal{R}_{(t-1)uv}^{n+1} + X_{PP'}\mathcal{R}_{tuv}^{n+1} \\ \mathcal{R}_{t(u+1)v}^n &= u\mathcal{R}_{t(u-1)v}^{n+1} + Y_{PP'}\mathcal{R}_{tuv}^{n+1} \\ \mathcal{R}_{tu(v+1)}^n &= v\mathcal{R}_{tu(v-1)}^{n+1} + Z_{PP'}\mathcal{R}_{tuv}^{n+1} \end{aligned} \tag{4.79}$$

In terms of the functions $\mathcal{R}_{tuv}$, we may write the Hermite integrals (4.75) as

$$V_{tuv;t'u'v'} = \frac{2\pi^{\frac{5}{2}}}{pp'\sqrt{(p+p')}}(-1)^{t'+u'+v'}\mathcal{R}_{t+t',u+u',v+v'} \tag{4.80}$$

a fairly simple expression compared to the other Hermite integrals we have discussed.

4.6.4 INT2C1: $\langle g_{\mu\nu,v}| \, r_{12}^{-1} \, |\chi_{\sigma\tau}\rangle$

We also need Coulomb operator matrix elements between geminals and orbitals. These are given by

$$\begin{aligned}
&\left\langle \exp(-\gamma_v r_{12}^2)\tilde{\chi}_{\mu\nu}\right| r_{12}^{-1} \left|\chi_{\sigma\tau}\right\rangle \\
&\quad = \iint \exp(-\gamma_v r_{12}^2)\tilde{\chi}_{\mu\nu} r_{12}^{-1} \chi_{\sigma\tau} \mathrm{d}r_1 \mathrm{d}r_2 \\
&\quad = \iint \Omega_{\tilde{\mu}\sigma}\left(1\right) \Omega_{\tilde{\nu}\tau}\left(2\right) r_{12}^{-1} \exp(-\gamma_v r_{12}^2) \mathrm{d}r_1 \mathrm{d}r_2 \\
&\quad = \sum_{tuv} E_{tuv}^{\tilde{\mu}\sigma} \sum_{t'u'v'} E_{t'u'v'}^{\tilde{\nu}\tau} V_{tuv;t'u'v'}
\end{aligned} \tag{4.81}$$

Setting $\gamma_v = 0$ reduces (4.81) to the repulsion integral INT2C0 and this is a simple way to check a part of our implementation.

Hermite integrals

The Hermite integrals in (4.81) may be expressed as

$$\begin{aligned}
&V_{tuv;t'u'v'} \\
&\quad = \iint \Lambda_{tuv}(\mathbf{r}_1, p, \mathbf{P}) \Lambda_{t'u'v'}(\mathbf{r}_2, p', \mathbf{P}') r_{12}^{-1} \exp(-\gamma_v r_{12}^2) \mathrm{d}r_1 \mathrm{d}r_2 \\
&\quad = \partial_P^{tuv} \partial_{P'}^{t'u'v'} \iint \exp(-p r_{1P}^2) \exp(-p' r_{2P'}^2) r_{12}^{-1} \exp(-\gamma_v r_{12}^2) \mathrm{d}r_1 \mathrm{d}r_2 \\
&\quad = \frac{2\pi^{\frac{5}{2}}}{(q+\gamma_v)(p+p')^{\frac{3}{2}}} \partial_P^{tuv} \partial_{P'}^{t'u'v'} \left(K_{PP'} F_0\right)
\end{aligned} \tag{4.82}$$

where we have applied the relation

$$q = \frac{pp'}{p+p'} \tag{4.83}$$

and relations

$$\begin{aligned}
K_{PP'} &= \exp(-\beta R_{PP'}^2) = \exp\left(-\frac{q\gamma_v}{q+\gamma_v} R_{PP'}^2\right) \\
F_0 &= F_0\left(\alpha R_{PP'}^2\right) = F_0\left(\frac{q^2}{q+\gamma_v} R_{PP'}^2\right)
\end{aligned} \tag{4.84}$$

By invoking the binomial formula (4.41), the differentiation part of (4.82) may be

written

$$\begin{aligned}
&\partial_P^{tuv}\partial_{P'}^{t'u'v'}\left(K_{PP'}F_0\right)\\
&=\sum_{\overline{x}=0}^{t}\sum_{\overline{y}=0}^{u}\sum_{\overline{z}=0}^{v}\sum_{\overline{x}'=0}^{t'}\sum_{\overline{y}'=0}^{u'}\sum_{\overline{z}'=0}^{v'}\binom{t}{\overline{x}}\binom{u}{\overline{y}}\binom{v}{\overline{z}}\binom{t'}{\overline{x}'}\binom{u'}{\overline{y}'}\binom{v'}{\overline{z}'}\\
&\qquad\times\left(\partial_P^{t-\overline{x},u-\overline{y},v-\overline{z}}\partial_{P'}^{t'-\overline{x}',u'-\overline{y}',v'-\overline{z}'}K_{PP'}\right)\left(\partial_P^{\overline{xyz}}\partial_{P'}^{\overline{x}'\overline{y}'\overline{z}'}F_0\right)
\end{aligned}\tag{4.85}$$

For both differentiations in (4.85) we have already developed recurrence relations. The K functions may be obtained from (4.63) while the Boys functions may be obtained from (4.79). Using these expressions we may write the Hermite integral (4.82) as

$$\begin{aligned}
V_{tuv;t'u'v'} &= \frac{2\pi^{\frac{5}{2}}}{(q+\gamma_v)(p+p')^{\frac{3}{2}}}\\
&\quad\times\sum_{\overline{x}=0}^{t}\sum_{\overline{x}'=0}^{t'}\binom{t}{\overline{x}}\binom{t'}{\overline{x}'}(-1)^{\overline{x}'}\,\mathcal{S}^{t-\overline{x},t'-\overline{x}'}\\
&\qquad\sum_{\overline{y}=0}^{u}\sum_{\overline{y}'=0}^{u'}\binom{u}{\overline{y}}\binom{u'}{\overline{y}'}(-1)^{\overline{y}'}\,\mathcal{T}^{u-\overline{y},u'-\overline{y}'}\\
&\qquad\qquad\sum_{\overline{z}=0}^{v}\sum_{\overline{z}'=0}^{v'}\binom{v}{\overline{z}}\binom{v'}{\overline{z}'}(-1)^{\overline{z}'}\,\mathcal{U}^{v-\overline{z},v'-\overline{z}'}\mathcal{R}_{\overline{x}+\overline{x}',\overline{y}+\overline{y}',\overline{z}+\overline{z}'}
\end{aligned}\tag{4.86}$$

which may be compared to the Hermite integral (4.65).

4.6.5 INT4C1: $\langle g_{\mu\nu,v}|\, P_1P_2r_{12}^{-1}\,|\chi_{\sigma\tau}\rangle$

The quasi four-electron integrals are, as the name reveals, not a true four-electron integral; it may be decomposed into a product of two-electron integrals

$$\begin{aligned}
&\left\langle\exp(-\gamma_v r_{12}^2)\tilde{\chi}_{\mu\nu}\right|P_1P_2r_{12}^{-1}\,|\chi_{\sigma\tau}\rangle\\
&\qquad=\sum_{k,l}\left\langle\exp(-\gamma_v r_{12}^2)\tilde{\chi}_{\mu\nu}|\varphi_k\varphi_l\right\rangle\langle\varphi_k\varphi_l|\,r_{12}^{-1}\,|\chi_{\sigma\tau}\rangle
\end{aligned}\tag{4.87}$$

The overlap integral in (4.87) is discussed in section 4.8.1 and the repulsion integral has already been discussed in 4.6.3. We therefore proceed to the next type of integrals, the nuclear attraction integrals.

4.7 Nuclear attraction integrals

4.7.1 INT2V1: $\langle g_{\mu\nu,v}| V_{2C} |\chi_{\sigma\tau}\rangle$

To obtain GTG-MP2 energies we need two types of nuclear attraction integrals, both of which are two-electron integrals. For the coupling between geminals and virtual orbitals we need matrix elements

$$\begin{aligned}
&\left\langle \exp(-\gamma_v r_{12}^2)\tilde{\chi}_{\mu\nu}\right| \sum Z_C r_{2C}^{-1} \left|\chi_{\sigma\tau}\right\rangle \\
&\qquad = \iint \exp(-\gamma_v r_{12}^2)\tilde{\chi}_{\mu\nu} \left(\sum_C Z_C r_{2C}^{-1}\right) \chi_{\sigma\tau} \mathrm{d}r_1 \mathrm{d}r_2 \\
&\qquad = \sum_C Z_C \iint \Omega_{\tilde{\mu}\sigma}(1)\, \Omega_{\tilde{\nu}\tau}(2)\, r_{2C}^{-1} \exp(-\gamma_v r_{12}^2) \mathrm{d}r_1 \mathrm{d}r_2 \\
&\qquad = \sum_{tuv} E_{tuv}^{\tilde{\mu}\sigma} \sum_{t'u'v'} E_{t'u'v'}^{\tilde{\nu}\tau} \sum_C Z_C V_{tuv;t'u'v'}^C
\end{aligned} \tag{4.88}$$

where the Hermite integrals $V_{tuv;t'u'v'}^C$ are dependent of the position of some nucleus C. The Hermite integrals in (4.88) may be evaluated as

$$\begin{aligned}
&V_{tuv;t'u'v'}^C \\
&\qquad = \partial_P^{tuv} \partial_{P'}^{t'u'v'} \iint \exp(-p r_{1P}^2) \exp(-p' r_{2P'}^2) r_{2C}^{-1} \exp(-\gamma_v r_{12}^2) \mathrm{d}r_1 \mathrm{d}r_2 \\
&\qquad = \left(\frac{\pi}{p+\gamma_v}\right)^{\frac{3}{2}} \left(\frac{2\pi}{s}\right) \partial_P^{tuv} \partial_{P'}^{t'u'v'} (K_{PP'} F_0)
\end{aligned} \tag{4.89}$$

where we have used relations

$$\begin{aligned}
q &= p\gamma_v (p+\gamma_v)^{-1} \\
\alpha &= qp'(q+p')^{-1} \\
s &= q + p' \\
s\mathbf{S} &= q\mathbf{P} + p'\mathbf{P}'
\end{aligned} \tag{4.90}$$

and

$$\begin{aligned}
K_{PP'} &= \exp(-\alpha R_{PP'}^2) \\
F_0 &= F_0(s R_{SC}^2)
\end{aligned} \tag{4.91}$$

The partial derivatives in (4.89) is given by (4.85), but the Boys function in this expression must be recurred using relations (4.51) rather than relations (4.79). The r_1 and r_2 are for the nuclear attraction integrals given by

$$\begin{aligned}
r_1 &= \frac{\partial X_{SC}}{\partial P_x} = \frac{q}{s} \\
r_2 &= \frac{\partial X_{SC}}{\partial P'_x} = \frac{p'}{s}
\end{aligned} \tag{4.92}$$

where X_{SC} is the x-component of $\mathbf{R}_{SC} = \mathbf{S} - \mathbf{R}_C$ and $\mathbf{R}_C$ is the position of some nucleus C.

If we insert the results obtained in (4.85) and (4.51) into (4.89), the nuclear attraction Hermite integral may be written in the final form

$$\begin{aligned} V^C_{tuv;t'u'v'} = &\left(\frac{\pi}{p+\gamma_v}\right)^{\frac{3}{2}} \left(\frac{2\pi}{s}\right) \\ &\times \sum_{\overline{x}=0}^{t}\sum_{\overline{x}'=0}^{t'} \binom{t}{\overline{x}}\binom{t'}{\overline{x}'} \left(\frac{r_2}{r_1}\right)^{\overline{x}} \mathcal{S}^{t-\overline{x},t'-\overline{x}'} \\ &\sum_{\overline{y}=0}^{u}\sum_{\overline{y}'=0}^{u'} \binom{u}{\overline{y}}\binom{u'}{\overline{y}'} \left(\frac{r_2}{r_1}\right)^{\overline{y}} \mathcal{T}^{u-\overline{y},u'-\overline{y}'} \\ &\sum_{\overline{z}=0}^{v}\sum_{\overline{z}'=0}^{v'} \binom{v}{\overline{z}}\binom{v'}{\overline{z}'} \left(\frac{r_2}{r_1}\right)^{\overline{z}} \mathcal{U}^{v-\overline{z},v'-\overline{z}'} \mathcal{R}_{\overline{x}+\overline{x}',\overline{y}+\overline{y}',\overline{z}+\overline{z}'} \end{aligned} \tag{4.93}$$

which closely resembles both (4.65) and (4.86).

4.7.2 INT2V2: $\langle g_{\mu\nu,v}| V_{2C} |g_{\sigma\tau,w}\rangle$

The nuclear attraction integral needed for the coupling between two geminals is

$$\begin{aligned} &\left\langle \exp(-\gamma_v r_{12}^2)\tilde{\chi}_{\mu\nu}\right| \sum Z_C r_{2C}^{-1} \left|\exp(-\gamma_w r_{12}^2)\tilde{\chi}_{\sigma\tau}\right\rangle \\ &\quad = \iint \exp(-\gamma_v r_{12}^2)\tilde{\chi}_{\mu\nu} \left(\sum_C Z_C r_{2C}^{-1}\right) \exp(-\gamma_w r_{12}^2)\tilde{\chi}_{\sigma\tau} \mathrm{d}r_1 \mathrm{d}r_2 \\ &\quad = \sum_C Z_C \iint \Omega_{\tilde{\mu}\tilde{\sigma}}(1)\, \Omega_{\tilde{\nu}\tilde{\tau}}(2)\, r_{2C}^{-1} \exp\left(-(\gamma_v+\gamma_w) r_{12}^2\right) \mathrm{d}r_1 \mathrm{d}r_2 \\ &\quad = \sum_{tuv} E^{\tilde{\mu}\tilde{\sigma}}_{tuv} \sum_{t'u'v'} E^{\tilde{\nu}\tilde{\tau}}_{t'u'v'} \sum_C Z_C V^C_{tuv;t'u'v'} \end{aligned} \tag{4.94}$$

where the Hermite integrals may be obtained using (4.93) if we replace all occurrences of γ_v with $\gamma_v + \gamma_w$.

4.8 Overlap integrals

The overlap integrals come both as two-electron and three-electron integrals. These integrals are separable in the Cartesian directions and may be evaluated without any numerical integrations or functional approximations.

4.8.1 INT21: $\langle g_{\mu\nu,v}|\chi_{\sigma\tau}\rangle$

The overlap between a geminal and an orbital product is

$$\begin{aligned}
&\left\langle \exp(-\gamma_v r_{12}^2)\tilde{\chi}_{\mu\nu}|\chi_{\sigma\tau}\right\rangle \\
&\qquad = \iint \exp(-\gamma_v r_{12}^2)\tilde{\chi}_{\mu\nu}\chi_{\sigma\tau}\mathrm{d}r_1\mathrm{d}r_2 \\
&\qquad = \iint \Omega_{\tilde{\mu}\sigma}\left(1\right)\Omega_{\tilde{\nu}\tau}\left(2\right)\exp\left(-(\gamma_v+\gamma_w)r_{12}^2\right)\mathrm{d}r_1\mathrm{d}r_2 \\
&\qquad = \sum_{tuv} E_{tuv}^{\tilde{\mu}\sigma}\sum_{t'u'v'} E_{t'u'v'}^{\tilde{\nu}\tau} V_{tuv;t'u'v'}
\end{aligned} \tag{4.95}$$

where the Hermite integral $V_{tuv;t'u'v'}$ may be evaluated as

$$\begin{aligned}
&V_{tuv;t'u'v'} \\
&\qquad = \partial_P^{tuv}\partial_{P'}^{t'u'v'}\iint \exp(-pr_{1P}^2)\exp(-p'r_{2P'}^2)\exp(-\gamma_v r_{12}^2)\mathrm{d}r_1\mathrm{d}r_2 \\
&\qquad = \frac{\pi^3}{(pp'+\gamma_v(p+p'))^{\frac{3}{2}}}\partial_P^{tuv}\partial_{P'}^{t'u'v'}K_{PP'}
\end{aligned} \tag{4.96}$$

where we have used relations

$$q = \frac{pp'}{p+p'} \tag{4.97}$$

and

$$K_{PP'} = \exp\left(-\alpha R_{PP'}^2\right) = \exp\left(-\frac{q\gamma_v}{q+\gamma_v}R_{PP'}^2\right) \tag{4.98}$$

It is not optimal to calculate overlap integrals by first calculating Hermite integrals using (4.96) and then inserting these into (4.95), as this does not allow us to exploit the separability into Cartesian directions. However, it provides us with a simple means to double-check the overlap integrals, and furthermore, it gives us a very important opportunity to check the Hermite to Cartesian transformation for the other two-electron integrals.

To take advantage of the separability we notice that the Hermite integral (4.96) may be decomposed into Cartesian directions

$$V_{tuv;t'u'v'} = V_{t;t'}^x \times V_{u;u'}^y \times V_{v;v'}^z \tag{4.99}$$

where $V_{t;t'}^x$ is the x-component of the Hermite integral. It is given by

$$V_{t;t'}^x = \frac{\pi}{\sqrt{pp'+\gamma_v(p+p')}}(-1)^{t'}\partial_P^{t+t'}\exp\left(-\alpha X_{PP'}^2\right) \tag{4.100}$$

The overlap integral (4.95) may be expressed directly in terms of decomposed Hermite integrals as

$$\left\langle \exp(-\gamma_v r_{12}^2)\tilde{\chi}_{\mu\nu}|\chi_{\sigma\tau}\right\rangle = I_x \times I_y \times I_z \tag{4.101}$$

where, for instance, I_x is given by

$$I_x = \sum_t E_t^{\tilde{\mu}\sigma} \sum_{t'} E_{t'}^{\tilde{\nu}\tau} V_{t;t'}^x \tag{4.102}$$

4.8.2 INT22: $\langle g_{\mu\nu,v} | g_{\sigma\tau,w} \rangle$

The overlap integral between two geminal may be calculated as

$$\left\langle \exp(-\gamma_v r_{12}^2)\tilde{\chi}_{\mu\nu} \right| \exp(-\gamma_w r_{12}^2)\tilde{\chi}_{\sigma\tau} \Big\rangle = I_x \times I_y \times I_z \tag{4.103}$$

where I_x, I_y, and I_z may be calculated using the expressions developed for the INT21 integrals by substituting γ_v by $\gamma_v + \gamma_w$.

4.8.3 INT32: $\langle g_{\mu\nu,v} | \, P_2 \, | g_{\sigma\tau,w} \rangle$

The three-electron overlap integrals are matrix elements of a projection operator between two geminals. They are given by

$$\begin{aligned}
&\left\langle \tilde{\chi}_{\mu\nu} \exp(-\gamma_v r_{12}^2) \right| P_2 \left| \tilde{\chi}_{\sigma\tau} \exp(-\gamma_w r_{12}^2) \right\rangle \\
&\quad = \sum_k \iiint \exp(-\gamma_v r_{12}^2)\tilde{\chi}_{\mu\nu}(1,2)\,\phi_k(2)\,\phi_k(3)\,\tilde{\chi}_{\sigma\tau}(1,3)\,\mathrm{d}r_1\mathrm{d}r_2\mathrm{d}r_3 \\
&\quad = \sum_{\eta\xi} D_{\eta\xi} \iiint \Omega_{\tilde{\mu}\tilde{\sigma}}(1)\,\Omega_{\tilde{\nu}\xi}(2)\,\Omega_{\tilde{\tau}\eta}(3) \exp(-\gamma_v r_{12}^2)\mathrm{d}r_1\mathrm{d}r_2\mathrm{d}r_3 \\
&\quad = \sum_{tuv} E_{tuv}^{\tilde{\mu}\tilde{\sigma}} \sum_{\eta\xi} D_{\eta\xi} \left(\sum_{t'u'v'} E_{t'u'v'}^{\tilde{\nu}\xi} \sum_{t''u''v''} E_{t''u''v''}^{\tilde{\tau}\eta} V_{tuv;t'u'v';t''u''v''} \right)
\end{aligned} \tag{4.104}$$

We note that the Hermite to Cartesian transformation of (4.104) is identical to that of the cyclic three-electron integral discussed in section 4.5.1. The Hermite integral may be calculated as

$$\begin{aligned}
&V_{tuv;t'u'v';t''u''v''} \\
&\quad = \partial_P^{tuv} \partial_{P'}^{t'u'v'} \partial_{P''}^{t''u''v''} \iiint \exp(-pr_{1P}^2) \exp(-p'r_{2P'}^2) \exp(-p''r_{3P''}^2) \\
&\qquad\qquad \times \exp(-\gamma_v r_{12}^2) \exp(-\gamma_w r_{13}^2)\mathrm{d}r_1\mathrm{d}r_2\mathrm{d}r_3 \\
&\quad = \partial_P^{tuv} \partial_{P'}^{t'u'v'} \partial_{P''}^{t''u''v''} V_{000;000;000}
\end{aligned} \tag{4.105}$$

where the spherical Hermite integral is

$$\begin{aligned}
V_{000;000;000} &= \left(\frac{\pi}{p + \gamma_v + \gamma_w} \right)^{\frac{3}{2}} K_{PP'} K_{PP''} \\
&\quad \times \iint \exp(-sr_{2S}^2) \exp(-s'r_{3S'}^2) \exp(-qr_{23}^2)\mathrm{d}r_2\mathrm{d}r_3 \\
&= \left(\frac{\pi}{p + \gamma_v + \gamma_w} \right)^{\frac{3}{2}} \left(\frac{\pi^2}{ss' + sq + s'q} \right) K_{PP'} K_{PP''} K_{SS'}
\end{aligned} \tag{4.106}$$

The s, s', q, $K_{PP'}$, $K_{PP''}$ and $K_{SS'}$ of (4.106) are defined exactly as for the cyclic three-electron integral, that is, by (4.37) and (4.38). This implies, for instance, that we may use relations (4.44)–(4.46) to recur the KKK functions for the INT32 integrals.

In principle, we should get a performance enhancement if we calculate (4.104) separately for each Cartesian direction as in (4.101) and (4.102). However, this requires a substantial amount of additional code to be implemented and our experience with the two-electron overlap integrals discourages this as not worth the effort. Note, however, that the two-electron overlap integrals should still be calculated by means of I_x, I_y, and I_z as these integrals are needed for the kinetic energy integrals.

4.9 Kinetic energy integrals

The kinetic energy integrals are given a special treatment as there are two different ways to calculate each integral. The second formula may be deduced from the following relation

$$\nabla_2 \langle g_{\mu\nu,v} | \nabla_2 \chi_{\sigma\tau} \rangle = \langle \nabla_2 g_{\mu\nu,v} | \nabla_2 \chi_{\sigma\tau} \rangle + \left\langle g_{\mu\nu,v} \middle| \nabla_2^2 \chi_{\sigma\tau} \right\rangle \tag{4.107}$$

Since an integral is just a number, it yields zero upon differentiation. We may therefore conclude that

$$\langle g_{\mu\nu,v} | \nabla_2^2 | \chi_{\sigma\tau} \rangle = - \langle \nabla_2 g_{\mu\nu,v} | \nabla_2 \chi_{\sigma\tau} \rangle \tag{4.108}$$

While the latter of these forms are often used to calculate the conventional one-electron kinetic energy integrals, this is not necessarily the best way to calculate integrals containing two-electron functions. We shall therefore study both approaches.

Moreover, as kinetic energy integrals symmetric in electron one and two exhibit certain symmetries, we work out formulas for symmetric operators like $\nabla_1^2 + \nabla_2^2$ as well as non-symmetric operators like ∇_2^2. Also, we start by using the ∇_1 operator rather than the ∇_2 operator, even though this is somewhat out of the line of the treatment given to other integrals so far.

4.9.1 INT2K1: $\langle g_{\mu\nu,v} | \nabla_1^2 | \chi_{\sigma\tau} \rangle$

The operator for kinetic energy is $-\frac{1}{2}\nabla^2$. To keep formulas as simple as possible, we disregard the factor $-\frac{1}{2}$ in the discussion below.

For the kinetic energy integral between a geminal and an orbital product, we have

$$\begin{aligned} &\langle g_{\mu\nu,v} | \nabla_1^2 | \chi_{\sigma\tau} \rangle \\ &\quad = \left\langle \chi_A(1)\chi_C(2) \exp(-\gamma_v r_{12}^2) \middle| \nabla_1^2 | \chi_B(1)\chi_D(2) \right\rangle \\ &\quad = T_x^1 I_y I_z + I_x T_y^1 I_z + I_x I_y T_z^1 \end{aligned} \tag{4.109}$$

where I_x, I_y, and I_z are overlap integrals decomposed into Cartesian directions, as discussed in section 4.8.1. The integrals represented by a T hold the differential operator. T_x^1, for instance, is given by

$$\begin{aligned} T_x^1 = \iint & G_k(x_1, a, A) G_m(x_2, c, C) \exp(-\gamma_v x_{12}^2) \\ & \times \frac{\partial^2}{\partial x_1^2} G_l(x_1, b, B) G_n(x_2, d, D) \mathrm{d}x_1 \mathrm{d}x_2 \end{aligned} \tag{4.110}$$

The super-index in T_x^1 denotes differentiation with respect to electron 1. The differential operator in (4.109) works only on $G_l(x_1, b, B)$ and leaves $G_n(x_2, d, D)$ unchanged. Setting $G_l \equiv G_l(x_1, b, B)$, we obtain

$$\begin{aligned} \frac{\partial^2}{\partial x_1^2} G_l &= \frac{\partial}{\partial x_1}(l G_{l-1} - 2b G_{l+1}) \\ &= l(l-1) G_{l-2} - 2b(l+1) G_l + 4b^2 G_{l+2} \end{aligned} \tag{4.111}$$

allowing us to write the $T^1 \equiv T_x^1$ integral as

$$T^1 = l(l-1) I^{k(l-2)mn} - 2b(l+1) I^{klmn} + 4b^2 I^{k(l+2)mn} \tag{4.112}$$

that is, as a linear combination of overlap integrals with angular momentum increased ($I^{k(l+2)mn}$), identical (I^{klmn}) and decreased ($I^{k(l-2)mn}$) relative to the kinetic energy integrals to be calculated. Calculating kinetic energy integrals up to d-orbitals thus requires the calculation of overlap integrals up to g-orbitals. Note that, we have set $I^{klmn} \equiv I_x^{klmn}$ to avoid overloading formulas unnecessarily.

The corresponding T^2 integral may be found by inspection. Adding integrals T^1 and T^2 to form a symmetric integral T^{12}, gives

$$\begin{aligned} T^{12} = & \, l(l-1) I^{k(l-2)mn} - 2b(l+1) I^{klmn} + 4b^2 I^{k(l+2)mn} \\ & + n(n-1) I^{klm(n-2)} - 2d(n+1) I^{klmn} + 4d^2 I^{klm(n+2)} \end{aligned} \tag{4.113}$$

By comparing (4.112) with (4.113), we see that there is no major advantage by using kinetic energy operators symmetric in the electron coordinates.

4.9.2 INT2K1: $-\langle \nabla_1 g_{\mu\nu,v} | \nabla_1 \chi_{\sigma\tau} \rangle$

Calculating the kinetic energy integrals using the right-hand-side of (4.108) leads to a different T^1 integrals, but the rest is equal.

$$\begin{aligned} T^1 = -\iint & \frac{\partial}{\partial x_1} \{ G_k(x_1, a, A) G_m(x_2, c, C) \exp(-\gamma_v x_{12}^2) \} \\ & \times \frac{\partial}{\partial x_1} G_l(x_1, b, B) G_n(x_2, d, D) \mathrm{d}x_1 \mathrm{d}x_2 \end{aligned} \tag{4.114}$$

The two derivatives of (4.114) are

$$\frac{\partial}{\partial x_1} G_k \exp(-\gamma_v x_{12}^2) = (kG_{k-1} - 2\gamma_v x_{12} G_k - 2aG_{k+1}) \exp(-\gamma_v x_{12}^2) \tag{4.115}$$

and

$$\frac{\partial}{\partial x_1} G_l = lG_{l-1} - 2bG_{l+1} \tag{4.116}$$

Using these expressions, we may rewrite (4.114) as

$$\begin{aligned} T^1 = -\iint & (kG_{k-1} - 2\gamma_v x_{12} G_k - 2aG_{k+1}) G_m \exp(-\gamma_v x_{12}^2) \\ & \times (lG_{l-1} - 2bG_{l+1}) G_n \mathrm{d}x_1 \mathrm{d}x_2 \end{aligned} \tag{4.117}$$

To be able to express (4.117) as a linear combination of overlap integrals, we must rewrite the factor x_{12} in terms of x_{1A} and x_{2C} or x_{1B} and x_{2D} using either

$$x_{12} = x_{1A} - x_{2C} + X_{AC} \tag{4.118}$$

or

$$x_{12} = x_{1B} - x_{2D} + X_{BD} \tag{4.119}$$

If we resolve the two parentheses of (4.117), we get

$$\begin{aligned} & (kG_{k-1} - 2\gamma_v x_{12} G_k - 2aG_{k+1})(lG_{l-1} - 2bG_{l+1}) \\ & \quad = klG_{k-1}G_{l-1} - 2bkG_{k-1}G_{l+1} - 2alG_{k+1}G_{l-1} \\ & \qquad + 4abG_{k+1}G_{l+1} - 2\gamma_v l x_{12} G_k G_{l-1} + 4b\gamma_v x_{12} G_k G_{l+1} \end{aligned} \tag{4.120}$$

The strategy for substituting x_{12} is to avoid increasing individual angular momenta with more than one. Therefore we substitute the first x_{12} in (4.117) using (4.119) and the second using (4.118). This allows us to write T^1 as

$$\begin{aligned} T^1 = & - klI^{(k-1)(l-1)mn} \\ & + 2\gamma_v l X_{BD} I^{k(l-1)mn} - 2\gamma_v l I^{k(l-1)m(n+1)} \\ & + 2bkI^{(k-1)(l+1)mn} + 2alI^{(k+1)(l-1)mn} \\ & + 2\gamma_v l I^{klmn} \\ & - 4b\gamma_v X_{AC} I^{k(l+1)mn} \\ & - 4b(a+\gamma_v) I^{(k+1)(l+1)mn} \\ & + 4b\gamma_v I^{k(l+1)m(n+1)} \end{aligned} \tag{4.121}$$

The expression for T^2 may be deduced from (4.121) by inspection. Adding T^1 and T^2 we get

$$\begin{aligned} T^{12} = & - klI^{(k-1)(l-1)mn} - mnI^{kl(m-1)(n-1)} \\ & + 2\gamma_v X_{BD}[lI^{k(l-1)mn} - nI^{klm(n-1)}] \\ & - 2\gamma_v[lI^{k(l-1)m(n+1)} + nI^{k(l+1)m(n-1)}] \\ & + 2bkI^{(k-1)(l+1)mn} + 2alI^{(k+1)(l-1)mn} \\ & + 2dmI^{kl(m-1)(n+1)} + 2cnI^{kl(m+1)(n-1)} \\ & + 2\gamma_v(l+n)I^{klmn} \\ & - 4\gamma_v X_{AC}[bI^{k(l+1)mn} - dI^{klm(n+1)}] \\ & - 4b(a+\gamma_v)I^{(k+1)(l+1)mn} + 4b\gamma_v I^{k(l+1)(m+1)n} \\ & - 4d(c+\gamma_v)I^{kl(m+1)(n+1)} + 4d\gamma_v I^{(k+1)lm(n+1)} \end{aligned} \tag{4.122}$$

If we compare (4.113) with (4.122), we see that the latter includes far more terms. This, however, is compensated for by a faster calculation of overlap integrals.

4.9.3 INT2K2: $\langle g_{\mu\nu,v}| \nabla_1^2 |g_{\sigma\tau,w}\rangle$

The kinetic energy integrals having geminals both in bra and ket may be expressed in the same way as the INT2K1 integrals of the previous sections

$$\begin{aligned} & \langle g_{\mu\nu,v}| \nabla_1^2 |g_{\sigma\tau,w}\rangle \\ & \quad = \left\langle \chi_A(1)\chi_C(2)\exp(-\gamma_v r_{12}^2)\right| \nabla_1^2 \left|\chi_B(1)\chi_D(2)\exp(-\gamma_w r_{12}^2)\right\rangle \\ & \quad = T_x^1 I_y I_z + I_x T_y^1 I_z + I_x I_y T_z^1 \end{aligned} \tag{4.123}$$

For the INT2K2 integrals, however, the T_x^1 factors become more complicated

$$\begin{aligned} T_x^1 = \iint & G_k(x_1,a,A)G_m(x_2,c,C)\exp(-\gamma_v x_{12}^2) \\ & \times \frac{\partial^2}{\partial x_1^2} G_l(x_1,b,B)G_n(x_2,d,D)\exp(-\gamma_w x_{12}^2)\mathrm{d}x_1\mathrm{d}x_2 \end{aligned} \tag{4.124}$$

By carrying out the differentiation in (4.124), we get

$$\begin{aligned} & \frac{\partial^2}{\partial x_1^2} G_l \exp(-\gamma_w x_{12}^2) \\ & \quad = \frac{\partial}{\partial x_1}(lG_{l-1} - 2\gamma_w x_{12} G_l - 2bG_{l+1})\exp(-\gamma_w x_{12}^2) \\ & \quad = \left\{ l(l-1)G_{l-2} - [2b(2l+1) + 2\gamma_w]G_l + 4b^2 G_{l+2} \right. \\ & \qquad \left. -4\gamma_w l x_{12} G_{l-1} + 4\gamma_w^2 x_{12}^2 G_l + 8b\gamma_w x_{12} G_{l+1} \right\} \exp\left(-\gamma_w x_{12}^2\right) \end{aligned} \tag{4.125}$$

which also includes a term that is second-order in the inter-electronic distance x_{12} as well as two terms that are of first-order. For all these terms, we replace x_{12} by

$$x_{12} = x_{1B} - x_{2D} + X_{BD} \tag{4.126}$$

Substituting the resulting expression back into (4.124) and collecting GTOs of equal angular momentum, we find that the $T^1 \equiv T^1_x$ integral is given by the following linear combination of overlap integrals

$$\begin{aligned} T^1 =& l(l-1)I^{k(l-2)mn} - 4\gamma_w l X_{BD} I^{k(l-1)mn} \\ &+ 4\gamma_w l I^{k(l-1)m(n+1)} \\ &- [2b(2l+1) + 2\gamma_w(2l+1) - 4\gamma_w^2 X_{BD}^2] I^{klmn} \\ &+ 8\gamma_w X_{BD}[(b+\gamma_w)I^{k(l+1)mn} - \gamma_w I^{klm(n+1)}] \\ &- 8\gamma_w(b+\gamma_w)I^{k(l+1)m(n+1)} \\ &+ 4(b+\gamma_w)^2 I^{k(l+2)mn} + 4\gamma_w^2 I^{klm(n+2)} \end{aligned} \tag{4.127}$$

The corresponding T^2 integral may be deduced from (4.127) by swapping l and n and b and d, and replacing X_{BD} by $-X_{BD}$. Adding T^1 and T^2, we get

$$\begin{aligned} T^{12} =& l(l-1)I^{k(l-2)mn} + m(m-1)I^{klm(n-2)} \\ &+ 4\gamma_w X_{BD}\left(nI^{klm(n-1)} - lI^{k(l-1)mn}\right) \\ &+ 4\gamma_w\left(nI^{k(l+1)m(n-1)} + lI^{k(l-1)m(n+1)}\right) \\ &- [2b(2l+1) + 2d(2m+1) + 4\gamma_w(l+m+1) - 8\gamma_w^2 X_{BD}^2] I^{klmn} \\ &+ 8\gamma_w X_{BD}\left[(2\gamma_w+b)I^{k(l+1)mn} - (2\gamma_w+d)I^{klm(n+1)}\right] \\ &- 8\gamma_w\left(b+d+2\gamma_w\right) I^{k(l+1)m(n+1)} \\ &+ 4\left[(b+\gamma_w)^2 + \gamma_w^2\right] I^{k(l+2)mn} \\ &+ 4\left[(d+\gamma_w)^2 + \gamma_w^2\right] I^{klm(n+2)} \end{aligned} \tag{4.128}$$

Note that, setting $\gamma_w = 0$ in (4.128), the expression reduces to that of (4.113) thus providing us with a valuable means to check parts of the expressions.

4.9.4 INT2K2: $-\langle \nabla_1 g_{\mu\nu,v} | \nabla_1 g_{\sigma\tau,w} \rangle$

If we calculate the kinetic energy integral using the expression on the right hand side of (4.108), we get a different T^1 integral, but the rest is equal.

$$\begin{aligned} T^1 = -\iint & \frac{\partial}{\partial x_1}\{G_k(x_1,a,A)G_m(x_2,c,C)\exp(-\gamma_v x_{12}^2)\} \\ & \times \frac{\partial}{\partial x_1}\{G_l(x_1,b,B)G_n(x_2,d,D)\exp(-\gamma_w x_{12}^2)\}\mathrm{d}x_1\mathrm{d}x_2 \end{aligned} \tag{4.129}$$

The two terms to be differentiated in this integral are given by

$$\begin{aligned}\frac{\partial}{\partial x_1}G_k\exp(-\gamma_v x_{12}^2) &= (kG_{k-1} - 2\gamma_v x_{12}G_k - 2aG_{k+1})\exp(-\gamma_v x_{12}^2)\\ \frac{\partial}{\partial x_1}G_l\exp(-\gamma_w x_{12}^2) &= (lG_{l-1} - 2\gamma_w x_{12}G_l - 2bG_{l+1})\exp(-\gamma_w x_{12}^2)\end{aligned} \tag{4.130}$$

If we multiply the two equations of (4.130)but leave the correlation factors out, we get

$$\begin{aligned}&(kG_{k-1} - 2\gamma_v x_{12}G_k - 2aG_{k+1})(lG_{l-1} - 2\gamma_w x_{12}G_l - 2bG_{l+1})\\ &\quad= klG_{k-1}G_{l-1} - 2bkG_{k-1}G_{l+1} - 2alG_{k+1}G_{l-1} + 4abG_{k+1}G_{l+1}\\ &\qquad- 2\gamma_w kx_{12}G_{k-1}G_l - 2\gamma_v lx_{12}G_kG_{l-1}\\ &\qquad+ 4a\gamma_w x_{12}G_{k+1}G_l + 4b\gamma_v x_{12}G_kG_{l+1}\\ &\qquad+ 4\gamma_v\gamma_w x_{12}^2G_kG_l\end{aligned} \tag{4.131}$$

To be able to express the T^1 integral as a linear combination of overlap integrals, we must rewrite x_{12} using either (4.118) or (4.119). In each case, we choose the formulation leading to least increase in individual angular momenta. When the resulting expressions are substituted back into (4.129), we get

$$\begin{aligned}T^1 =& - klI^{(k-1)(l-1)mn}\\ &+ 2\gamma_w kX_{AC}I^{(k-1)lmn} + 2\gamma_v lX_{BD}I^{k(l-1)mn}\\ &- 2\gamma_w kI^{(k-1)l(m+1)n} - 2\gamma_v lI^{k(l-1)m(n+1)}\\ &+ 2bkI^{(k-1)(l+1)mn} + 2alI^{(k+1)(l-1)mn}\\ &+ 2(\gamma_w k + \gamma_v l - 2\gamma_v\gamma_w X_{AC}X_{BD})I^{klmn}\\ &+ 4\gamma_w X_{BD}[\gamma_v I^{kl(m+1)n} - (a+\gamma_v)I^{(k+1)lmn}]\\ &+ 4\gamma_v X_{AC}[\gamma_w I^{klm(n+1)} - (b+\gamma_w)I^{k(l+1)mn}]\\ &- 4(ab + a\gamma_w + b\gamma_v + \gamma_v\gamma_w)I^{(k+1)(l+1)mn}\\ &- 4\gamma_v\gamma_w I^{kl(m+1)(n+1)}\\ &+ 4(a+\gamma_v)\gamma_w I^{(k+1)lm(n+1)}\\ &+ 4(b+\gamma_w)\gamma_v I^{k(l+1)(m+1)n}\end{aligned} \tag{4.132}$$

The linear combination of overlap integrals that give the T^2 integrals may be deduced directly from (4.132) saving us from doing tedious algebra all over again. To obtain T^2, we simply swap all occurrences of $1A$ by $2C$, $2B$ by $2D$, k by m and l by n. We also replace X_{AC} by $-X_{AC}$ and X_{BD} by $-X_{BD}$ as well as a by c and b by d.

Adding the resulting T^2 with the T^1 of (4.132), we get the T^{12} integrals that are

symmetric in the electron coordinates

$$
\begin{aligned}
T^{12} = & - klI^{(k-1)(l-1)mn} - mnI^{kl(m-1)(n-1)} \\
& + 2\gamma_w X_{AC}[kI^{(k-1)lmn} - mI^{kl(m-1)n}] \\
& + 2\gamma_v X_{BD}[lI^{k(l-1)mn} - nI^{klm(n-1)}] \\
& - 2\gamma_w mI^{(k+1)l(m-1)n} - 2\gamma_v nI^{k(l+1)m(n-1)} \\
& - 2\gamma_w kI^{(k-1)l(m+1)n} - 2\gamma_v lI^{k(l-1)m(n+1)} \\
& + 2bkI^{(k-1)(l+1)mn} + 2alI^{(k+1)(l-1)mn} \\
& + 2dmI^{kl(m-1)(n+1)} + 2cnI^{kl(m+1)(n-1)} \\
& + 2[(k+m)\gamma_w + (l+n)\gamma_v - 4\gamma_v\gamma_w X_{AC}X_{BD}]I^{klmn} \\
& + 4\gamma_w X_{BD}[(c+2\gamma_v)I^{kl(m+1)n} - (a+2\gamma_v)I^{(k+1)lmn}] \\
& + 4\gamma_v X_{AC}[(d+2\gamma_w)I^{klm(n+1)} - (b+2\gamma_w)I^{k(l+1)mn}] \\
& - 4[(a+\gamma_v)(b+\gamma_w) + \gamma_v\gamma_w]I^{(k+1)(l+1)mn} \\
& - 4[(c+\gamma_v)(d+\gamma_w) + \gamma_v\gamma_w]I^{kl(m+1)(n+1)} \\
& + 4[(a+\gamma_v)\gamma_w + (d+\gamma_w)\gamma_v]I^{(k+1)lm(n+1)} \\
& + 4[(b+\gamma_w)\gamma_v + (c+\gamma_v)\gamma_w]I^{k(l+1)(m+1)n}
\end{aligned}
\tag{4.133}
$$

Note that, the number of overlap integrals in this linear combination only increases from 16 to 23 when the integral is made symmetric, that is, when we calculate it using (4.133) rather than (4.132). We also note that, setting $\gamma_w = 0$ reduces (4.133) to (4.122).

Chapter 5

Symmetry-adapted integrals over many-electron basis functions

This chapter is based on a paper published by Dahle and Taylor in 2001 [47]. The two texts are identical in content, but the paper has been modified somewhat with respect notation and so forth, in order to fit in with the rest of the thesis.

5.1 Introduction

One of the strategies that can be used to reduce the computational effort in quantum-chemical calculations is to exploit molecular symmetry. Symmetry serves to reduce the number of non-vanishing terms that must be processed, as well as to relate quantities that are equal and thus need be calculated only once, reducing redundant work. The first stage of most calculations is the computation of integrals involving various operators over some form of one-electron basis. The molecular Hamiltonian comprises one- and two-electron operators, and for a one-electron basis this leads to one- and two-electron integrals. The greatest economy from symmetry in later stages of the calculation is obtained if the one-electron basis is symmetry-adapted, that is, the elements of this basis transform as basis functions for irreducible representations of the molecular point group. Integrals over such symmetry-adapted basis functions will be referred to as *symmetry-adapted integrals* in this work. Typically, the basis functions used in molecular calculations are centred on individual atoms, and thus symmetry-adapted basis functions must be formed as appropriate linear combinations of the original basis. We shall refer to the original basis functions as *atomic orbitals* (AOs) and the symmetry-adapted combinations as *symmetry orbitals* (SOs) in what follows.

Probably the most elegant and powerful technique for obtaining symmetry-adapted integrals is the method of double coset decompositions introduced by Davidson [48]. This approach unifies the enumeration of *symmetry-distinct integrals* —

the list of distinct integrals over AOs — with the construction of symmetry-adapted integrals by combining these distinct integrals with appropriate weights. In his original paper Davidson considered one- and two-electron integrals over *totally symmetric* operators $\mathcal{O}$, that is operators for which

$$G^{-1}\mathcal{O}G = \mathcal{O} \;\; \forall \;\; G \in \mathscr{G}, \tag{5.1}$$

where $\mathscr{G}$ is the molecular point group, of order g. Integrals over operators that are not totally symmetric have been discussed by Taylor [49], as have integrals over basis functions that are differentiated with respect to certain parameters, such as the coordinates of their centres [50].

In the current work we use basis functions that depend on the coordinates of more than one electron (see section 6.1). In AO basis these functions may be written in the general product form

$$g^{\mathrm{AO}}_{\mu\nu,w}(\mathbf{r}_1, \mathbf{r}_2, r_{12}) = f_w(r_{12})\chi_\mu(\mathbf{r}_1)\chi_\nu(\mathbf{r}_2) \tag{5.2}$$

where the correlation factor $f_w(r_{12})$ may be a Gaussian-type function having the form $\exp(-\gamma_w r_{12}^2)$ or simply the linear function r_{12}. For either form the correlation factor will be totally symmetric

$$Gf_w(r_{12}) = f_w(r_{12}) \;\; \forall \;\; G \in \mathscr{G}. \tag{5.3}$$

Even for a Hamiltonian comprising only one- and two-electron operators, a much richer set of integrals arises once two-electron basis functions are admitted. For the simplest treatment of electron correlation, second-order perturbation theory, at least three-electron integrals are needed, and as the correlation treatment becomes more elaborate four-electron integrals and even five-electron and higher integrals can appear. The scaling of the computational effort for these many-electron integrals is very great, and indeed it is difficult to see that a method that requires, say, four-electron integrals can find wide applicability. Nevertheless, for any desired order of integrals there are the same opportunities to use molecular symmetry to reduce the work needed to calculate the integrals and the work performed using them in later stages of the calculation. We have therefore generalised the double coset decomposition (DCD) procedure to integrals of any order. In this work we first review DCDs and their application to one- and two-electron integrals, in part to establish notation. We then develop a general formula, proved by induction. Finally, we use this general formula to discuss computational considerations and the example of three-electron integrals, which are programmed in the GREMLIN [51] integral package.

5.2 Symmetry-adapted integrals over one-electron basis functions

At the outset of this work we found ourselves in a notational quandary. There is a rather well-established notation for all of the various quantities that comprise the formulas for symmetry-adapted integrals, and all of the previous work has consistently used these conventions. Unfortunately, this notation makes heavy use of different alphabetical sequences for different quantities, and there are simply not enough letters in the (Roman) alphabet to do the job for higher-order integrals. After many attempts to use different fonts for different quantities and endless difficulties with multiple levels of subscripts, we have reluctantly concluded that a change in notation is unavoidable. In this section, therefore, we will briefly review one- and two-electron integrals over one-electron basis functions in the usual notation, and then make a transition to the more general notation we shall use later, in order to make clear the connections to earlier work.

In most computational implementations of DCDs, the molecular symmetry treated has been restricted to D_{2h} and its subgroups. These are Abelian groups in which each element is its own inverse. Further, any function on a given centre is taken into a single "image" function on another centre under any group operation, rather than a linear combination of functions. Let an AO on centre A be denoted f_{aA}, where all other properties of the AO (angular type, s, p_x, etc., Gaussian or Slater exponent or exponents and contraction coefficients) are subsumed into the index a. Then

$$G f_{aA} = p_a(G) f_{aG(A)}, \tag{5.4}$$

where $G(A)$ is the transformed centre obtained by applying G to centre A, and $p_a(G)$ is a parity factor (for D_{2h} and its subgroups) that depends on the angular behaviour of f_{aA}. An SO F^{α}_{aA} for irreducible representation (irrep) α can be constructed from this AO and its images by projection:

$$F^{\alpha}_{aA} = g^{-1} \sum_{G} \chi^{\alpha}(G) G f_{aA}, \tag{5.5}$$

where g is the order of the group and χ^{α} the group character for the desired irrep.

We note that there is some subgroup $\mathscr{U} \subset \mathscr{G}$ for which $U(A) = A$. $\mathscr{U}$ is known as the *stabiliser* of A. If the order of $\mathscr{U}$ is denoted u. Under the stabiliser AOs on A transform as

$$U f_{aA} = p_a(U) f_{aA}. \tag{5.6}$$

In fact, each f_{aA} transforms as a basis function for some irrep υ of the subgroup $\mathscr{U}$, giving

$$\sum_{U} \chi^{\upsilon}(U) p_a(U) = u. \tag{5.7}$$

Consider now another AO, f_{bB}, with stabiliser $\mathscr{V}$. From two subgroups $\mathscr{U}$ and $\mathscr{V}$ we can form *double cosets*

$$\mathscr{U}G\mathscr{V} \quad \forall \quad G \in \mathscr{G}. \tag{5.8}$$

Two double cosets are either distinct (no elements in common) or identical. Unlike cosets, $G\mathscr{U}$ or $\mathscr{U}G$, a given element of $\mathscr{G}$ may occur multiple times in a given double coset. For D_{2h} and its subgroups this degeneracy is independent of G in (5.8) and is given by the expression $\lambda_{\mathbb{G}} = |\mathscr{U} \cap \mathscr{V}|$. A group can thus be decomposed into distinct double cosets in this way: a double coset decomposition. By selecting a set of operators $\mathbb{R}$ chosen one from each *distinct* double coset, a sum over group elements can be replaced with a sum over elements of $\mathscr{U}$, $\mathscr{V}$, and $\mathbb{R}$, with a weighting factor of $\lambda_{\mathbb{R}}$. The elements of $\mathbb{R}$ are termed *double coset representatives*. For example

$$F^{\alpha}_{aA} = g^{-1}\lambda_{\mathbb{R}}^{-1} \sum_{U} \sum_{R} \sum_{V} \chi^{\alpha}(URV) URV f_{aA}. \tag{5.9}$$

Using DCDs, it is possible to write a symmetry-adapted integral as a sum of symmetry-distinct integrals with appropriate weight factors. The most important cases are totally symmetric one- and two-electron operators, whose integrals over SOs take the form

$$(F^{\alpha}_{aA}|O|F^{\alpha}_{bB}) = uvg^{-1}\lambda_{\mathbb{R}}^{-1} I_{\alpha\beta} \sum_{R} \chi^{\beta}(R) p_b(R) \left(f_{aA}|O|f_{bR(B)}\right) \tag{5.10}$$

and

$$\begin{aligned} \left(F^{\alpha}_{aA}F^{\beta}_{bB}|F^{\gamma}_{cC}F^{\delta}_{dD}\right) = g^{-3}uvwx I_{\alpha\beta\gamma\delta}\lambda_{\mathbb{T}}^{-1} \sum_{R} \sum_{S} \sum_{T} \chi^{\beta}(R)\chi^{\gamma}(T)\chi^{\delta}(TS) \\ \times \; p_b(R)p_c(T)p_d(TS) \left(f_{aA}f_{bR(B)}|f_{cT(C)}f_{dTS(D)}\right). \end{aligned} \tag{5.11}$$

Here the selection rule factor $I_{\alpha\beta\ldots}$ is given by

$$I_{\alpha\beta\ldots} = g^{-1} \sum_{G} \chi^{\alpha}(G)\chi^{\beta}(G)\ldots, \tag{5.12}$$

which vanishes unless the direct product $\alpha \otimes \beta \otimes \ldots$ contains the totally symmetric irrep, and the DCR $\mathbb{R}$, $\mathbb{S}$, and $\mathbb{T}$ are obtained from DCDs involving respectively $\mathscr{U}$ and $\mathscr{V}$, $\mathscr{W}$ and $\mathscr{X}$, and $\mathscr{U} \cap \mathscr{V}$ and $\mathscr{W} \cap \mathscr{X}$. $\mathscr{U}$, $\mathscr{V}$, $\mathscr{W}$ and $\mathscr{X}$ are the respective stabilisers of centres A, B, C, and D. $\mathscr{U} \cap \mathscr{V}$ is the stabiliser of the *pair* of centres A and B, and thus of the charge distribution $f_{aA}f_{bB}$, and similarly $\mathscr{W} \cap \mathscr{X}$ for $f_{cC}f_{dD}$. Finally, we may note that if the charge distribution $f_{cC}f_{dD}$ is the same as $f_{aA}f_{bB}$ the DCD defining $\mathbb{T}$ can be expanded, see Refs. [48] and [49].

We will later make use of a particular property of the selection rule (5.12) for D_{2h} and its subgroups. We note first that since all irreps are 1-dimensional, it follows that any direct product of irreps is 1-dimensional. Further, for the totally

symmetric irrep all characters are unity, of course, whereas for all other irreps half of the g characters are $+1$ and half are -1. The result is that when (5.12) is satisfied we have the stronger condition

$$\chi^{\alpha}(G)\chi^{\beta}(G)\ldots = 1 \;\; \forall \;\; G \in \mathscr{G}. \tag{5.13}$$

We may term this stronger condition a super-selection rule.

The formulas of (5.10) and 5.11 are relatively straightforward. Each comprises a set of summations over group operators that generate distinct AO integrals, and a product of selection rule and parity factor terms that give the weight with which each distinct integral contributes to the non-vanishing symmetry-adapted integrals. Computational implementation is also relatively straightforward: Almlöf' MOLECULE program [52] computed symmetry-adapted integrals in this way almost thirty years ago, although the author arrived at the necessary formulas via a quite different route. Several current integral programs use an implementation very close to that described here, including the program SEWARD [53] as well as the integral routines in the package DALTON [54].

As noted above the notation used in this brief review is exactly that introduced by Davidson [48], and in retrospect it can be seen to be profligate in its use of alphabetical symbols even though it is economical of subscripts and superscripts. In order to generalise these formulas to higher-order integrals we will have to revise the notation. Going forward, then, we will denote different AOs by $f[a_i, A_i]$, with different choice of subscripts i, and similarly the possible SOs derived from $f[a_i, A_i]$ and its images as $F[a_i, A_i, \alpha_p]$, where irreps are now labelled as α_p. Group operators in $\mathscr{G}$ will be denoted G_j; the stabiliser of centre A_i becomes $\mathscr{U}^i$ with elements U^i and order u_i. Here i, j and p are integers, counting from one up. The selection rule $I_{\alpha\beta\ldots}$ becomes $I(\alpha_1\alpha_2\ldots)$; the parity factors become $p_{a_i}(G_k)$. Each set of DCR will be denoted $\mathbb{T}^k$, with k again an integer counting index. It is essential to understand that the superscript notation denotes a specific *set* of DCR or a subgroup of $\mathscr{G}$, and not an *element* of a set. That is, the elements of the set $\mathbb{T}^1$ are labelled T^1, and similarly for an element $U^i \in \mathscr{U}^i$. The factor λ associated with each set of DCR is written as $\lambda_{\mathbb{T}^i}$.

In this notation the one- and two-electron symmetry-adapted integrals introduced above would become

$$\begin{aligned}\Big(F[a_1, A_1, \alpha_1] \,\Big|\, O \,\Big|\, F[a_2, A_2, \alpha_2]\Big) = \\ u_1 u_2 g^{-1} \lambda_{\mathbb{T}^1}^{-1} I(\alpha_1\alpha_2) \sum_{T^1} \chi^{\alpha_2}(T^1) p_{a_2}(T^1) \Big(f[a_1, A_1] \,\Big|\, O \,\Big|\, f[a_2, T^1(A_2)]\Big)\end{aligned} \tag{5.14}$$

and

$$\Big(F[a_1,A_1,\alpha_1]F[a_2,A_2,\alpha_2]\;\Big|\;F[a_3,A_3,\alpha_3]F[a_4,A_4,\alpha_4]\Big) =$$
$$g^{-3}u_1u_2u_3u_4I(\alpha_1\alpha_2\alpha_3\alpha_4)\lambda_{\mathbb{T}^3}^{-1}$$
$$\times\sum_{T^1}\sum_{T^2}\sum_{T^3}\chi^{\alpha_2}(T^1)\chi^{\alpha_3}(T^3)\chi^{\alpha_4}(T^3T^2)p_{a_2}(T^1)p_{a_3}(T^3)p_{a_4}(T^3T^2) \tag{5.15}$$
$$\times\Big(f[a_1,A_1]f[a_2,T^1(A_2)]\;\Big|\;f[a_3,T^3(A_3)]f[a_4,T^3T^2(A_4)]\Big).$$

Comparison with (5.10) and 5.11 should make all of the notational changes clear. With this notation we can now establish a general formula for symmetry-adapted integrals.

5.3 General formula for symmetry-adapted integrals

We begin by reminding the reader that we are using two-electron basis functions of the general form of (5.2). We then redefine the operator in a general many-electron integral so that the two-electron factors are absorbed into the operator. For example, if we have a two-electron operator $\mathcal{O}_{12}$ and the cyclic three-electron integral discussed in section 4.5.1 we get

$$\iiint\chi_\mu(r_1)\chi_\nu(r_2)\chi_\eta(r_3)f_v(r_{13})\mathcal{O}_{12}f_w(r_{23})\chi_\sigma(r_1)\chi_\tau(r_2)\chi_\xi(r_3)\mathrm{d}r_1\mathrm{d}r_2\mathrm{d}r_3, \tag{5.16}$$

we define a new operator

$$\mathcal{O}_{123}^{vw}=f_v(r_{13})\mathcal{O}_{12}f_w(r_{23}) \tag{5.17}$$

and rewrite the integral as

$$\iiint\chi_\mu(r_1)\chi_\nu(r_2)\chi_\eta(r_3)\mathcal{O}_{123}^{ab}\chi_\sigma(r_1)\chi_\tau(r_2)\chi_\xi(r_3)\mathrm{d}r_1\mathrm{d}r_2\mathrm{d}r_3, \tag{5.18}$$

Assuming for the moment that $\mathcal{O}_{12}$ is a totally symmetric operator, and that the correlation factors are also totally symmetric, it follows that the new operator $\mathcal{O}_{123}^{vw}$ is also totally symmetric. (We will relax these restrictions subsequently.) This is of course also true for any operator we construct in this way, irrespective of how many correlation factors appear. We can therefore write a general symmetry-adapted integral over such a many-electron operator (say n-electron) as

$$\int\ldots\int F[a_1,A_1,\alpha_1](r_1)\,F[a_3,A_3,\alpha_3](r_2)\ldots F[a_{2n-1},A_{2n-1},\alpha_{2n-1}](r_n)$$
$$\times\mathcal{O}_{12\ldots n}^{vw\ldots}F[a_2,A_2,\alpha_2](r_1)\,F[a_4,A_4,\alpha_4](r_2)\ldots F[a_{2n},A_{2n},\alpha_{2n}](r_n)\mathrm{d}r_1\ldots\mathrm{d}r_n, \tag{5.19}$$

where we have specifically indicated the electron coordinates associated with each symmetry orbital, or in a more convenient charge distribution notation as

$$\Big(F[a_1,A_1,\alpha_1]F[a_2,A_2,\alpha_2]\;\Big|\;F[a_3,A_3,\alpha_3]F[a_4,A_4,\alpha_4]\;\Big|\;\ldots\;\Big|\;F[a_{2n-1},A_{2n-1},\alpha_{2n-1}]F[a_{2n},A_{2n},\alpha_{2n}]\Big), \tag{5.20}$$

by analogy with the LHS of (5.15). Here each pair of symmetry orbitals between vertical bars involves a single electron coordinate: a charge distribution.

We now assert that the integral of (5.20) can be written in terms of distinct integrals over AO charge distributions as

$$\begin{aligned}
&\Big(F[a_1,A_1,\alpha_1]F[a_2,A_2,\alpha_2]\;\Big|\;F[a_3,A_3,\alpha_3]F[a_4,A_4,\alpha_4]\;\Big|\\
&\quad\cdots\;\Big|\;F[a_{2n-1},A_{2n-1},\alpha_{2n-1}]F[a_{2n},A_{2n},\alpha_{2n}]\Big) =\\
&g^{-(2n-1)}u_1\ldots u_{2n}I(\alpha_1\ldots\alpha_{2n})\lambda^{-1}_{\mathbb{T}^{2n-1}}\\
&\times\sum_{T^1}\cdots\sum_{T^{2n-1}}\chi^{\alpha_2}(T^1)\chi^{\alpha_3}(T^{2n-1})\chi^{\alpha_4}(T^{2n-1}T^2)\ldots\chi^{\alpha_{2n}}(T^{2n-1}T^{2n-2}\ldots T^n)\\
&\times p_{a_2}(T^1)p_{a_3}(T^{2n-1})p_{a_4}(T^{2n-1}T^2)\ldots p_{a_{2n}}(T^{2n-1}T^{2n-2}\ldots T^n)\\
&\times\Big(f[a_1,A_1]f[a_2,T^1(A_2)]\;\Big|\;f[a_3,T^{2n-1}(A_3)]f[a_4,T^{2n-1}T^2(A_4)]\;\Big|\\
&\cdots f[a_{2n-1},T^{2n-1}\ldots T^{n+1}(A_{2n-1})]f[a_{2n},T^{2n-1}\ldots T^n(A_{2n})]\Big).
\end{aligned} \tag{5.21}$$

In this expression we have adopted the following numbering convention for DCRs. DCR $\mathbb{T}^1$ generates distinct charge distributions from orbital pair $f[a_1,A_1]f[a_2,A_2]$, DCR $\mathbb{T}^2$ generates distinct charge distributions from $f[a_3,A_3]f[a_4,A_4]$, and so on through $\mathbb{T}^n$ for $f[a_{2n-1},A_{2n-1}]f[a_{2n},A_{2n}]$. The DCR $\mathbb{T}^{n+1}$ arises from a DCD involving the respective stabilisers of products $f[a_{2n-3},A_{2n-3}]f[a_{2n-2},T^{n-1}(A_{2n-2})]$ and $f[a_{2n-1},A_{2n-1}]f[a_{2n},T^n(A_{2n})]$, then DCR $\mathbb{T}^{n+2}$ arises from the stabilisers of $f[a_{2n-5},A_{2n-5}]f[a_{2n-4},T^{n-2}(A_{2n-4})]$ and the *quadruplet*

$$f[a_{2n-3},A_{2n-3}]f[a_{2n-2},T^{n-1}(A_{2n-2})]f[a_{2n-1},T^{n+1}(A_{2n-1})]f[a_{2n},T^{n+1}T^n(A_{2n})], \tag{5.22}$$

and so on recursively back to T^{2n-1}. We shall prove (5.21) by induction, by constructing from this n-electron integral and an additional pair of symmetry orbitals an $n+1$-electron symmetry-adapted integral.

For further manipulation we make some indexing changes in the integral, numbering orbitals from 3 to $2n+2$ instead of 1 to $2n$, with a corresponding shift in DCR numbering from 2 to $2n$ instead of 1 to $2n-1$. We also expand the selection rule (after re-sequencing) as

$$I(\alpha_3\ldots\alpha_{2n+2}) = g^{-1}\sum_i \chi^{\alpha_3}(G_i)\ldots\chi^{\alpha_{2n+2}}(G_i) \tag{5.23}$$

and multiply the AO integral by G_i for each term in this sum. The integral is a scalar and unaffected by this operation, of course. We thus rewrite (5.21) as

$$\begin{aligned}
&\Big(F[a_3,A_3,\alpha_3]F[a_4,A_4,\alpha_4]\;\Big|\;F[a_5,A_5,\alpha_5]F[a_6,A_6,\alpha_6]\;\Big|\\
&\quad\cdots\;\Big|\;F[a_{2n+1},A_{2n+1},\alpha_{2n+1}]F[a_{2n+2},A_{2n+2},\alpha_{2n+2}]\Big)=\\
&g^{-(2n)}u_3\ldots u_{2n+2}\sum_i\chi^{\alpha_3}(G_i)\ldots\chi^{\alpha_{2n+2}}(G_i)\lambda^{-1}_{\mathbb{T}^{2n}}\\
&\times\sum_{T^2}\cdots\sum_{T^{2n}}\chi^{\alpha_4}(T^2)\chi^{\alpha_5}(T^{2n})\chi^{\alpha_6}(T^{2n}T^3)\ldots\chi^{\alpha_{2n+2}}(T^{2n}T^{2n-1}\ldots T^{n+1})\\
&\times p_{a_4}(T^2)p_{a_5}(T^{2n})p_{a_6}(T^{2n}T^3)\ldots p_{a_{2n+2}}(T^{2n}T^{2n-1}\ldots T^{n+1})\\
&\times\Big(G_if[a_3,A_3]\,G_if[a_4,T^2(A_4)]\;\Big|\;G_if[a_5,T^{2n}(A_5)]\,G_if[a_6,T^{2n}T^3(A_6)]\;\Big|\\
&\cdots G_if[a_{2n+1},T^{2n}\ldots T^{n+2}(A_{2n+1})]\,G_if[a_{2n+2},T^{2n}\ldots T^{n+1}(A_{2n+2})]\Big).
\end{aligned}\tag{5.24}$$

We now wish to develop an $n+1$-electron integral by extending the existing integral with an additional charge distribution. In SOs we take this charge distribution to be $F[a_1,A_1,\alpha_1]F[a_2,A_2,\alpha_2]$, giving

$$\begin{aligned}
&\Big(F[a_1,A_1,\alpha_1]F[a_2,A_2,\alpha_2]\;\Big|\;F[a_3,A_3,\alpha_3]F[a_4,A_4,\alpha_4]\;\Big|\\
&\quad\cdots\;\Big|\;F[a_{2n+1},A_{2n+1},\alpha_{2n+1}]F[a_{2n+2},A_{2n+2},\alpha_{2n+2}]\Big)=\\
&g^{-(2n)}u_3\ldots u_{2n+2}\sum_i\chi^{\alpha_3}(G_i)\ldots\chi^{\alpha_{2n+2}}(G_i)\lambda^{-1}_{\mathbb{T}^{2n}}\\
&\times\sum_{T^2}\cdots\sum_{T^{2n}}\chi^{\alpha_4}(T^2)\chi^{\alpha_5}(T^{2n})\chi^{\alpha_6}(T^{2n}T^3)\ldots\chi^{\alpha_{2n+2}}(T^{2n}T^{2n-1}\ldots T^{n+1})\\
&\times p_{a_4}(T^2)p_{a_5}(T^{2n})p_{a_6}(T^{2n}T^3)\ldots p_{a_{2n+2}}(T^{2n}T^{2n-1}\ldots T^{n+1})\\
&\times\Big(F[a_1,A_1,\alpha_1]F[a_2,A_2,\alpha_2]\;\Big|\;G_if[a_3,A_3]\,G_if[a_4,T^2(A_4)]\;\Big|\\
&\quad\cdots G_if[a_5,T^{2n}(A_5)]\,G_if[a_6,T^{2n}T^3(A_6)]\;\Big|\\
&\quad\cdots G_if[a_{2n+1},T^{2n}\ldots T^{n+2}(A_{2n+1})]\,G_if[a_{2n+2},T^{2n}\ldots T^{n+1}(A_{2n+2})]\Big).
\end{aligned}\tag{5.25}$$

We expand the charge distribution $F[a_1,A_1,\alpha_1]F[a_2,A_2,\alpha_2]$ using a DCD as

$$\begin{aligned}
&F[a_1,A_1,\alpha_1]F[a_2,A_2,\alpha_2]=\\
&\quad g^{-2}u_1u_2\lambda^{-1}_{\mathbb{T}^1}\sum_j\sum_{T^1}\chi^{\alpha_1}(G_j)\chi^{\alpha_2}(G_j)\chi^{\alpha_2}(T^1)p_{a_2}(T^1)G_jf[a_1,A_1]\,G_jf[a_2,T^1(A_2)]
\end{aligned}\tag{5.26}$$

and substitute this into the RHS of (5.25) to give

$$\begin{aligned}
&\Big(F[a_1,A_1,\alpha_1]F[a_2,A_2,\alpha_2]\;\Big|\;F[a_3,A_3,\alpha_3]F[a_4,A_4,\alpha_4]\;\Big|\\
&\quad\cdots F[a_{2n+1},A_{2n+1},\alpha_{2n+1}]F[a_{2n+2},A_{2n+2},\alpha_{2n+2}]\Big)=\\
&g^{-(2n+2)}u_1\ldots u_{2n+2}\sum_i\sum_j\chi^{\alpha_1}(G_j)\chi^{\alpha_2}(G_j)\chi^{\alpha_3}(G_i)\ldots\chi^{\alpha_{2n+2}}(G_i)\lambda_{\mathbb{T}^1}^{-1}\lambda_{\mathbb{T}^{2n}}^{-1}\\
&\times\sum_{T^1}\sum_{T^2}\ldots\sum_{T^{2n}}\chi^{\alpha_2}(T^1)\chi^{\alpha_4}(T^2)\chi^{\alpha_5}(T^{2n})\\
&\times\chi^{\alpha_6}(T^{2n}T^3)\ldots\chi^{\alpha_{2n+2}}(T^{2n}T^{2n-1}\ldots T^{n+1})\\
&\times p_{a_2}(T^1)p_{a_4}(T^2)p_{a_5}(T^{2n})p_{a_6}(T^{2n}T^3)\ldots p_{a_{2n+2}}(T^{2n}T^{2n-1}\ldots T^{n+1})\\
&\times\Big(G_jf[a_1,A_1]\,G_jf[a_2,T^1(A_2)]\;\Big|\;G_if[a_3,A_3]\,G_if[a_4,T^2(A_4)]\;\Big|\\
&\quad\cdots G_if[a_5,T^{2n}(A_5)]G_if[a_6,T^{2n}T^3(A_6)]\;\Big|\\
&\quad\cdots G_if[a_{2n+1},T^{2n}\ldots T^{n+2}(A_{2n+1})]\,G_if[a_{2n+2},T^{2n}\ldots T^{n+1}(A_{2n+2})]\Big).
\end{aligned}\tag{5.27}$$

We replace G_i with G_jG_i using the Rearrangement Theorem and then rotate the AO integral by G_j, giving

$$\begin{aligned}
&\Big(F[a_1,A_1,\alpha_1]F[a_2,A_2,\alpha_2]\;\Big|\;F[a_3,A_3,\alpha_3]F[a_4,A_4,\alpha_4]\;\Big|\\
&\quad\cdots\;\Big|\;F[a_{2n+1},A_{2n+1},\alpha_{2n+1}]F[a_{2n+2},A_{2n+2},\alpha_{2n+2}]\Big)=\\
&g^{-(2n+2)}u_1\ldots u_{2n+2}\sum_i\sum_j\chi^{\alpha_1}(G_j)\ldots\chi^{\alpha_{2n+2}}(G_j)\chi^{\alpha_3}(G_i)\ldots\chi^{\alpha_{2n+2}}(G_i)\lambda_{\mathbb{T}^1}^{-1}\lambda_{\mathbb{T}^{2n}}^{-1}\\
&\times\sum_{T^1}\sum_{T^2}\ldots\sum_{T^{2n}}\chi^{\alpha_2}(T^1)\chi^{\alpha_4}(T^2)\chi^{\alpha_5}(T^{2n})\\
&\times\chi^{\alpha_6}(T^{2n}T^3)\ldots\chi^{\alpha_{2n+2}}(T^{2n}T^{2n-1}\ldots T^{n+1})\\
&\times p_{a_2}(T^1)p_{a_4}(T^2)p_{a_5}(T^{2n})p_{a_6}(T^{2n}T^3)\ldots p_{a_{2n+2}}(T^{2n}T^{2n-1}\ldots T^{n+1})\\
&\times\Big(f[a_1,A_1]f[a_2,T^1(A_2)]\;\Big|\;G_if[a_3,A_3]\,G_if[a_4,T^2(A_4)]\;\Big|\\
&\quad\cdots G_if[a_5,T^{2n}(A_5)]\,G_if[a_6,T^{2n}T^3(A_6)]\;\Big|\\
&\quad\cdots G_if[a_{2n+1},T^{2n}\ldots T^{n+2}(A_{2n+1})]\,G_if[a_{2n+2},T^{2n}\ldots T^{n+1}(A_{2n+2})]\Big).
\end{aligned}\tag{5.28}$$

We now use a DCD derived from the stabiliser (denoted $\mathscr{U}^I$) of $f[a_1,A_1]f[a_2,A_2]$ and the stabiliser (denoted $\mathscr{U}^{II}$) of the set of canters $\{A_3\ldots A_{2n+2}\}$, with DCR T^{2n+1}.

(We note that this notation for the stabilisers can be arbitrary since they do not appear in any final expressions.) From the properties of the stabilisers we have

$$U^{II} f[a_k, A_k] = p_{a_k}(U^{II}) f[a_k, A_k] \;\; \forall \;\; k \geq 3 \;\; \text{and} \;\; U^{II} \in \mathscr{U}^{II}. \tag{5.29}$$

We replace the sum over G_i using this DCD, and note that we can collapse the sum over G_j into the usual selection rule to give

$$\begin{aligned}
&\Big(F[a_1, A_1, \alpha_1] F[a_2, A_2, \alpha_2] \;\Big|\; F[a_3, A_3, \alpha_3] F[a_4, A_4, \alpha_4] \;\Big| \\
&\quad \cdots \;\Big|\; F[a_{2n+1}, A_{2n+1}, \alpha_{2n+1}] F[a_{2n+2}, A_{2n+2}, \alpha_{2n+2}] \Big) = \\
&g^{-(2n+1)} u_1 \dots u_{2n+2} I(\alpha_1 \dots \alpha_{2n+2}) \lambda^{-1}_{\mathbb{T}^1} \lambda^{-1}_{\mathbb{T}^{2n}} \lambda^{-1}_{\mathbb{T}^{2n+1}} \\
&\times \sum_{U^I} \sum_{U^{II}} \sum_{T^{2n+1}} \sum_{T^1} \sum_{T^2} \cdots \sum_{T^{2n}} \chi^{\alpha_3}(U^I) \cdots \chi^{\alpha_{2n+2}}(U^I) \\
&\times \chi^{\alpha_3}(U^{II}) \cdots \chi^{\alpha_{2n+2}}(U^{II}) \chi^{\alpha_3}(T^{2n+1}) \cdots \chi^{\alpha_{2n+2}}(T^{2n+1}) \\
&\times \chi^{\alpha_2}(T^1) \chi^{\alpha_4}(T^2) \chi^{\alpha_5}(T^{2n}) \chi^{\alpha_6}(T^{2n} T^3) \dots \chi^{\alpha_{2n+2}}(T^{2n} T^{2n-1} \dots T^{n+1}) \\
&\times p_{a_2}(T^1) p_{a_4}(T^2) p_{a_5}(T^{2n}) p_{a_6}(T^{2n} T^3) \dots p_{a_{2n+2}}(T^{2n} T^{2n-1} \dots T^{n+1}) \\
&\times \Big(f[a_1, A_1] f[a_2, T^1(A_2)] \;\Big|\; U^I T^{2n+1} U^{II} f[a_3, A_3] U^I T^{2n+1} U^{II} f[a_4, T^2(A_4)] \;\Big| \\
&\quad \cdots U^I T^{2n+1} U^{II} f[a_5, T^{2n}(A_5)] \, U^I T^{2n+1} U^{II} f[a_6, T^{2n} T^3(A_6)] \;\Big| \\
&\quad \cdots U^I T^{2n+1} U^{II} f[a_{2n+1}, T^{2n} \dots T^{n+2}(A_{2n+1})] \\
&\quad \times U^I T^{2n+1} U^{II} f[a_{2n+2}, T^{2n} \dots T^{n+1}(A_{2n+2})] \Big).
\end{aligned} \tag{5.30}$$

If we carry out the transformations by T^{2n+1} and U^{II} we obtain

$$
\begin{aligned}
&\Big(F[a_1,A_1,\alpha_1]F[a_2,A_2,\alpha_2]\,\Big|\,F[a_3,A_3,\alpha_3]F[a_4,A_4,\alpha_4]\,\Big|\\
&\quad\cdots\,\Big|\,F[a_{2n+1},A_{2n+1},\alpha_{2n+1}]F[a_{2n+2},A_{2n+2},\alpha_{2n+2}]\Big)=\\
&g^{-(2n+1)}u_1\dots u_{2n+2}I(\alpha_1\dots\alpha_{2n+2})\lambda_{\mathbb{T}^1}^{-1}\lambda_{\mathbb{T}^{2n}}^{-1}\lambda_{\mathbb{T}^{2n+1}}^{-1}\\
&\times\sum_{U^I}\sum_{U^{II}}\sum_{T^{2n+1}}\sum_{T^1}\sum_{T^2}\cdots\sum_{T^{2n}}\chi^{\alpha_3}(U^I)\cdots\chi^{\alpha_{2n+2}}(U^I)\\
&\times\chi^{\alpha_3}(U^{II})\cdots\chi^{\alpha_{2n+2}}(U^{II})\chi^{\alpha_3}(T^{2n+1})\cdots\chi^{\alpha_{2n+2}}(T^{2n+1})\\
&\times\chi^{\alpha_2}(T^1)\chi^{\alpha_4}(T^2)\chi^{\alpha_5}(T^{2n})\chi^{\alpha_6}(T^{2n}T^3)\dots\chi^{\alpha_{2n+2}}(T^{2n}T^{2n-1}\dots T^{n+1})\\
&\times p_{a_2}(T^1)p_{a_4}(T^2)p_{a_5}(T^{2n})p_{a_6}(T^{2n}T^3)\dots p_{a_{2n+2}}(T^{2n}T^{2n-1}\dots T^{n+1})\\
&\times p_{a_3}(T^{2n+1})\dots p_{a_{2n+2}}(T^{2n+1})p_{a_3}(U^{II})\dots p_{a_{2n+2}}(U^{II})\\
&\times\Big(f[a_1,A_1]f[a_2,T^1(A_2)]\,\Big|\,U^If[a_3,T^{2n+1}(A_3)]U^If[a_4,T^{2n+1}T^2(A_4)]\,\Big|\\
&\quad\cdots U^If[a_5,T^{2n+1}T^{2n}(A_5)]\,U^If[a_6,T^{2n+1}T^{2n}T^3(A_6)]\,\Big|\\
&\quad\cdots U^If[a_{2n+1},T^{2n+1}T^{2n}\dots T^{n+2}(A_{2n+1})]\\
&\quad\times U^If[a_{2n+2},T^{2n+1}T^{2n}\dots T^{n+1}(A_{2n+2})]\Big),
\end{aligned}
\tag{5.31}
$$

and by rotating the AO integral by U^I we obtain

$$
\begin{aligned}
&\Big(F[a_1,A_1,\alpha_1]F[a_2,A_2,\alpha_2]\,\Big|\,F[a_3,A_3,\alpha_3]F[a_4,A_4,\alpha_4]\,\Big|\\
&\quad\cdots\,\Big|\,F[a_{2n+1},A_{2n+1},\alpha_{2n+1}]F[a_{2n+2},A_{2n+2},\alpha_{2n+2}]\Big)=\\
&g^{-(2n+1)}u_1\dots u_{2n+2}I(\alpha_1\dots\alpha_{2n+2})\lambda_{\mathbb{T}^1}^{-1}\lambda_{\mathbb{T}^{2n}}^{-1}\lambda_{\mathbb{T}^{2n+1}}^{-1}\\
&\times\sum_{U^I}\sum_{U^{II}}\sum_{T^{2n+1}}\sum_{T^1}\sum_{T^2}\cdots\sum_{T^{2n}}\chi^{\alpha_3}(U^I)\cdots\chi^{\alpha_{2n+2}}(U^I)\\
&\times\chi^{\alpha_3}(U^{II})\cdots\chi^{\alpha_{2n+2}}(U^{II})\chi^{\alpha_3}(T^{2n+1})\cdots\chi^{\alpha_{2n+2}}(T^{2n+1})\\
&\times\chi^{\alpha_2}(T^1)\chi^{\alpha_4}(T^2)\chi^{\alpha_5}(T^{2n})\chi^{\alpha_6}(T^{2n}T^3)\dots\chi^{\alpha_{2n+2}}(T^{2n}T^{2n-1}\dots T^{n+1})\\
&\times p_{a_2}(T^1)p_{a_4}(T^2)p_{a_5}(T^{2n})p_{a_6}(T^{2n}T^3)\dots p_{a_{2n+2}}(T^{2n}T^{2n-1}\dots T^{n+1})\\
&\times p_{a_3}(T^{2n+1})\dots p_{a_{2n+2}}(T^{2n+1})p_{a_3}(U^{II})\dots p_{a_{2n+2}}(U^{II})p_{a_1}(U^I)p_{a_2}(U^I)\\
&\times\Big(f[a_1,A_1]f[a_2,T^1(A_2)]\,\Big|\,f[a_3,T^{2n+1}(A_3)]\\
&\quad\times f[a_4,T^{2n+1}T^2(A_4)]\,\Big|\,f[a_5,T^{2n+1}T^{2n}(A_5)]f[a_6,T^{2n+1}T^{2n}T^3(A_6)]\,\Big|\\
&\quad\cdots f[a_{2n+1},T^{2n+1}T^{2n}\dots T^{n+2}(A_{2n+1})]f[a_{2n+2},T^{2n+1}T^{2n}\dots T^{n+1}(A_{2n+2})]\Big).
\end{aligned}
\tag{5.32}
$$

Now, from the super-selection rule (5.13)

$$\chi^{\alpha_1}(G_i)\cdots\chi^{\alpha_{2n+2}}(G_i) = 1 \;\; \forall \;\; G_i \in \mathscr{G}, \tag{5.33}$$

or the integral would anyway vanish under (5.12). Hence

$$\chi^{\alpha_1}(G_i)\chi^{\alpha_2}(G_i) = \chi^{\alpha_3}(G_i)\cdots\chi^{\alpha_{2n+2}}(G_i). \tag{5.34}$$

In turn, then,

$$\begin{aligned}\sum_{U^I}&\chi^{\alpha_3}(U^I)\cdots\chi^{\alpha_{2n+2}}(U^I)p_{a_1}(U^I)p_{a_2}(U^I)\\ &= \sum_{U^I}\chi^{\alpha_1}(U^I)\chi^{\alpha_2}(U^I)p_{a_1}(U^I)p_{a_2}(U^I) = \lambda_{\mathbb{T}^1},\end{aligned} \tag{5.35}$$

(cf. (5.7) and Refs. [48, 49]), and also

$$\sum_{U^{II}}\chi^{\alpha_3}(U^{II})\cdots\chi^{\alpha_{2n+2}}(U^{II})p_{a_3}(U^{II})\cdots p_{a_{2n+2}}(U^{II}) = \lambda_{\mathbb{T}^{2n}}, \tag{5.36}$$

yielding finally

$$\begin{aligned}&\Big(F[a_1,A_1,\alpha_1]F[a_2,A_2,\alpha_2]\;\Big|\;F[a_3,A_3,\alpha_3]F[a_4,A_4,\alpha_4]\;\Big|\\ &\quad\cdots\;\Big|\;F[a_{2n+1},A_{2n+1},\alpha_{2n+1}]F[a_{2n+2},A_{2n+2},\alpha_{2n+2}]\Big) =\\ &g^{-(2n+1)}u_1\ldots u_{2n+2}I(\alpha_1\ldots\alpha_{2n+2})\lambda^{-1}_{\mathbb{T}^{2n+1}}\\ &\times\sum_{T^1}\cdots\sum_{T^{2n+1}}\chi^{\alpha_2}(T^1)\chi^{\alpha_3}(T^{2n+1})\chi^{\alpha_4}(T^{2n+1}T^2)\ldots\chi^{\alpha_{2n+2}}(T^{2n+1}T^{2n}\ldots T^{n+1})\\ &\times p_{a_2}(T^1)p_{a_3}(T^{2n+1})p_{a_4}(T^{2n+1}T^2)\ldots p_{a_{2n+2}}(T^{2n+1}T^{2n}\ldots T^{n+1})\\ &\times\Big(f[a_1,A_1]f[a_2,T^1(A_2)]\;\Big|\;f[a_3,T^{2n+1}(A_3)]f[a_4,T^{2n+1}T^2(A_4)]\;\Big|\\ &\cdots f[a_{2n+1},T^{2n+1}\ldots T^{n+2}(A_{2n+1})]f[a_{2n+2},T^{2n+1}\ldots T^{n+1}(A_{2n+2})]\Big).\end{aligned} \tag{5.37}$$

This is exactly the same as the formula of (5.21) except that the index ranges are larger. Hence coupling a new charge distribution into the n-electron integral formula has produced the same formula as extending the indices in the original formula. This, together with the observation that we obtain the correct result for the two-electron case from the one-electron case, is sufficient to establish (5.21) as correct by induction.

The above derivation assumed a totally symmetric many-electron operator in the integral, which allowed us to ignore the operator itself in our derivation. If the many-electron operator is of symmetry species α_0, say, not necessarily the totally

symmetric irrep, then provided the operator does not depend on any centre coordinates the only change to the symmetry-adapted integral formula is that the selection rule I becomes $I(\alpha_0\alpha_1\ldots\alpha_{2n})$, that is, includes an extra factor for α_0. This allows us to generalise the two-electron function $f_v(r_{12})$ in (5.2) to include angular terms like x_{12}. If $f_v(r_{12})$ depends on any centre coordinates, then in order to obtain an expression that involves no redundant terms in the summation it is necessary to introduce another double coset decomposition, based on the stabiliser of the centre(s) appearing in the operator and the stabiliser of *all* the charge distributions [48, 49].

5.4 Discussion

It is edifying to look at a specific case to illustrate the formulas. The most obvious new case would be a three-electron integral. We see from above that a cyclic three-electron integral over the electron repulsion operator would be given by

$$\begin{aligned}
&\iiint F[a_1,A_1,\alpha_1](r_1)\,F[a_3,A_3,\alpha_3](r_2)\,F[a_5,A_5,\alpha_5](r_3)\\
&\quad\times f_v(r_{13})r_{12}^{-1}f_w(r_{23})\\
&\quad\times F[a_2,A_2,\alpha_2](r_1)\,F[a_4,A_4,\alpha_4](r_2)\,F[a_6,A_6,\alpha_6](r_3)\mathrm{d}r_1\mathrm{d}r_2\mathrm{d}r_n\\
&\quad\equiv \Big(F[a_1,A_1,\alpha_1]F[a_2,A_2,\alpha_2]\;\Big|\;F[a_3,A_3,\alpha_3]F[a_4,A_4,\alpha_4]\;\Big|\\
&\qquad\cdots F[a_5,A_5,\alpha_5]F[a_6,A_6,\alpha_6]\Big)\\
&\quad= g^{-5}u_1u_2u_3u_4u_5u_6I(\alpha_1\alpha_2\alpha_3\alpha_4\alpha_5\alpha_6)\lambda_{\mathbb{T}^5}^{-1}\\
&\qquad\times\sum_{T^1}\sum_{T^2}\sum_{T^3}\sum_{T^4}\sum_{T^5}\chi^{\alpha_2}(T^1)\chi^{\alpha_3}(T^5)\chi^{\alpha_4}(T^5T^2)\chi^{\alpha_5}(T^5T^4)\chi^{\alpha_6}(T^5T^4T^3)\\
&\qquad\times p_{a_2}(T^1)p_{a_3}(T^5)p_{a_4}(T^5T^2)p_{a_5}(T^5T^4)p_{a_5}(T^5T^4T^3)\\
&\qquad\times\Big(f[a_1,A_1]f[a_2,T^1(A_2)]\;\Big|\;f[a_3,T^5(A_3)]f[a_4,T^5T^2(A_4)]\;\Big|\\
&\qquad\cdots f[a_5,T^5T^4(A_5)]f[a_6,T^5T^4T^3(A_6)]\Big)
\end{aligned}\tag{5.38}$$

This expression is long but not complicated. It comprises a selection rule, some numerical factors which weight each integral according to the irreps it contributes to, with what phase, and how many equivalent integrals are accounted for. The various DCR ensure first that only distinct charge distributions appear, and then that only distinct *combinations* of those charge distributions appear. The five sets of DCR arise as follows. $\mathbb{T}^1$, $\mathbb{T}^2$ and $\mathbb{T}^3$ generate distinct charge distributions from the original pairs $f[a_1,A_1]f[a_2,A_2]$, $f[a_3,A_3]f[a_4,A_4]$ and $f[a_5,A_5]f[a_6,A_6]$, respectively. Then $\mathbb{T}^4$ generates distinct quadruplets from $f[a_3,A_3]f[a_4,T^2(A_4)]$

and $f[a_5, A_5]f[a_6, T^3(A_6)]$, and finally $\mathbb{T}^5$ generates distinct hextuplets from pairs $f[a_1, A_1]f[a_2, T^1(A_2)]$ and $f[a_3, A_3]f[a_4, T^2(A_4)]f[a_5, T^4(A_5)]f[a_6, T^4T^3(A_6)]$. There is no structural difference between the three-electron formula and the two-electron formula. For example, DALTON [54] includes a matrix multiplication formulation of the two-electron integral formula, developed by Helgaker (unpublished), and we have had little trouble implementing the appropriate loop structure and formulas to extend this to the case of three-electron integrals over Gaussian-type geminal basis functions.

In applications such as MP2 calculations with correlation factors of Gaussian or linear r_{12} type, three- and perhaps four-electron integrals appear in partial trace expressions where they are contracted with the SCF density matrix. It is possible to simplify symmetry processing in such trace calculations somewhat by defining new density matrices that include some of the phase and weighting factors [49].

5.5 Conclusions

A general formula has been developed for computing integrals over symmetry-adapted basis functions to any order, extending existing work for one- and two-electron integrals. The formula expresses integrals over symmetry-adapted two-electron basis functions of the general form of (5.2) in terms of symmetry-distinct integrals. The formula has been proved by induction and holds for arbitrarily many electrons.

Chapter 6

Computational aspects

Up to this point we have only discussed theoretical aspects of GTG theory. In this chapter, we shall consider the implementation of this theory made in the GREMLIN and DALTON programs [51, 54]. We do not consider real applications, however, but discuss computational aspects like integral timings, parallelisation, and integral prescreening. We shall also investigate the quality of the Gaussian-type correlation factors (GCFs) we have used for applications, and see how energies and strong orthogonality measures change with different values of the level-shift parameter η. We start by describing the different two-electron basis sets and one-electron basis sets we have used, and develop notation that will be used throughout this work.

6.1 Two-electron basis sets of GTGs

We started section 3.4.3 by stating that pair functions must be expanded in r_{12}-dependent functions if pair energies close to the limit are to be obtained. A set of such functions, referred to as geminals, were introduced in (3.75) and defined as

$$g^{\mathcal{P}}_{pq,v}(\mathbf{r}_1, \mathbf{r}_2, r_{12}) = f_v(r_{12})\phi^{\mathcal{P}}_{pq}(\mathbf{r}_1, \mathbf{r}_2) \tag{6.1}$$

where $\mathbf{r}_1$ and $\mathbf{r}_2$ are the positions of electron 1 and 2, respectively, and r_{12} is the relative distance between the two electrons. The function $\phi^{\mathcal{P}}_{pq}$, is a symmetry-adapted pair of orbitals, and $f_v(r_{12})$ is a correlation factor "tieing" the orbitals together into a geminal.

For practical reasons we have used the general MO indices p and q in the orbital product (6.1), but this is not necessarily an optimal choice. In this section, we suggest different forms for both the orbital product and the correlation factor. For the orbital product, this includes replacing p and q by less general indices, but may also include replacing the MOs by other one-electron functions like AOs or approximated MOs. We therefore reformulate (6.1) as

$$g_{xy,v}(\mathbf{r}_1, \mathbf{r}_2, r_{12}) = f_v(r_{12})\tilde{\phi}_{xy}(\mathbf{r}_1, \mathbf{r}_2) \tag{6.2}$$

where we for simplicity have left out the parity-adaption. In this equation xy are non-specified indices, and the tilde indicates that the product of one-electron functions no longer have to be the Hartree-Fock (HF) orbitals. Note that, while a tilde in the previous chapter denoted a near complete basis set, this is not the case here. Rather, the one-electron functions used to construct $\tilde{\phi}_{xy}$ are expanded in a basis set that is *smaller* than the basis set used to describe Hartree–Fock orbitals.

Before we discuss (6.2) in more detail, recall from chapter 1 that according to the electron-electron cusp condition [4], the wave function of a two-electron system behaves as

$$\Psi(\mathbf{r}_1, \mathbf{r}_2, r_{12}) = \Psi(\mathbf{r}_c, \mathbf{r}_c, 0) \left\{ 1 + \frac{1}{2} r_{12} + \mathcal{O}(r_{12}^2) \right\} \tag{6.3}$$

when the two electrons are close in space. The mathematical form of (6.3), gives rise to the well-known Coulomb hole shape of the wave function (see Figure 1.2). We assume that the Hartree–Fock wave function gives a reasonable description of $\Psi(\mathbf{r}_c, \mathbf{r}_c, 0)$. In order to be able to describe the Coulomb hole, therefore, we need the first-order wave function correction to behave as

$$u_{ij}(\mathbf{r}_c, \mathbf{r}_c, r_{12}) \sim r_{12} \Psi(\mathbf{r}_c, \mathbf{r}_c, 0) \tag{6.4}$$

Leaving the virtual orbital approximation out of the current discussion, the pair function in (6.4) may be written as a linear combination of geminals

$$u_{ij}(\mathbf{r}_c, \mathbf{r}_c, r_{12}) = \sum_v c_v f_v(r_{12}) \sum_{xy} c_{ij}^{xy} \tilde{\phi}_{xy}(\mathbf{r}_1, \mathbf{r}_2) \tag{6.5}$$

If we compare (6.4) with (6.5) we see that the *sum* of correlation factors have to scale linearly with r_{12} for small inter-electronic distances and not necessarily the individual terms. At first sight, the obvious expansion for the correlation factor is the one-term expansion

$$f(r_{12}) = r_{12} \tag{6.6}$$

Although a correlation factor of the form (6.6) looks mathematically simple, there are certain problems connected with it. First of all, it leads to three-electron integrals that cannot be expressed in closed form, and this is very inconvenient if, for instance, energy derivatives are to be obtained. Next, the linear term does not level off as the inter-electronic distance increases, but goes to infinity as the two electrons are moved infinitely far apart. This deficiency may be reduced or removed completely, however, if a damping factor is introduced. Samson and Klopper [55], for instance, have proposed a Gaussian-type damping factor, and using this, their correlation factor takes the form

$$f(r_{12}) = r_{12} \exp(-\gamma r_{12}^2) \tag{6.7}$$

Rather than using the Gaussian-type function as a damping factor only, it may also be used directly as a correlation factor, that is, we may write

$$f_v(r_{12}) = \exp(-\gamma_v r_{12}^2) \tag{6.8}$$

Such Gaussian-type correlation factors (GCFs), originally introduced by Boys [56] and Singer [57], go to zero as the electrons are moved infinitely far apart and not to infinity. Moreover, all many-electron integrals can be expressed in either closed form, or in a form that involves a one-dimensional numerical integration or functional approximation [46, 56, 58]. A drawback, however, is that the Gaussian-type correlation factor does not have the correct linear behaviour for small values of r_{12}. Although, this behaviour cannot be obtained with a single GCF, a linear combination of GCFs can be made arbitrarily close to r_{12}, by including sufficiently many terms in the expansion

$$r_{12} = 1 + \lim_{v\to\infty} \sum_v c_v \exp(-\gamma_v r_{12}^2) \tag{6.9}$$

This relationship, which is similar to the expansion of a single STO using several GTOs, has been studied by Persson and Taylor [59] and is investigated further in section 6.9. A drawback of using a linear combination of GCFs, is that the number of many-electron integrals grows as the square of the number of GCFs. For this approach to be successful, therefore, a short expansion must be sufficient.

Comparing (6.4) with (6.5) again, we see that the sum of functions $\tilde{\phi}_{xy}$ should be equal to the wave function when $\mathbf{r}_1 = \mathbf{r}_2 = \mathbf{r}_c$.

$$\Psi(\mathbf{r}_c, \mathbf{r}_c, 0) = \sum_{xy} c_{ij}^{xy} \tilde{\phi}_{xy}(\mathbf{r}_c, \mathbf{r}_c) \equiv G_{ij}^{\mathrm{xy}}(\mathbf{r}_c) \tag{6.10}$$

where we have introduced the function G^{xy} to simplify equations.

Since our basic knowledge about $\Psi(\mathbf{r}_c, \mathbf{r}_c, 0)$ is that provided by the Hartree–Fock orbitals, a first approximation to G^{xy} may be

$$G_{ij}^{\mathrm{ij}} = \phi_{ij} \tag{6.11}$$

and this is, essentially, the ansatz used in the MP2-R12 implementations [60–62] which are based on the linear correlation factor. A deficiency with the functional form of (6.11), is that it is not invariant to rotations among the occupied orbitals. The energy obtained using the canonical Hartree–Fock orbitals may therefore be different from the energy obtained with some non-canonical orbitals. The simplest way to remedy this is to include all occupied orbitals in G_{ij}^{xy}, that is

$$G_{ij}^{\mathrm{kl}} = \sum_{k\le l} \tilde{\phi}_{kl} c_{ij}^{kl} \tag{6.12}$$

and this was first suggested by Klopper [63]. Note that the tilde is back in the expression again to emphasise that the orbital product ϕ_{kl} does not have to be constructed from the exact Hartree–Fock orbitals.

Since the Hartree–Fock wave function is not equal to the exact wave function, it may be far to restrictive to limit the sum in (6.12) to occupied orbitals only. As

an alternative, we may include the complete basis set in the expansion of G^{xy}. This gives

$$G_{ij}^{\mathrm{pq}} = \begin{cases} \sum\limits_{p \le q} \tilde{\phi}_{pq} c_{ij}^{pq}, & \text{MO formulation} \\ \sum\limits_{p \le q} \tilde{\chi}_{pq} c_{ij}^{pq}, & \text{AO formulation} \end{cases} \tag{6.13}$$

where χ_{pq} is the product of the atomic orbitals χ_p and χ_q. Note that, as all basis function are used, the space spanned by a pair of MOs is also spanned by some linear combination of pairs of AOs. And by using the AO formulation, we may avoid the CPU intensive MO transformations.

Bukowski *et al.* [64] have combined the AO formulation of (6.13) with Gaussian-type correlation factors to a Gaussian-type geminals (GTG) formulation of MP2 theory. In contrast to the linear r_{12} implementations mentioned above, these authors have expanded the pair functions in geminals only and do not use the virtual orbital expansion at all. Furthermore, they only use *s*-, *p*-, and *d*-orbitals in their basis sets, but compensate for this by optimising all nonlinear parameters (also orbital centres) present in the geminals. The GTG-MP2 implementation of Bukowski also differs from the MP2-R12 implementations in the way pair functions are optimised. While the GTGs are optimised using the WO functional, that is, following the far left path of Figure 3.2, the MP2-R12 implementations use the SO functional with a modified Q_{occ} operator, that is, they follow the far right path of Figure 3.2.

While (6.13) allows for a very flexible description of pair functions, it is also hampered with severe deficiencies. First, if we multiply an entire basis set by itself, linear dependencies may be encountered even for relatively small basis sets, and if we add flexible correlation factors $f_v(r_{12})$, the problem will increase. Another problem with the G^{pq} ansatz, is that the number of elements in the matrix $\mathbf{H}_{\mathrm{gg}}$ in (3.83), grows as the forth power of the basis set size. Even though we are able to hold large equation systems in memory, we are likely to get convergence problems when we try to solve them. The form proposed for G^{xy} in (6.13), will therefore in our case probably be of limited use only.

To alleviate the size problems and at the same time maintain some flexibility in the description of the pair function, we may restrict one of the general indices in $\tilde{\phi}_{pq}$ to run over occupied orbitals only,

$$G_{ij}^{\mathrm{kq}} = \begin{cases} \sum\limits_{k \le q} \tilde{\phi}_{kq} c_{ij}^{kq}, & \text{MO formulation} \\ \sum\limits_{kq} \tilde{\varphi}_k \tilde{\chi}_q c_{ij}^{kq}, & \text{AO formulation} \end{cases} \tag{6.14}$$

where we once again have both an MO and an AO formulation available. Note, however, that the AO formulation includes more functions than the MO formulation since the summation is not restricted. The AO formulation, therefore, includes redundant functions.

Both formulations of G^{kq} are invariant to rotations among the occupied orbitals, and this is also true for the G^{pq} ansätze. Moreover, the AO approaches are less CPU demanding than the MO approaches and may also be used relatively straightforwardly with local methods (LMP2). The MO approaches, on the other hand, have the advantage that when we do a G^{pq} calculation, for instance, the integrals needed for both G^{kq} and G^{kl} calculatons are directly available. We may therefore do calculations for three models at the cost of one.

The integral program GREMLIN [51] which has been used for all MP2 calculations presented in this work, can handle geminals constructed from Gaussian-type correlation factors and all the above G^{xy} ansätze. GREMLIN is a module of the DALTON [54] program.

6.2 AO basis sets and notation

If we do a MP2-GTG calculation using the G^{ij} option, this calculation is in the following referred to as using the *ij-ansatz*. Likewise, if we use the G^{kl} option, the calculation is referred to as using the *kl-ansatz*, and so forth. As noted in section 6.1, the kq- and pq-ansätze have both an MO and an AO formulation. Unless otherwise stated, we assume that the MO formulation has been chosen for the former, and that the AO formulation has been chosen for the latter. Note that, whenever we refer to one of the ansätze above, it is implicitly understood that the virtual orbital expansion is also included in the expansion of the pair function.

Whether or not we choose the MO formulation, the different ansätze need to be expanded in some AO basis. Dunning and coworkers [65–69] have developed a number of correlation-consistent basis sets which give a systematic improvement in the description of the electronic structure towards the limit of an infinite basis set, at least for the correlation energy. These basis sets are widely used throughout the quantum chemistry community, and shall be our number one choice. It should be pointed out, however, that the Dunning basis set have been optimised for orbital expansions and not geminal expansions.

Most of the Dunning basis sets are conveniently retrieved from the *Extensible Computational Chemistry Environment Basis Set Database* [70], also known as the EMSL Gaussian Basis Set Library. Wherever possible, basis sets used in the current work have been obtained from this library.

The original correlation-consistent basis sets of Dunning are denoted cc-pVXZ, where $X \in$\{D, T, Q, 5, 6\} specifies the zeta level ranging from double through sextuple zeta. X is usually referred to as the cardinal number of the basis set. For some molecular properties, the original set of functions does not perform sufficiently well, and diffuse or contracted functions must be included. Correlation-consistent basis sets that have been augmented with diffuse functions are called aug-cc-pVXZ, while basis sets given additional core functions are denoted cc-pCVXZ. A basis set

may also be augmented with both diffuse and contracted functions, in which case the basis sets are called aug-cc-pCVXZ.

The cc-pVXZ basis sets are composed as principal expansions [1], meaning that they belong to either of the following orbital spaces $(2s1p)$, $(3s2p1f)$, $(4s3p2f1g)$, and so forth. In order to explore convergence for partial-wave type expansions as well as principal expansions, we often truncate the correlation-consistent basis sets at some angular momentum level. The orbital types still present in the basis set, are given in parentheses after the basis set name. Thus, for hydrogen and helium, cc-pVTZ(sp) denotes a basis set where the d-orbital is excluded, while for the second period elements it denotes a basis set where the $2d1f$ part is excluded. In case a system consists of atoms having different expansions, as with hydrogen and oxygen, both expansions must be given in parentheses. We do this by writing the expansion for the heavier atom first. Thus, cc-pVTZ(spd,sp) denotes a basis set where we have excluded the f-orbital for oxygen and the d-orbital for hydrogen.

Unfortunately, Dunning and co-workers did not include lithium and beryllium in their original work. Although there are cc-pVXZ basis sets available for both lithium and beryllium [65, 71], and cc-pCVXZ basis sets for lithium [65], it is not clear how to augment these sets with diffuse functions. This has encouraged us to look for other basis sets when describing systems containing these elements. Because of the large number of basis functions available, we have chosen to use the *Roos augmented triple zeta ANO* basis set [72] as well as a smaller basis set also presented by Roos and co-workers [73]. These basis sets, which are extensions to basis sets originally made by van Duijneveldt [74], are given in appendix C.

6.3 GCF expansions

Even though the range of useful correlation factors $f_v(r_{12})$ are more limited than the range of of useful AO basis sets, we may still vary both the number of terms in the expansion as well as the exponent in each term. It is of particular interest to investigate whether a given GCF expansion may be used to recover high-quality correlation energies for all systems. If this turns out to be the case, GTG-MP2 calculations become "black box" calculations which is important if the method is to become widely used. In this section we shall try and find such an expansion and shall use this expansion in all subsequent calculations.

In their original work, Persson and Taylor [59] used 6, 9, and 15 terms expansions of GCFs which all fitted the linear r_{12} nicely within the fitting region. In these expansions the exponents γ_v were simply chosen as an even-tempered sequence $a/3^v$, where a was a power of three. We assimilate this sequence in the current work and make the *ad hoc* assumption that a ratio of 3 gives GCF expansions that are sufficiently saturated within the fitting region. In section 6.9 we show cusp fit plots indicating that this is indeed the case.

A question left, however, is how many terms we should include in the GCF expansion and what the largest and smallest exponents should be. Clearly, the exponents should not be chosen very small, as this makes the corresponding correlation factors close to one. Geminals constructed from such GCFs are essentially products of orbitals and cannot, by the Brillouin theorem, contribute much to the correlation energy unless both orbitals are virtual. Moreover, the part of the GCF expansion containing small exponents describes the outer part of the Coulomb hole, a region that is already described by the simpler virtual orbital expansion (VOE). This leads us to making another *ad hoc* assumption, namely that $\gamma_{\min} = 1/9$ is an appropriate choice for the most diffuse exponent.

Although, the VOE part of the pair function describes the outer part of the Coulomb hole properly, it cannot describe the innermost parts. This is also the reason for introducing explicitly correlated basis functions in the first place. It is therefore important to ensure that the GCF expansion includes sufficiently high exponents.

In Tables 6.1 and 6.2 we have presented energies obtained for the neon atom and the water molecule using different GCF expansions, all having 1/9 as the most diffuse exponent.[1] Both systems were described with two different basis sets in order to check whether the energy response to different GCF expansions are independent or not of the chosen AO basis set. Within each basis set we start by giving the correlation energy for a GCF expansion of zero length. For such expansions the pair function reduces to an expansion of virtual orbitals, and the energy for each ansatz become identical to the conventional MP2 energy for the basis set in question. This is observed in both tables.

Investigating the neon energies presented in Table 6.1, we see that the energy hardly changes for the kl- and kq-ansätze as the most diffuse GCF is included in the expansion, whereas the the energy makes a significant jump for the pq-ansatz. As commented above, GTGs made from diffuse GCFs will essentially be orbital products, and from conventional MP2 and the Brillouin theorem we know that only products of virtual orbitals may contribute to the energy. Only the pq-ansatz contains such products thus explaining the difference.

As more contracted GCFs are included in the expansion, the energies for the kl- and kq-ansätze are also improved. For the former, however, we note that whereas the energy increases somewhat when going from one to two GCFs for basis set cc-pVDZ, there is hardly any improvement for the basis set aug-cc-pCVTZ(spd). This is indicated in Table 6.1 using numbers written in bold face. For the larger basis set, therefore, the energy recovered by the two most diffuse GCFs has already been recovered by the virtual orbital expansion.

The third and fourth terms in the GCF expansion have exponents 1.0 and 3.0

[1]The level-shift parameter was set to $\eta = 0.1$ for all calculation. This choice is discussed in more detail in section 6.4.

Table 6.1: All electron second-order correlation energies ($-E/\mathrm{mE_h}$) for the neon atom using basis sets A:cc-pVDZ and B:aug-cc-pCVTZ(spd) and different lengths of the GCF expansion. GCF exponents are taken from the sequence $\{\frac{1}{9}, \frac{1}{3}, 1, \ldots, 729\}$.

Basis	#GCFs	KL	KQ	PQ
A	0	**187.567**	**187.567**	**187.567**
A	1	**187.655**	**187.758**	206.325
A	2	196.870	240.497	280.170
A	3	229.085	294.675	307.021
A	4	274.410	320.640	331.566
A	5	290.017	335.968	345.550
A	6	296.844	343.290	352.874
A	7	299.810	345.784	355.252
A	8	300.708	346.621	356.144
A	9	300.976	346.932	356.372
B	0	**309.078**	**309.078**	**309.078**
B	1	**309.078**	**309.126**	335.423
B	2	**309.368**	337.466	364.538
B	3	319.221	362.224	376.800
B	4	337.957	374.004	382.839
B	5	346.125	380.437	385.912
B	6	350.167	383.779	387.156
B	7	352.651	385.416	387.591
B	8	353.695	386.062	387.905
B	9	353.914	386.232	388.008

and make significant energy contributions for all three ansätze. As more GCFs are included, the energy contribution gradually decreases, and when we have reached a nine terms expansion, all energies are probably converged to within $0.1\,\mathrm{mE_h}$. An investigation shows that the last three GCFs included in the expansion mainly improve on the $1s1s$ singlet energy (ϵ^1_{1s1s}).

Proceeding to the water calculations presented in Table 6.2, we see that the discussion made for neon applies equally well to water.[2] We therefore decide to use the sequence $\{729, 243, \ldots, 1/9\}$ for all applications, and shall in the following refer to these exponents as the *standard set*. Calculations with GCF expansions differing from the standard expansion are left for future studies.

[2]Due to memory requirements, we had to replace the four d-orbitals given for oxygen in the aug-cc-pCVTZ(spd) basis set by the single d-orbital taken from cc-pVDZ when using the pq-ansatz.

Table 6.2: All electron second-order correlation energies ($-E/\mathrm{mE_h}$) for the water molecule using basis sets A:cc-pVDZ and B:aug-cc-pCVTZ(spd,sp) and different lengths of the GCF expansion. GCF exponents are taken from the sequence $\{\frac{1}{9}, \frac{1}{3}, 1, \ldots, 729\}$.

Basis	#GCFs	KL	KQ	PQ
A	0	**203.960**	**203.960**	**203.960**
A	1	**204.108**	**204.336**	229.849
A	2	214.375	258.213	283.429
A	3	256.603	300.181	311.034
A	4	282.174	318.251	328.142
A	5	291.235	328.599	337.294
A	6	295.723	332.119	340.936
A	7	297.408	333.661	342.411
A	8	297.943	334.166	342.837
A	9	298.068	334.279	342.966
B	0	**300.215**	**300.215**	**300.215**
B	1	**300.215**	**300.321**	306.818
B	2	**300.898**	326.684	339.975
B	3	315.805	344.656	350.890
B	4	328.492	352.240	356.551
B	5	332.665	356.029	358.705
B	6	335.495	358.090	359.524
B	7	337.086	359.207	359.917
B	8	337.637	359.563	360.115
B	9	337.753	359.651	360.141

6.4 The level-shift parameter

The GTG-MP2 energy is not only dependent on the AO and GCF basis sets. Equations (3.77) and (3.78) show that the optimisation of pair functions, and therefore also the pair energy, depends on the level-shift parameter η as well. This dependency is discussed in some detail in appendix A and has also been covered by Szalewicz and co-workers in the context of MP2 energies [13] and MP3 energies [75]. Szalewicz showed that, as we increase the level-shift parameter, the pair functions become more strongly orthogonal to the occupied orbitals, but at the expense of higher MP2 energies. If we decrease the value for the level-shift parameter, on the other hand, we get better MP2 energies but at the expense of losing orthogonality.

Whereas pair functions have to be strongly orthogonal to the occupied orbitals

Table 6.3: All-electron second-order correlation energies ($-E/\mathrm{mE_h}$) and SO measures for the neon atom for different values of the level-shift parameter η. Basis A is cc-pVDZ and basis B is aug-cc-pCVTZ(spd). See text for further details.

Basis	$\log_{10}\eta$	KL	SO	KQ	SO	PQ	SO
A	+3	252.462	1.94	315.307	2.62	336.135	2.64
A	+2	282.105	1.45	335.286	2.06	348.959	2.08
A	+1	297.655	1.20	344.908	1.79	355.068	1.82
A	0	300.625	1.15	346.721	1.74	356.235	1.77
A	−1	300.976	1.15	346.932	1.72	356.372	1.76
A	−2	301.014	1.13	346.954	1.66	356.386	1.72
A	−3	301.048	0.77	346.960	1.18	356.390	1.26
B	+3	334.630	4.05	384.519	4.91	387.811	11.59
B	+2	345.706	3.07	385.761	4.19	387.926	10.67
B	+1	352.384	2.60	386.162	3.94	387.996	10.28
B	0	353.749	2.51	386.225	3.89	388.008	10.23
B	−1	353.914	2.49	386.232	3.89	388.008	10.39
B	−2	353.932	2.44	386.232	3.81	388.009	10.22
B	−3	353.940	1.48	386.232	2.47	388.009	9.67

if we want to calculate MP3 energies, such orthogonality is not important for MP2, as the SO operator, Q_{occ}, is present in the energy expression. For MP2, therefore, the level-shift parameter should be chosen "as small as possible", which means zero if the basis set is complete (cf. appendix A). For finite basis sets, however, we have to be more careful as the operator $\tilde{f}(1) + \tilde{f}(2) - \varepsilon_i - \varepsilon_j$ of equation (3.79) is only guaranteed to be positive definite if the level-shift term Λ_{ij} is sufficiently large. According to (3.78), we may increase the value of this term by increasing the parameter η. For some value of η (possibly zero), the computed pair energy $J_{ij}[\tilde{u}_{ij}]$ will obey the relation $J_{ij}[\tilde{u}_{ij}] \geq \epsilon_{ij}$. The value of η needed to provide this depends on the electron pair but also on the quality of the one-electron basis set, as we shall see below. Note, however, that in the WO functional for two electrons in the lowest occupied orbital we have $\Lambda_{ij} = \eta$, and if we let $\eta = 0$, the optimisation of this pair will be without "level-shift protection". Since we shall use the same parameter value for all pairs, the use of finite basis sets require us to have $\eta > 0$.

To illustrate how the MP2 energy and the strong orthogonality varies with the level-shift parameter, we have repeated the calculations from the previous section. This time, however, we have used the standard set of 9 GCFs in all calculations and have only varied the level-shift parameter. The results are given in Table 6.3 for the neon atom and in Table 6.4 for the water molecule.

Table 6.4: All-electron second-order correlation energies ($-E/\mathrm{mE_h}$) and SO measures for the water molecule for different values of the level-shift parameter η. Basis A is cc-pVDZ and basis B is aug-cc-pCVTZ(spd,sp). See text for further details.

Basis	$\log_{10}\eta$	KL	SO	KQ	SO	PQ	SO
A	+3	254.517	2.78	310.842	3.07	332.845	3.36
A	+2	279.408	1.75	325.490	2.39	338.875	2.55
A	+1	294.245	1.31	332.712	2.05	342.171	2.20
A	0	297.652	1.22	334.116	1.98	342.882	2.12
A	−1	298.068	1.21	334.279	1.97	342.966	2.11
A	−2	298.112	1.14	334.295	1.92	342.975	2.09
A	−3	298.130	0.92	334.299	1.27	342.976	1.44
B	+3	319.069	4.33	357.426	4.95	359.490	9.96
B	+2	329.197	3.27	358.941	4.15	359.822	8.92
B	+1	335.908	2.62	359.524	3.78	360.095	8.74
B	0	337.549	2.47	359.637	3.71	360.165	8.52
B	−1	337.753	2.45	359.651	3.70	360.141	8.58
B	−2	337.775	2.44	359.652	3.68	360.184	7.29
B	−3	337.778	1.98	359.652	3.00	360.176	7.25

The reported strong orthogonality (SO) measures are based on the measure, χ_{ij}^{SO}, which is discussed in appendix A

$$\chi_{ij}^{\mathrm{SO}} = \frac{\langle \tilde{u}_{ij}| \, P_{\mathrm{occ}}(1) + P_{\mathrm{occ}}(2) \, |\tilde{u}_{ij}\rangle}{\langle \tilde{u}_{ij}|\tilde{u}_{ij}\rangle} \tag{6.15}$$

This measure is calculated for the 25 *states* (15 singlets and 10 triplets) of the neon atom and the water molecule. Next, we calculate the arithmetic mean, $\bar{\chi}^{\mathrm{SO}}$, of these measures for each system, and finally we represent this mean by the negative logarithm $-\log_{10}\bar{\chi}^{\mathrm{SO}}$.

Focusing on the neon energies, we see that these hardly changes when the level-shift parameter is varied in the range $0.001 < \eta < 1$. We also note that the changes are larger for the smaller of the two basis sets (A). This is in agreement with the general discussion we make in appendix A where we show that the energy becomes less dependent of the level-shift parameter as the AO basis improves in quality, and for a complete basis it is entirely independent.

Within each basis set we also note that energies vary more with η for the kl-ansatz than they do for the kq- and pq-ansätze. This is also in agreement with our discussion in appendix A where we state that the optimisation of the pair function is made so as to fulfil the SO condition $u_{ij} = Q_{\mathrm{occ}} u_{ij}$. The greater the flexibility

in the basis set for u_{ij}, the better this condition is fulfilled. Pair functions based on the pq-ansatz therefore have smaller components lying in the "SO violating" spaces than pair functions based on the kq-ansatz, which in turn have smaller "SO violating" components than the kl-ansatz. Since only energy contributions coming from these components (called $u_{ij}^{(2)}$ and $u_{ij}^{(3)}$) are dependent on the value of the level-shift parameter, the order of sensitivity to η for the different ansätze, kl > kq > pq, is just as expected.

A brief look at Table 6.4, reveals that the discussion made for neon, also applies to the water molecule[3]. Since there is nothing extraordinary about these two systems, there is reason to think that these results can be extrapolated to all closed shell atoms and molecules consisting of first and second row elements. We therefore conclude that for such systems, MP2 energies change insignificantly when the level-shift parameter is varied in the range $0 < \eta < 1$.

There is, however, one thing that differs the water energies from the neon energies. For water, the energies obtained for the larger basis using the pq-ansatz, does not decrease monotonically against some limit as the level-shift parameters become very small. Instead, the energy starts oscillating at the $\mu\mathrm{E_h}$ level. This *may* be due to lacking positive definiteness, but since the basis set must be considered a rather good one, this is not likely. Also, for the smaller basis set this problem is not observed. Instead, the oscillations may be caused by numerical problems due to lacking internal machine precision, and as one of the equation systems that have to be solved is 4.887×4.887, this is a plausible explanation. It is supported by the fact that the kq-ansatz performs nearly as well as the pq-ansatz, implying that both *two-electron* basis sets are nearly complete. For such basis set, linear dependencies must be expected to be a problem. Problems related to linear dependencies and numerical precision are briefly touched in section 6.8.

Turning to the SO measure, we see that the extent to which our optimised pair functions are strongly orthogonal to the occupied orbitals, is controlled by the flexibility in the two-electron basis. This flexibility is determined by the ansatz we choose for pair functions as well as the one-electron basis. Thus, the SO measures are better for the large AO basis than for the small AO basis, and better for the pq-ansatz than for the kq- and kl-ansätze. The kq-ansatz, in turn, gives better SO measures than the kl-ansatz. We also note that for the smaller AO basis set the SO measure only improves marginally as we go from the kl-ansatz to the pq-ansatz, whereas the change is significant for the larger AO basis.

For all calculations, energies and SO measures change little as $\log_{10}\eta$ is increased from -1 to 0. The SO measures improve significantly, however, for the change -3 to -1, while the energy is practically unchanged. To be able to enjoy a better SO measure without too much loss in the energy, we shall therefore set $\eta = 0.1$ in all

[3]Due to memory requirements, we had to replace the four *d*-orbitals given for oxygen in the aug-cc-pCVTZ(spd) basis set by the single *d*-orbital taken from cc-pVDZ when using the pq-ansatz.

applications in this work. Note that, the additional orthogonality this provides us, also makes the WO functional a better approximation to the SO functional.

6.5 Integral timings—where do we spend CPU time?

We do not have to implement GTG-MP2 theory to realize that the integrals needed for a GTG-MP2 calculation, within a given one-electron basis consume considerably more CPU time than the integrals needed for a conventional MP2 calculation. Indeed, apart from the two-electron overlap integrals, the two-electron repulsion integrals (INT2C0) needed for MP2, are among the simplest integrals needed for GTG-MP2. This was observed in chapter 4.

It is of interest to know how large proportions of the total calculation time the different parts of a GTG-MP2 calculation consume. This knowledge may be obtained by running a number of different calculations where we carefully measure the amount of CPU time consumed by the MO transformation and the different integral type. If we let these calculations vary sufficiently in both system size and one-electron basis set, we should also be able to draw some general conclusions about integral timings.

In Table 6.5 we present timings for six different calculations. As the calculations have been done on different machines we only give the percentage of CPU time consumed by each part for a given calculation. Integrals have been labelled according to the INTXYZ notation introduced in section 4.4. There is one exception, however, namely the label INT3CE which specifies that the integrals INT3C1 and INT3E1 have been calculated simultaneously. This is possible since the only difference for these two integrals is the way they are combined with density matrix elements. If the geminals and the virtual orbitals expansion are described using different one-electron basis sets, however, the integrals will also differ.

For each calculation we have employed the highest possible Abelian symmetry which is D_{2h} for the neon atom and C_{2v}, C_{2h} and C_2 for the water, the *t*-H_2O_2, and the *g*-H_2O_2 molecules, respectively. The geminals have been described using the kq-ansatz (see section 6.1) with the standard set of 9 even-tempered GCFs $\{729, 243, \ldots, 1/9\}$ (see section 6.3).

Table 6.5 tells us that the two-electron integrals are unimportant for the total calculation time (recall that INT4C1 is just a combination of two-electron integrals). This is just as expected. We also note that the MO transformation is relatively inexpensive. This situation may change when the basis sets get bigger, of course, but then we can switch from the MO formulation of the kq-ansatz to the AO formulation, thus removing the most CPU intensive MO transformations completely.

Turning to the three-electron integrals, we note that except for the INT3E2 integrals, these integrals are, relatively speaking, equally expensive to compute. The INT3C2 integrals take about five times as much CPU time to compute as the INT3P1

Table 6.5: The percentage of total CPU time consumed by the MO transformation and each integral type when the kq-ansatz is used.

	aug-cc-pVDZ				aug-cc-pVTZ	
	Ne	H_2O	t-H_2O_2	g-H_2O_2	Ne	H_2O
INT21	.00	.00	.00	.00	.00	.00
INT22	.03	.01	.00	.00	.00	.00
INT2C0	.00	.00	.00	.00	.00	.00
INT2C1	.01	.00	.00	.00	.00	.00
INT4C1	.00	.00	.00	.00	.00	.00
INT2K1	.09	.02	.01	.00	.01	.00
INT2K2	.49	.13	.03	.02	.06	.04
INT2V1	.05	.02	.00	.00	.02	.00
INT2V2	.23	.10	.02	.01	.09	.03
INT3P1	5.26	5.11	4.56	4.71	5.46	5.51
INT3CE	5.30	5.15	4.59	4.61	5.56	5.58
INT3C2	26.06	25.15	23.17	23.35	27.45	27.34
INT3E2	34.17	39.05	43.75	46.86	31.68	36.21
INT32	27.16	24.77	23.41	20.20	28.93	25.05
MOTRANS	.59	.45	.45	.23	.46	.18
OTHER	.54	.04	.01	.01	.18	.09
TOTAL	100.00	100.00	100.00	100.00	100.00	100.00

integrals, but there are also five times as many of them ($N_{\mathrm{GCF}}(N_{\mathrm{GCF}}+1)/2$ versus N_{GCF}, where $N_{\mathrm{GCF}}=9$).

The INT3E2 integrals, however, are more CPU intensive than the other three-electron integrals. We also note in Table 6.5 that when the ability to exploit local symmetry is reduced, the proportion of the total calculation time consumed by the cyclic three-electron integrals is increased. The presence of local symmetry allows us to take codal short cuts when we evaluate an integral since certain quantities are known to be zero. As the code for the INT3E2 integrals is the most complex, these integrals are also the ones that benefit the most from this kind of symmetry.

Figure 6.1 shows the outcome when we profile[4] the calculation of INT3E2 integrals for the t-H_2O_2 molecule given in Table 6.5. The figure lists the most important subroutines and the proportion of total CPU time used by the subroutines or subroutines called from within them. Some of the names represent a set of subroutines rather than one, and these names are explained below.

GEM3INT is one of the top subroutines in the calculation of three-electron integrals and has four main branches. In the first, GEM3MIX, the three-electron integrals

[4]The profiling has been done using the gprof tool.

Figure 6.1: The percentage of total CPU time consumed by different subroutines when calculating the cyclic three-electron integrals for the *t*-H_2O_2 molecule with basis aug-cc-pVDZ. Only the most important subroutines have been included.

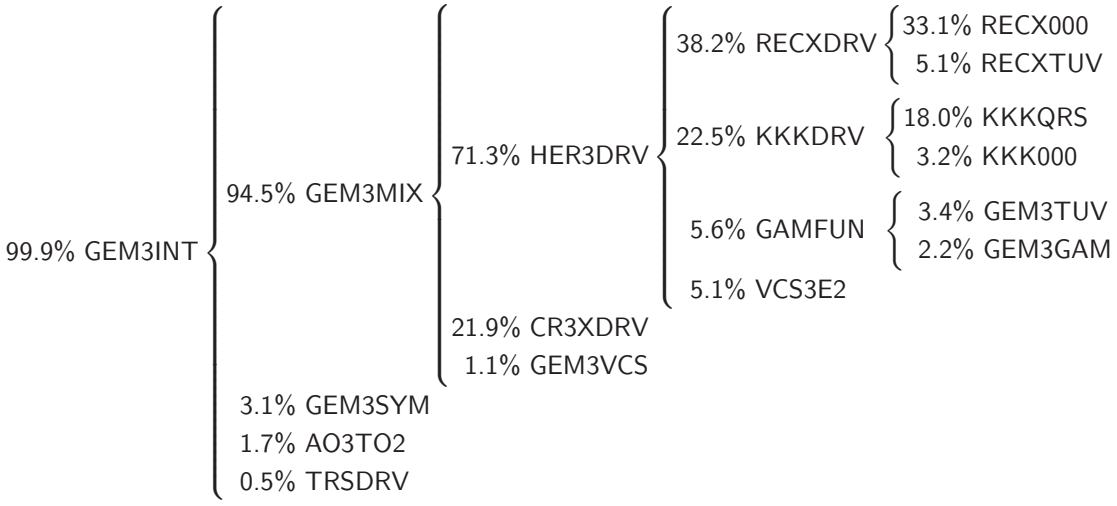

are calculated. In the second, GEM3SYM, these integrals are symmetry-adapted. In the third, AO3TO2, three-electron integrals are contracted with density matrix elements to form four-index matrix elements. And finally, these matrix elements are transformed to MO-basis in the subroutine TRSDRV.

When three-electron integrals are calculated in GEM3MIX, a number of vectors containing orbital exponents, orbital centres and integral prefactors have to be set up. This is done in the subroutine GEM3VCS. In HER3DRV, the integrals are calculated in a Hermite basis and in in subroutines CR3XDRV they are transformed to a spherical Cartesian basis. This transformation is performed one electron at a time, and the first transformation is the most CPU intensive

$$21.9\%\ \text{CR3XDRV} \begin{cases} 14.3\%\ \text{CR33DRV} \\ 5.6\%\ \text{CR32DRV} \\ 2.0\%\ \text{CR31DRV} \end{cases} \tag{6.16}$$

The reason is that the number of angular components decrease with each transformation, and more importantly, that each transformation also converts a number of primitive integrals into contracted integrals, thus decreasing the vector length.

Note, in Table 6.5, that the proportion of the total calculation time spent calculating cyclic three-electron integrals go down as we include higher angular momentum in the basis set. This is because the subroutines that are common to all three-electron integrals, here represented mainly by CR3XDRV, increase more in computation time than the calculation of Hermite integrals.

Before the Hermite integrals may be calculated in HER3DRV a number of new vectors are set up in the subroutine VCS3E2 (see equation 4.37). This is followed by the calculation of KKK functions in KKKDRV (equations (4.46)), the calculation of Boys functions (incomplete gamma functions) in GAMFUN (equations (4.51)), and finally, the combination of these into Hermite integrals in the RECXDRV subroutines (equation (4.52)).

The combining of KKK functions and Boys functions into Hermite functions is a major bottle-neck in the calculation. To speed this part up, we exploit translational symmetry (see section 4.3). This means that angular momentum for one of the electrons is generated from angular momentum for the other two electrons. This is done in the subroutines RECXTUV by means of efficient recurrence relations. To be able to recur angular momentum like this, we must first calculate unrecurred Hermite integrals that has augmented angular momentum for the other electrons. These unrecurred integrals are calculated in subroutines RECX000.

The electron that has its angular momentum recurred is always the one with the lowest angular momentum. If two electrons are equal, the one with the lowest label, that is, 1, 2 or 3, is recurred. This leads to the following distribution of calculation times

$$38.2\%\ \text{RECXDRV} \begin{cases} 18.8\%\ \text{REC1DRV} \\ 12.1\%\ \text{REC2DRV} \\ 7.2\%\ \text{REC3DRV} \end{cases} \tag{6.17}$$

where the X in RECXTUV is a label for the electron that is recurred.

The KKK functions are, in a similar manner, recurred in the subroutine KKKQRS, from a set of start functions generated in the subroutine KKK000. As these start functions are calculated using very simple expressions, the most time consuming part of the KKK evaluation is the recurrence. For the Hermite integrals it was opposite, and the start functions consumed the most calculation time.

Note finally, that even though the profiling has been done for the cyclic three-electron integrals, the program flow is similar for the other three-electron integrals. In the case of the overlap integral, INT32, Hermite integrals are constructed from the KKK functions alone. For the other three-electron integrals, vectors are set up in subroutines VCS3XX rather than VCS3E2, and in the subroutine KREC the K functions (equation (4.63)) are made. These functions replace the more complex KKK functions and this also gives us a faster execution in subroutine REC3000.

6.6 Parallelisation

Since a large amount of time is spent calculating integrals we have to look for ways to speed up the code. This may be done by tuning the implementation or recoding it using different algorithms. However, even though this may give some speedup,

more than a factor of 2–3 would seem unrealistic. In addition to tuning, we may also introduce integral prescreening based on the Cauchy–Schwartz inequality, for instance. Even though this may be useful for large molecular systems it is of little importance for the systems treated in this work. This is shown in section 6.7 where we discuss integral prescreening.

6.6.1 Implementation

A commonly used technique for speeding up calculations is parallelisation [76]. The potential of this technique was early realized by the quantum chemistry community who used it to parallelise Hartree–Fock calculations [77–81]. Parallelisation typically gives an overall increase in consumed CPU time, while the effective calculation time goes down, often linearly with the number of processors. For computer programs to achieve such speedups, however, they must contain a large number of independent tasks. Since each GTG-integral may be calculated independently of all others, GTG-type calculations are well suited for parallelisation.

In Table 4.1 of section 4.1, we outlined pseudo-code for the construction of Fock matrix elements, built up by adding together integrals INT2K1, INT2V1, INT3C1 and INT3E1. If we look closer into the pseudo-code for these matrix elements, we see that two loops are readily available for parallelisation. These are the outer loop that runs over correlation factors, v, and second outer loop that runs over overlap distributions for electron 1, $\mu\tilde{\sigma}$. Before we go into discussing whether or not both loops are parallelised, we recall that in order to get the GTG-MP2 energy we must set up the equation system (3.83). This requires us to calculate a number of different matrix elements, whose construction could also be represented by pseudo-code similar to that in Table 4.1. These matrix elements are made up of integrals (INT21), (INT22), (INT2K2+INT2V2+INT3C2+INT3E2), (INT32), (INT2C1+INT3P1), (INT4C1), and (INT2C0), where we have included parentheses to show which integrals occur in the same matrix element. Adding up, we see that a total of 8 double loops have to be parallelised. In Table 6.6 we have outlined pseudo-code for such a parallelisation built around a master/slave paradigm. This pseudo-code is rather crude, however, and is only intended to roughly show how the parallelisation is implemented.

The major challenge in the parallelisation is to handle the eight matrix elements simultaneously. While the master process may have advanced to matrix element number three, for instance, one or more slaves may still be calculating integrals for matrix element number two, or maybe even one. It is not a good idea to have the master wait for all slaves before proceeding to the next matrix element, as this will make slaves idle. The code must therefore be flexible enough to handle a number special cases that, more or less frequently, arise.

The outer loop that runs over correlation factors is parallelised in all eight matrix elements. The inner loop that runs over overlap distributions (ODs) is also parallelised, but the implementation allows for more than one pair of $\mu\sigma$ indices to

Table 6.6: Simple pseudo code describing the parallelisation

Master

for X **in** 8 parallelisation jobs
    do v
        do $\mu\sigma$
            receive request for tasks **from** slave N
            send $(X, v, \mu\sigma)$ **to** slave N
        end do
        receive all integrals for index v
    end do
end for
do symmetrisations and parity-adaptions

Slaves

do 8 parallelisation jobs
    while $(X_{\text{new}} = X_{\text{old}})$ **do**
        send request for tasks **to** master
        receive $(X_{\text{new}}, v_{\text{new}}, \mu\sigma)$ **from** master
        return integrals for indices $(X_{\text{old}}, v_{\text{old}})$ **if** $(v_{\text{new}} \neq v_{\text{old}})$
        calculate MO integrals
    end while
end do

be sent to each slave in the same task. This way, we may adjust the granularity of the tasks executed by the slaves. Some jobs, like INT21 and INT22, are so quickly executed that it is no point in splitting the inner loop up in small tasks. All indices $\mu\sigma$ are therefore sent to the same slave. For other jobs, however, like the construction of Fock matrix elements between two geminals, it is advantageous to keep the task size as small as possible. Here it should be pointed out that $\mu\sigma$ is *one* index running over classes of ODs, and that it should *not*, for instance, be interpreted as a double loop running over the traditional *blocks of shells*. The class structure used in the implementation has been taken directly from the ERI program [82] developed by T. Helgaker. One of the key features with this structure is that the atomic orbitals have been made independent of the kind of centre, usually a nucleus, they are attached to. This means, for instance, that *dd*-distributions consisting of oxygen orbitals and *dd*-distributions consisting of hydrogen orbitals can be present in the same class. This, in turn, allows these ODs to be present in the same vector during an integral calculation. When integrals contain *d*-orbitals or orbitals of higher angular momentum, this is very important for the efficiency.

This class structure may also have a negative side-effect for the parallelisation, however. As more and more ODs are gathered in the same class, integrals made from this class become increasingly CPU intensive to compute. If one or more tasks get so big that the slaves receiving them are still busy calculating long after all other slaves have gone idle, this may have a crucial impact on the efficiency. In fact, for the calculations presented in the next section, this turns out to be what limits the performance as the number of processors increase.

6.6.2 Speedups for some neon and water calculations

In Tables 6.7 and 6.8 we have presented the speedups obtained for two different water and neon calculation. For each system we have used one small and one (relatively) large basis set. The number of processors ranges from 1 to 256 for all calculations. In each table we have listed the calculation time given in minutes. Note that all times refer to "wall" times and not CPU times. For a calculation using N processors, the speedup has been calculated simply as t_1/t_N, where t_1 and t_N are the calculation times for 1 and N processors, respectively. For both water calculations, t_1 had to be estimated as $3t_4$ in order to avoid incorrect, super-linear scaling. The actually computed one-processor times for basis A and B were 137.67 and 2001.17, respectively. Usually, the speedups are what attract most attention in tables. The higher the speedup the better. Another performance measure which is devoted less attention is the efficiency, which gives a measure of how well a calculation utilises its allocated resources. We define the efficiency as the percentage of processors that are effectively used, and calculate this percentage by $100 \cdot N \cdot (t_N/t_1)$.

In Figure 6.2 we have plotted the speedups for the water and neon calculation. For the water calculation, given in the upper figure, we see that the larger calculation scales slightly better than the small one. However, both calculations readily obtain a speedup of more than one hundred. This leads to a substantial drop in the calculation time, implying that calculations normally requiring a year, say, to be calculated, may be completed in just a few days.

From Table 6.7 we see that the calculation time of the smaller basis set (A) has dropped to just a little more than a minute when a speedup of one hundred is reached. In most cases, the parallelisation has served its purpose long before we get down to this time scale, where we start pushing system resources like network latency and bandwidth. The water molecule with basis set A should therefore be considered a test case only, as it does not give a correct picture of the "true" parallel performance. For this the calculation is too small. The larger water calculation, however, gives a more representative picture of the parallelisation. Indeed, for 96 processors it shows a speedup of 91. Since the best possible speedup in our master/slave paradigm would be 95, this must be considered excellent.

Turning to the speedups for the neon atom shown in the bottom part of Figure 6.2, we see that the performance is far less impressive. Using 96 processors,

Table 6.7: Parallelisation results for the water molecule. Times are given in minutes and refer to wall times. Basis sets A and B are aug-cc-pVDZ(sp,s) and aug-cc-pVDZ respectively.

Basis	Procs	Timing	Speedup	Efficiency	Proc loss
A	1	135.39	1.00	100.00	0
A	4	45.13	3.00	75.00	1.00
A	8	19.45	6.96	87.00	1.04
A	16	9.28	14.59	91.19	1.41
A	32	4.70	28.81	90.03	3.19
A	64	2.38	56.89	88.89	7.11
A	96	1.68	80.59	83.94	15.41
A	128	1.30	104.15	81.37	23.85
A	160	1.07	126.53	79.08	33.47
A	192	.95	142.52	74.23	49.48
A	224	.92	147.16	65.70	76.84
A	256	.85	159.28	62.22	96.72
B	1	1955.40	1.00	100.00	0
B	4	651.80	3.00	75.00	1.00
B	8	279.50	7.00	87.50	1.00
B	16	130.78	14.95	93.45	1.05
B	32	63.75	30.67	95.85	1.33
B	64	31.98	61.14	95.54	2.86
B	96	21.53	90.82	94.60	5.18
B	128	17.57	111.31	86.96	16.69
B	160	14.47	135.13	84.46	24.87
B	192	12.22	160.02	83.34	31.98
B	224	11.48	170.33	76.04	53.67
B	256	10.68	183.09	71.52	72.91

even the larger of the two neon calculation only achieves a speedup of 75. We also note that while the speedup curves for the two water calculations start to level off around two hundred processors, the neon curves have levelled off already when a hundred processors are being used. This may be explained by looking at the kind if tasks available in each calculation. Since the only thing differing the four parallelisations is the loop over OD classes for electron 1, we shall take a closer look at this. Table 6.9 gives the total number of OD classes that has to be looped over in each calculation.

Comparing the two basis A numbers, we note that the water calculation has a few more OD classes we must loop over. The difference, however, is not large enough

Table 6.8: Parallelisation results for the neon atom. Timings are given in minutes and refer to wall times. Basis sets A and B are aug-cc-pVDZ and aug-cc-pVTZ respectively.

Basis	Procs	Timing	Speedup	Efficiency	Proc loss
A	1	94.25	1.00	100.00	0
A	4	31.57	2.98	74.50	3.12
A	8	13.92	6.77	84.63	1.33
A	16	6.45	14.61	91.33	1.39
A	32	3.20	29.45	92.04	2.55
A	64	1.92	49.09	76.70	14.91
A	96	1.50	62.93	65.45	33.07
A	128	1.42	66.37	51.85	61.63
A	160	1.38	68.30	42.68	91.70
A	192	1.33	70.71	36.83	121.29
A	224	1.33	70.71	31.57	153.29
A	256	1.23	76.62	29.93	179.38
B	1	2912.28	1.00	100.00	0
B	4	1123.72	2.59	64.79	1.41
B	8	445.47	6.55	81.90	1.45
B	16	211.02	13.80	86.26	2.20
B	32	103.87	28.04	87.61	3.96
B	64	52.46	55.51	86.74	8.49
B	96	38.80	75.06	78.19	20.94
B	128	35.57	81.88	63.97	46.12
B	160	32.58	89.38	55.86	70.62
B	192	29.72	97.99	51.04	94.01
B	224	28.12	103.58	46.24	120.42
B	256	28.23	103.15	40.29	152.85

to explain why the water calculation scales so much better. The answer, instead, must be found by looking at the granularity of the tasks to be distributed. Recall that basis A is not the same basis set for the two systems. While it only includes basis functions up to p-orbitals for the water molecule, also d-orbitals are included for the neon atom. A task having integrals containing d-orbitals consumes more CPU time than a task only having p-orbitals in its integrals. This is exactly what we observe. When the neon atom calculation approaches a minute and a half of calculation time, the time required to calculated the largest of its tasks is probably reached. This efficiently limits any further performance enhancement.

Note that, if we compare the total CPU time consumed with the number of OD

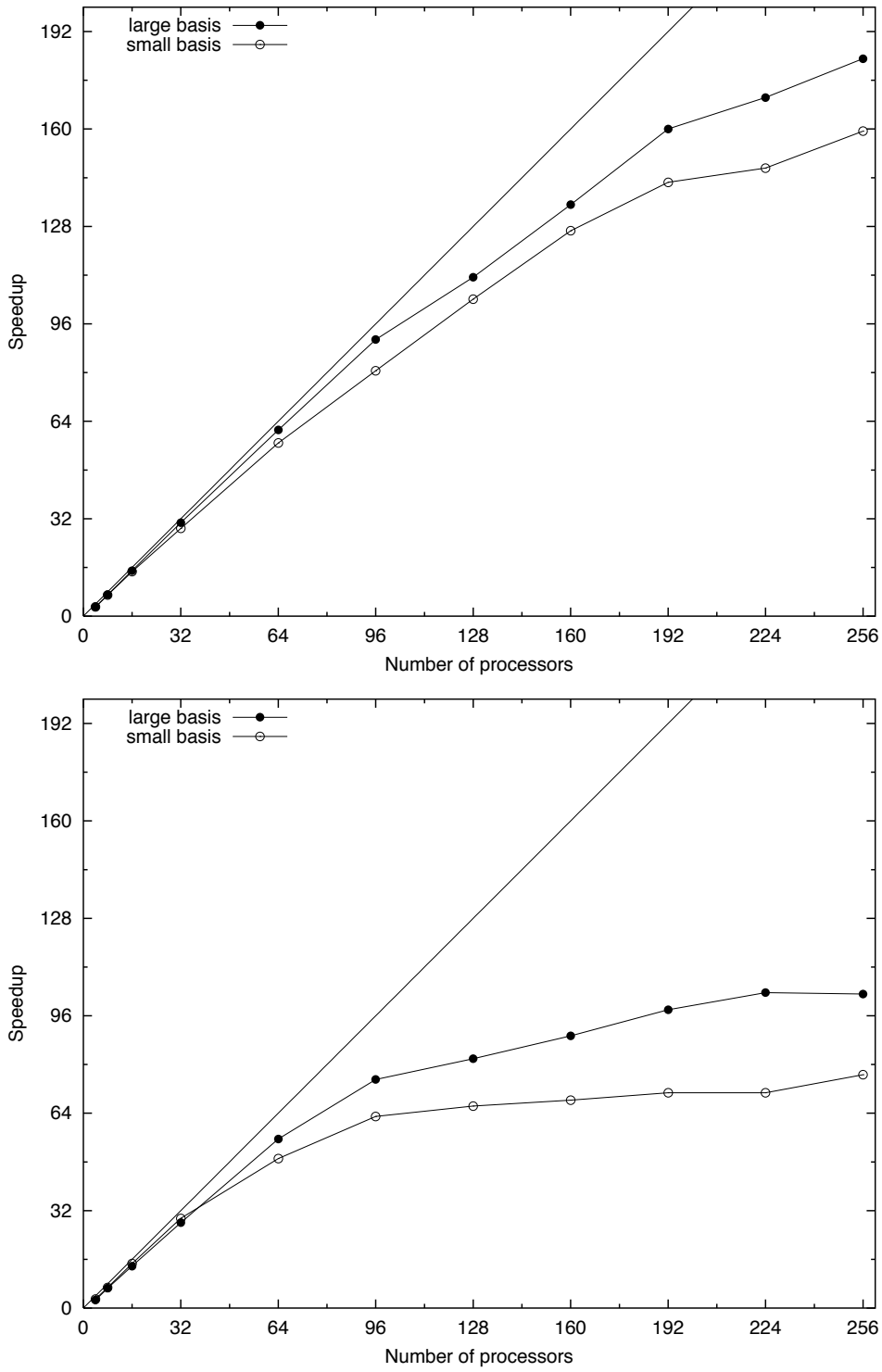

Figure 6.2: Speedups for the water (top) and neon (bottom) calculations. All calculations were done using a cluster of 512 MIPS R14000 (600 MHZ) processors.

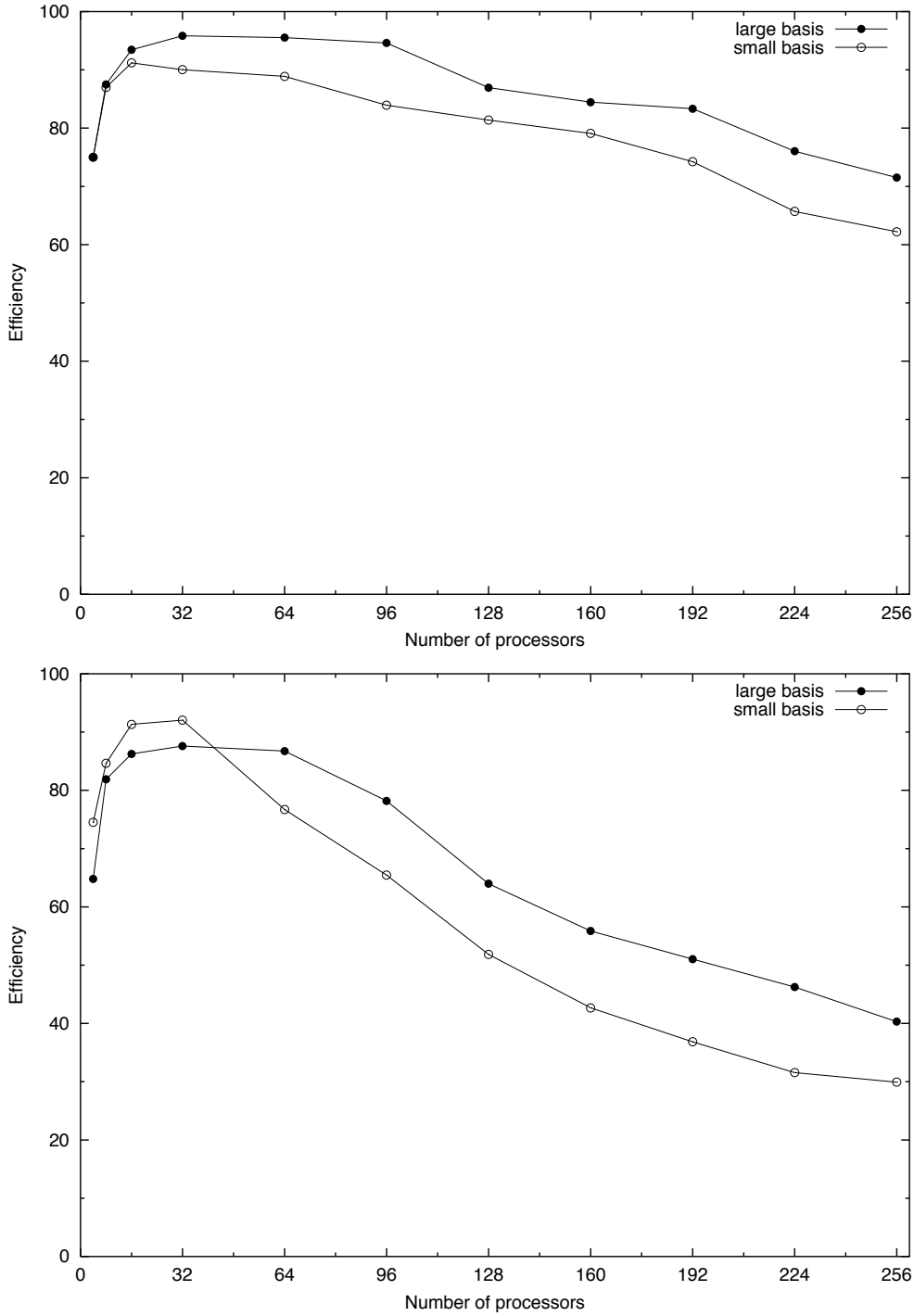

Figure 6.3: Efficiencies for the water calculations (top) and the neon calculation (bottom). Denoting the calculation time for N processors, t_N, the efficiency is defined as $100N(t_N/t_1)$ and gives the percentage of processors that are effectively utilised.

Table 6.9: Total number of OD classes available for parallelisation

	Basis A	Basis B
Water	26	45
Neon	21	32

classes available, we see that *on average* the neon tasks are actually more fine-grained than the water tasks (94/21 vs. 135/26). Normally this would make us expect better scaling for the former. However, when comparing the speedup plots, we find that this is definitely not so. The granularity among the neon tasks, therefore, must vary from fine-grained to the coarse-grained, and this is exactly what we find if we compare their basis sets.

Basis B for the water molecule and basis A for the neon atom are both aug-cc-pVDZ and may therefore be considered equivalent. Accordingly, we would expect the granularity of the tasks to be distributed to be similar for both systems. The reason that the water calculation scales so much better, therefore, must be that the calculation is larger both with respect to total CPU time and the number of tasks available. Overall, this gives better scaling.

The same kind of reasoning may be used for the neon calculation with basis B, but the presence of f-orbitals in this basis set complicates the picture. Since integrals containing f-orbitals are orders of magnitude more time consuming to calculate than integrals containing d-orbitals, we get very coarse-grained tasks in this calculation. From the timings given in Table 6.8, we estimate the largest of these tasks to require around 28 minutes of computation time, or slightly less.

Even though a high speedup is attractive, we cannot justify the allocation of hundreds of processors unless these processors are efficiently utilised. In Figure 6.3 we have plotted efficiencies taken from Tables 6.7 and 6.8. These two figures show for what range of processors we use the resources sensibly and for what range we are wasting them.

Since the implemented master/slave algorithm, puts aside one of the processors just to distribute tasks and keep the other processors busy, we cannot expect the efficiency to be good when only a small number of processors is allocated. This is also clearly depicted in all four efficiency plots of Figure 6.3. As the number of processors increase, we start benefiting from the dynamic load balancing, and when the number of processors is really large, it is impossible to get a good performance unless one process is reserved for administration only. The two water calculations exhibit a fairly good efficiency even when the number of processors is large. Notice also that the fall-off is only moderate throughout the plots. This indicates that the implemented master/slave paradigm has sufficient flexibility for handling the eight

matrix elements simultaneously for a large range of processors.

For the two neon calculations the efficiency drops quickly when the top has been reached. This is explained by the same means used to explain the flattening out for the corresponding speedup plots.

We conclude this section by claiming that the scaling and efficiency that will be obtained for real applications will be better than what have been presented here. Typically, the calculations presented in chapter 7 that were run in parallel, were exceedingly CPU consuming calculations that had to run overnight or for several days also when parallelisation was used. Since we typically used between 8 and 64 processors, we should expect nearly optimal load balancing to be obtained for such long calculation times.

6.7 Prescreening of AO integrals

In the previous section, we showed that through parallelisation we may speed up a calculation significantly. Moreover, calculations that are too time-consuming to be feasible for a single processor, may sometimes be handled if a sufficient amount of processors are available for parallelisation. Parallelisation, however, does not relieve the most fundamental problem with the GTG-MP2 theory presented in this thesis; when we increase the number of basis functions, N, the number of three-electron integrals increases as N^6.

If we do calculations on atoms or small molecular systems, this integral growth cannot be escaped. For large molecules, however, it is possible to reduce the scaling by exploiting the local nature of the electron-electron correlation (cf. page 32). Since the electron-electron correlation is a short-range interaction, only integrals containing orbitals that are located relatively close in space survive. Integrals in which two or more atomic orbitals are separated by a large distance are likely to be redundant, assuming, of course, that orbitals are not too diffuse. Nowadays, state-of-the-art quantum chemistry programs have implemented different sort of means to identify redundant two-electron integrals. One of the more powerful of these is the Cauchy–Schwarz inequality.

6.7.1 Cauchy–Schwarz inequality for two-electron integrals

Consider the two-electron repulsion integral given in section 4.6.3

$$A_{\mu\nu\sigma\tau} \equiv \langle \chi_{\mu\nu} | \, r_{12}^{-1} \, | \chi_{\sigma\tau} \rangle = \iint \Omega_{\mu\sigma}(1) \, \Omega_{\nu\tau}(2) \, r_{12}^{-1} \mathrm{d}r_1 \mathrm{d}r_2 \tag{6.18}$$

In the following, we regard $A_{\mu\nu\sigma\tau}$ as a matrix where index $\mu\nu$ specify the row number and index $\sigma\tau$ specify the column number.

To maintain a certain numerical precision in the energy, integrals must be calculated with a somewhat higher precision as some precision is lost when the matrix

equation (3.83) is solved. Additionally, some precision may be lost when integrals are combined to form the matrix elements of (3.83). The precision held in each of these matrix elements is determined by the magnitude and the precision of the integrals constituting it. If numerically large integrals having high precision are combined with numerically small integrals having low precision the precision of the resulting matrix element may end up either high or low. If the largest integral has low precision, however, the matrix element itself also have low precision no matter the precision of the other integrals. The numerical precision of a matrix element is thus tightly connected to the precision of its largest integral.

To obtain a certain precision in the energy it is therefore sufficient to ensure that the matrix elements are good to some decimal place. To identify this decimal place we have do a certain amount calculations where we compare the precision maintained in the energy with the precision used for integrals. Once this threshold value has been established we know that integrals smaller than this do not influence the energy (within the required precision) and may therefore be discarded. In order to avoid calculating redundant integrals, i.e. have them prescreened, we must be able to estimate the size of an integral before doing an exact evaluation. This estimate should be computationally inexpensive to obtain, and must also represent an upper bound to the true integral. By comparing the estimate with the threshold value, we may decide whether or not the integral needs to be evaluated exactly. An efficient approach for obtaining integral estimates is to approximate the integrals using the Cauchy–Schwarz inequality. Using this inequality we may approximate all N^4 integrals from a subset of N^2 integrals. The equality is only valid for inner products, though, and before applying it to a new kind of integrals, we must first check that these integrals satisfy the requirements for inner products.

For the repulsion integral given in (6.18), a mere inspection is enough to verify that most inner product requirements are fulfilled. To prove that $A_{\mu\nu\mu\nu} > 0$ for any choice of $\mu\nu$ is not as straight forward, however, and a proof is therefore given below.

Consider a two-electron function $\chi(1,2)$ given as an expansion over all products of AO basis functions

$$\chi(1,2) = \sum_{\mu,\nu} \chi_\mu(1)\chi_\nu(2)c_\mu c_\nu \equiv \sum_{\mu\nu} \chi_{\mu\nu}(1,2)c_{\mu\nu} \tag{6.19}$$

Using this function, we construct the following two-electron integral

$$I[\chi] = \iint \chi(1,2)\chi(1,2)r_{12}^{-1}\mathrm{d}r_1\mathrm{d}r_2 \tag{6.20}$$

Since $\chi^2(1,2)$ and r_{12}^{-1} are both positive functions in their entire domain, the integrand in (6.20) is always greater than or equal to zero. The integral itself, is therefore positive definite

$$I[\chi] > 0 \tag{6.21}$$

Using the expansion for $\chi(1,2)$, we may rewrite the inequality (6.21) in the form

$$\sum_{\mu\nu}\sum_{\sigma\tau} c_{\mu\nu} A_{\mu\nu\sigma\tau} c_{\sigma\tau} > 0 \tag{6.22}$$

This equation constitutes the definition of a positive definite matrix. As a corollary, the diagonal elements are positive

$$A_{\mu\nu\mu\nu} > 0 \tag{6.23}$$

The two-electron integrals given in (6.18) therefore satisfy the condition for inner products in a metric defined by r_{12}^{-1}. Application of the Cauchy–Schwarz inequality then yields

$$|A_{\mu\nu\sigma\tau}| \leq \sqrt{A_{\mu\nu\mu\nu}} \cdot \sqrt{A_{\sigma\tau\sigma\tau}} \tag{6.24}$$

As the quantities on the right-hand side of (6.24) are two-index quantities, the process of finding an approximate value for $A_{\mu\nu\sigma\tau}$ goes as N^2 rather than N^4.

The expression for prescreening given in (6.24) is slightly different from the one usually encountered in literature [1, 83], namely

$$|A_{\mu\nu\sigma\tau}| \leq \sqrt{A_{\mu\mu\sigma\sigma}} \cdot \sqrt{A_{\nu\nu\tau\tau}} \tag{6.25}$$

The integrals appearing on the right-hand side of (6.25) are one-centre integrals, and since the Boys function need not be evaluated for such integrals, they are considerably faster to calculate than the two-centre integrals needed in (6.24).

Unfortunately, even though the inequality (6.25) is the preferred one for two-electron integrals, it has no counterpart for three-electron integrals. The alternative inequality given in (6.24), on the other hand, may rather easily be generalised to three-electron integrals and more generally also to N-electron integrals. Before considering such integrals, however, we shall study two-electron integrals in more detail.

Consider a general two-electron integral, $A_{\mu\nu\sigma\tau}$, given by the expression

$$A_{\mu\nu\sigma\tau} = \langle \chi_{\mu\nu} | \, \mathcal{O}(1,2) \, | \chi_{\sigma\tau} \rangle \tag{6.26}$$

This integral may be turned into any of the two-electron integrals discussed in chapter 4 by giving the operator $\mathcal{O}(1,2)$ the appropriate definition.[5] For example, letting

$$\mathcal{O}(1,2) = \begin{cases} \exp(-\gamma_v r_{12}^2) & \textsf{(INT21)} \\ r_{12}^{-1} & \textsf{(INT2C0)} \\ \exp(-\gamma_v r_{12}^2) r_{12}^{-1} & \textsf{(INT2C1)} \\ \exp(-\gamma_v r_{12}^2) r_{2C}^{-1} & \textsf{(INT2V1)} \\ \exp(-\gamma_v r_{12}^2) \nabla_2^2 & \textsf{(INT2K1)} \end{cases} \tag{6.27}$$

[5]Note that by defining the two-electron integrals as in (6.26), we have moved the correlation factors (GCFs) out of the geminals and into the operator, thus leaving pure orbital products in the bra and the ket.

we may construct all two-electron integrals containing one geminal. The two-electron integrals with two geminals, INT22, INT2V2, and INT2K2, may be formed by adding $\exp(-\gamma_w r_{12}^2)$ to the corresponding one-geminal operators in (6.27).

For the Cauchy–Schwarz inequality to be applicable to a certain integral type, the integral must be an inner product. We have already proven this for the INT2C0 integral, and noting that this integral only differs from the others in the $\mathcal{O}(1,2)$ operator, it is sufficient to show that this operator is everywhere positive. For all two-electron integrals except the kinetic energy integrals, this is a trivial task to do. For the kinetic energy integrals, however, the differentiation operator makes things more complicated, and we cannot prove that these integrals are inner products using the simple technique presented above. For the kinetic energy integrals, therefore, we have to investigate other techniques, possibly involving the turn-over rule.

6.7.2 Cauchy–Schwarz inequality for three-electron integrals

Following the same approach as for two-electron integrals, it is straight forward to show that all three-electron integrals given in section 4 are inner products.

First, we note that all three-electron integrals generically may be given as

$$\begin{aligned} A_{\mu\nu\eta\sigma\tau\xi} &= \langle \chi_{\mu\nu\eta} | \, \mathcal{O}(1,2,3) \, | \chi_{\sigma\tau\xi} \rangle \\ &\equiv \iiint \Omega_{\mu\sigma}(1) \, \Omega_{\nu\tau}(2) \, \Omega_{\eta\xi}(3) \, \mathcal{O}(1,2,3) \mathrm{d}r_1 \mathrm{d}r_2 \mathrm{d}r_3 \end{aligned} \tag{6.28}$$

where the different integrals only differ in the operator $\mathcal{O}(1,2,3)$. The alternative forms of this operator are

$$\mathcal{O}(1,2,3) = \begin{cases} \exp(-\gamma_v r_{12}^2) r_{23}^{-1} & \text{(INT3E1)} \\ \exp(-\gamma_v r_{12}^2) r_{23}^{-1} \exp(-\gamma_w r_{13}^2) & \text{(INT3E2)} \\ \exp(-\gamma_v r_{12}^2) \exp(-\gamma_w r_{23}^2) & \text{(INT32)} \end{cases} \tag{6.29}$$

where we have left out entries for INT3C1, INT3P1, and INT3C2 as the operator for these integrals is similar to that of integral INT3E1.

In the following, the integral $A_{\mu\nu\eta\sigma\tau\xi}$ is regarded as a matrix element with $\mu\nu\eta$ giving the row number and $\sigma\tau\xi$ giving the column number.

Consider the three-electron integral

$$I[\chi] = \iiint |\chi(1,2,3)|^2 \mathcal{O}(1,2,3) \mathrm{d}r_1 \mathrm{d}r_2 \mathrm{d}r_3 \tag{6.30}$$

where we have introduced a three-electron function $\chi(1,2,3)$ that may be expanded in orbitals as

$$\chi(1,2,3) = \sum_{\mu,\nu,\eta} \chi_\mu(1) \chi_\nu(2) \chi_\eta(3) c_\mu c_\nu c_\eta \equiv \sum_{\mu\nu\eta} \chi_{\mu\nu\eta}(1,2,3) c_{\mu\nu\eta} \tag{6.31}$$

Using the same reasoning as for two-electron integrals, it is not difficult to verify that $I[\chi] > 0$. Inserting the expansion for $\chi(1,2,3)$ into (6.30) we obtain

$$\sum_{\mu\nu\eta}\sum_{\sigma\tau\xi} c_{\mu\nu\eta} A_{\mu\nu\eta\sigma\tau\sigma} c_{\sigma\tau\xi} > 0 \tag{6.32}$$

which leads us directly to the Cauchy–Schwarz inequality for three-electron integrals

$$|A_{\mu\nu\eta\sigma\tau\xi}| \leq \sqrt{A_{\mu\nu\eta\mu\nu\eta}} \cdot \sqrt{A_{\sigma\tau\xi\sigma\tau\xi}} \tag{6.33}$$

Equation (6.33) is hence the three-electron counterpart of (6.24). Using this expression to prescreen integrals we may potentially reduce the scaling from N^6 to N^3. Keep in mind though, that this kind of reduction is only realistic for large molecular systems. The kind of scaling that is realistic for medium-sized systems is studied in more detail in section 6.7.4 where we present some numerical examples.

Some caution must be exercised if prescreening is used together with multiple basis sets. Consider, as an example, the integral INT3C1 given in section 4.6.1. If we assign basis functions used in describing geminals with a tilde, the Cauchy–Schwarz inequality for this integral reads

$$|A_{\tilde{\mu}\tilde{\nu}\eta\sigma\tau\xi}| \leq \sqrt{A_{\tilde{\mu}\tilde{\nu}\eta\tilde{\mu}\tilde{\nu}\eta}} \cdot \sqrt{A_{\sigma\tau\xi\sigma\tau\xi}} \tag{6.34}$$

If orbitals and geminals are expanded in the same basis set, the integrals used for prescreening are also needed in the pair function optimisations and energy calculations. When multiple basis sets are used as in (6.34), this is no longer necessarily true.

6.7.3 Further prescreening techniques

The operators $\mathcal{O}$ for both two-electron and three-electron integrals vary with the choice of correlation factors, and are therefore more appropriately denoted $\mathcal{O}_v$ or $\mathcal{O}_{vw}$, depending on whether the integral is of type orbital-geminal or geminal-geminal. Accordingly, three-electron integrals, for instance, are more appropriately expressed as $A^{v}_{\mu\nu\eta\sigma\tau\xi}$ or $A^{v,w}_{\mu\nu\eta\sigma\tau\xi}$.

Let us assume that we have calculated all INT32 integrals corresponding to the pair of indices (v, w_1), and that we are about to calculate integrals corresponding to the pair (v, w_2). Since we use the Cauchy–Schwarz inequality for prescreening, the "prescreen-integrals", $A^{v,w_1}_{\mu\nu\eta} \equiv A^{v,w_1}_{\mu\nu\eta\mu\nu\eta}$, should currently be available either in memory or on disk. When we start calculating the (v, w_2) integrals, the current prescreen-integrals must be replaced by integrals $A^{v,w_2}_{\mu\nu\eta}$. Before we throw away the former integrals, however, we may use these to prescreen the latter. To show this, we consider their difference

$$\begin{aligned} A^{v,w_1}_{\mu\nu\eta} - A^{v,w_2}_{\mu\nu\eta} \\ = \iiint |\chi_{\mu\nu\eta}(1,2,3)|^2 \exp(-\gamma_v r_{12}^2) \exp(-\gamma_{w_1} r_{23}^2) \left[1 - \frac{\exp(-\gamma_{w_2} r_{23}^2)}{\exp(-\gamma_{w_1} r_{23}^2)}\right] \mathrm{d}r_1 \mathrm{d}r_2 \mathrm{d}r_3 \end{aligned} \tag{6.35}$$

The first three terms of the integrand in (6.35) are always positive, as discussed above. The last term is positive if $\gamma_{w_1} < \gamma_{w_2}$, negative if $\gamma_{w_1} > \gamma_{w_2}$, and zero if the two exponents are equal.

Therefore, when calculating integrals containing GTGs, we should always sort the GCFs in descending order and calculate the integrals with the most diffuse GCF first. This enables us to use the prescreen-integrals based on the current GCFs to prescreen the prescreen-integrals for the GCFs coming up next. The integral with the most diffuse GCFs, in turn, may be prescreened by the integral for which γ_w has been set to zero. In the current example with INT32 this integral reduces to a two-electron integral

$$A^{v,w}_{\mu\nu\eta}[\gamma_w = 0] = \iint |\chi_{\mu\nu}(1,2)|^2 \exp(-\gamma_v r_{12}^2) \mathrm{d}r_1 \mathrm{d}r_2 = A^v_{\mu\nu} \tag{6.36}$$

assuming that the atomic orbital have been normalised. Integral (6.36), in turn, may be prescreened by the integral for which γ_v has been set to zero. These additional levels of prescreening open for the possibility to further reduce the scaling from the N^3 potentially offered by the Cauchy–Schwarz inequality.

6.7.4 Size distribution of AO integrals in t-H_2O_2 and $(H_2O)_2$

As the prescreening schemes discussed in the previous sections are currently not implemented, we cannot present tables or figures showing how the Cauchy–Schwarz inequality actually performs for each integral type. It is, however, not difficult to get an idea of the potential the suggested prescreening algorithms have for a given system. By counting the fraction of AO integrals that, in absolute value, are smaller than the threshold set for integrals, we may find an upper limit to prescreening for this particular system, no matter what algorithms we use. Doing a thorough investigation of prescreening would require us to do this kind of study for a large variety of molecules. This is, however, outside the scope of this text and we restrict the discussion to five molecular systems: the C_2 molecule, the cyclic C_3 molecule, the tetraedric C_4 molecule, the *trans*-H_2O_2 molecule, and the water dimer.

The C_2, C_3, and C_4 molecules represent one-, two- and three-dimensional systems, respectively, that are directly comparable, and through these molecules we may investigate the effects geometry have on prescreening. The three carbon allotropes are particularly well suited for this purpose, as their regular structures allow each molecule to be uniquely specified by one carbon–carbon distance only. Also, by varying this distance in the range 100–800 pm, we may systematically study how prescreening improves with increasing inter-nuclear distance.

The C_2 and C_3 molecules have been studied using both the cc-pVDZ and the aug-cc-pVDZ basis sets, and this allows us to study the effect diffuse functions have on prescreening. Due to high computational cost, the C_4 molecule was only described using the smaller of the two sets.

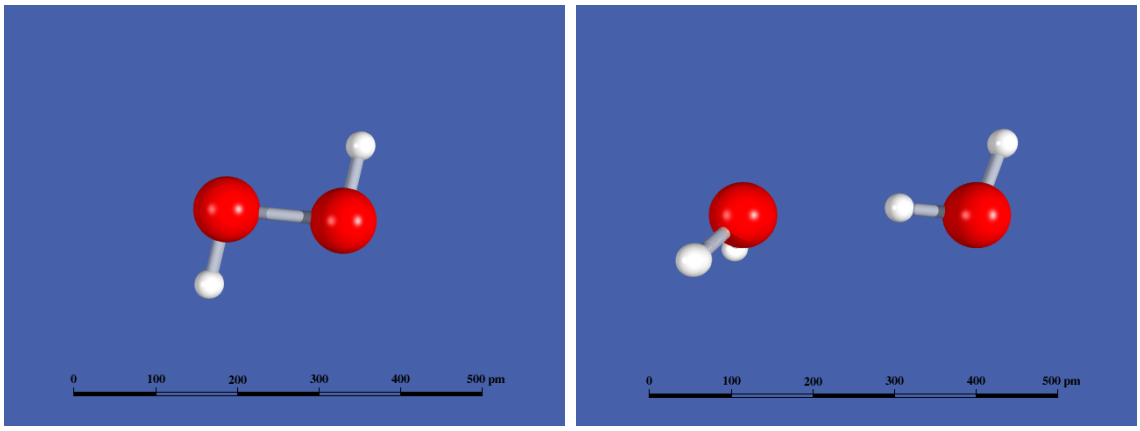

Figure 6.4: The *trans*-H_2O_2 molecule (left) and the water dimer (right).

While the three carbon molecules may be considered somewhat artificial systems, the peroxide molecule and the water dimer, provide us with a couple of "real-world" systems. These systems have been studied using the cc-pVDZ basis set and with fixed structures. The current section is devoted to these two systems only.

In the context of a Hartree–Fock calculation or a conventional MP2 calculation the *trans*-H_2O_2 molecule and the water dimer, both depicted in Figure 6.4, are small systems, and using a Cauchy–Schwarz type prescreening (or any other type of prescreening) do not have much effect. In the context of GTG-MP2 calculations, however, these systems are considered fairly large, and for prescreening to be really useful, these systems ought to contain a significant amount of redundant integrals that may be identified using a Cauchy–Schwarz inequality.

The amount of redundant integrals present in a certain system, depends on the exponents used in the GCF part of the geminals (see equations (6.1) and (6.8)). If we increase the size of an exponent, the corresponding geminal becomes more short-range and fewer of the integrals it contributes to become significant. It is therefore of fundamental importance to understand how the size of AO integrals depends on the size of the GCF exponents. Considering the set of 9 GCF exponents discussed in section 6.3, we note that for each, say, INT3E2 integral, there are $9 \times (9+1)/2 = 45$ integrals having the same six AO labels but differing in GCF exponents γ_v and/or γ_w. Studying all these variations is merely an exercise in pointlessness and we focus on diagonal elements for which $\gamma_v = \gamma_w$. Since the integrals either increase or decrease monotonically in size along the diagonal, we expect a few diagonal elements to be sufficient for obtaining a trend. Having decided to use three diagonal elements, the GTG space is probably best spanned if we use the exponents 1/3, 9, and 243.

AO integrals typically range in size from zero to one. However, as machine precision is encountered when integrals get very small, there is no point in distinguishing between integrals of size 10^{-21}, say, and integrals of size 10^{-20}. For our purpose it

turns out that 10^{-15} is suitable as the lower limit for distinguishing between integral sizes. All integrals smaller than this therefore count as if they had the size 10^{-15}. Similarly, we use 1 as an upper limit.

Integral sizes are most conveniently reported using a logarithmic scale, and once an integral has been calculated we convert its size using $-\log_{10}|I_{\text{size}}|$. Also, chopping off the decimals, the logarithm is reduced to on of the integers $\{0, 1, 2, \ldots, 15\}$. These 16 integers may now be regarded as labels for 16 stacks of integrals. On stack 10, for instance, we put integrals that have size in the range 10^{-10} to 10^{-11}, while stack 15 holds all integrals smaller than 10^{-15}.

Note, that generally we cannot put an integral onto a stack based on its own size only, as each integral typically is part of a batch in which there are tens, hundreds, or even thousands of other integrals. These integrals have the same set of orbital exponents and orbital angular momenta but their orbitals differ in their spatial orientation (e.g. p_x, p_y, p_z). From a prescreening point of view it helps us nothing that 999 out of 1000 integrals are close to zero if the last integral is, say, 10^{-1}. They all have to be calculated, no matter. Integrals belonging to the same AO batch are therefore better collectively represented by the largest integral in the batch. Our 999 integrals of size zero shall therefore join the integral going to the 10^{-1} stack implying that a total of 1000 integrals are added to this stack.

As integrals are calculated, the different stacks gradually fill up, and on some stacks large numbers are quickly encountered. We are, however, not interested in the exact number of integrals that are put onto each stack, but the relative sizes of the different stacks, i.e. the size distributions. Rather than reporting the number of integrals on each stack, we therefore report the fraction of the total number of integrals that have been put onto the different stacks. This fraction is in the following referred to as the frequency. From the definition of the frequency, we note that adding up all frequencies within a certain integral type give us 1.

The size distributions for the *trans*-H_2O_2 molecule and the water dimer using the cc-pVDZ basis set and GCFs with exponents 1/3, 9 or 243 are reported in Tables B.1 and B.2. These tables have been put in the appendices as we focus on trends rather than numbers. Since trends are better seen using graphical visualisation, we have illustrated Table B.1 graphically in Figure 6.5. The illustration shows that for a GCF exponent of 1/3 there are almost no integrals smaller than 10^{-5}, implying that there is nothing to be gained from prescreening. When the GCF exponent is increased to 9 a shift in the direction of smaller integrals is observed, as expected. This shift is most pronounced for the three-electron exchange integrals INT32 and INT3E2 which both have their maximum frequency shifted from stack 3 to stack 6. Although this is a considerable shift, we note that there is no significant amount of integrals smaller than 10^{-9} and we cannot expect prescreening to be useful for these integrals. When the GCF exponent is increased to 243, however, prescreening may prove to become important. Now, integrals INT3E2 and INT32 have their largest frequencies for stack 9 and 10, respectively, and a considerable amount of integrals

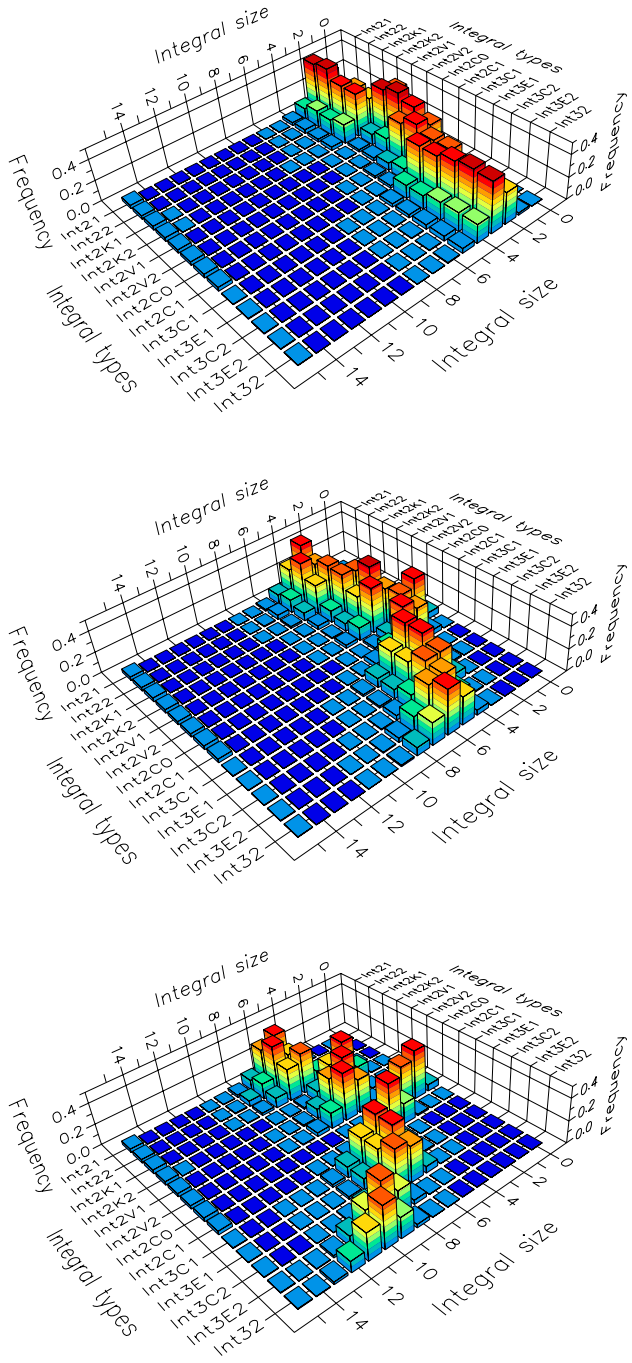

$\boxed{\gamma_v = \gamma_w = \frac{1}{3}}$

$\boxed{\gamma_v = \gamma_w = 9}$

$\boxed{\gamma_v = \gamma_w = 243}$

Figure 6.5: The size distribution of AO integrals for the *trans*-H_2O_2 molecule with basis set cc-pVDZ and one GCF. The stack each integral belongs to is obtained from the expression $-\mathrm{int}(\log_{10}|I_{\mathrm{size}}|)$. Frequencies given on stacks 0–15 add up to 1 within each integral type.

is therefore smaller than 10^{-10}. This is an interesting observation as some three-electron integrals probably have numerical precision of this order. This is explained shortly.

It is a well-known fact that numerical precision is lost when two almost equal numbers are subtracted. Due to the large number of additions/subtractions needed to generate them, three-electron integrals are especially exposed to this. Equation (4.52) which gives the Hermite integrals needed to produce integrals INT3E2, is a good example. Note that the summations run over angular momenta, and integrals are therefore more likely to lose numerical precision as their angular momentum increase. An integral consisting purely of s-orbitals, however, can be constructed without any subtractions and may consequently be given with machine precision.

By calculating an integral using two different algorithms and comparing the numbers, we may get an idea of how precisely the integral has been calculated. In a small test study, the Hermite integrals needed to construct INT3E1 integrals for the water molecule were calculated with and without the use of translational symmetry. When an integral batch consisting of f-orbitals were considered, out of the 592 704 integrals, 2 differed in the 9th figure, 28 differed in the 10th figure, and 191 differed in the 11th figure. Although this was a somewhat artificial test case, it suggests that we ought to be careful trusting the numerical value of three-electron integrals as small as 10^{-10}. Integrals belonging to stack 9 or 10 may therefore turn out to be redundant due to limited machine precision.

Table B.2, which gives the size distribution of AO integrals in the water dimer, has been visualised in Figure 6.6. Considering the most diffuse GCF first, we note that integral sizes are more evenly distributed in the dimer than in the peroxide molecule. This becomes particularly clear if we compare the number of stacks having a zero frequency i.e. containing no integrals. These stacks may be identified by their dark blue colour. Interestingly, there also seems to be a small fraction of integrals that may be prescreened even for this diffuse GCF. Moving on to the size distribution for the GCF with exponent 9, we see that the amount of integrals that may be prescreened have increased considerably, especially for INT32 and INT3E2. Finally, using the most contracted GCF, we see that for the three-electron exchange integrals only a small fraction of integrals actually need to be calculated.

6.7.5 Size distribution of AO integrals in the C_2, C_3, and C_4 molecules as a function of the carbon–carbon distance

When we turn to applications in chapter 7, we see that augmented basis sets like aug-cc-pVDZ generally performs a lot better than the corresponding non-augmented basis sets. Since the augmented functions are diffuse, we expect poorer prescreening when these are present. In the next couple of sections we have used the molecules C_2 and C_3 to study the effect diffuse functions have on prescreening. Using these molecules, we have also studied how integrals decrease in magnitude as the carbon–

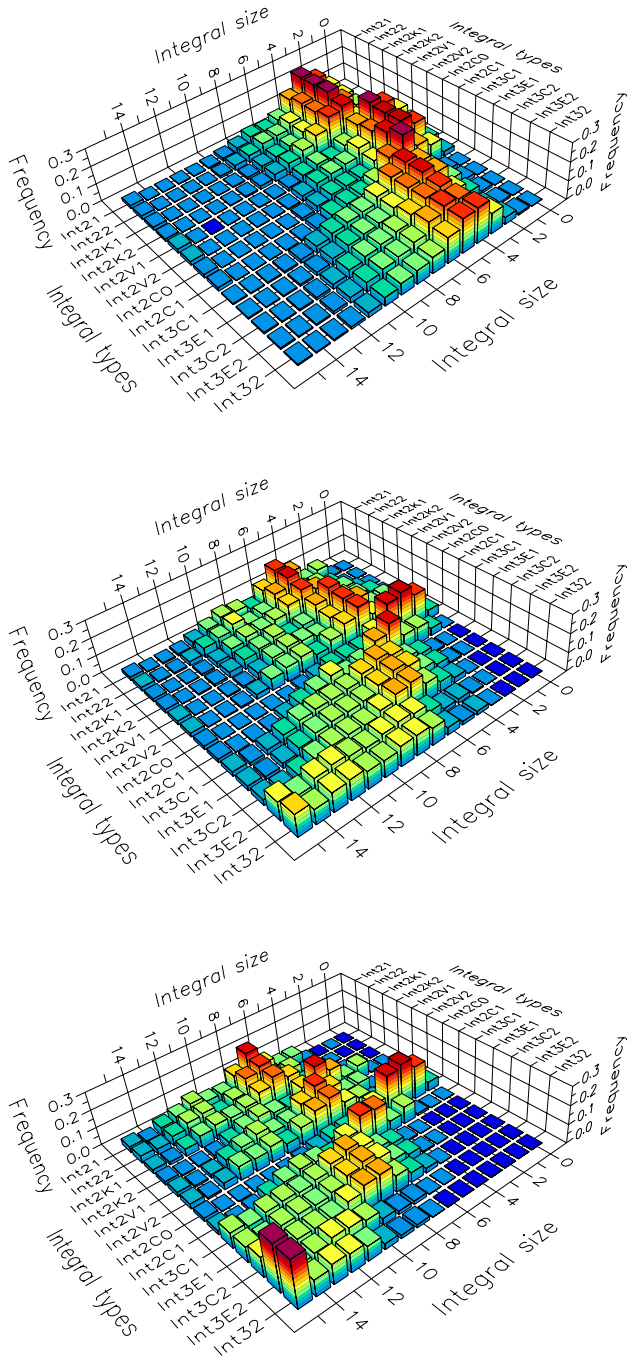

Figure 6.6: The size distribution of AO integrals for the water dimer with basis set cc-pVDZ and one GCF. The stack each integral belongs to is obtained from the expression $-\mathrm{int}(\log_{10}|I_{\mathrm{size}}|)$. Frequencies given on stacks 0–15 add up to 1 within each integral type.

carbon distance increases. This distance dependency have been investigated for the tetraedric C_4 molecule as well, but in this case only the cc-pVDZ basis set were used.

Since the basis sets for carbon are more diffuse than the corresponding basis sets for the nitrogen, oxygen and hydrogen atoms, the results presented below ought to be applicable to a wide range of organic molecules.

The C_2 molecule

Guided by the discussion in the previous section we assume that all integrals smaller than 10^{-10} are insignificant and may be prescreened. If we add up the fraction of integrals smaller than this value, therefore, we get the fraction of integrals that may be prescreened for each integral type. This fraction is obtained directly from the size distribution table by adding up the frequencies given in stacks 10–15 for the integral type in question.

In Table 6.10 we present the fraction of integrals that may be prescreened in the C_2 molecule when we use basis sets cc-pVDZ and aug-cc-pVDZ, eight different inter-nuclear separations, and 3 different GCF exponents. All calculations have been done using symmetric overlap distributions, making diagonal elements $\Omega_{\mu\mu}$ slightly over-represented. The fractions in Table 6.10 are therefore somewhat too small.

For accountability we have also included a few of the size distribution tables that Table 6.10 is based on. These tables are located in appendix B as Tables B.3 and B.4.

We begin studying the uppermost part of Table 6.10 which gives the fraction of prescreenable integrals when using basis set cc-pVDZ and a GCF exponent of 1/3. Looking through the numbers we see that these naturally may be divided into three categories. Those belonging to two-electron integrals, those belonging to the three-electron integrals of type INT3C1, INT3E1, and INT3C2 and those belonging to the three-electron integrals INT3E2 and INT32. The three categories are in the following referred to as category 1, 2 and 3, respectively. Within each category the different integral types behave similarly. Note, however, that the two-electron Coulomb integral does not really fit into category 1. Since it is not a geminal integral this is to be expected, and it is included for reference only.

As the inter-nuclear distance increases the fraction of integrals that has to be calculated drops. It drops slowest for the two-electron integrals in category 1, somewhat faster for the three-electron integrals in category 2 and fastest for the three-electron integrals in category 3. When the carbon–carbon distance has increased to approximately 800 pm, however, all fractions have reached or nearly reached their maximum value. This maximum value gives the largest fraction of integrals that may be prescreened. Since there is nothing more to be gained from prescreening when the carbon atoms are moved further apart, the integrals still surviving must all be one-centre integrals.

Table 6.10: The fraction of integrals that may be prescreened (size $< 10^{-10}$) in the C_2 molecule using basis sets cc-pVDZ (upper part of table) and aug-cc-pVDZ (lower part of table). The inter-nuclear distance r(C–C) is given in picometer.

	r(C–C)	I21	I22	I2K1	I2K2	I2V1	I2V2	I2C0	I2C1	I3C1	I3E1	I3C2	I3E2	I32
$\gamma = \frac{1}{3}$	100	.0999	.0949	.0916	.0836	.1023	.0977	.0961	.0947	.0217	.0217	.0215	.0214	.0217
	200	.0908	.0908	.0972	.0907	.0931	.0931	.0908	.0908	.0213	.0213	.0213	.0212	.0213
	300	.0908	.0919	.1137	.1057	.0931	.0948	.0908	.0908	.0226	.0226	.0236	.0238	.0234
	400	.1546	.1605	.1508	.1641	.1386	.1448	.1440	.1496	.2853	.2853	.3438	.3743	.3403
	500	.4863	.5891	.4796	.5902	.4600	.5404	.4128	.5177	.6787	.6787	.7565	.7835	.7586
	600	.6861	.7680	.7184	.7831	.6535	.7403	.5629	.7267	.8266	.8266	.8488	.9159	.9018
	700	.8237	.8579	.8261	.8538	.7649	.7867	.6498	.8344	.9120	.9120	.9281	.9693	.9634
	800	.9178	.9237	.9261	.9362	.8705	.8879	.7661	.9215	.9440	.9440	.9444	.9826	.9827
$\gamma = 9$	100	.0933	.0928	.0852	.0933	.0901	.0910	.0961	.0931	.0212	.0212	.0211	.0208	.0210
	200	.0921	.0927	.0972	.0924	.0937	.0926	.0908	.0921	.0216	.0216	.0216	.0218	.0219
	300	.0931	.0942	.1163	.0933	.0996	.0994	.0908	.0929	.0502	.0502	.0747	.2836	.3664
	400	.4053	.4995	.4197	.3296	.3107	.3985	.1440	.3248	.6539	.6539	.7013	.8956	.9022
	500	.7493	.7563	.7679	.7506	.7173	.7312	.4128	.7374	.8334	.8334	.8453	.9341	.9409
	600	.8097	.8515	.8313	.7991	.7708	.7811	.5629	.7905	.9034	.9034	.9181	.9813	.9827
	700	.9235	.9241	.9273	.9293	.8743	.8914	.6498	.9179	.9437	.9437	.9442	.9828	.9828
	800	.9241	.9240	.9372	.9373	.8938	.8932	.7661	.9239	.9473	.9473	.9482	.9827	.9827
$\gamma = 243$	100	.0935	.0935	.0849	.0940	.0917	.0917	.0961	.0935	.0211	.0211	.0211	.0206	.1099
	200	.0926	.0926	.0966	.0930	.0939	.0939	.0908	.0926	.0216	.0216	.0218	.2307	.7645
	300	.1288	.1768	.1576	.0933	.1082	.1203	.0908	.0954	.3122	.3122	.4180	.9276	.9788
	400	.7240	.7392	.7247	.4385	.6726	.6953	.1440	.5769	.8133	.8133	.8314	.9795	.9828
	500	.8064	.8429	.8276	.7646	.7620	.7767	.4128	.7674	.9033	.9033	.9207	.9827	.9828
	600	.9208	.9239	.9241	.8309	.8480	.8864	.5629	.8873	.9442	.9442	.9456	.9827	.9827
	700	.9240	.9241	.9371	.9366	.8943	.8943	.6498	.9240	.9481	.9481	.9487	.9827	.9827
	800	.9240	.9240	.9372	.9372	.8943	.8943	.7661	.9240	.9481	.9481	.9497	.9827	.9827
$\gamma = \frac{1}{3}$	100	.0927	.0905	.0908	.0827	.0914	.0873	.0909	.0903	.0191	.0191	.0190	.0190	.0191
	200	.0837	.0836	.0865	.0806	.0678	.0677	.0843	.0837	.0187	.0187	.0187	.0186	.0187
	300	.0821	.0822	.0930	.0849	.0668	.0671	.0821	.0821	.0187	.0187	.0189	.0188	.0188
	400	.0915	.0933	.1027	.1001	.0733	.0748	.0900	.0912	.0782	.0782	.1013	.1163	.1002
	500	.2381	.2818	.2468	.2833	.2091	.2461	.2110	.2497	.3314	.3314	.4046	.4365	.4007
	600	.3783	.4638	.4062	.4762	.3393	.4259	.2847	.4135	.5529	.5529	.6009	.7069	.6748
	700	.5510	.6004	.5664	.6088	.4998	.5425	.3933	.5661	.7253	.7253	.7666	.8550	.8360
	800	.7142	.7615	.7353	.7803	.6633	.7230	.5357	.7355	.8311	.8311	.8488	.9295	.9202
$\gamma = 9$	100	.0898	.0897	.0869	.0894	.0847	.0853	.0909	.0898	.0189	.0189	.0189	.0187	.0188
	200	.0837	.0837	.0872	.0831	.0665	.0668	.0843	.0835	.0187	.0187	.0187	.0187	.0188
	300	.0827	.0827	.0939	.0820	.0681	.0683	.0821	.0825	.0228	.0228	.0276	.0982	.1423
	400	.1776	.2219	.1962	.1436	.1263	.1614	.0900	.1432	.3058	.3058	.3580	.6145	.6426
	500	.4341	.4471	.4549	.4295	.4019	.4108	.2110	.4254	.5408	.5408	.5751	.8170	.8466
	600	.5679	.6057	.5952	.5381	.5202	.5435	.2847	.5379	.7384	.7384	.7680	.9244	.9353
	700	.7446	.7825	.7746	.7049	.7067	.7357	.3933	.7051	.8460	.8460	.8571	.9454	.9491
	800	.8221	.8296	.8382	.8176	.7820	.7889	.5357	.8128	.8783	.8783	.8855	.9569	.9630
$\gamma = 243$	100	.0900	.0900	.0868	.0897	.0860	.0861	.0909	.0900	.0189	.0189	.0189	.2406	.8332
	200	.0836	.0836	.0872	.0832	.0672	.0672	.0843	.0836	.0188	.0188	.0190	.4407	.9405
	300	.0911	.1078	.1132	.0820	.0703	.0748	.0821	.0828	.1132	.1132	.1719	.8838	.9899
	400	.3932	.4204	.4020	.1926	.3516	.3797	.0900	.2769	.5003	.5003	.5503	.9703	.9941
	500	.5496	.6013	.5901	.4399	.4881	.5222	.2110	.4643	.7426	.7426	.7870	.9815	.9943
	600	.7421	.7801	.7798	.5781	.6878	.7286	.2847	.6489	.8613	.8613	.8798	.9843	.9944
	700	.8266	.8354	.8488	.7565	.7895	.7975	.3933	.7992	.8984	.8984	.9147	.9850	.9944
	800	.8523	.8681	.8717	.8317	.8080	.8151	.5357	.8323	.9257	.9257	.9388	.9850	.9943

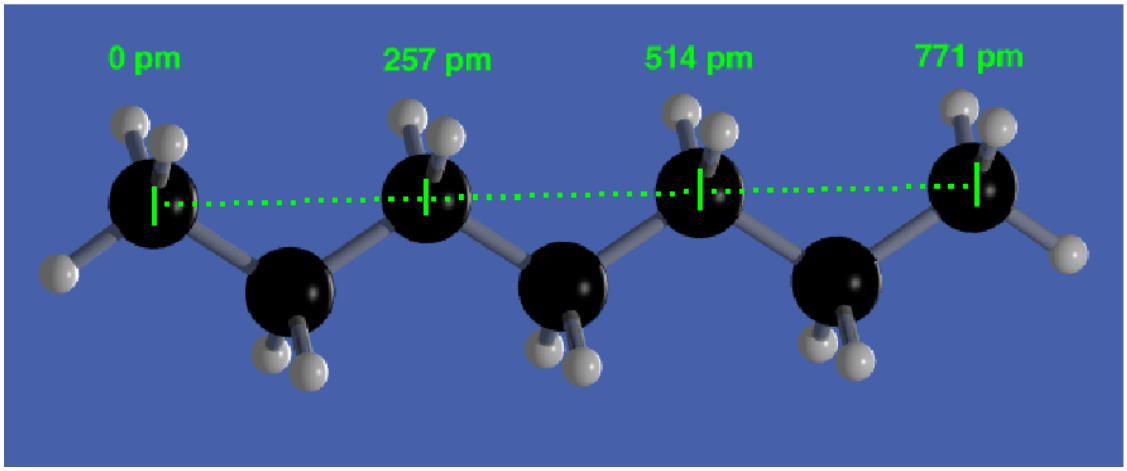

Figure 6.7: Some C–C distances in the n-heptane molecule. This figure is included to illustrate the range of the different C_2 integrals given in Table 6.10.

For comparison, we have in Figure 6.7 depicted the n-heptane molecule and some of its internal carbon–carbon distances. Since the two terminal carbon atoms in the chain are separated by nearly 800 pm, we conclude that geminal integrals constructed from basis set cc-pVDZ and GCFs having exponent 1/3, ranges over 7 carbon atoms in an alkane chain. This is a somewhat disappointing result. Note, also, that for inter-nuclear distances smaller than 300 pm there is hardly any integrals at all that can be prescreened. After that, however, the fraction of integrals that may be discarded increases rapidly within all three categories.

When the GCF exponent is increased to 9, integrals die off more quickly with orbital separation and the maximum fraction of prescreenable integrals is reached at a carbon–carbon distance of 700 pm for integrals in category 1 and 2 and at a distance of 600 pm for integrals in category 3. Again, the fraction of integrals that may be prescreened makes a jump after 300 pm. For the CPU intensive integrals in category 3 a noticeable amount of integrals may also be prescreened even at 300 pm.

Increasing the exponent to 243, the integrals in category 1 still reaches maximum prescreening at a carbon–carbon distance of 700 pm. For the three-electron integrals in category 2, however, maximum prescreening is now reached at 600 pm, and for the three-electron integrals INT3E2 and INT32 the maximum is reached at 400 pm and 300 pm, respectively. For the latter two integral types, this means that only few integrals range across more than 3 carbon atoms of an alkane chain.

Moving on to basis set aug-cc-pVDZ we expect less prescreening to be possible. The lower part of Table 6.10 shows that this is also the case. Note, for instance, that when using a GCF exponent of 1/3 no integral type has reached maximum possible prescreening even at a carbon–carbon distance of 800 pm. A comparison with fractions obtained with the GCF exponent 243 shows that. We also note that

while the fraction of integrals that may be prescreened took a jump after 300 pm for the cc-pVDZ basis, the corresponding jump now comes after 400 pm.

Continuing with the GCF exponent 9, we note that fractions increase slowly, and at an inter-nuclear distance of 800 pm, they have still not reached maximum for either of the integral types. Note, however, that there is a small jump after 300 pm again. We also note that some 60% of integrals in category 3 may be prescreened when the carbon–carbon distance is 400 pm. This, approximately, corresponds to the distance between atom number 1 and 4 in the carbon chain of n-heptane.

With the most contracted GCF, having an exponent of 243, the largest fraction of integrals that may be prescreened is reached at a inter-nuclear distance of 800 pm for the integrals in category 3. For the other integrals the limit is still not reached at that distance.

Note, finally, that a larger fraction of integrals may be prescreened for the aug-cc-pVDZ basis set than for the cc-pVDZ basis set. This, which at first may seem strange, only states that the relative amount of one-centre integrals is smaller in the larger basis set.

The cyclic C_3 molecule

Before drawing conclusions from Table 6.10 alone, some caution should be exercised. Since the C_2 molecule is a two-centre molecule, only one- and two-centre integrals are present in a calculation. Three-electron integrals, however, may have up to six different canters, and the more different centres there are in an integral, the more likely the integral is prescreenable. Also, for a large molecule, there is more three-centre integrals than two-centre integrals, more four-centre integrals than three-centre integrals, and so forth. The numbers given in Table 6.10 may therefore be far too pessimistic.

To check whether this is indeed the case, we have repeated all calculations, but this time for the cyclic C_3 molecule (regular triangle). Since this molecule contains three atoms, three-centre integrals appear.

In Table 6.11 we have presented the fraction of prescreenable integrals for the C_3 molecule. We shall not describe this table in detail, as it exhibits the same trends as Table 6.10. Note, especially, that integrals become redundant at about the same inter-nuclear distances in the C_3 molecule as they did in the C_2 molecule, and there is no major shift in the direction of shorter distances. For a given distance, however, the amount of integrals that may be prescreened is significantly larger in the C_3 molecule than in the C_2 molecule.

The tetraedric C_4 molecule

It may still be argued, however, that a 2D system is also too small to give a representable picture of the prescreening potentials. To investigate whether this is true, we have included the tetraedric C_4 molecule in our study. As with the C_3 molecule,

Table 6.11: The fraction of integrals that may be prescreened (size $< 10^{-10}$) in the cyclic C_3 molecule using basis sets cc-pVDZ (upper part of table) and aug-cc-pVDZ (lower part of table). The inter-nuclear distance r(C–C) is given in picometer.

	r(C–C)	I21	I22	I2K1	I2K2	I2V1	I2V2	I2C0	I2C1	I3C1	I3E1	I3C2	I3E2	I32
$\gamma = \frac{1}{3}$	100	.0298	.0295	.0271	.0260	.0168	.0161	.0299	.0295	.0034	.0034	.0034	.0034	.0034
	200	.0302	.0299	.0292	.0278	.0153	.0154	.0305	.0301	.0034	.0034	.0034	.0034	.0034
	300	.0303	.0307	.0321	.0302	.0154	.0161	.0306	.0303	.0091	.0091	.0165	.0205	.0151
	400	.1766	.2551	.1527	.2244	.1243	.1854	.1339	.2026	.5047	.5047	.5827	.6557	.6111
	500	.6128	.7043	.5832	.7018	.5509	.6618	.4980	.6466	.8418	.8418	.8889	.9256	.9108
	600	.8099	.8732	.8170	.8797	.7778	.8528	.6633	.8373	.9360	.9360	.9465	.9791	.9743
	700	.8979	.9158	.9004	.9150	.8716	.8887	.7597	.9037	.9727	.9727	.9791	.9925	.9903
	800	.9706	.9763	.9741	.9804	.9473	.9612	.8643	.9755	.9865	.9865	.9867	.9978	.9976
$\gamma = 9$	100	.0288	.0285	.0253	.0278	.0145	.0146	.0299	.0286	.0033	.0033	.0032	.0032	.0033
	200	.0309	.0309	.0290	.0299	.0147	.0144	.0305	.0309	.0035	.0035	.0035	.0035	.0036
	300	.0386	.0508	.0388	.0331	.0183	.0214	.0306	.0343	.1565	.1565	.2272	.6176	.6821
	400	.5404	.6344	.5275	.4519	.4211	.5039	.1339	.4525	.8279	.8279	.8559	.9629	.9673
	500	.8475	.8613	.8547	.8371	.8187	.8312	.4980	.8313	.9384	.9384	.9441	.9833	.9850
	600	.9005	.9130	.9077	.8959	.8782	.8817	.6633	.8911	.9674	.9674	.9755	.9977	.9976
	700	.9761	.9765	.9786	.9764	.9556	.9618	.7597	.9732	.9863	.9863	.9866	.9976	.9977
	800	.9767	.9767	.9813	.9812	.9631	.9630	.8643	.9766	.9880	.9880	.9881	.9976	.9976
$\gamma = 243$	100	.0286	.0286	.0252	.0279	.0145	.0145	.0299	.0286	.0033	.0033	.0033	.0031	.1094
	200	.0311	.0313	.0291	.0300	.0145	.0145	.0305	.0308	.0037	.0037	.0042	.4870	.9637
	300	.2157	.2776	.1977	.0399	.1177	.1745	.0306	.0806	.5625	.5625	.6620	.9823	.9973
	400	.8163	.8301	.8112	.5734	.7705	.7944	.1339	.7217	.9217	.9217	.9378	.9975	.9978
	500	.8973	.9121	.9054	.8581	.8744	.8787	.4980	.8775	.9680	.9680	.9770	.9977	.9977
	600	.9760	.9766	.9768	.9069	.9370	.9612	.6633	.9218	.9866	.9866	.9873	.9977	.9976
	700	.9767	.9767	.9812	.9806	.9630	.9631	.7597	.9767	.9881	.9881	.9883	.9976	.9976
	800	.9766	.9766	.9811	.9811	.9630	.9631	.8643	.9766	.9883	.9883	.9884	.9976	.9976
$\gamma = \frac{1}{3}$	100	.0256	.0254	.0248	.0238	.0109	.0107	.0257	.0254	.0027	.0027	.0027	.0027	.0027
	200	.0257	.0256	.0252	.0242	.0093	.0093	.0259	.0257	.0027	.0027	.0027	.0027	.0027
	300	.0257	.0258	.0261	.0246	.0090	.0092	.0259	.0257	.0030	.0030	.0036	.0038	.0035
	400	.0509	.0777	.0488	.0698	.0256	.0427	.0410	.0599	.1467	.1467	.1919	.2456	.2120
	500	.2730	.3384	.2584	.3309	.2287	.2922	.2197	.2931	.4738	.4738	.5531	.6400	.5967
	600	.4708	.5637	.4818	.5714	.4228	.5234	.3117	.5095	.7265	.7265	.7681	.8661	.8441
	700	.6625	.7113	.6736	.7268	.6264	.6711	.4656	.6767	.8661	.8661	.8923	.9504	.9411
	800	.8072	.8541	.8221	.8652	.7777	.8208	.6234	.8250	.9300	.9300	.9388	.9794	.9764
$\gamma = 9$	100	.0252	.0251	.0240	.0246	.0101	.0101	.0257	.0251	.0027	.0027	.0027	.0026	.0026
	200	.0258	.0257	.0252	.0251	.0089	.0089	.0259	.0257	.0027	.0027	.0027	.0027	.0028
	300	.0275	.0295	.0275	.0258	.0096	.0102	.0259	.0265	.0273	.0273	.0464	.2338	.2924
	400	.2008	.2663	.2013	.1494	.1234	.1702	.0410	.1503	.4537	.4537	.4983	.7596	.7920
	500	.5022	.5264	.5144	.4839	.4681	.4841	.2197	.4836	.7066	.7066	.7431	.9290	.9436
	600	.6762	.7090	.6970	.6456	.6340	.6574	.3117	.6475	.8739	.8739	.8942	.9794	.9825
	700	.8464	.8642	.8531	.8074	.7980	.8342	.4656	.8120	.9374	.9374	.9445	.9869	.9884
	800	.9015	.9067	.9082	.8930	.8791	.8869	.6234	.8912	.9575	.9575	.9623	.9903	.9916
$\gamma = 243$	100	.0251	.0251	.0240	.0247	.0101	.0101	.0257	.0251	.0027	.0027	.0027	.2181	.8480
	200	.0257	.0257	.0253	.0251	.0089	.0090	.0259	.0256	.0028	.0028	.0030	.6286	.9911
	300	.0734	.0929	.0718	.0272	.0309	.0465	.0259	.0351	.2058	.2058	.3006	.9739	.9987
	400	.4585	.4832	.4564	.2198	.3992	.4341	.0410	.3342	.6561	.6561	.7193	.9950	.9992
	500	.6558	.6962	.6894	.5094	.5945	.6291	.2197	.5582	.8797	.8797	.9105	.9970	.9992
	600	.8439	.8695	.8654	.6848	.7804	.8243	.3117	.7422	.9493	.9493	.9596	.9977	.9993
	700	.9083	.9170	.9218	.8523	.8845	.8927	.4656	.8761	.9692	.9692	.9753	.9979	.9992
	800	.9272	.9356	.9376	.9056	.9072	.9119	.6234	.9131	.9792	.9792	.9839	.9979	.9993

Table 6.12: The fraction of integrals that may be prescreened (size $< 10^{-10}$) in the C_4-molecule using the basis set cc-pVDZ. The inter-nuclear distance r(C–C) is given in picometer.

	r(C–C)	I21	I22	I2K1	I2K2	I2V1	I2V2	I2C0	I2C1	I3C1	I3E1	I3C2	I3E2	I32
$\gamma = \frac{1}{3}$	100	.0125	.0121	.0114	.0111	.0120	.0118	.0128	.0121	.0008	.0008	.0008	.0007	.0008
	200	.0135	.0132	.0154	.0147	.0131	.0129	.0140	.0133	.0010	.0010	.0010	.0010	.0010
	300	.0195	.0204	.0241	.0215	.0190	.0198	.0188	.0201	.0177	.0177	.0385	.0541	.0368
	400	.2430	.3585	.2117	.3244	.1824	.2744	.1601	.2857	.6434	.6434	.7188	.7919	.7525
	500	.6966	.7895	.6772	.7886	.6464	.7520	.5692	.7292	.9122	.9122	.9414	.9696	.9613
	600	.8788	.9227	.8833	.9269	.8566	.9086	.7335	.8985	.9711	.9711	.9765	.9929	.9911
	700	.9412	.9525	.9420	.9512	.9258	.9362	.8286	.9456	.9895	.9895	.9923	.9979	.9971
	800	.9864	.9896	.9880	.9917	.9733	.9826	.9112	.9892	.9952	.9952	.9953	.9995	.9994
$\gamma = 9$	100	.0120	.0119	.0105	.0114	.0105	.0106	.0128	.0119	.0008	.0008	.0008	.0007	.0007
	200	.0136	.0137	.0159	.0132	.0135	.0133	.0140	.0136	.0011	.0011	.0011	.0017	.0019
	300	.0478	.0740	.0431	.0348	.0272	.0367	.0188	.0350	.2812	.2812	.3719	.7815	.8290
	400	.6719	.7379	.6454	.5929	.5559	.6311	.1601	.5937	.8991	.8991	.9167	.9844	.9865
	500	.8998	.9148	.9052	.8860	.8762	.8896	.5692	.8831	.9719	.9719	.9751	.9942	.9949
	600	.9408	.9501	.9455	.9392	.9303	.9319	.7335	.9365	.9873	.9873	.9908	.9994	.9995
	700	.9894	.9899	.9908	.9893	.9802	.9829	.8286	.9884	.9952	.9952	.9953	.9994	.9994
	800	.9900	.9901	.9920	.9920	.9837	.9838	.9112	.9900	.9958	.9958	.9959	.9994	.9994
$\gamma = 243$	100	.0119	.0119	.0105	.0115	.0105	.0105	.0128	.0119	.0008	.0008	.0008	.0007	.1391
	200	.0144	.0147	.0163	.0132	.0132	.0134	.0140	.0137	.0016	.0016	.0025	.7027	.9880
	300	.3258	.3943	.3008	.0537	.1859	.2600	.0188	.1285	.7127	.7127	.7932	.9941	.9993
	400	.8684	.8839	.8662	.6972	.8299	.8476	.1601	.7956	.9623	.9623	.9720	.9993	.9996
	500	.9390	.9492	.9440	.9079	.9269	.9301	.5692	.9272	.9874	.9874	.9916	.9995	.9994
	600	.9896	.9900	.9899	.9447	.9674	.9827	.7335	.9575	.9953	.9953	.9956	.9995	.9994
	700	.9900	.9900	.9920	.9915	.9839	.9839	.8286	.9901	.9961	.9961	.9961	.9994	.9994
	800	.9900	.9900	.9920	.9920	.9839	.9840	.9112	.9900	.9961	.9961	.9961	.9994	.9994

the structure of the C_4 molecule is fully described by one C–C distance.

The results are presented in Table 6.12. Due to the high CPU requirements, we did not consider the aug-cc-pVDZ basis set for this molecule. The relationship between augmented and non-augmented basis sets were covered extensively for the C_2 and C_3 molecules, and it is unlikely that a different relationship would be revealed for the C_4 molecule.

The numbers given in Table 6.12 reveal the same trends as found in the two smaller molecules, and no matter which system we consider integrals start becoming redundant at about the same distance. For a given inter-nuclear distance, however, the fraction of prescreenable integrals increases significantly with the system size.

Considering the results presented for the three carbon allotropes in this section, we conclude that implementing Cauchy–Schwarz prescreening by itself is not sufficient to break barriers for how big systems we can treat with GTG-MP2 theory. Especially not if decent basis sets like aug-cc-pVDZ are to be used.

6.8 Linear dependencies and numerical stability

In Tables 6.1 and 6.2 presented in section 6.3, we saw that the pq-ansatz performs better than the kq-ansatz, and that the kq-ansatz, in turn, outperforms the kl-ansatz. As our energies are obtained variationally and therefore bound to improve when the basis set is increased, this is to be expected.

Unfortunately, the improved energies does not come without cost. Using $\mathrm{LDL}^{\mathrm{T}}$ factorisation to solve the linear equations (3.95), $\mathcal{O}(N^3)$ arithmetic operations must be performed when N linear equations are present. Since the kq- and pq-ansätze give larger basis sets than the kl-ansatz they also give a larger number of linear equations and thus more calculation time. For the kl-ansatz the number of equations to solve depends on the number of GCFs and the number of occupied orbitals only, and N is therefore typically of modest size. For the kq-ansatz, however, N grows linearly with the one-electron basis set, and for the pq-ansatz the growth is quadratic. For the kq- and pq-ansätze, therefore, the CPU time spent in the equation solver can become very large.

The CPU time spent in the integral calculation, on the other hand, is less affected by the choice of ansatz. The integral code is essentially the same for all ansätze and the only significant difference lies in the MO transformation. For the current implementation, however, this transformation consumes only a small part of the total calculation time, something Table 6.5 clearly indicates. Moreover, since the AO formulation of the pq-ansatz (6.13) involves no MO transformations at all, this ansatz may be expected to have the slightly faster integral calculation.

Due to the equation solver, calculations involving the kq- and pq-ansätze generally require more CPU time than calculations involving the kl-ansatz. More importantly, however, they also require more memory. In the case of the pq-ansatz this is actually a critical issue. As we experienced in section 6.3, the water molecule can not be described with the aug-cc-pCVTZ(spd,sp) basis set when using the pq-ansatz. Containing 71 contracted AOs, this basis set is not particularly big, and the pq-ansatz can therefore be expected to have limited applicability only. Fortunately, the kq-ansatz, which performs nearly as good as the pq-ansatz, is less memory intensive, and what currently limits the use of this ansatz is CPU time requirements rather than memory requirements.

The kq- and pq-ansätze outperforms the kl-ansatz since they use a wider range of AO combinations in their respective two-electron basis sets. This, however, also makes the ansätze more exposed to numerical instabilities. Partly, because more arithmetic operations are needed to solve their equation systems, but also because their basis sets (cf. (6.2)) are more likely to contain linear dependencies. A linear dependency may arise, for instance, if a two-electron basis functions like $g_{kq,v}$ becomes to resemblant to another function $g_{kr,v}$ or $g_{kq,w}$.

For a given ansatz and one-electron basis set we can check for this kind of linear dependencies by diagonalising the geminal-geminal overlap matrix INT22. A small

eigenvalue indicates that a basis function (or linear combination of basis functions) are similar to another basis function (or linear combination of basis functions). A zero eigenvalue implies that there is an exact overlap.

To investigate whether linear dependency indeed may represent a problem for either of the ansätze, we have calculated some INT22 matrices for the neon atom and the water molecule and diagonalised these. For comparison with sections 6.3 and 6.4 we have used basis sets cc-pVDZ and aug-cc-pCVTZ(spd)/(spd,sp) once more. For the latter basis set, the original four d-orbitals for oxygen were replaced by the single d-orbital taken from the cc-pVDZ basis when the water molecule was described with the pq-ansatz. Different GCF expansions were also used to investigate how linear dependency is related to the choice of GCF exponents and the number of GCFs included in the expansion of a geminal.

After diagonalising the INT22 matrices, their eigenvalues λ were transformed to the integers 0–15 using the relations

$$\Delta(\lambda) = \begin{cases} 0, & \text{if} \quad \lambda \geq 1 \\ -\text{int}(\log_{10}\lambda), & \text{if} \quad 1 > \lambda > 10^{-16} \\ 15, & \text{if} \quad \lambda \leq 10^{-16} \end{cases} \tag{6.37}$$

Thus, eigenvalues lying in the range $10^{-4} \geq \lambda > 10^{-5}$, for instance, were transformed to $\Delta = 4$.

In Table 6.13 we have listed transformed eigenvalues for the neon atom. Each entry in the table gives the total number of eigenvalues transformed to a particular Δ. For each ansatz four different expansions of GCFs were investigated. Three of the expansions consisted of a single GCF having exponent 1/3, 9, or 243, while the fourth expansion was the standard set of GCFs discussed in section 6.3. This expansion is denoted "Full" in the table.

Beginning with the kl-ansatz, we see that the distribution of eigenvalues is quite sensitive to the choice of GCF exponent. The larger the exponent, the larger the overlap between different geminals. For the kl-ansatz, however, the distribution of eigenvalues is insensitive to the choice of one-electron basis.

Moving to the kq-ansatz, we see that the distribution of eigenvalues is even more sensitive to the choice of GCF exponent than for the kl-ansatz. This is also true for the pq-ansatz. Furthermore, we note that for the kq- and pq-ansätze the degree of linear dependency increases, i.e. the number of small eigenvalues increases, when the one-electron basis set is increased. Note, especially, that there is a considerable amount of eigenvalues smaller than 10^{-15} for the pq-ansatz. These eigenvalues corresponds to GCFs or linear combinations of GCFs that, within numerical precision, is identical to linear combinations of other GCFs.

This is not a fortunate situation as the equation solver may fail to converge in certain situations, as seen in Table 7.10. Exactly when a calculation is going to fail to converge is difficult to say, however. When using the AO formulation of

Table 6.13: Distribution of eigenvalues (λ) for some INT22 matrices for the neon atom. Geminals are constructed using basis sets cc-pVDZ (upper part of table) and aug-cc-pCVTZ(spd) (lower part of table) and using either one GCF having exponent $\frac{1}{3}$, 9 or 243 or the full set of 9 GCFs that was discussed in section 6.3. Eigenvalues are reported as $\Delta = -\mathrm{int}(\log_{10}\lambda)$.

	KL				KQ				PQ			
Δ	1/3	9	243	Full	1/3	9	243	Full	1/3	9	243	Full
0	15	1		19	59	1		67	80	2		115
1		13	1	25	1	20	1	70	24	34	1	108
2				22		15		77	1	26	1	124
3		1	9	28		17	20	100		21	31	162
4			4	23		7	9	83		21	19	155
5				13			9	60		1	13	104
6			1	3			10	36			6	71
7				1				20			14	35
8				1			8	12			9	32
9							3	7			11	27
10								5				4
11								3				8
12												
13												
14												
15												
0	15	1		19	227	15		309	440	78	4	750
1		13	1	25	42	82	5	266	298	118	22	609
2				22	16	59	10	337	168	109	34	791
3		1	9	28		39	49	415	107	127	57	931
4			4	23		38	41	323	18	131	73	1018
5				13		25	32	220	4	91	63	865
6			1	3		12	29	197		104	87	727
7				2		11	22	130		99	72	671
8						1	27	125		86	66	567
9							36	93		31	86	438
10						3	16	57		28	95	416
11							6	48		27	91	373
12							8	18		3	64	317
13							4	15		3	66	225
14								12			36	171
15											119	446

the kq-ansatz (see Equation (6.14)), for instance, redundant two-electron basis sets are produced. These redundant basis sets bring several singularities into the linear equations. A few test calculations on neon and water, however, produced exactly the same pair energies as those obtained with the non redundant MO formulation. The LDL^T factorisation therefore seems to be rather robust with respect to linear dependencies.

Even though a calculation converges, the resulting pair energies can only have limited accuracy. Exactly what accuracy we have obtained for each energy, however, is hard to tell. When we later turn to applications in section 7, we try and resolve this problem by using a series of systematically increasing basis sets for each system. This way, the energy converges in a systematic manner, and as the larger basis sets reproduce figures obtained in smaller sets, these figures are trusted as reliable.

Before leaving Table 6.13 completely, we note that the distribution of eigenvalues for the full set of GCFs seems to follow the distribution pattern outlined by the calculations where one GCF was used. This holds true for all three ansätze regardless of whether the small or the large one-electron basis set is used. If the overlap between geminals having different GCF exponents had been high, a shift in the direction of smaller eigenvalues would have been expected when the full expansion was used. Since such a shift is not observed, we conclude that the exponents in the standard set have been chosen sufficiently different.

In Table 6.14 we have presented the distribution of eigenvalues obtained for the water molecule. We shall not discuss this table in much detail as it reveals exactly the same trends as found for the neon atom. Note however, that for the water molecule there has been a shift in the direction of smaller eigenvalues. This is probably related to the lower point-group symmetry of the water molecule.

The equation solver employed in this work calls subroutines in the LINPACK [84] library. The LDL^T approach implemented in this library, utilises the pivoting strategy of Bunch and Kaufman [85] for general symmetric matrices. Higham [86] has shown that this gives a stable factorisation, and linear dependencies is not expected to create severe numerical instabilities in the equation solver. If such instabilities should be encountered, however, there are a number of possible ways to reduce or resolve this problem. One way is to replace the LDL^T factorisation with a singular value decomposition (SVD). This method is not as efficient as the LDL^T factorisation in solving equation, but it is designed to treat equation systems with singular values by explicitly removing the singularities from the equation system.

In the next section we discuss another approach which rather than removing singularities from the equation system, aims at removing them by fixation of the GCF expansion coefficients. An additional benefit of this approach is that it also decreases the memory requirements.

Table 6.14: Distribution of eigenvalues (λ) for some INT22 matrices for the water molecule. Geminals are constructed using basis sets cc-pVDZ (upper part of table) and aug-cc-pCVTZ(spd,sp) (lower part of table) and using either one GCF having exponent $\frac{1}{3}$, 9 or 243 or the full set of 9 GCFs that was discussed in section 6.3. Eigenvalues are reported as $\Delta = -\mathrm{int}(\log_{10}\lambda)$.

	KL				KQ				PQ			
Δ	1/3	9	243	Full	1/3	9	243	Full	1/3	9	243	Full
0	15	1		17	58	1		262	119	4		245
1		3	1	21	44	14	1	233	101	38	1	227
2		10		23	8	23		305	51	30	1	298
3		1	2	29		22	12	363	27	49	32	339
4			11	20		21	25	333	2	50	33	335
5			1	17		19	14	309		57	39	301
6				6		7	16	236		48	28	234
7				2		2	15	188		19	39	208
8						1	15	164		4	40	178
9							8	121		1	38	138
10							3	92			31	95
11								55			15	61
12							1	28			2	30
13								10			1	9
14								1				1
15												1
0	15	1		17	160	14		281	334	37	1	709
1		3	1	21	96	40	5	267	288	59	9	681
2		10		23	40	65	9	340	264	97	21	938
3		1	2	29	31	48	27	409	247	96	49	1161
4			11	20	11	38	38	346	192	141	59	1232
5			1	17	4	45	43	323	135	152	68	1200
6				6	3	34	40	251	76	178	85	1131
7				2		24	36	229	45	188	93	1051
8						19	40	187	12	178	108	986
9						3	34	144	3	155	138	932
10						8	32	122		121	144	863
11						5	18	88		67	157	762
12						2	10	53		54	148	668
13							7	35		34	145	536
14							5	19		17	116	461
15							1	11		22	255	1053

6.9 Approximating the Coulomb hole using a linear combination of GCFs

One of the motivations for using Gaussian-type geminals in MP2 theory, is that a linear combination of such functions are able to construct a linear r_{12} to any degree of accuracy. However, rather than using a fixed linear combination of GCFs, we have decided to let these expansion coefficients be optimised in each calculation. This provide us with a better energy, but as we have seen, this does not come for free.

Alternatively, we may use a fixed linear combination of GCFs in our GTGs. This ought to reduce the problems with linear dependencies, but at the same time energies must be expected to be less good.

In this section we discuss different ways to optimise the linear combination of GCFs, and we also show that such a linear combination indeed is a good representations of a linear r_{12}.

6.9.1 Fitting by means of least squares

Let us assume that the shape of the Coulomb hole for certain values of r_{12} is given exactly by the function $f(r_{12})$. Denoting the linear combination of GCFs that best fits this shape $g(r_{12})$, we may write

$$f(r_{12}) \approx g(r_{12}) = \sum_v h_v(r_{12}) c_v \tag{6.38}$$

where $\{h_v\}$ are basis functions expressed in terms of GCFs and $\{c_v\}$ are coefficients to be optimised. Typically, a fit like this is optimised using least squares, which minimises the quadratic error between g and the target function f

$$\frac{\partial}{\partial c_v} ||f - g||^2 = \frac{\partial}{\partial c_v} \int_0^b \left[f(r_{12}) - g(r_{12}) \right]^2 \mathrm{d}r_{12} = 0 \tag{6.39}$$

In this expression we have assumed that the function g is to fit f in the region $0 \leq r_{12} \leq b$. Taking partial derivatives with respect to each of the coefficients c_v we get a set of equations that may be written

$$\langle h_v | f \rangle - \sum_w \langle h_v | h_w \rangle \, c_w = 0 \tag{6.40}$$

or

$$t_v - \sum_w S_{vw} c_w = 0 \tag{6.41}$$

where the matrix $\mathbf{S}$ gives the overlap between any two basis functions and the vector $\mathbf{t}$ gives the overlap between any basis function and the function to be fitted. The

process of fitting the function g to function f is thus reduced to simple matrix algebra. The coefficients c_v that gives the best fit are

$$c_v = \sum_w S^{-1}_{vw} t_w \tag{6.42}$$

To obtain numerical values for these coefficients we must first choose what function $f(r_{12})$ to fit and then which basis to fit it in.

6.9.2 GCF basis sets used for the expansion

Two equivalent sets of basis functions may be formed from a set of GCFs

$$h_v(r_{12}) = \exp\left(-\gamma_v r_{12}^2\right) \qquad \text{(basis A)} \tag{6.43}$$

$$h_v(r_{12}) = 1 - \exp\left(-\gamma_v r_{12}^2\right) \qquad \text{(basis B)} \tag{6.44}$$

These basis functions look similar but give, in fact, quite different fits. Note also, in passing by, that each Gaussian correlation factor contains a nonlinear parameter γ_v. Optimising this parameter as well would probably give us less linearly dependent basis functions, but to avoid complicated optimisation schemes, we only consider the standard set given in section 6.3.

6.9.3 Fitting GCFs to the linear r_{12}

According to equation (6.3) the shape of the Coulomb hole is given by a function linear in r_{12} for small values of r_{12}. We therefore set the target function $f(r_{12}) = r_{12}$ and use the Gaussian correlation factors to fit this function. Depending on which of the basis sets (6.43)–(6.44) we choose, the fit (6.38) may be written either as

$$r_{12} - 1 \approx \sum_v c_v \exp\left(-\gamma_v r_{12}^2\right) \tag{6.45}$$

or as

$$r_{12} \approx \sum_v c_v \left[1 - \exp\left(-\gamma_v r_{12}^2\right)\right] \tag{6.46}$$

We start exploring the former of these fits and then return to the latter at the end of this section.

Basis A

To obtain the expansion coefficients given in (6.45), we must solve equation (6.42). The overlap matrices needed in this equation are

$$S_{vw} = \langle h_v | h_w \rangle = \int_0^b \exp\left(-\gamma_v r_{12}^2\right) \exp\left(-\gamma_w r_{12}^2\right) \mathrm{d}r_{12} \tag{6.47}$$

$$t_v = \langle h_i | f \rangle = \int_0^b \exp\left(-\gamma_v r_{12}^2\right)(r_{12} - 1)\, \mathrm{d}r_{12} \tag{6.48}$$

The integration limit b is the largest inter-electronic distance that is included in the fit. It may alternatively be denoted $r_{\max}$. To evaluate the integrals we start by making the substitution $r_{12} = r_{\max} u$. This gives

$$S_{vw} = \int_0^1 \exp\left(-\left(\gamma_v + \gamma_w\right) r_{max}^2 u^2\right) r_{\max}\, \mathrm{d}u \tag{6.49}$$

$$t_v = \int_0^1 \exp\left(-\gamma_v r_{max}^2 u^2\right) \left(r_{\max} u - 1\right) r_{\max}\, \mathrm{d}u \tag{6.50}$$

In both expressions we recognise the zeroth order Boys function, recalling that the nth order Boys function is given by the relation

$$F_n\left(x\right) = \int_0^1 \exp\left(-xt^2\right) t^{2n}\, \mathrm{d}t \tag{6.51}$$

Expressing both (6.49) and (6.50) in terms of the Boys function and substituting γ_{vw} for $\gamma_v + \gamma_w$ we arrive at

$$S_{vw} = r_{\max} F_0\left(\gamma_{vw} r_{\max}^2\right) \tag{6.52}$$

$$t_v = \frac{1}{2\gamma_v}\left[1 - \exp\left(-\gamma_v r_{\max}^2\right)\right] - r_{\max} F_0\left(\gamma_v r_{\max}^2\right) \tag{6.53}$$

Giving a value for the $r_{\max}$ is a question of which region we want our approximative function g to fit the exact function f. Since the Coulomb hole has been represented by a function linear in r_{12}, terms of higher order have been neglected. The Coulomb hole is therefore best represented for small values of r_{12}, suggesting a small value for $r_{\max}$. The $r_{\max}$, however, must also reflect the set of Gaussians actually used. This means that we must avoid fitting in a region where we have no basis functions, and also we must avoid having basis functions beyond the region we intend to fit. A choice of $r_{\max}$ that naturally limits the region a set of Gaussian functions can describe, is the first turning point of the most diffuse Gaussian. Denoting the exponent of this function γ_{min} the turning point r_{tp} is given by

$$r_{\mathrm{tp}} = \left(2\gamma_{min}\right)^{-\frac{1}{2}} \tag{6.54}$$

Using $r_{\max} = r_{\mathrm{tp}} \approx 2.121$, we have fitted the standard set of 9 GCFs to the linear r_{12} function. To show how sensitive the solution is to the upper integration limit, we have also fitted the GCFs with this limit set to $.5\, r_{\mathrm{tp}}$ and $2\, r_{\mathrm{tp}}$. The three fits are plotted in Figure 6.8 as fits 1, 2, and 3, respectively. The solution coefficients $\{c_v\}$, which have been normalised to unity after the plotting, are given in Table 6.15. These normalised coefficients do not reproduce the plots.

The plots in Figure 6.8 shows the importance of choosing an appropriate integration limit for the basis set in use. Particularly, we note that when the integration

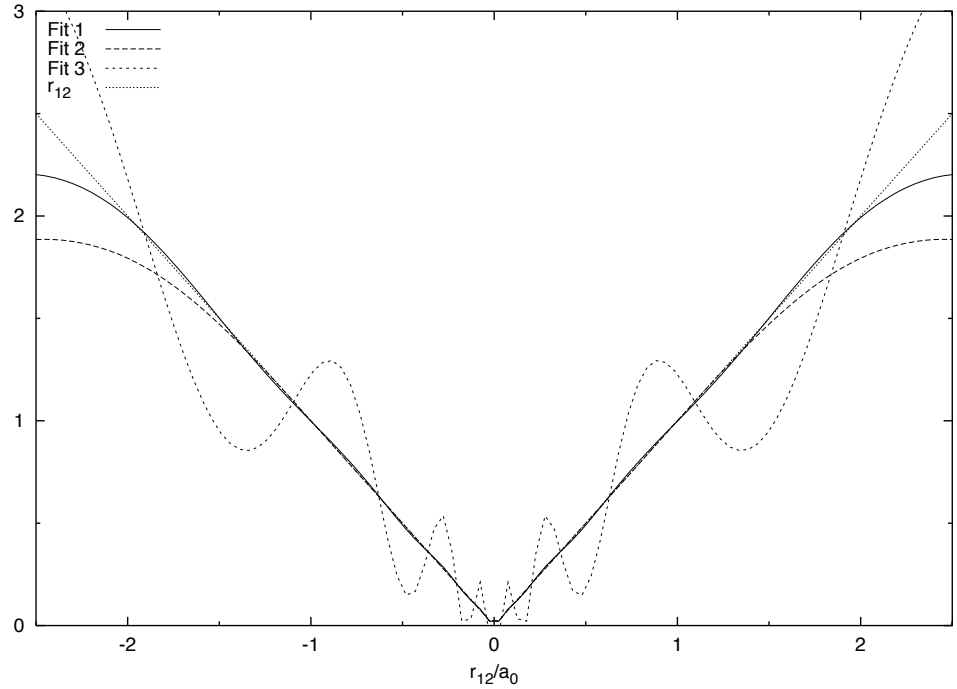

Figure 6.8: Fitting basis A to the linear r_{12} using three different fit regions. Fit 1: $[0, r_{\rm tp}]$, Fit 2: $[0, 0.5r_{\rm tp}]$, and Fit 3: $[0, 2r_{\rm tp}]$. Distance $r_{\rm tp} \approx 2.121$

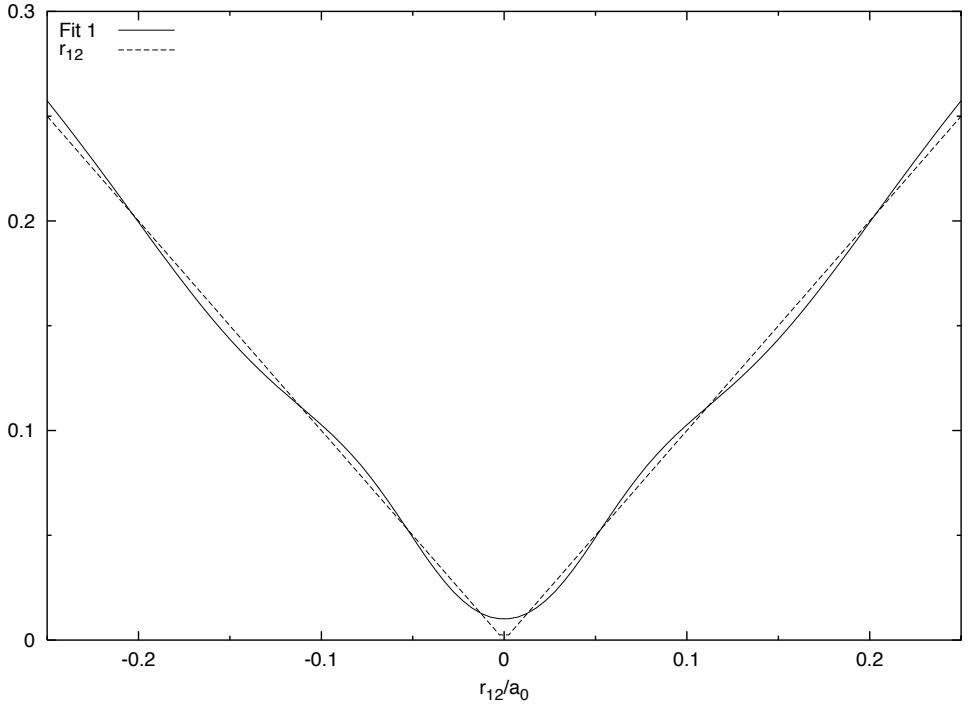

Figure 6.9: Figure 6.8 magnified 10 times. Only Fit 1 are included in the plot.

Table 6.15: Normalised solution coefficients $\{c_v\}$ when fitting basis A to the linear r_{12}.

Exp.	1/9	1/3	1	3	9	27	81	243	729
Fit 1	.535	−.788	.254	−.148	.052	−.052	.024	−.018	.002
Fit 2	.613	−.786	.047	−.052	−.024	−.013	−.010	−.001	−.007
Fit 3	.262	−.545	.498	−.421	.323	−.249	.175	−.105	.036

limit is chosen too large, like in Fit 3, we end up with a completely useless function. This is a direct consequence of fitting over a region where there are no appropriate basis functions. Note, however, that the function *does* represent a best fit in the mathematical sense, it just does not have the shape we want.

When the upper integration limit is chosen small, like in Fit 2, we see that the shape does not change much from that of Fit 1. The expansion coefficients given in Table 6.15, however, are very different for the two functions. As long as the shape for small values of r_{12} are similar, these two Coulomb hole representations ought to yield similar energies.

In Figure 6.9, we have plotted Fit 1 again, but this time the plot is zoomed 10 times nearby the origin. The magnified plot reveals that the optimised function meanders nicely about the straight r_{12} line all the way down to $r_{12} \approx 0.01$ Bohr. The results presented in section 6.3, suggests that such a Coulomb hole fit is sufficient to give us energies accurate to a few tenths of a $\mathrm{mE_h}$.

Basis B

To obtain Coulomb hole fits for basis B defined in (6.44), we need to work out formulas for the overlap matrices $\mathbf{S}$ and $\mathbf{t}$ corresponding to those given for basis A in (6.52)–(6.53). The formulas for basis B turns out to be slightly more complicated

$$S_{vw} = r_{\max}\left[1 - F_0\left(\gamma_v r_{\max}^2\right) - F_0\left(\gamma_w r_{\max}^2\right) + F_0\left(\gamma_{vw} r_{\max}^2\right)\right) \tag{6.55}$$

$$t_v = \frac{1}{2} r_{\max}^2 - \frac{1}{2\gamma_v}\left[1 - \exp\left(-\gamma_v r_{\max}^2\right)\right] \tag{6.56}$$

Fitting the linear r_{12} in basis B using the standard set of GCFs and the same values of $r_{\max}$ as for basis A, we get the functions plotted in Figure 6.10. Their respective expansion coefficients, which have been normalised, are given in Table 6.16. Note that these coefficients differ significantly from those presented in Table 6.15.

Again, the function for which $r_{\max} = r_{\mathrm{tp}}$ fits the linear r_{12} nicely. Increasing the upper integration limit to $2\,r_{\mathrm{tp}}$ also generates nice fits, which is not the case when basis A is used. When the integration limit is reduced to $0.5\,r_{\mathrm{tp}} \approx 1.061$, however, the fitted function is given an exponential increase shortly after the integration

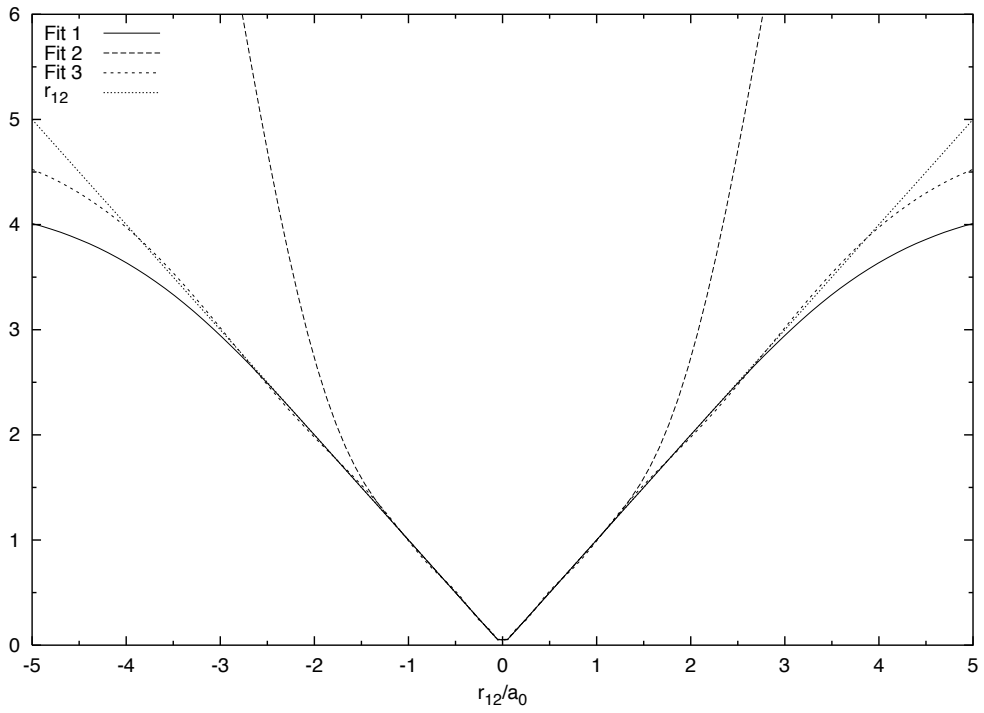

Figure 6.10: Fitting basis B to the linear r_{12} using three different fit regions. Fit 1: $[0, r_{\rm tp}]$, Fit 2: $[0, 0.5r_{\rm tp}]$, and Fit 3: $[0, 2r_{\rm tp}]$. Distance $r_{\rm tp} \approx 2.121$.

Table 6.16: Normalised solution coefficients $\{c_v\}$ when fitting basis B to the linear r_{12}.

Exp.	1/9	1/3	1	3	9	27	81	243	729
Fit 1	−.991	.021	−.114	−.045	−.033	−.013	−.016	.004	−.013
Fit 2	−.892	.442	−.093	.003	−.005	−.001	−.002	.001	−.002
Fit 3	−.879	.331	−.281	.118	−.124	.069	−.062	.032	−.017

limit, and does not level off until the functional value is approximately 16. The exact asymptotic value may be found by summing the expansion coefficients prior to normalisation.

6.9.4 Fitting GCFs to the linear r_{12} with damping

In their 1996 paper, Persson and Taylor [59] used an exponential weight $\exp(-r_{12})$ in their least-squares procedure. Since this exponential weight favours the inner part of the Coulomb hole, such a fit is expected to be less sensitive to the choice of upper integration limit. In particular, choosing the limit too large should give less

oscillation than observed in Figure 6.8

Introducing the exponential weight $\exp(-2\gamma r_{12})$ into equation (6.39), we get

$$\frac{\partial}{\partial c_v}||f-g||^2 = \frac{\partial}{\partial c_v}\int_0^b \exp\left(-2\lambda r_{12}\right)\left[f(r_{12})-g(r_{12})\right]^2 \mathrm{d}r_{12} = 0 \tag{6.57}$$

In addition to viewing this as a damped fit we may also regard it as a change of both the function to be fitted and the basis functions

$$f(r_{12}) \longrightarrow f(r_{12})\exp\left(-\lambda r_{12}\right) \tag{6.58}$$
$$h(r_{12}) \longrightarrow h(r_{12})\exp\left(-\lambda r_{12}\right) \tag{6.59}$$

Assuming basis function of type A, the two kinds of overlap matrices now becomes

$$S_{vw} = \exp\left(\gamma_{vw} r_{vw}^2\right)\left[(r_{vw}+r_{\max})F_0(\gamma_{vw}(r_{vw}+r_{\max})^2) - r_{vw}F_0(\gamma_{vw}r_{vw}^2)\right] \tag{6.60}$$

and

$$\begin{aligned} t_v = \exp\left(\gamma_v r_v^2\right)\Big[&\frac{1}{2\gamma_v}\left(\exp\left(-\gamma_v r_v^2\right) - \exp\left(-\gamma_v(r_v+r_{\max})^2\right)\right) \\ &+ r_v(r_v+1)F_0(\gamma_v r_v^2) \\ &- (r_v+r_{\max})(r_v+1)F_0(\gamma_v(r_v+r_{\max})^2)\Big] \end{aligned} \tag{6.61}$$

where we have introduced the simplifications $\gamma_{vw} = \gamma_v + \gamma_w$, $r_{vw} = \lambda/\gamma_{vw}$, $r_v = \lambda/\gamma_v$ and $r_w = \lambda/\gamma_w$. For basis B the corresponding formulas become

$$\begin{aligned} S_{vw} =&\frac{1}{2\lambda}\left[1-\exp(-2\lambda r_{\max})\right] \\ &- \left[(r_v+r_{\max})F_0(\gamma_v(r_v+r_{\max})^2) - r_v F_0(\gamma_v r_v^2)\right] \\ &- \left[(r_w+r_{\max})F_0(\gamma_w(r_w+r_{\max})^2) - r_w F_0(\gamma_w r_w^2)\right] \\ &+ \left[(r_{vw}+r_{\max})F_0(\gamma_{vw}(r_{vw}+r_{\max})^2) - r_{vw}F_0(\gamma_{vw}r_{vw}^2)\right] \end{aligned} \tag{6.62}$$

and

$$\begin{aligned} t_v = &\left(\frac{1}{2\lambda}\right)^2 - \left[\left(\frac{1}{2\lambda}\right)^2 + \frac{r_{\max}}{2\lambda}\right]\exp\left(-2\lambda r_{\max}\right) \\ &- \exp\left(\gamma_v r_v^2\right)\Big[\frac{1}{2\gamma_v}\left(\exp\left(-\gamma_v r_v^2\right) - \exp\left(-\gamma_v(r_v+r_{\max})^2\right)\right) \\ &\qquad + r_v(r_v+r_{\max})F_0(\gamma_v(r_v+r_{\max})^2) - r_v^2 F_0(\gamma_v r_v^2)\Big] \end{aligned} \tag{6.63}$$

where the definitions of r_v, r_w and r_{vw} are identical to those given above for basis A.

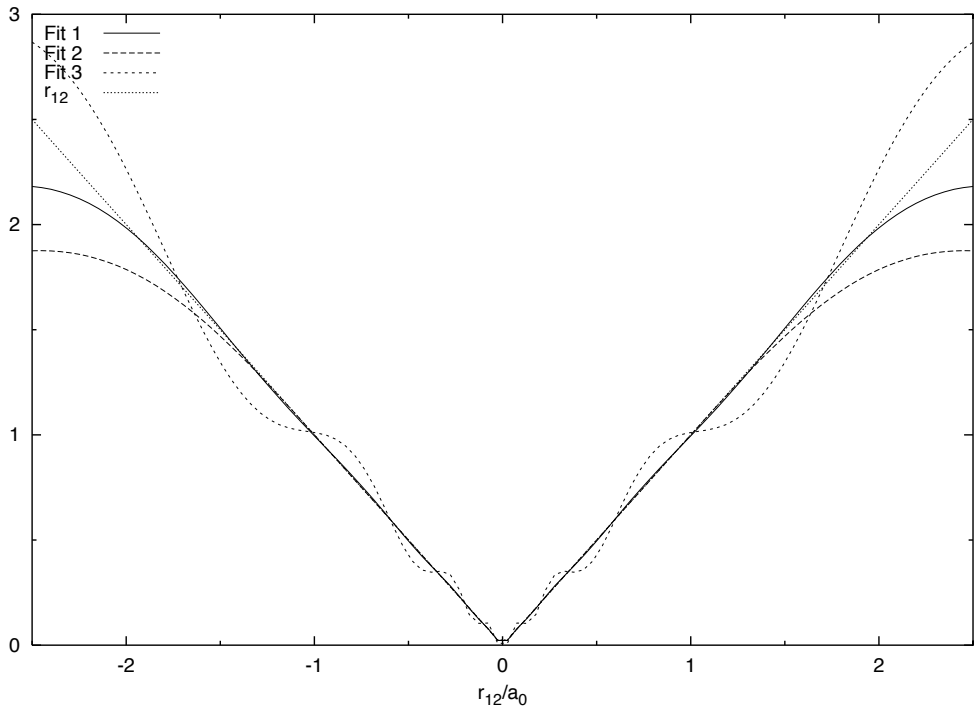

Figure 6.11: A damped with of basis A to the linear r_{12} using three different fit regions. Fit 1: $[0, r_{\rm tp}]$, Fit 2: $[0, 0.5r_{\rm tp}]$, and Fit 3: $[0, 2r_{\rm tp}]$. Distance $r_{\rm tp} \approx 2.121$.

Table 6.17: Solution coefficients $\{c_v\}$ when fitting basis A to linear r_{12} using damping.

Exp.	1/9	1/3	1	3	9	27	81	243	729
Fit 1	.556	−.796	.210	−.109	.016	−.025	.003	−.006	−.003
Fit 2	.618	−.783	.031	−.049	−.027	−.012	−.011	−.001	−.008
Fit 3	.471	−.766	.369	−.206	.088	−.061	.030	−.018	.003

In Figure 6.11 we have, once again, plotted the same type of fits as those presented in Figure 6.8. This time, however, we have used a damped fit with the damping factor λ set to unity. Normalised expansion coefficients for these fits are given in Table 6.17.

Note how the oscillation for Fit 3 is less pronounced. Apart from that, there are only minor changes.

Table 6.18: Second-order correlation energies ($-E/\mathrm{mE_h}$) for the helium atom using a fixed GCF expansion. Expansion coefficients are taken from Fit 1 of Tables 6.15 and 6.16 which represent GCF basis sets A and B, respectively. The results for basis A and B are presented in the upper and lower part of this table, respectively.

Orbital basis	VOE	IJ	KL	KQ	PQ
cc-pVDZ	25.828	—	27.426	28.459	35.052
cc-pVTZ	33.138	—	33.417	33.542	37.246
aug-cc-pVDZ	26.962	—	28.379	29.870	37.229
aug-cc-pVTZ	33.621	—	33.620	34.099	36.431
cc-pVDZ	25.828	—	26.488	26.665	31.304
cc-pVTZ	33.138	—	33.200	33.244	36.106
aug-cc-pVDZ	26.962	—	27.353	27.398	33.354
aug-cc-pVTZ	33.621	—	33.654	33.658	36.453

6.9.5 Sample calculations

To investigate the performance of fixed GCF expansions, we have done some calculations on the helium and neon atoms using the coefficients for Fit 1 taken from Tables 6.15 and 6.16. These coefficients have been obtained using GCF basis sets A and B, respectively. The results are presented in Tables 6.18 and 6.19.

Investigating the results for helium first, we note that these are somewhat odd. For several of the calculations, the kq-ansatz performs only slightly better than the kl-ansatz (which equals the ij-ansatz for two-electron systems), whereas for all other calculation presented in this work, the kq-ansatz performs significantly better. We also note that for the combination of GCF basis A and the pq-ansatz, the energy obtained using the aug-cc-pVDZ basis is lower than the energy obtained using the aug-cc-pVTZ basis. Assuming that the Fock operator expansion is sufficiently complete for both basis sets, this is a violation of the variational principle. For the aug-cc-pVTZ basis, we also get that the pure virtual orbital expansion gives a lower energy than the kl-ansatz. Adding to this the fact that basis sets A and B produce quite different results, the energies presented in Table 6.18 seem rather unreliable.

When expansion coefficients are fixed, flexibility is lost in the two-electron basis. As discussed in appendix A, such flexibility is crucial for strong orthogonality to be obtained. Strong orthogonality, in turn, is our insurance that the WO functional does a good job in optimising pair functions. Possibly, by fixing the expansion coefficients, we have reduced the flexibility to an extent where the WO functional no longer produces truly optimised pair functions. If so, the pair functions obtained do not correspond to the lowest pairs energies within the given two-electron basis.

Table 6.19: Second-order correlation energies ($-E/\mathrm{mE_h}$) for the neon atom using a fixed GCF expansion. Expansion coefficients are taken from Fit 1 of Tables 6.15 and 6.16 which represent GCF basis sets A and B, respectively. The results for basis A and B are presented in the upper and lower part of this table, respectively.

Orbital basis	VOE	IJ	KL	KQ	PQ
cc-pCVDZ	228.303	230.898	232.070	247.511	265.889
aug-cc-pCVDZ	249.895	252.082	252.822	269.187	298.257
cc-pCVDZ	228.302	228.652	228.680	228.886	263.458
aug-cc-pCVDZ	249.895	250.226	250.252	250.460	299.632

In Table 7.1 of the next chapter, calculations on helium using optimised expansion coefficients are presented. The optimised coefficients give far better energies than the fixed expansion coefficients no matter the ansatz. Also, there is no (visible) violations of the variational principle when expansion coefficients are optimised.

In Table 6.19, we have presented results for the neon atom using fixed expansion coefficients. Again, the performance of the kl- and kq-ansätze are rather miserable, especially when comparing to the results obtained with optimised expansion coefficients as presented in Table 7.10.

The kq-ansatz performs better with GCF basis A than with GCF basis B. For the other ansätze, however, there are only minor differences. Pair energies, therefore, seem to be sensitive to the choice of expansion coefficients in a rather unpredictable manner.

For the helium atom, the pq-ansatz performs reasonably well, especially when using GCF basis A. For the neon atom, however, the pq-ansatz performs poor with both GCF basis sets. Why the pq-ansatz performs better for helium than for neon is difficult to say, but it is probably related to the larger variety of pair functions present in the neon atom. For some reason, this degrades the overall performance of the optimisation.

We conclude this section by stating that using a fixed set of expansion coefficients for the Gaussian correlation factors (GCFs) does not turn out to be a success, as the energies obtained are both poor and unreliable. Whether this is due to the use of the WO functional to optimise pair functions, due to the fitting strategy or due to something else, cannot currently be stated.

A motivation for investigating the use of a fixed GCF expansion was the quest for a two-electron basis less hampered with linear dependencies. Due to the poor performance of the fixed expansions, we have not investigated whether the degree of linear dependencies really has decreased or not.

Finally, it should be pointed out that even if it is not such a good idea to fix

the entire GCF expansion, it may still be an alternative to fix parts of it. As the largest amount of linear dependencies is related to the inner part of the Coulomb hole, fixing only the expansion coefficients for the GCFs with the highest exponents may therefore still prove to be a good idea. This way we may get rid of the most severe linear dependency problems and at the same time have sufficient flexibility left in the two-electron basis.

Chapter 7

Applications

7.1 Introduction

In the preceding chapters we have studied the theoretical foundation of GTG-MP2 theory and have discussed different computational aspects of this method like integral timings, parallelisation, prescreening, and so forth. One of the more intriguing parts of method development, however, is finding out how the new method performs in real applications. The current chapter is devoted to this task.

In conventional MP2, the resulting pair energies depend only on the quality of the one-electron basis set, and exploring the performance of this method is therefore a rather straight forward task. For the GTG-MP2 theory presented here, however, things are unfortunately not that simple as the performance depends on several different parameters making a full exploration of the method a comprehensive task. Things that affect MP2-GTG energies include the choice of

- Level-shift parameter
- Two-electron basis (GTG ansatz)
- GCF expansion
- One-electron basis.

As discussed in section 6.4, the level-shift parameter (η) affects the optimisation of pair functions. A level-shift parameter of zero theoretically gives the lowest ($\approx$ best) pair energies, but at the expense of pair functions that are not strongly orthogonal to the occupied orbitals. Since the SO measure may give us valuable information about the quality of the optimised pair functions (cf. section A), using $\eta = 0$ is not a good idea. In section 6.4, we concluded that a level-shift parameter of 0.1 represents a compromise between low energies and good SO measures, and we use this η for all calculations in this chapter and do not investigate whether or not it is the optimal choice in each case.

Whereas pair energies are fairly insensitive to the choice of level-shift parameter, they depend strongly of the GTG ansatz. When constructing Gaussian-type geminals (see section 6.1) we may use several different ansätze for the orbital part, and each of these have upsides as well as downsides. Since the different ansätze lead to quite different performance for the GTG-MP2 method, the calculations presented in this chapter shall to as large an extent as possible employ the three major ansätze; kl, kq, and pq.

In addition to an orbital part, GTGs are also constructed from a Gaussian-type correlation factor (GCF) which "ties" the two orbitals into a two-electron function. The GCF exponent may be varied, and for the GTGs to properly describe the Coulomb hole, a linear combination of GCFs with different exponents have to be used. The number of GCFs included in the linear combination and the values of their exponents may both be varied, and this leaves us with a large "GCF-space" to explore. Note, also, that a linear combination that is optimal for one system, is not necessarily optimal for other systems. Fortunately, the GCF study performed in section 6.3, suggests that the GCF-space is rather well saturated if we use a set of 9 GCFs consisting of the even-tempered exponents $\{1/9, 1/3, \ldots, 729\}$, and we shall not pursue the choice of GCFs any further in this chapter.

Finally, pair energies also depend on the choice of one-electron basis set, just as with conventional MP2. In fact, the choice of one-electron basis is what influence the energy the most. Unfortunately, this dependency is rather complicated as the atomic orbitals enter the GTGs, the virtual orbital expansion, and the expansion of the Fock operator at the same time. If the orbital basis is improved, it is impossible to decouple the contributions each of these factors make to the change in energy, although pair energies are expected to be sensitive to the Fock operator expansion only if the basis set is small.

Since the choice of one-electron basis is so important, we have chosen to study each system using a wide range of basis sets, thus allowing us to monitor energy convergence with respect to both partial-wave expansions as well as principal expansions. The basis sets that are used for this study were discussed in section 6.2, along with some notational details.

7.2 Helium

The smallest atomic systems that contain electron-electron correlation are the two-electron systems H^-, He, Li^+, and so on. Since these systems are all two-electron, results obtained for one of them also apply to the others. With this in mind, we limit our investigation of one-centre two-electron systems to helium.

For helium, however, we shall not only study the atom but also the dimer. The existence of the helium dimer is entirely due to the electron-electron correlation, and in a world where this effect did not exist, two helium atoms would merely repel

each other. We shall calculate the depth of the MP2-GTG potential energy surface of the helium dimer, and show that our results are comparable to result presented in literature.

7.2.1 The helium atom

In Table 7.1 we present results for the helium atom using the three ansätze and various flavours of the correlation-consistent basis sets of Dunning and co-workers. For reference, we have also included the energies obtained using conventional MP2. These are listed in the VOE (virtual orbital expansion) column.

The number of figures included in the different energies vary, roughly reflecting the accuracy obtained in each case. For accountability, however, all energies are listed in Table B.5 using nine figures.

Table 7.1 shows that the kq- and pq-ansätze perform excellently while the performance of the kl-ansatz is only fair. Note, for instance, that while the best energy using the kl-ansatz is obtained with the aug-cc-pV6Z basis, better energies are obtained for the kq-ansatz in a basis consisting of s- and p-orbitals only.

We furthermore note that for the kq- and pq-ansätze, decent energies are obtained also when only s-orbitals are used; and when p-orbitals are included, the pair energy is converged to within $1\,\mu\mathrm{E_h}$. This is quite remarkable. Another interesting thing to note is that the kq- and pq-ansätze perform better with the aug-cc-pVXZ(sp) basis sets than the corresponding cc-pVXZ sets, indicating that saturating the low angular momentum spaces is more important for the pair energy than adding orbitals with high angular momentum. This property turns out to be general and is also encountered for the other systems discussed in this work.

The best helium energy is obtained using the pq-ansatz and the basis set aug-cc-pV6Z(spd). This basis is made from 50 orbitals ($7s6p5d$), which is not a large basis set the performance taken into account. Unfortunately, we could not use the basis set aug-cc-pV5Z(spdf) with the pq-ansatz, due to a current limit of 2GB internal memory usage (the 32 bit architecture limit).

In Table 7.2 we have compared our best helium pair energies with a few reference values found in literature. This table shows that our best value is close to the current energy limit obtained by Bukowski and co-workers [88]. They also used the weak orthogonality functional (3.77) in optimising the pair function, and expanded this in a set of Gaussian-type geminals. These GTGs, however, were defined differently from ours and read

$$g_i(1,2) = \exp\left[-\alpha_i(\mathbf{r}_1 - \mathbf{P}_i)^2 - \beta_i(\mathbf{r}_2 - \mathbf{Q}_i)^2 - \gamma_i r_{12}^2\right] \tag{7.1}$$

where the exponents α_i, β_i and γ_i were treated as variational parameters. Since these parameters enter an exponential function, expensive non-linear optimisation techniques must be used. The centres of the GTGs, $\mathbf{P}_i$ and $\mathbf{Q}_i$, did not have to be optimised, however, as their optimal location, due to symmetry, is on the helium

Table 7.1: Second-order correlation energies ($-E/\mathrm{mE_h}$) for the helium atom. The entry marked with a dagger (†) failed to converge in the equation solver. Refer to Table B.5 to have all energies listed with nine figures.

Orbital basis	VOE	KL	KQ	PQ
cc-pVDZ	25.83	33.75	36.713	36.9501
cc-pVTZ	33.14	35.87	37.183	37.2998
cc-pVQZ	35.48	36.77	37.326	37.3628
cc-pV5Z	36.41	37.09	37.363	37.3738
aug-cc-pVDZ(s)	11.50	29.39	36.941	37.0913
aug-cc-pVTZ(s)	12.90	29.48	37.053	37.2166
aug-cc-pVQZ(s)	13.28	29.57	37.208	37.3353
aug-cc-pV5Z(s)	13.44	29.59	37.235	37.3613
aug-cc-pV6Z(s)	13.47	29.59	37.239	37.3689
aug-cc-pVDZ	26.96	35.23	37.169	37.2926
aug-cc-pVTZ(sp)	31.11	35.77	37.251	37.3460
aug-cc-pVQZ(sp)	32.06	35.97	37.350	37.3724
aug-cc-pV5Z(sp)	32.35	36.02	37.369	37.3769
aug-cc-pV6Z(sp)	32.42	36.04	37.372	37.37720
aug-cc-pVTZ	33.62	36.52	37.255	37.3610
aug-cc-pVQZ(spd)	35.03	36.88	37.352	37.3755
aug-cc-pV5Z(spd)	35.46	36.98	37.371	37.37717
aug-cc-pV6Z(spd)	35.58	37.00	37.375	37.37729
aug-cc-pVQZ	35.72	37.06	37.354	37.3758
aug-cc-pV5Z(spdf)	36.29	37.19	37.3720	n/a
aug-cc-pV6Z(spdf)	36.47	37.22	37.3755	n/a
aug-cc-pV5Z	36.53	37.23	37.3725	n/a
aug-cc-pV6Z(spdfg)	36.78	37.26	†	n/a
aug-cc-pV6Z	36.88	37.305	n/a	n/a
d-aug-cc-pVDZ	27.01	35.29	37.190	37.3079
d-aug-cc-pVTZ(sp)	31.12	35.78	37.258	37.3547
d-aug-cc-pVQZ(sp)	32.06	35.98	37.351	37.3736
d-aug-cc-pV5Z(sp)	32.35	36.02	37.369	37.37697
d-aug-cc-pVTZ	33.63	36.53	37.263	37.3678
d-aug-cc-pVQZ(spd)	35.04	36.89	37.353	37.3762

Table 7.2: Second-order correlation energies ($-E/\mathrm{mE_h}$) for the helium atom. Comparison with literature data. Entries are listed chronologically. For helium the total correlation energy is $-42.044\,\mathrm{mE_h}$ [88].

Authors	$E^{(2)}$
This work	
kl-ansatz (aug-cc-pV6Z)	37.305
kq-ansatz (aug-cc-pV6Z-spdf)	37.375
pq-ansatz (aug-cc-pV6Z-spd)	37.37729
Lee and Park [87]	
Extrapolation	37.4052
Bukowski *et al.* [88]	
150 nonlinearly optimised GTGs	37.37744
Flores [89]	
FEM-MP2 with $l \leq 12$ and angular extrapolation	37.376
Termath *et al.* [41]	
MP2-R12/A with STO basis ($12s11p11d9f9g$)	37.375
MP2-R12/B with same basis as approximation A	37.362
Petersson *et al.* [90]	
CBS (complete basis set) model	37.59
Malinowski *et al.* [91]	
Partial-wave expansion with radial and angular extrapolation	37.359
Winter *et al.* [92]	
First order equation solved numerically	37.355

nucleus. From the definition (7.1) we see that the GTGs may be regarded as a pair of s-orbitals tied together with a GCF; p-orbitals or orbitals with higher angular momentum, are not used. For the helium atom this is not a shortcoming, however, as King [93] has shown that geminals of type (7.1), constitutes a complete basis for pair functions of atoms, when these (as for helium) belong to the totally symmetric representation.

To obtain their helium energy limit, Bukowski and co-workers used 150 GTGs. This number may be compared to the 2349 GTGs used to obtain our pq-ansatz limit, 153 GTGs used to obtain the kq-ansatz limit and 9 GTGs used to obtain the kl-ansatz limit. Note, also, that Bukowski obtained his limit using a pure GTG expansion for the pair function, while we supplement the GTGs with the conventional virtual orbitals expansion.

Being variational, the result obtained by Bukowski and co-workers currently ought to be considered the best value for the second order energy correction of helium. Interestingly, therefore, this is not always recognised in literature [87, 94, 95].

Although not the lowest correlation energy obtained for helium, it is the lowest energy obtained variationally, and, together with the pq-ansatz value presented here, the only correlation energy that is converged to within $1\,\mu E_h$.

When comparing the performance of different methods for larger system later in this chapter, it is probably worthwhile to keep in mind that the performance of most of these methods for helium, the simplest of all electron-electron correlated systems, is only fair.

7.2.2 The interaction energy of the helium dimer

Between all electronic systems there are weak interactions often referred to as London forces. These forces are most important in systems that are neutral and non-polar. Two helium atoms forming a helium dimer are two such systems.

When helium gas eventually condenses to liquid at around 4K, this is entirely due to the weak London forces. The last 15 years, these interactions have been studied in several papers. With the objective to obtain the interaction energy as accurately as possible, most attention has been given to higher order methods like CCSD(T), MRCI, or other multi-reference methods. Some of this methods have also been combined with extrapolation.

Anderson [96], for instance, used an exact quantum Monte Carlo calculation to estimate the interaction energy of the dimer, and obtained, for the correlation part of this energy, the value (10.98 ± 0.02)K. Jeziorska *et al.* [97], however, recently obtained (11.008 ± 0.008)K by combining the Gaussian geminal value of the CCSD energy with extrapolated orbital estimates of the CCSD(T) and FCI contributions. Although both of these values are claimed to be highly accurate, they disagree slightly.

Interesting, therefore, is the critical note on extrapolated helium pair potentials, where Klopper [98] argues that it is difficult, or even impossible, to obtain the interaction energy using extrapolation with significantly higher precision than what is already available today using directly computed potentials.

Even though good estimates of the total interaction energy are available, studying the helium dimer using GTG-MP2 is not irrelevant. First of all, it contributes to the exploration of GTG based methods. Second, if highly accurate estimates are obtained, they may be used when calibrating other methods.

One of the problems encountered when estimating the helium–helium interaction energy, is the basis set superposition error (BSSE). When calculating the energy of a dimer, each atom also benefits from the basis set used to describe its partner. If, therefore, the energy of the monomers are calculated without compensating for this, an unbalance arises in the description of the monomers and the dimer, leading to an interaction energy that is too large.

The simplest way to compensate for an unbalance, is to describe the monomers using a ghost basis. When setting up the input for the monomer calculation, one

removes one of the helium atoms from the dimer calculation, but leaves its basis set in place.

Interaction energies calculated using a ghost basis are said to be counterpoise-corrected (CP). When the corrected energy differs from the non corrected energy, as it usually does, this indicates a deficit in the original basis. As we shall see, within a Gaussian-type geminal basis, it is not difficult to construct basis sets that make the counterpoise-correction superfluous at the second-order energy correction level.

In Table B.7 we have recalculated the second-order energy correction of the helium atom, but this time with a ghost basis at a $5.6a_0$ distance, which is the accepted equilibrium bond length of the helium dimer. Due to high computational cost we were not able to consider all basis sets appearing in Table 7.1, but only a subset of those. The table is included for reference only, and have therefore been placed in the appendices. We shall not discuss it in any detail here.

In Table 7.3, however, we give the second-order energy correction of the helium dimer at its equilibrium distance (refer to Table B.6 to get all energies listed with nine figures). Again we see that the kq- and the pq-ansätze completely outperform the kl-ansatz which suffers from the basis set limitation. The best value for the kl-ansatz is $74.18\,\mathrm{mE_h}$ obtained with the aug-cc-pVQZ basis set, while the best value obtained with the kq-ansatz is $74.801\,\mathrm{mE_h}$ obtained with the aug-cc-pV6Z(spd) basis set. This basis set is highly saturated in the s-, p-, and d-orbital spaces. For the pq-ansatz, the best value obtained is $74.8042\,\mathrm{mE_h}$ obtained with the basis set aug-cc-pV6Z(sp). This value is is converged to within $10\,\mu\mathrm{E_h}$ of the limit and maybe even down to $1\,\mu\mathrm{E_h}$.

It is possible to evaluate the convergence of this value by using the best available energy for the helium atom along with some upper limit for the interaction energy of the dimer. The best available energy for the helium atom is $37.37744\,\mathrm{mE_h}$, as concluded in the previous section. Using 16.0K as an upper limit for the interaction energy (see Table 7.5), and the conversion factor $1\mathrm{K}{=}3.1577466\,\mu\mathrm{E_h}$ obtained from Ref.[99], we arrive at the value $74.8055\,\mathrm{mE_h}$ as the upper limit for the second-order energy correction of the helium dimer. We have, therefore, reason to believe that our best estimate of the second-order correlation energy of the dimer is converged to within 99.99% of the limit for both the kq- and the pq-ansätze.

Unfortunately, we could not explore the use of d-orbitals with the pq-ansatz beyond the aug-cc-pVTZ basis set, and a basis set like aug-cc-pV6Z(sp) cannot be trusted to give a reliable estimating of the interaction energy. A basis consisting of s- and p-functions only, describe the atom better than the dimer, and this gives a unbalanced treatment of the two systems, inevitably leading to an underestimated interaction energy.

In Table 7.4 we give counterpoise-corrected second-order correlation interaction energies for the helium dimer. The counterpoise-correction energy is given in parentheses, except for the pq-ansatz. For this ansatz, energies are given without correction, as the ghost basis introduced singularities that could not be handled by the

Table 7.3: Second-order correlation energies ($-E/\mathrm{mE_h}$) for the helium dimer. An inter-nuclear distance of $5.6\mathrm{a_0}$ was used.

Orbital basis	VOE	KL	KQ	PQ
cc-pVDZ	51.66	67.97	73.56	73.94
cc-pVTZ	66.29	71.85	74.41	74.64
cc-pVQZ	70.98	73.62	74.70	n/a
aug-cc-pVDZ(s)	23.00	59.39	73.93	74.20
aug-cc-pVTZ(s)	25.79	59.41	74.14	74.45
aug-cc-pVQZ(s)	26.56	59.59	74.44	74.69
aug-cc-pV5Z(s)	26.87	59.62	74.50	74.74
aug-cc-pV6Z(s)	26.94	59.64	74.51	74.75
aug-cc-pVDZ	53.97	70.66	74.40	74.64
aug-cc-pVTZ(sp)	62.26	71.67	74.55	74.74
aug-cc-pVQZ(sp)	64.16	72.07	74.75	74.795
aug-cc-pV5Z(sp)	64.73	72.16	74.78	74.802
aug-cc-pV6Z(sp)	64.88	72.20	74.791	74.8042
aug-cc-pVTZ	67.29	73.11	74.57	74.77
aug-cc-pVQZ(spd)	70.11	73.84	74.76	n/a
aug-cc-pV5Z(spd)	70.96	74.03	74.794	n/a
aug-cc-pV6Z(spd)	71.21	74.08	74.801	n/a
aug-cc-pVQZ	71.50	74.18	74.76	n/a
d-aug-cc-pVDZ	54.07	70.76	74.44	74.67
d-aug-cc-pVTZ(sp)	62.28	71.68	74.57	74.76
d-aug-cc-pVQZ(sp)	64.17	72.07	74.75	74.797
d-aug-cc-pV5Z(sp)	64.73	72.16	74.786	74.8038
d-aug-cc-pVTZ	67.32	73.16	74.58	n/a
d-aug-cc-pVQZ(spd)	70.12	73.86	74.76	n/a

implemented equation solver.

Since the basis sets employed are small, we cannot expect the interaction energies obtained with the virtual orbital expansion to be approaching the limit. The energies presented, however, give us an idea of how the conventional MP2 method converges with the size of the basis set.

For the kl-ansatz, all calculations except the one using the aug-cc-pVQZ basis, yield interaction energies that are far off the limit. Moreover, all interaction energies are too high, and this somewhat counter-intuitive result, suggests that the basis sets employed are far too small to be used with the kl-ansatz.

Table 7.4: Second-order correlation interaction energies ($E/\mu\mathrm{E_h}$) for the helium dimer. An inter-nuclear distance of $5.6\mathrm{a_0} \approx 296\,\mathrm{pm}$ was used. All energies except for those given for the pq-ansatz, are counterpoise (CP) corrected. The number in parentheses is the decrease in interaction energy caused by the correction. The bond energy marked with a dagger is erroneous due to a poorly described Fock operator.

Orbital basis	VOE	KL	KQ	PQ
cc-pVDZ	−5.11 (1.62)	−472.26 (.80)	−118.21 (16.47)	−38.02
cc-pVTZ	−16.93 (1.97)	−121.05 (1.77)	−40.97 (3.42)	−42.96
cc-pVQZ	−26.95 (1.36)	−78.73 (1.22)	−42.34 (1.58)	n/a
aug-cc-pVDZ(s)	+4.32 (4.17)	−606.97 (1.42)	−45.17 (2.31)	−23.35
aug-cc-pVTZ(s)	+4.23 (1.36)	−443.05 (.41)	−36.72 (.77)	−20.24
aug-cc-pVQZ(s)	+4.10 (.44)	−443.69 (.29)	−25.76 (.10)	−18.19
aug-cc-pV5Z(s)	+4.02 (.32)	−443.73 (.28)	−26.86 (.03)	−16.71
aug-cc-pV6Z(s)	+3.96 (.36)	−451.39 (.35)	−26.83 (.02)	−17.11
aug-cc-pVDZ	−34.66(15.22)	−176.80(15.46)	−63.30 (1.20)	−51.45
aug-cc-pVTZ(sp)	−34.90 (3.50)	−117.52 (4.21)	−51.57 (1.04)	−50.92
aug-cc-pVQZ(sp)	−34.88 (1.08)	−119.62 (1.47)	−47.32 (.25)	−49.88
aug-cc-pV5Z(sp)	−34.87 (.52)	−122.75 (1.22)	−46.47 (.10)	−48.55
aug-cc-pV6Z(sp)	−35.19 (.37)	−122.50 (.70)	−46.47 (.03)	−49.76
aug-cc-pVTZ	−43.94 (4.13)	−73.99 (4.67)	−55.65 (1.26)	−52.53
aug-cc-pVQZ(spd)	−45.39 (1.89)	−73.00 (3.07)	−51.73 (.35)	n/a
aug-cc-pV5Z(spd)	−45.93 (1.05)	−72.24 (1.49)	−51.07 (.15)	n/a
aug-cc-pV6Z(spd)	−46.30 (.53)	−71.33 (.62)	−50.48 (.00)	n/a
aug-cc-pVQZ	−46.72 (1.97)	−60.02 (2.98)	−51.67 (.36)	n/a
d-aug-cc-pVDZ(sp)	−35.11(22.24)	−167.64(12.59)	−60.94(−1.10)†	−51.01
d-aug-cc-pVTZ(sp)	−35.51 (4.59)	−116.50 (4.79)	−52.10 (.95)	−50.36
d-aug-cc-pVQZ(sp)	−35.58 (1.25)	−119.49 (1.61)	−47.82 (.13)	−50.03
d-aug-cc-pV5Z(sp)	−35.58 (.59)	−122.43 (1.26)	−46.97 (.07)	−49.91
d-aug-cc-pVTZ	−45.37(11.29)	−85.25(11.45)	−56.21 (3.28)	n/a
d-aug-cc-pVQZ(spd)	−46.03 (2.98)	−72.10 (4.21)	−52.13 (.38)	n/a

Table 7.5: Second-order correlation interaction energies ($-E/K$) for the helium dimer. Comparison with literature data. Entries are listed chronologically.

Authors	$E^{(2)}$
This work	
kq-ansatz and basis aug-cc-pV6Z(spd)	15.99
MP2 using 326 basis functions (d-aug-cc-pV6Z)	15.92
Jeziorska *et al.* [97]	
MP2 using 545 basis functions	15.980
MP2 with X^{-3} extrapolation	16.000
MP2 with X^{-2} extrapolation	16.013
Bukowski *et al.* [88]	
Nonlinearly optimised GTGs	16.00
Klopper [100]	
MP2-R12/A	15.98
MBPT2 using same basis as R12/A calculation	15.92
Gutowski and Chałasiński [101]	
Orbital estimate	15.95

The results obtained with the kq- and pq-ansätze, however, are encouraging. In accordance with the discussion above, interaction energies obtained using a s-orbital basis, underestimate the interaction energy. The same holds for the basis sets consisting of both s- and p-orbitals, but the underestimation is smaller. When d-orbitals are added, the underestimation decreases further, and adding f-orbitals to the aug-cc-pVQZ(spd) basis set, hardly changes the interaction energy, suggesting that f-orbitals are less important for a balanced description of monomer and dimer.

We also note how the basis sets are gradually saturated within each angular momentum level. This is observed as a decrease in the correction energy. For the kq-ansatz, the singly augmented basis sets become saturated to a degree where the counterpoise-correction are insignificant. Using the pq-ansatz, these basis sets should prove to be even better saturated.

In Table 7.5 we compare our best estimate of the second-order correlation interaction energy with values obtained from literature. The best interaction energy calculated in this work, was obtained using the kq-ansatz and the basis set aug-cc-pV6Z(spd). Our estimate is in agreement with literature data, but the energy are not converged, and claiming that there is a certain element of "luck" involved in this excellent agreement, is probably not unfair.

Note, however, that in order obtain a value like 15.99K without having to rely on cancellation of errors, both the energy of the atom and the dimer must be converged

to within $0.01\,\mu E_h$. For the helium atom, Bukowski and co-workers [88] are probably close to this, but for the helium dimer, no-one has up to this point reported a value that is anywhere near such an accuracy.

For reference, we have also included an estimate obtained using conventional MP2 and the basis set d-aug-cc-pV6Z. This calculation is used for the construction of the potential surface of the helium dimer, and is discussed in some more detail in the next section.

7.2.3 The potential energy surface of the helium dimer

When evaluating the relative performance of different methods, it is important to compare the interaction energies at some inter-nuclear reference distance. It is also valuable to calculate interaction energies for different inter-nuclear distances, however, as this allows us to investigate whether the energy difference between two methods is constant or a function of the inter-nuclear distance.

To check whether the GTG ansätze scale correctly, we have calculated the potential energy surface for the helium dimer at inter-nuclear distances in the range 4.8 to $8.5a_0$. For the Hartree–Fock wave function we used the doubly augmented cc-pV6Z basis, while the considerably smaller aug-cc-pVQZ(spd) basis was used for the MP2 correction. For consistency, all calculations had to be counterpoise-corrected, and this excluded the pq-ansatz from the investigation.

As a reference surface, we used a potential energy surface obtained with conventional MP2 and the basis set d-aug-cc-pV6Z. This basis set was also used for the Hartree–Fock part of the calculation. With such a large basis set, the potential energy surface is expected to be given with approximately the same accuracy, for all inter-nuclear distances employed in the investigation.

In Table 7.6 we show total MP2 interaction energies obtained with the GTG methods and the reference method. The absolute energies used to obtain the interaction energies in Table 7.6 are given in Tables B.8–B.10. As these energies are enclosed for accountability only, they have been given in the appendices.

In Figure 7.1, we have plotted the potential energy surfaces using the unit Kelvin. We notice, that the surface obtained with the kl-ansatz undershoot the other two surfaces by several Kelvin. From the results obtained in the previous section, we knew this would be the case, and this observation is therefore not particularly interesting. More interesting is the fact that this surface has its minimum value for a different inter-nuclear distance than the other two. While these have their minima at around $5.8a_0$, the surface obtained with the kl-ansatz have its minimum around $5.7a_0$. This difference may be explained by consulting Table 7.6.

At an inter-nuclear distance of $5.0a_0$, the kl-surface lies $8.19K$ under the reference surface. When the inter-nuclear distance has increased to $5.8a_0$ this gap has decreased to $6.85K$, and when the two helium atoms are separated by $8.0a_0$, the gap is down to $4.64K$. In essence, this shows that the kl-ansatz used with the basis

Table 7.6: Total MP2 interaction energies for the helium dimer at various inter-nuclear distances.

Distance	VOE		KL		KQ	
a_0	μHartree	Kelvin	μHartree	Kelvin	μHartree	Kelvin
4.8	−73.0322	−23.13	−46.3169	−14.67	−71.2158	−22.55
5.0	−23.7596	−7.52	2.1112	.67	−22.1793	−7.02
5.1	−8.4106	−2.66	16.9836	5.38	−6.8991	−2.18
5.2	2.6275	.83	27.5179	8.71	4.0949	1.30
5.4	15.6516	4.96	39.4808	12.50	17.0873	5.41
5.6	21.0696	6.67	43.8058	13.87	22.5278	7.13
5.8	22.3173	7.07	43.9706	13.92	23.8326	7.55
6.0	21.4109	6.78	42.0267	13.31	23.0583	7.30
6.5	16.1130	5.10	34.4947	10.92	17.8891	5.67
7.0	11.0220	3.49	27.8054	8.81	12.8907	4.08
7.5	7.3868	2.34	23.0669	7.30	9.3826	2.97
8.0	4.9830	1.58	19.6317	6.22	6.7154	2.13
8.5	3.4180	1.08	16.5757	5.25	4.8839	1.55

set aug-cc-pVQZ(spd) scales incorrectly.

If we consider the kq-ansatz, however, the distances between the kq-surface and the reference surface are $.50K$, $.48K$, and $.55K$, at the same inter-nuclear separations as above. This variation is marginal, and suggests that the kq-ansatz scales correctly with bond lengths. Note, that it may be difficult to realize this only by looking at Figure 7.1, as the gap visually seems to widen up with the helium–helium distance.

To conclude this section on helium, we have seen that the performance of the kl-ansatz depends extensively on the basis set in use. The kq- and pq-ansätze are less sensitive to the basis set, and perform well also when no higher than d-orbitals are included. For the kl-ansatz to perform satisfactorily, f-orbitals and higher must also be present in the basis set.

7.3 Beryllium

The beryllium atom is the simplest neutral four-electron system that we can study. From the periodic table of the elements, we identify the beryllium atom as a closed-shell system having electron configuration $1s^2 2s^2$. This implies that the Hartree–Fock wave function can only contain s-orbitals. There is no such restriction applying to the wave function corrections, though, and the first-order wave function correction of beryllium may contain orbitals of any order of angular momentum. This is also true for the helium atom, but in this case s-orbitals turn out to be sufficient to obtain

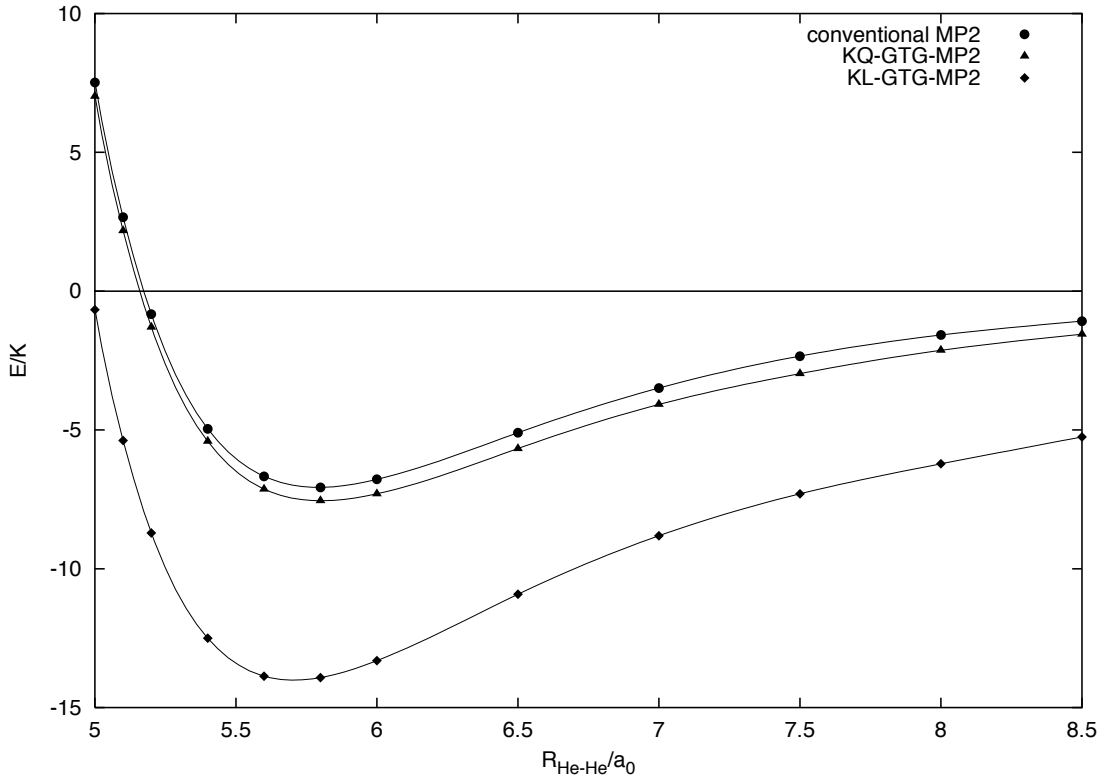

Figure 7.1: Potential energy curves of the helium dimer. The curve plotted from conventional MP2 energies (●) are compared to the curves plotted from KL-ansatz (▲) and KQ-ansatz (♦).

the second-order correlation energy to within 99.99% of the total MP2 correction. This performance is not surprising, however, as the orbital interacting most with the $1s^2$ ground state of helium is also an s-orbital. This orbital, the $2s$-orbital, lies $1.0\,\mathrm{E_h}$ above the $1s$-orbital in energy, while the closest p- and d-orbitals follows some $0.2\,\mathrm{E_h}$ and $0.7\,\mathrm{E_h}$ higher up, respectively. s-orbitals are therefore expected to be more important in the wave function correction.

For the beryllium atom, things are different, and the lowest unoccupied orbital is not a s-orbital but the three $2p$-orbitals, which lie only $0.3\,\mathrm{E_h}$ higher in energy than the occupied $2s$-orbitals. The $2p$-orbitals are followed by the $3s$- and $3p$-orbitals, a mere $0.01\,\mathrm{E_h}$ and $0.04\,\mathrm{E_h}$ higher up, respectively. Both s- and p-orbitals are therefore expected to be important for the wave function correction for beryllium. Our second-order correlation energies for beryllium, which are presented in Table 7.7, supports this assumption.

According to Table 7.7, the best correlation energy obtained for beryllium within a pure s-orbital basis, is only $68.217\,\mathrm{E_h}$. Assuming that the MP2 correction limit is $76.358\,\mathrm{E_h}$ (see Table 7.8), s-orbitals manage to recover only 89% of the correlation

Table 7.7: All-electron second-order correlation energies ($-E/\mathrm{mE_h}$) for the beryllium atom. The ANO basis sets are listed in appendix C. Basis sets marked with an asterisk (*) are used uncontracted. Refer to Table B.11 to have all energies listed with nine figures.

Orbital basis		VOE	KL	KQ	PQ
ANO–1	$(3s)$	2.05	51.97	59.59	60.05
ANO–1	$(4s)$	3.75	52.58	61.10	62.20
ANO–1	$(5s)$	6.79	53.76	64.91	66.35
ANO–1	$(6s)$	14.84	55.61	65.94	67.04
ANO–1	$(10s)^*$	15.68	55.67	66.04	67.42
ANO–1	$(6s1p)$	34.86	68.22	75.31	75.98
ANO–1	$(6s2p)$	36.40	68.44	75.42	76.18
ANO–1	$(6s3p)$	38.63	69.54	75.70	76.25
ANO–1	$(6s4p)$	42.00	70.21	75.74	76.26
ANO–1	$(10s4p)^*$	42.84	70.28	75.81	76.28
ANO–1	$(6s4p1d)$	44.89	71.14	76.072	76.299
ANO–1	$(6s4p2d)$	45.49	71.29	76.097	76.304
ANO–1	$(6s4p3d)$	45.61	71.35	76.108	76.307
ANO–1	$(10s4p3d)^*$	46.45	71.43	76.167	76.317
ANO–2	$(14s)^*$	15.91	55.76	66.239	68.217
ANO–2	$(14s4p)^{*a}$	43.10	70.33	75.866	76.333
ANO–2	$(14s9p)^*$	64.05	74.18	75.939	76.349
ANO–2	$(14s9p3d)^{*b}$	67.67	75.27	76.314	76.3555
ANO–2	$(14s9p4d)^*$	68.28	75.39	76.318	n/a
ANO–2	$(14s9p4d3f)^*$	69.40	75.62	76.345	n/a

[a] Using the four p-orbitals from the ANO–1 basis set.
[b] Using the three d-orbitals from the ANO–1 basis set.

energy, even for the pq-ansatz. When p-orbitals are added, however, the energy increases to $76.349\,\mathrm{E_h}$ which is 99.99% of the estimated limit. Both s- and p-orbitals are therefore essential for the recovery of correlation energy.

By contrast, d-orbitals are not crucial, since the $3d$-orbitals lie some $0.5\,\mathrm{E_h}$ higher in energy than the $2s$-orbital, which is considerably higher than the $2p$-, $3s$-, and $3p$-orbitals.

Even though the pq-ansatz manages to recover a large fraction of the correlation energy without the use of d- and f-orbitals, this is not the case for the other two ansätze. For the kq-ansatz, for instance, the best energy obtained with a basis consisting of merely s- and p-orbitals is $75.939\,\mathrm{E_h}$. This is "only" 99.5% of the limit,

Table 7.8: All-electron second-order correlation energies ($-E/\mathrm{mE_h}$) for the beryllium atom. Comparison with literature data. Entries are listed chronologically. The total correlation energy is $-94.332\,\mathrm{mE_h}$ [107].

Authors	$E^{(2)}$
This work	
kl-ansatz (ANO–2 $14s9p4d3f^*$)	75.62
kq-ansatz (ANO–2 $14s9p4d3f^*$)	76.345
pq-ansatz (ANO–2 $14s9p3d^*$)	76.355
Bukowski *et al.* [102]	
350 nonlinearly optimised GTGs for each pair	76.358
Noga *et al.* [103]	
MBPT-R12 ($16s10p6d5f4g$)	76.248
Termath *et al.* [41]	
MP2-R12/A (STO basis $15s12p11d11f10g$)	76.373
MP2-R12/B (STO basis $15s12p11d11f10g$)	76.311
Salomonsen and Öster [104]	
Extrapolated partial-wave expansion ($l \leq 10$) with numerical orbitals	76.358
Petersson *et al.* [90]	
CBS (complete basis set) model	77.27
Alexander *et al.* [105]	
Nonlinearly optimised GTGs	76.350
Janowski *et al.* [106]	
Partial-wave expansion with $l \leq 9$	75.98
Malinowski *et al.* [91]	
Partial-wave expansion with radial and angular extrapolation	76.29

and by comparing the energy obtained with the basis set $(14s4p)^*$ with the energy obtained with the basis set $(14s9p)^*$, we conclude that the energy does not improve substantially if more p-orbitals are added. Rather, we have to add several d- and f-orbitals if we want a kq-ansatz performance comparable to that obtained with the pq-ansatz used in a basis of s- and p-orbitals.

For the kl-ansatz, we also have to include g-orbitals, if decent correlation energies are to be obtained. The kl-ansatz performs far better than the virtual orbital expansion, however, which are far from the limit even for the largest basis set.

In Table 7.8, we compare our results with some reference values found in literature. The best correlation energy listed, is the energy obtained by Bukowski and co-workers [102] and Salomonsen and Öster [104]. These authors independently obtained the same energy using very different methods. The energy obtained by Bukowski and co-workers, however, has the advantage that it is obtained variation-

Table 7.9: Second-order pair correlation energies ($-E/\mathrm{mE_h}$) for the beryllium atom.

Pair	R12/A[a]	R12/B[a]	GTG[b]	KL[c]	KQ[c]	PQ[d]
$1s^2$	40.334	40.325	40.340	39.883	40.341	40.343
$1s2s$, ^{1}S	3.252	3.249	3.251	3.211	3.253	3.253
$1s2s$, ^{3}S	2.217	2.217	2.219	2.165	2.219	2.219
$2s^2$	30.570	30.520	30.540	30.363	30.532	30.540
$E^{(2)}$	76.373	76.311	76.350	75.622	76.345	76.355

[a] MP2-R12/A(STO) and MP2-R12/B(STO) from Ref.[41].
[b] Nonlinearly optimised GTGs from Ref.[105].
[c] Using basis set ANO–2 $(14s9p4d3f)^*$
[d] Using basis set ANO–2 $(14s9p3d)^*$

ally. We know, therefore, that the limit value for the pair energy is lower than $-76.358\,\mathrm{E_h}$.

The best estimate of the second-order correlation energy for beryllium obtained in this work is $-76.355\,\mathrm{mE_h}$. This value, which was obtained using the pq-ansatz and a $14s9p3d$ basis set, is only $3\,\mu\mathrm{E_h}$ higher than the current best estimate. This is remarkably good, especially considering the size of the orbital basis and the fact that GCF exponents were not optimised.

Using the kq-ansatz we obtain a correlation energy that is $13\,\mu\mathrm{E_h}$ higher than the best estimate. Even though this performance is inferior to the performance of the pq-ansatz, it is still 99.98% of the best estimate, which is acceptable.

We also note, that the MP2-R12 energies obtained by Termath *et al.*, are considerably better than the energy we have obtained with the kl-ansatz. This clearly shows that a good result can only be obtained with the kl-ansatz, if we use a basis set containing orbitals with high angular momentum. Since the GTGs do not contribute to the correlation energy beyond s-orbitals, the largest proportion of the energy must be recovered by the virtual orbital expansion.

When the MP2-R12/B calculation was extrapolated, Termath obtained the value $-76.316\,\mathrm{mE_h}$ as the basis set limit value for the second-order correlation energy. This estimate is $42\,\mu\mathrm{E_h}$ higher than the Bukowski estimate.

In Table 7.9, we compare the pair energies obtained with the different GTG-ansätze with pair energies found in literature. There are a few interesting things to note. First, we see that the pq-ansatz performs better than the kq-ansatz mainly for the $2s^2$ pair, while the performance is rather similar for the other pairs. Next, we note that the performance of the MP2-R12/A method is somewhat inconsistent. For the $1s2s$ singlet and triplet pairs, the linear r_{12} method performs well, and is only a

few μE_h above the energies obtained with the pq-ansatz. For the $1s^2$ pair, however, the method overshoot the pq-ansatz by $9\,\mu E_h$, and for the $2s^2$ pair it undershoots the pq-ansatz with $30\,\mu E_h$. Since a large orbital basis set was used, it is hard to see why the R12/A method should perform this differently for the different electron pairs. We note finally that the MP2-R12/B method is not hampered with this inconsistency.

7.4 Neon

The all-electron second-order correlation energies obtained for the neon atom are presented in Table 7.10. In the first part of this table we list correlation energies obtained with the cc-pV*X*Z series of basis sets. We see that the trends observed for helium using these basis sets are reproduced for neon; the energy convergence is relatively fast for the kq- and pq- ansätze, but only moderate for the kl-ansatz. The latter, however, performs far better than the conventional virtual orbital expansion.

The cc-pV*X*Z basis sets do not contain flexible core orbitals, and are therefore not suited for describing core-core and core-valence correlation. To remedy this, Dunning and co-workers generated sets of tight functions that were added to the original cc-pV*X*Z basis sets. In the second part of Table 7.10, we have used these basis sets, generically denoted cc-pCV*X*Z, to investigate the importance of the extra core functions. The energy improvements turns out to be significant within all ansätze. Note, also, that for the virtual orbital expansion and the kl-ansatz, the improvements are numerically larger for the triple-zeta basis set than for the double-zeta basis set. This results, which at first may seem surprising, arises because the number of tight functions added to each of these basis sets are different. For the double zeta basis, one *s*- and one *p*-orbital are added. For the triple zeta basis, however, two *s*-orbitals and two *p*-orbitals are added, as is an extra *d*-orbital.

While the cc-pCV*X*Z basis sets contain extra functions for describing the core, the aug-cc-pV*X*Z basis sets have been supplemented with diffuse functions to improve the description of the outer valence. Independently of the cardinal number X, one diffuse function is added for each angular momentum present in the basis.

Depending of the ansatz, additional diffuse functions turn out to be more important for the correlation energy than the tight functions provided by the cc-pCV*X*Z basis sets. From Table 7.10 we see that the virtual orbital expansion and the kl-ansatz benefit more from additional core functions, while additional diffuse functions are more important for the kq- and pq-ansätze. It is fairly obvious, however, that since the tight functions and the diffuse functions expand different parts of the orbital space, we should eventually use both in combination. The basis sets aug-cc-pCV*X*Z have been made for this.

The aug-cc-pCV*X*Z sets provide sufficient flexibility for both core and valence, and perform very well for neon. In fact, the current best estimate of the MP2

Table 7.10: All-electron second-order correlation energies ($-E/\mathrm{mE_h}$) for the neon atom. A dagger (†) is given for calculations that failed to converge, and a double dagger (††) is given for calculations that are currently too computationally demanding. The (‡) is explained on page 171. Refer to Table B.12 to have all energies listed with ten digits.

Orbital basis	VOE	KL	KQ	PQ
cc-pVDZ	187.57	300.98	346.93	356.37
cc-pVTZ	277.29	350.32	380.61	383.99
cc-pVQZ	326.26	371.77	386.19	387.30
cc-pCVDZ	228.30	310.43	356.40	364.16
cc-pCVTZ	329.10	362.47	383.67	385.49
cc-pCVQZ	361.51	378.51	†	n/a
aug-cc-pVDZ	209.06	323.58	369.27	380.66
aug-cc-pVTZ	285.91	358.89	384.86	387.55
aug-cc-pVQZ	330.01	375.51	387.21	n/a
aug-cc-pCVDZ (sp)	157.71	265.30	344.39	356.17
aug-cc-pCVTZ (sp)	187.48	273.91	357.11	364.54
aug-cc-pCVQZ (sp)	190.94	275.73	358.59	365.74
aug-cc-pCV5Z (sp)	191.74	276.26	359.24	366.36
aug-cc-pCVDZ	249.90	333.13	375.05	384.56
aug-cc-pCVTZ (spd)	309.08	353.91	386.23	388.008
aug-cc-pCVQZ (spd)	319.34	358.23	387.14	n/a
aug-cc-pCV5Z (spd)	321.57	359.37	††	n/a
aug-cc-pCVTZ	337.29	370.72	387.14	388.189
aug-cc-pCVQZ (spdf)	354.18	377.17	†	n/a
aug-cc-pCVQZ	365.16	382.12	††	n/a
aug-cc-pCV5Z‡	375.93	385.54	††	n/a

correction energy for the neon atom, is obtained using the pq-ansatz and the basis set aug-cc-pCVTZ (see Table 7.11). With this basis set, the kq-ansatz retrieves 99.7% of the estimated limit, while the kl-ansatz and the virtual orbital expansion retrieves 95.5% and 86.9%, respectively. For the latter methods, the lack of high angular momentum functions is apparent. The best energy estimate for the kl-ansatz is obtained using the aug-cc-pCV5Z basis set, consisting of orbitals $11s10p8d6f4g2h$. Using this basis set we manage to retrieve 99.3% of the correlation energy, which is satisfactory.

Three-electron integrals could not be calculated using the exact aug-cc-pCV5Z

basis set however. Due to the high level of contraction in the s-block of atomic orbitals, the integral calculation ran out of memory. In order to push the calculation through, the two atomic orbitals with highest exponent were removed from the basis set, thus reducing the number of contracted primitives from 10 to 8. For the conventional MP2 calculation this removal merely increased the pair energy from $-375.933\,\mathrm{mE_h}$ to $-375.931\,\mathrm{mE_h}$, and we do not expect the removal to be significantly more important for the kl-ansatz. The aug-cc-pCV5Z basis set has been marked with a ‡ to notify the change, however.

Since the aug-cc-pCVXZ basis sets give excellent results for the neon atom, we have used these to explore partial-wave expansions. Having electron configuration $1s^2 2s^2 2p^6$, the smallest partial-wave expansion that makes sense for the neon atom must contain both s- and p-orbitals. Although sensible, Table 7.10 shows that basis sets without high angular momentum functions give poor energy estimates. This is in accordance with the observations made for beryllium. As we shall see below, polarisation functions are needed for neon mainly due to the ^{1}D coupling between $2p$ orbitals. Without d-orbitals or higher, this interaction cannot be properly described.

The best energy obtained in a basis set consisting of s- and p-orbitals, is 94.4% of the estimated limit for the pq-ansatz, 92.5% for the kq-ansatz, and 71.2% for the kl-ansatz. Once d-orbitals are included, however, these percentages rise to 99.97%, 99.7%, and 92.6%, respectively. For the kq- and pq-ansätze, therefore, it is sufficient to include d-orbitals unless very accurate energies are requested.

In Table 7.11 we compare our results with values obtained from the literature. Accurate estimates for the MP2 correction energy of neon are given by several authors. Among these estimates, the pq-ansatz energy is not the lowest, but since it is the only value that has been obtained variationally, we still consider it the best. Comparing the energies obtained with the pq-ansatz and basis sets aug-cc-pCVDZ, aug-cc-pCVTZ(spd), and aug-cc-pCVTZ, however, it is reasonable to conclude that the true limit is "considerably" lower than $-388.19\,\mathrm{mE_h}$, probably also lower than $-388.31\,\mathrm{mE_h}$; the value obtained by Lindgren and Salomonsen.

Before moving to the next table, we note that the energy estimate obtained by Wenzel and co-workers [14] using nonlinearly optimised GTGs, is not among the best. This is somewhat surprising, considering the fact that the best energy estimates for the helium and beryllium atoms were obtained using this method. For the neon atom Wenzel and co-workers defined geminal basis functions as

$$\begin{aligned} g_i(1,2) = {} & x_{1P}^{l_1} y_{1P}^{m_1} z_{1P}^{n_1} x_{2Q}^{l_2} y_{2Q}^{m_2} z_{2Q}^{n_2} \\ & \times \exp\left[-\alpha_i(\mathbf{r}_1 - \mathbf{P}_i)^2 - \beta_i(\mathbf{r}_2 - \mathbf{Q}_i)^2 - \gamma_i r_{12}^2\right] \end{aligned} \tag{7.2}$$

which is similar to (7.1), except for the angular factors in front of the exponential term. As for the helium atom, all GTGs are centred on the neon atom, that is $\mathbf{P}_i = \mathbf{Q}_i = \mathbf{0}$. The exponents α_i, β_i and γ_i were optimised for each geminal under

Table 7.11: All-electron second-order correlation energies ($-E/\mathrm{mE_h}$) for the neon atom. Comparison with literature data. Entries are listed chronologically. The total correlation energy is $-390.47\,\mathrm{mE_h}$ [112].

Authors	$E^{(2)}$
This work	
kl-ansatz (aug-cc-pCV5Z‡)	385.54
kq-ansatz (aug-cc-pVQZ)	387.21
pq-ansatz (aug-cc-pCVTZ)	388.19
Wind *et al.* [108]	
MP2-R12-SO (exact 3-electron integrals in basis $20s14p11d9f7g5h$)	388.06
MP2-R12/A ($20s14p11d9f7g5h$)	388.29
MP2-R12/B ($20s14p11d9f7g5h$)	388.00
Flores [89]	
FEM-MP2 with $l \leq 12$ and angular extrapolation	388.10
Petersson *et al.* [90]	
CBS (complete basis set) model	386.38
Wenzel *et al.* [14]	
Nonlinearly optimised GTGs	385.26
Lindgren and Salomonsen [109, 110]	
Numerical integration of the Coupled-Cluster equations	388.31
Janowski and Malinowski [111]	
Calculated	384.98
Radially and angular extrapolated	387.92

the restrictions

$$\alpha_i\beta_i + \alpha_i\gamma_i + \beta_i\gamma_i > 0 \quad \text{and} \quad \alpha_i + \beta_i + \gamma_i > 0 \tag{7.3}$$

and using a modification of the weak orthogonality functional. This functional, which is referred to as the *modified weak orthogonality* (MWO) *functional*, is described in Ref. [14]. The non-negative integers $l_1, m_1, n_1, l_2, m_2, n_2$ define the angular symmetry of the basis function $g_i(1,2)$, and are chosen according to the completeness criteria given by King [93]. As discussed in section 7.2, pair functions belonging to the totally symmetric representation may be expanded completely in basis functions for which $l_1, m_1, n_1, l_2, m_2, n_2$ are equal to zero.

In neon, however, there are also pairs belonging to representations different from the totally symmetric representation, and for these pairs, appropriate angular factors must be included. For the $1s2p_x$ singlet and triplet interactions, for instance, Wenzel used basis functions with angular symmetry $(l_1, m_1, l_2, m_2) = (0, 0, 1, 0)$. Likewise, for the $2p_x2p_y$ triplet interaction, basis functions with angular symmetry (1,0,0,1) and (0,1,1,0) was used, and for the singlet interaction (0,0,1,1) was also included.

Table 7.12: Second-order pair energies ($-E/\mathrm{mE_h}$) for the neon atom using different methods.

Pair		GTG[a]	R12/SO[b]	KL[c]	KQ[d]	PQ[e]	PQ[f]
$1s^2$		40.22	40.252	40.150	39.965	40.224	40.229
$1s2s$,	^{1}S	3.95	3.974	3.960	3.929	3.974	3.975
$1s2s$,	^{3}S	1.58	1.582	1.567	1.566	1.585	1.585
$2s^2$		12.00	12.038	11.984	12.033	12.044	12.046
$1s2p$,	^{1}P	8.10	8.176	8.055	8.103	8.139	8.161
$1s2p$,	^{3}P	13.86	13.911	13.846	13.763	13.825	13.880
$2s2p$,	^{1}P	59.85	60.472	59.765	60.438	59.702	60.532
$2s2p$,	^{3}P	26.55	26.708	26.633	26.679	26.439	26.757
$2p^2$,	^{1}S	45.24	45.565	45.450	45.553	45.544	45.574
$2p^2$,	^{1}D	87.06	88.042	86.907	87.891	65.957	88.031
$2p^2$,	^{3}P	86.85	87.341	87.224	87.296	87.110	87.417
$E^{(2)}$		385.26	388.061	385.541	387.215	364.543	388.189

[a] MP2-R12-SO from Ref. [108].
[b] Nonlinearly optimised GTGs from Ref. [14].
[c] Orbital basis aug-cc-pCV5Z.
[d] Orbital basis aug-cc-pVQZ.
[e] Orbital basis aug-cc-pCVTZ (sp).
[f] Orbital basis aug-cc-pCVTZ (spd).

To describe each pair function, Wenzel and co-workers used a 40 term GTG expansion, whereas Bukowski *et al.* [102] used 150 and 350 GTGs, respectively, to obtain their excellent helium and beryllium energies. Although Bukowski and co-workers obtained descent pair energies even for 30 terms expansions, the 40 GTGs of Wenzel had to describe all symmetry components of the $2p^2$ interactions, leaving less variationally flexibility for each. And as discussed below, the relatively poor performance of the GTG approach by Wenzel and co-workers, are mainly due to a deficient description of the $2p^2$ interactions.

In Table 7.12, we give pair energies obtained by some selected methods, including the GTG approach by Wenzel *et al.*. The pair energies given in the two rightmost columns are both obtained using the pq-ansatz, but their one-electron basis sets differ slightly in that one of them also contains *d*-orbitals. As a result, seven out of eleven pair energies differ by less than $0.10\,\mathrm{mE_h}$, three pair energies differ by less than $1\,\mathrm{mE_h}$, while the last pair energy, the $^1\mathrm{D}(2p^2)$ interaction, differ by more than $22\,\mathrm{mE_h}$. For this interaction, therefore, *d*-orbitals are essential. In terms of MP2-R12 theory, Klopper [41, 100] has also made the observations that the $^1\mathrm{D}(2p^2)$ interaction is the most difficult to converge.

Note, however, that for the nonlinearly optimised GTGs, Wenzel and co-workers obtain an excellent estimate of the ^{1}D interaction, considering that only s- and p-orbitals are used. This is very intriguing as the pq-ansatz, at least in principle, should be able to produce pair energies of similar quality. The major difference is that in the nonlinear optimisation of exponents, negative values for α_i, β_i, and γ_i are allowed, providing these exponents fulfil (7.3). Table III of Ref. [14], which lists the 40 optimal exponents for the $2s2p_x$ interaction in neon, shows that some of the GTGs in fact *do* get negative exponents. Most likely, therefore, the excellent estimate of the ^{1}D interaction is due to these basis functions.

Since the pair functions presented in this work are constructed from pairs of orbitals, only the GCF exponent may be chosen negative. Currently, it is somewhat unclear, however, how much the implementation much be modified in order to allow for negative GCF exponents.

In a last glance at Table 7.12, we also note, that the kq-ansatz performs poorly relative to the pq-ansatz for the $1s^2$ pair. In fact, for all pairs involving the $1s$ orbital, except the singlet $1s2p$ interaction, the pair energies listed for the kq-ansatz in Table 7.12 are also inferior to the energies listed for the kl-ansatz. Since the kl-ansatz exploits a smaller subset of the MO space than the kq-ansatz, this is purely a basis set effect. A comparison of the basis sets used for the different GTG ansätze listed in Table 7.12, shows that the basis set giving the best energy for the kq-ansatz is the only one not containing flexible core functions. This explains the inferior performance observed for the core–core and core–valence correlation energies.

In Table 7.13 we compare the kl-ansatz with the rotational variant ij-ansatz and different MP2-R12 methods. As explained in section 6.1, the difference between the ij- and kl-ansätze is that in the latter the pair function of a specific pair ij is expanded using all pairs of occupied orbitals kl, whereas in the former only the pair ij is utilised. In addition to being rotational invariant, the kl-ansatz also gives a larger variation space, and consequently a better energy. For the basis set aug-cc-pCVDZ, for instance, the difference between the two ansätze is more than $6\,\mathrm{mE_h}$. As the orbital basis increases, however, the difference in performance diminishes, and for the basis set aug-cc-pCV5Z, it is down to $0.6\,\mathrm{mE_h}$.

The ansatz denoted IJ-SO in Table 7.13, refers to the MP2-R12/SO implementation of Wind *et al.* [108], in which three-electron integrals are calculated explicitly. This approach is less approximate than the usual MP2-R12 methods, and the resolution-of-the-identity (RI) approximation is largely avoided. Wind and co-workers did not employ the usual orbital invariant approach, however, and energies obtained with the MP2-R12/SO method should therefore be compared with the ij-ansatz rather than the kl-ansatz.

In Table 7.13 we see that the MP2-R12/SO method gives lower energies than the ij-ansatz for most of the basis sets. This somewhat counter-intuitive result may be a MP2-R12 effect caused by the RI approximation. The WO functional is only a good approximation to the SO functional if the pair function is sufficiently flexible,

Table 7.13: All-electron second-order correlation energies ($-E/\mathrm{mE_h}$) for the neon atom compared with linear r_{12} methods.

Orbital basis	VOE	KL-1A'[a]	KL-1B[a]	IJ-SO[b]	IJ	KL
cc-pVDZ	187.57	—	—	306.6	290.49	300.98
cc-pVTZ	277.29	—	—	343.1	343.19	350.32
cc-pVQZ	326.26	—	—	365.9	367.63	371.77
cc-pCVDZ	228.30	302.89	288.45	318.7	303.98	310.43
cc-pCVTZ	329.10	357.46	355.56	362.4	360.37	362.47
cc-pCVQZ	361.51	375.21	373.26	377.1	377.40	378.51
aug-cc-pVDZ	209.06	—	—	322.7	313.00	323.58
aug-cc-pVTZ	285.91	—	—	356.1	351.85	358.89
aug-cc-pVQZ	330.01	—	—	373.2	371.42	375.51
aug-cc-pCVDZ	249.90	312.28	302.91	—	326.54	333.13
aug-cc-pCVTZ	337.29	362.35	360.07	—	368.78	370.72
aug-cc-pCVQZ	365.16	377.35	375.88	—	381.14	382.12
aug-cc-pCV5Z	375.93	384.46	383.92	—	384.97[c]	385.54[c]

[a] Referring to the MP2-R12/1A' and MP2-R12/1B methods described in Ref. [42]. Both methods are based on the kl-ansatz.

[b] Referring to the MP2-R12/SO method described in Ref. [108]. This method is based on the ij-ansatz.

[c] Using the quenched aug-cc-pCV5Z basis set described on page 171.

however, and the results may therefore also be a GTG effect. The fact that we have expanded correlation factors in a set of GCFs instead of using a linear r_{12}, is not an issue however. The set of GCFs employed in our calculations is saturated to within $0.1\,\mathrm{mE_h}$ for the inner part of the Coulomb hole (cf. section 6.3), and for the outer part of the hole, the expansion of GCFs ought to provide a better description than a single r_{12}.

For the basis set cc-pCVQZ the situation is reversed, however, and the ij-ansatz gives a lower energy than the MP2-R12/SO method. Assuming that the RI approximation holds sufficiently well for this basis set (due to size and saturation), this result is in agreement with the larger variation space offered by the ij-ansatz.

In Table 7.13 we also list correlation energies obtained with two of the conventional MP2-R12 methods. These methods use the rotational invariant formulations, and should therefore be compared to the kl-ansatz. Moreover, in the formulation of the MP2-R12 methods listed here, the resolution of the identity is expanded in a separate basis set of quality $32s24p18d15f12g9h6i$. The RI-approximation may therefore be assumed to hold, allowing a direct comparison with the kl-ansatz. We

Table 7.14: Second-order correlation energies ($-E/\mathrm{mE_h}$) for the hydrogen molecule. An inter-nuclear distance of 74.08481 pm was used. Energies marked with a double-dagger (‡) undershoot the true energy, probably due to a non-positive-definite Fock operator. Refer to Table B.13 to have all energies listed with nine digits.

Orbital basis	VOE	KL	KQ	PQ
cc-pVDZ	26.38	31.63	33.580	33.8019
cc-pVTZ	31.68	33.48	34.151	34.2263
cc-pVQZ	33.11	34.00	34.226	n/a
aug-cc-pVDZ(s)	15.95	29.82	33.535	33.7943
aug-cc-pVTZ(s)	17.91	30.07	33.836	34.1317
aug-cc-pVQZ(s)	18.36	30.11	33.934	34.3232‡
aug-cc-pV5Z (s)	18.43	30.13	33.943	34.3680‡
aug-cc-pVDZ	27.29	32.74	33.879	34.0464
aug-cc-pVTZ(sp)	29.88	33.31	34.177	34.2434
aug-cc-pVQZ(sp)	30.45	33.50	34.220	34.2460
aug-cc-pV5Z (sp)	30.65	33.53	34.229	34.2491
aug-cc-pVTZ	31.99	33.82	34.209	34.2525
aug-cc-pVQZ(spd)	32.74	34.06	34.240	n/a
aug-cc-pV5Z (spd)	32.98	34.11	34.247	n/a
aug-cc-pVQZ	33.25	34.14	34.241	n/a

see that the GTG approach generally performs better than the MP2-R12 methods. The variation space is larger for the former, however, and this result is therefore in excellent agreement with the reasoning already made for the ij-ansatz.

7.5 The hydrogen molecule

The smallest system containing a chemical bond is the hydrogen molecule. This molecule has the same number of electrons as the helium atom, but since the symmetry is lower, we cannot expect the energy to be obtained with the same accuracy as for helium. If we cannot manage to get a decent correlation energy for hydrogen, however, our GTG-MP2 ansätze will probably not perform well for other molecules either. The hydrogen molecule is therefore an important test system.

In Table 7.14 we give our second-order correlation energies for a hydrogen molecule with bond length $1.4a_0 = 74.0848$pm. In the upper part of the table we give

Table 7.15: Second-order correlation energies ($-E/\mathrm{mE_h}$) for a hydrogen molecule with an inter-nuclear distance of 71.42857 pm. Entries are listed chronologically. The total correlation energy is $-40.8461\,\mathrm{mE_h}$ [115].

Authors	$E^{(2)}$
This work	
kl-ansatz (aug-cc-pVQZ)	34.14
kq-ansatz (aug-cc-pVQZ)	34.247
pq-ansatz (aug-cc-pV5Z-spd)	34.252
Bukowski *et al.* [88]	
120 nonlinearly optimised GTGs	34.244
Klopper and Kutzelnigg [113]	
MP2-R12/A ($9s8p4d1f$)	34.23
MP2-R12/B ($9s8p4d1f$)	34.17
Jeziorski *et al.* [114]	
40 nonlinearly optimised GTGs	34.20

correlation energies obtained with the cc-pVXZ series of basis sets. We shall not discuss these values in any detail, merely comment that the pq-ansatz used with the cc-pVTZ basis set gives the same energy as the kq-ansatz used with the cc-pVQZ basis set.

In the rest of Table 7.14 we use the aug-cc-pVXZ series of basis sets to explore partial-wave expansions in the *s*-, *sp*-, and *spd*-orbital spaces.

Expansion of the pair function in *s*-orbitals appears to give good energy estimates with the kq- and pq-ansätze, and may therfore, at first sight, seem like a good idea. If we compare with energies obtained with the full aug-cc-pVTZ basis set, however, inconsistencies are seen. Clearly, the energies obtained with the pq-ansatz and the two largest *s*-expansions are undershooting the true MP2 correction energy. In section 3.4.1 we argued that pair energies obtained by minimising the WO or SO functionals may undershoot the true pair energy if the Fock operator is poorly described. A quick look at the Hartree–Fock orbitals obtained with the aug-cc-pVQZ basis set shows that the occupied 1σ orbital contains small amounts of p-functions, as well as smaller amounts of d- and f-functions. It is therefore reasonable to assume that the undershooting observed in Table 7.14 is due to a poorly described Fock operator. Since the Fock operator are of equal or less quality for all *s*-expansions, we conclude that energies obtained with *s*-orbitals are all incorrect even though most of them are well above the MP2 correction limit.

The pair energies obtained with *sp*-expansions are all above the limit, and for the larger expansions we have reason to assume that the Fock operator is described accurately. For the largest expansion we also get good energy estimates, and the

pq-, kq- and kl-ansätze recover some 99.99%, 99.93%, and 97.9% of the estimated limit, respectively (see Table 7.15). When d-orbitals are included in the partial-wave expansions, the pq-ansatz give the current best estimate of the MP2 correction energy, while the kq- and kl-ansätze recover some 99.98% and 99.6%, respectively, of this limit estimate. The best correlation energy using the kl-ansatz is obtained with the aug-cc-pVQZ basis set. In this case some 99.7% of the correlation energy is recovered.

In Table 7.15, we compare our best correlation energies with values obtained from the literature. Note, that there are fewer energy estimates available for molecules than for atoms, as several of the methods giving accurate correlation energies, are either specialised for atoms [89, 109, 111] or only implemented for atoms [108].

The best correlation energies given in Table 7.15 are the energy estimates obtained with the pq- and kq-ansätze in this work. These estimates of $-34.252\,\mathrm{mE_h}$ and $-34.247\,\mathrm{mE_h}$ were obtained using 1710 and 171 GTGs, respectively. The value obtained by Bukowski and co-workers [88] using 120 nonlinearly optimised GTGs is only a few $\mu\mathrm{E_h}$ behind, however. Bukowski defined the pair function as for the helium atom (see Equation 7.1), but included the coordinates of the GTGs lying in the direction of the molecular axis in the optimisation. For linear molecules it has been shown [116, 117] that any two-electron pair function belonging to the totally symmetric representation can be represented by geminals with no angular components. If Bukowski and co-workers include more GTGs in their pair function expansion, therefore, they ought to be able to improve on the energy estimate presented here.

The energies obtained by Klopper and Kutzelnigg [113] using the two MP2-R12 approximations are also acceptable, especially considering the size of the basis set that was used.

7.6 Lithium hydride

In Table 7.16 we present all-electron second-order correlation energies for a lithium hydride molecule with bond length $3.015a_0 = 159.6\mathrm{pm}$. We have not listed any energies for the pq-ansatz, however, as singularities in the equation solver prevented us from using this ansatz. The problems observed for lithium hydride are similar to those experienced for the helium calculations involving a ghost basis set. These problems are of technical nature, however, and if we remove the singularities, energy estimates may also be obtained for the pq-ansatz. Since the systems studied in previous sections of this work obtained their best energy estimates with the pq-ansatz, we will probably not be able to exploit the full potential of the GTG-MP2 method for the lithium hydride molecule.

As mentioned in section 6.2, we have not used the correlation-consistent basis sets to describe the lithium hydride molecule. Instead we have used two sets of atomic natural orbitals (ANOs) developed by Roos and co-workers [72, 73]. The

Table 7.16: All electron second-order correlation energies ($-E/\mathrm{mE_h}$) for the lithium hydride molecule with an inter-nuclear distance of r(Li–H)=159.5469 pm. Due to problems with singular matrices the pq-ansatz could not be used. Basis sets marked with an asterisk (*) are used uncontracted. Refer to Table B.14 for more precise energies.

Orbital basis (Li,H)		VOE	KL	KQ
ANO–1	$(10s4p, 7s)^*$	28.97	58.13	70.549
ANO–1	$(10s4p3d, 7s)^*$	32.83	60.76	71.419
ANO–1	$(10s4p, 7s3p)^*$	40.80	63.79	72.373
ANO–1	$(10s4p3d, 7s3p)^*$	41.80	64.50	72.511
ANO–2	$(14s9p, 8s)^*$	49.99	63.81	70.900
ANO–2	$(14s9p4d, 8s)^*$	54.41	66.72	71.808
ANO–2	$(14s9p, 8s4p)^*$	61.78	69.52	72.678
ANO–2	$(14s9p4d, 8s4p)^*$	63.06	70.38	72.809
ANO–2	$(14s9p4d3f, 8s4p)^*$	63.68	70.79	72.850
ANO–2	$(14s9p4d, 8s4p3d)^*$	65.24	71.20	72.864
ANO–2	$(14s9p4d3f, 8s4p3d)^*$	65.40	71.33	72.877

basis function exponents for these basis sets are given in Appendix C.

Even though the pq-ansatz could not be used, Table 7.16 shows that the correlation energies obtained with the kq-ansatz are also good. This is in agreement with observations made for the hydrogen molecule. When the kq-ansatz is combined with the basis set $(14\mathrm{s9p4d3f}, 8\mathrm{s4p3d})^*$ we get $-72.877\,\mathrm{mE_h}$, which is our best correlation energy for the lithium hydride molecule. A comparison with Table 7.17 shows that we have recovered 99.98% of the estimated limit. Note also, that reasonably good correlation energies are obtained even when the f-orbitals on lithium are not used.

For the kl-ansatz the best correlation energy obtained is $-71.20\,\mathrm{mE_h}$ which is only 97.9% of the limit. For this ansatz, therefore, far better correlation energies are obtained for the hydrogen molecule.

In Table 7.17 we compare our best correlation energies with literature data. The best correlation energy for the lithium hydride molecule is given by Bukowski and co-workers [102]. Using 350 GTGs of type (7.1) in which five of the nonlinear parameters were optimised variationally, they obtained $-72.890\,\mathrm{mE_h}$. This excellent result is almost matched by Noga *et al.* [103] who obtained $-72.869\,\mathrm{mE_h}$ using the MBPT-R12/B method. This method is not variational, however, and it is therefore somewhat difficult to evaluate the quality of the result. The complete-basis-set (CBS) value of Petersson [90], on the other hand, is far off the limit.

When comparing with literature data, we see that the kq-ansatz performs very well. In Table 7.18 we have split the best correlation energy obtained with this ansatz

Table 7.17: Second-order correlation energies ($-E/\mathrm{mE_h}$) for the lithium hydride molecule with an inter-nuclear distance of r(Li–H)=159.5469 pm. Comparison with literature data. Entries are listed chronologically. The total correlation energy is approximately $-83.2\,\mathrm{mE_h}$ [75].

Authors	$E^{(2)}$
This work	
kl-ansatz [ANO–2 ($14s9p4d3f$, $8s4p3d$)*]	71.33
kq-ansatz [ANO–2 ($14s9p4d3f$, $8s4p3d$)*]	72.877
Bukowski *et al.* [102]	
350 nonlinearly optimised GTGs	72.890
Noga *et al.* [103]	
MBPT-R12/A ($11s8p6d5f$, $9s8p6d5f$)	72.973
MBPT-R12/B ($11s8p6d5f$, $9s8p6d5f$)	72.869
Klopper and Kutzelnigg [113]	
MP2-R12/A ($11s7p4d1f, 9s6p3d1f$)	72.76
MP2-R12/B ($11s7p4d1f, 9s6p3d1f$)	72.16
Petersson *et al.* [90]	
CBS (complete basis set) model	73.54
Alexander *et al.* [118]	
700 nonlinearly optimised, randomly tempered GTGs	72.781

Table 7.18: Second-order pair correlation energies ($-E/\mathrm{mE_h}$) for the lithium hydride molecule with an inter-nuclear distance of r(Li–H)=159.5469 pm.

Pair		R12/A[a]	R12/B[a]	GTG[b]	KL[c]	KQ[c]
$1\sigma^2$	$^1\Sigma^+$	39.51	39.45	39.590	38.527	39.609
$1\sigma2\sigma$	$^1\Sigma^+$	1.48	1.41	1.471	1.409	1.490
	$^3\Sigma^+$	1.37	1.30	1.324	1.284	1.340
$2\sigma^2$	$^1\Sigma^+$	30.41	30.00	30.396	30.106	30.437
$E^{(2)}$		72.76	72.16	72.781	71.326	72.877

[a] Energies are obtained with the MP2-R12/A and MP2-R12/B methods in a basis of quality ($11s8p6d5f$, $9s8p6d5f$). From Ref. [113].
[b] Using nonlinearly optimised GTGs. From Ref. [118].
[c] Using basis set ANO–2 ($14s9p4d3f, 8s4p3d$)*.

into separate pair energies. Also presented are the best pair energies obtained with the kl-ansatz as well as pair energies obtained from literature. Unfortunately, neither Bukowski nor Noga listed pair energies in their papers, and we are therefore left to compare with the pair energies given by Alexander *et al.* [118] and Klopper and Kutzelnigg [113]. Except for the $1\sigma 2\sigma$ triplet energy obtained with the MP2-R12/A method, we see that the kq-ansatz give slightly lower energies for all pairs.

7.7 Hydrogen fluoride

Having established that our ansätze perform well for the smaller hydrogen and lithium hydride molecules, we turn to the slightly larger hydrogen fluoride molecule. This ten-electron system is also linear, but differs from H_2 and LiH in that it has electron pairs that do not belong to the totally symmetric representation. Based on our experience with the neon atom, we expect d-orbitals centred at the fluorine atom to be important for such pairs.

In Table 7.19 we present our second-order correlation energies for a hydrogen fluoride molecule with a bond length of $1.73280a_0 = 91.6958$pm. For all calculations we have used the correlation consistent basis sets of Dunning and co-workers [65–69] with emphasis on the aug-cc-pCVXZ series. Note that, for this molecule, singularities is not a problem with the pq-ansatz. For many of the basis sets, however, the pq-ansatz is not applicable due to extensive memory requirements. Moreover, as we shall see below, some of the correlation energies obtained with the pq-ansatz cannot be fully trusted.

Most of the correlation energies given in Table 7.19 have been obtained using subsets of the different aug-cc-pCVXZ basis sets. By comparing some of these energies, the importance of d-orbitals becomes evident. For the kq-ansatz, for instance, the energy obtained with the aug-cc-pCVQZ(sp,sp) basis set, $-358.65\,\mathrm{mE_h}$, is rather poor, although the basis set is well saturated in the s- and p-orbital spaces. If we use the value $-384.38\,\mathrm{mE_h}$ as an estimate of the limit (cf. Table 7.20), we find that merely 93.3% of the correlation energy has been recovered. Once d-orbitals are added on the fluorine atom, however, the energy recovery increases to 99.5%. The same trend is observed for the pq-ansatz. With the basis set aug-cc-pCVTZ(sp,s), only 93.7% of the correlation energy is recovered, while for the basis set aug-cc-pCVTZ(spd,s), the recoverage is 99.8%. For the hydrogen fluoride molecule, therefore, good correlation energy estimates may be obtained if we use basis sets saturated in the s-, p- and d-orbital spaces for fluorine and the s- and p-orbital spaces for hydrogen. This agrees with results obtained for the neon atom and the hydrogen molecule.

For the kl-ansatz, however, much larger basis sets must be used. Based on our experience with the neon atom, basis sets should be of aug-cc-pCV5Z quality or better if more than 99% of the correlation energy is to be recovered. For the hydrogen fluoride molecule, however, we were not able to use a better basis set than

Table 7.19: All electron second-order correlation energies ($-E/\mathrm{mE_h}$) for the hydrogen fluoride molecule. For the structure we have used r(H–F)=91.6958 pm. Refer to Table B.15 to have energies listed with ten digits.

Orbital basis (F, H)	VOE	KL	KQ	PQ
cc-pVDZ	203.78	306.89	350.48	360.21
cc-pCVDZ	242.85	316.33	356.63	365.24
aug-cc-pVDZ	224.56	328.36	369.51	379.21
aug-cc-pCVDZ (sp ,s)	173.76	270.15	342.20	353.93
aug-cc-pCVDZ (sp ,sp)	181.81	277.41	347.24	359.99
aug-cc-pCVDZ (spd,s)	260.01	334.59	373.02	381.59
aug-cc-pCVDZ	263.71	337.79	374.03	382.01
aug-cc-pCVTZ (sp ,s)	197.21	276.21	350.87	360.05
aug-cc-pCVTZ (sp ,sp)	207.60	285.11	357.05	366.66
aug-cc-pCVTZ (spd,s)	309.14	351.26	381.36	383.685
aug-cc-pCVTZ (spd,sp)	313.51	354.70	382.35	n/a
aug-cc-pCVTZ (spd,spd)	317.00	357.35	382.64	n/a
aug-cc-pCVTZ	339.89	370.41	383.690	n/a
aug-cc-pCVQZ (sp ,s)	200.46	277.74	352.03	361.17
aug-cc-pCVQZ (sp ,sp)	212.02	287.47	358.65	367.92
aug-cc-pCVQZ (spd,s)	318.47	354.94	382.25	n/a
aug-cc-pCVQZ (spd,sp)	323.31	358.65	383.221	n/a
aug-cc-pCVQZ (spd,spd)	327.53	361.68	383.529	n/a

the aug-cc-pCVTZ basis, for which only $-370.41\,\mathrm{mE_h}$, or 96.4%, of the second-order correlation energy was recovered.

In Table 7.20, we compare our best correlation energies for the hydrogen fluoride molecule with literature data. The current best estimate of the limit, $-384.38\,\mathrm{mE_h}$, has been obtained by Klopper [119] using the MP2-R12/B method. Klopper obtained this estimate using a basis set of $19s14p8d6f4g3h$ quality for fluorine and $9s6p4d3f$ quality for hydrogen. Even though the MP2-R12/B method is not variational, experience shows that correlation energies obtained with this method converges to the limit from above. Since a rather large one-electron basis set was employed, the value obtained by Klopper ought to be considered the best. The best correlation energy obtained in this work, $-383.69\,\mathrm{mE_h}$, has been obtained using the kq-ansatz and the aug-cc-pCVTZ basis set. A comparison with the value of Klopper, shows that 99.82% has been recovered. The true limit is probably somewhat lower than the value obtained by Klopper, however. If we assume that the basis set

Table 7.20: Second-order correlation energies ($-E/\mathrm{mE_h}$) for the hydrogen fluoride molecule. Comparison with literature data. An inter-nuclear distance r(H–F)=91.6958 pm was used. Entries are listed chronologically. The total correlation energy is approximately $-388\,\mathrm{mE_h}$ [120].

Authors	$E^{(2)}$
This work	
kl-ansatz (aug-cc-pCVTZ)	370.41
kq-ansatz (aug-cc-pCVTZ)	383.69
pq-ansatz (aug-cc-pCVTZ-spd-s)	383.69
Klopper [119]	
MP2-R12/B (19s14p8d6f4g3h, 9s6p4d3f)	384.38
Müller *et al.* [120]	
MP2-R12/A (18s12p10d8f6g, 10s7p5d)	384.36
MP2-R12/B (18s12p10d8f6g, 10s7p5d)	384.17
Klopper [100]	
MP2-R12/A (15s9p7d5f3g1h, 9s7p5d3f1g)	384.47
MP2 (15s9p7d5f3g1h, 9s7p5d3f1g)	371.68
Petersson *et al.* [90]	
CBS (complete basis set) model	378.80

observations made for the neon atom also applies to the hydrogen fluoride molecule, the true second-order correlation energy is slightly more than $1\,\mathrm{mE_h}$ lower in energy than our aug-cc-pCVTZ value, or approximately $-384.8\,\mathrm{mE_h}$.

All highly accurate correlation energies reported in literature have been obtained using different MP2-R12 approaches with one-electron basis sets of high quality. As shown in Table 7.20, these estimates are in good agreement with each other.

An estimate of the correlation energy, has also been reported by Petersson [90] using his CBS theory. Although he obtains better energies than conventional MP2, the performance of the CBS theory is clearly inferior to that of the MP2-R12 methods.

Note also, that there are no correlation energies listed in Table 7.20 for the GTG method where the nonlinear parameters are optimised. Although Wenzel and Zabolitzky [121] have reported pair energies for three totally symmetric pairs, there are no total correlation energies available. The pair energies given are those of the $1\sigma^2$, $2\sigma^2$, and $3\sigma^2$ pairs and are $40.2\,\mathrm{mE_h}$, $12.4\,\mathrm{mE_h}$, and $27.2\,\mathrm{mE_h}$, respectively. We add that these pair energies were computed to illustrate a new optimisation technique only.

In Table 7.21 we compare pair energies for hydrogen fluoride using some selected methods. The two rightmost columns list pair energies obtained with the pq-ansatz

Table 7.21: Second-order pair energies ($-E/\mathrm{mE_h}$) for a hydrogen fluoride molecule with an inter-nuclear distance of r(H–F)=91.6958 pm.

	Pair	R12/A[a]	KL[b]	KQ[b]	PQ[c]	PQ[d]
Singlets	$1\sigma^2$	40.57	40.038	40.546	40.558	40.570
	$1\sigma 2\sigma$	3.60	3.493	3.614	3.598	3.616
	$2\sigma^2$	13.06	12.643	13.057	13.471	13.107
	$1\sigma 3\sigma$	2.07	1.859	2.076	2.064	2.075
	$2\sigma 3\sigma$	20.16	19.230	20.116	19.057	20.236
	$3\sigma^2$	29.30	28.574	29.243	28.878	29.271
	$1\sigma 1\pi$	4.99	4.422	4.981	5.010	5.006
	$2\sigma 1\pi$	39.97	37.670	39.884	38.653	39.818
	$3\sigma 1\pi$	33.15	31.201	32.998	25.370	32.517
	$1\pi^2$	71.30	68.057	71.067	60.887	71.531
Triplets	$1\sigma 2\sigma$	1.59	1.455	1.596	1.614	1.598
	$1\sigma 3\sigma$	3.31	3.082	3.300	3.217	3.293
	$2\sigma 3\sigma$	8.81	8.590	8.802	8.826	8.783
	$1\sigma 1\pi$	8.56	7.957	8.532	8.558	8.570
	$2\sigma 1\pi$	18.79	18.143	18.764	18.586	18.836
	$3\sigma 1\pi$	56.49	55.711	56.416	53.246	56.143
	$1\pi^2$	28.74	28.287	28.699	28.457	28.717
	$E^{(2)}$	384.47	381.412	383.691	360.050	383.687

[a] MP2-R12/A from Ref. [100].
[b] Using basis aug-cc-pCVTZ
[c] Using basis aug-cc-pCVTZ (sp, s)
[d] Using basis aug-cc-pCVTZ (spd, s)

but different one-electron basis sets. The two basis sets differ only in that one of them has four d-orbitals for the fluorine atom while the other has none. Differences observed in pair energies between the two columns, therefore, illustrate the importance of d-orbitals.

For electron pairs involving σ-orbitals only, there is little difference between the two columns. This is to be expected as σ-orbitals are symmetric around the bond axis, and the interaction between two such orbitals has little to gain from the angular flexibility provided by d-orbitals. For electron pairs involving π-orbitals, however, some large differences are observed between the two columns. Assuming that the molecular bond lies along the z-axis, a π-orbital consists of either p_x- or p_y-orbitals as well as small amounts of appropriate d-orbitals. For the major part, these p- and

d-orbitals come from the fluorine atom, but if they are provided for hydrogen, small amounts of these orbitals also participate in the π-orbital. This is not the case here, however, and the π-orbitals therefore behave as fluorine p-orbitals. As expected, Table 7.21 shows that the largest basis set dependency is observed for the singlet interaction between two such π-orbitals. This is in full agreement with observations made for neon pair energies in Table 7.12. Note also, that the singlet interactions between the 3σ-orbital and the two 1π-orbitals also need d-functions in order to be properly described. This is easily explained by a high p_z content in the 3σ-orbital.

The pair energy decomposition given in Table 7.21 also shows something else. For the ${}^1(2\sigma^2)$, ${}^1(1\sigma 1\pi)$, ${}^3(1\sigma 2\sigma)$, and ${}^3(2\sigma 3\sigma)$ interactions, the pair energies obtained with the pq-ansatz in the small aug-cc-pCVTZ(sp,s) basis set are lower than the energies obtained in the aug-cc-pCVTZ(spd,s) basis. Although this may seem as a violation of the variation principle, it is merely due to deficiencies in the Fock operator. A similar problem was observed for the hydrogen molecule and we concluded then that p-orbitals were needed on each hydrogen atom. A similar conclusion may be drawn here. Note that, the pair energies obtained with the aug-cc-pCVTZ(spd,s) basis set does not seem unreasonably low. The additional d-orbitals provided by this basis set may therefore relieve the deficiency caused by the lack of hydrogen p-orbitals.

We conclude this section by noting that since our pair energies are supposedly variational, we may combine pair energies obtained with the kq- and pq-ansätze, depending of which gives the better energy, in pursuit of the second-order correlation energy limit. Assuming that the energies obtained with the pq-ansatz and the aug-cc-pCVTZ(spd,s) basis set may be trusted, this approach gives $-384.53\,\mathrm{mE_h}$ as an upper bound to the second-order correlation energy of the hydrogen fluoride molecule.

7.8 Water

7.8.1 The second-order correlation energy

As our systems grow larger, the increased number of three-electron integrals makes it harder to utilise basis sets of high quality. For the water molecule, for instance, the aug-cc-pCVTZ basis set contains 105 basis functions, while the corresponding number for the hydrogen fluoride molecule and the neon atom are only 82 and 59, respectively. Since the number of three-electron integrals grows as N_{basis}^6, the aug-cc-pCVTZ basis set quickly becomes inaccessible as our systems grow larger; at least with the current approach of calculating all three-electron integrals exactly.

The computation time does not only increase with the number of basis functions, however, but also with a reduced amount of local symmetry. Local symmetry is symmetry in either of the x-, y-, and z-planes and is related to point-group symmetry

Table 7.22: All electron second-order correlation energies ($-E/\mathrm{mE_h}$) for the water molecule. Except for the calculation marked with an [b], all geometries are as specified in tablenote [a]. Refer to Table B.16 to have energies listed with ten digits.

Orbital basis (O,H)	VOE	KL	KQ	PQ
cc-pVDZ	203.96	298.07	334.28	342.97
cc-pCVDZ	241.33	307.05	339.13	346.65
aug-cc-pVDZ	221.83	315.79	349.94	357.71
aug-cc-pCVDZ (sp ,s)	171.61	258.93	320.69	332.67
aug-cc-pCVDZ (sp ,sp)	192.98	277.17	332.42	346.64
aug-cc-pCVDZ (spd,s)	249.81	317.45	351.79	359.35
aug-cc-pCVDZ	259.24	324.72	353.48	359.66
aug-cc-pCVTZ (sp ,s)	190.51	263.39	326.71	337.51
aug-cc-pCVTZ (sp ,sp)	217.65	285.90	341.10	352.56
aug-cc-pCVTZ (spd,s)	289.59	330.18	357.66	360.65
aug-cc-pCVTZ (spd,sp)	300.21	337.75	359.65	n/a
aug-cc-pCVTZ (spd,spd)	307.86	342.83	360.35	n/a
aug-cc-pCVTZ[b]	324.28	351.48	361.39	n/a
aug-cc-pCVQZ (sp ,s)	193.84	264.84	327.87	338.84
aug-cc-pCVQZ (sp ,sp)	223.42	289.00	342.91	n/a
aug-cc-pCVQZ (spd,s)	298.20	333.20	358.52	n/a
aug-cc-pCVQZ (spd,sp)	309.62	341.34	360.49	n/a

[a] Structure: $\angle$(HOH)=104.52° and r(O–H)=95.720 pm.
[b] Structure: $\angle$(HOH)=104.34° and r(O–H)=95.885 pm.

as well as the choice of coordinate system. In molecules with no symmetry planes, there is no local symmetry, but the reverse is not necessarily true. Local symmetry is important since it allows us to take short-cuts in the integral evaluation as certain quantities are known to be zero. For the hydrogen peroxide conformations presented in section 7.9, for instance, the calculation time of the *trans*-conformation is only half that of the *gauche*-conformation due to local symmetry.

In this section we study the water molecule. Whereas the hydrogen fluoride molecule studied in the previous section had local symmetry in both the x- and y-planes, the water molecule only have local symmetry in the x-plane. This does not only give us additional computation time in the integral code, but also require different parts of the integral code to be used. Bugs that were not observed for smaller molecules may therefore potentially turn up for water.

In Table 7.22 we present our second-order correlation energies for the water

Table 7.23: Second-order correlation energies ($-E/\mathrm{mE_h}$) for the water molecule. Comparison with literature data. Entries are listed chronologically. Except for the energies marked with an [b], the water geometry was as specified in tablenote [a]. The total correlation energy is approximately $-370\,\mathrm{mE_h}$ [120].

Authors	$E^{(2)}$
This work	
kl-ansatz (aug-cc-pCVTZ)	351.49[b]
kq-ansatz (aug-cc-pCVTZ)	361.39[b]
pq-ansatz (aug-cc-pCVDZ)	359.79
Klopper [119]	
MP2-R12/B (19s14p8d6f4g3h, 9s6p4d3f)	361.92
Müller *et al.* [120]	
MP2-R12/A (17s11p9d7f5g, 10s7p5d)	362.32
MP2-R12/B (17s11p9d7f5g, 10s7p5d)	361.52
Klopper [100]	
MP2-R12/A (15s9p7d5f3g1h, 9s7p5d3f1g)	362.01
Bukowski *et al.* [15]	
Nonlinearly optimised GTGs	356.43

[a] Structure: $\angle$(HOH)=104.52° and r(O–H)=95.720 pm.
[b] Structure: $\angle$(HOH)=104.34° and r(O–H)=95.885 pm.

molecule. Essentially, we have used the same basis set combinations that were used for the hydrogen fluoride molecule. As also observed for hydrogen fluoride, there are several basis sets for which the pq-ansatz could not be used. Especially, we miss results for the basis set aug-cc-pCVTZ(spd) which showed excellent performance for the neon atom.

Our best correlation energy for the water molecule, $-361.39\,\mathrm{mE_h}$, was obtained with the aug-cc-pCVTZ basis set and the kq-ansatz. Unfortunately, this basis set was only used in the linearisation study presented below, and in this case, the geometry of the bent water molecule was slightly different. The correlation energies obtained with this different geometry are given in Table B.17. If we compare the correlation energies obtained with the two different geometries and the kq-ansatz and the aug-cc-pCVQZ(spd,sp) basis set, we see that the different structure gives us an energy which is too low by some 0.10–0.15 $\mathrm{mE_h}$.

In Table 7.23 we compare our best correlation energies with values obtained from literature. The best estimate of the second-order correlation energy for water is that obtained by Klopper [119] with the MP2-R12/B method. His energy estimate of $-361.92\,\mathrm{mE_h}$ was obtained using a large one-electron basis set, and as commented

in section 7.7, experience shows that such MP2-R12/B values in practice are upper bounds to the true correlation energy. If we correct our best energy estimate for the shift caused by the geometry difference, we find that some 99.78% of the energy obtained by Klopper is recovered. Table 7.24, which lists pair energies for some selected methods, suggests that the remaining energy fraction of 0.22% is evenly distributed among the 25 pairs.

As for hydrogen fluoride, all highly accurate energy estimates presented in the literature have been obtained using a combination of high quality basis sets and MP2-R12 methods. For the water molecule, however, there is also a reasonably good energy estimate obtained using nonlinearly optimised GTGs. This estimate of $-356.43\,\mathrm{mE_h}$ is given by Bukowski *et al.* [15] who used approximately 150 GTGs to describe each electron pair. Bukowski and co-workers show that GTGs constitute a complete basis for the two-electron space for C_{2v} symmetry if the geminal centres are optimised in the molecular plane. Due to high computational cost or complexity, however, they did not optimise the geminal centres in the water calculation, but compensated for this by adding d-functions for the oxygen atom and p-functions for the hydrogen atom. The quality of their energy estimate, suggests that a lot more functions need to be added in order to fully compensate for the fixation of centres.

7.8.2 The second-order correction to the barrier to linearity

In the middle of the 1990s, rovibrational states characteristic for the water molecule were identified in the sunspot spectrum of the sun [122, 123]. In combination with an increased spectroscopic capability to detect higher-lying bending states [124, 125], this discovery initiated a renewed interest in the barrier to linearity of the water molecule [126–133]. Although the barrier is relatively large, approximately $11\,100\,\mathrm{cm^{-1}}$, it has become an important issue as it not only affects the prediction of high-lying vibrational bending states, but also low-lying bending states and the rotational states supported by these [126–130].

While the Hartree–Fock limit to the barrier is easily established, this is not the case for the MP2 correlation contribution [131, 132]. Using the aug-cc-pV6Z basis set [134], for instance, Tarczay *et al.* [132] calculated the valence contribution explicitly to be $-330\,\mathrm{cm^{-1}}$, whereas they with extrapolation techniques estimated the complete basis set limit to be $-348\,\mathrm{cm^{-1}}$. The large aug-cc-pV6Z basis set, therefore, only managed to recover some 95% of the MP2 contribution. If we go beyond MP2, the corrections seem to be less dependent of the quality of the basis set, making the MP2 limit particularly important for the *ab initio* estimate of the barrier.

In order to compute the barrier to linearity, we have calculated correlation energies for a linear and a bent geometry of the water molecule. The angles and bond lengths used in these geometries are given in Table 7.25 along with the barrier estimates. Estimates are presented for all ansätze, but since only a few basis sets could

Table 7.24: Second-order pair correlation energies ($-E/\mathrm{mE_h}$) for the water molecule. The water geometry differ slightly for some of the calculations. See Table 7.23 for details.

	Pair	R12/A[a]	GTG[b]	KL[c]	KQ[d]	PQ[e]
Singlets	$1a_1^2$	40.86	40.76	40.36	40.842	40.849
	$1a_1 2a_1$	3.21	3.20	3.12	3.229	3.234
	$2a_1^2$	13.31	13.17	12.98	13.293	13.324
	$1a_1 3a_1$	2.16	2.14	1.92	2.154	2.113
	$2a_1 3a_1$	17.67	17.21	16.96	17.639	17.582
	$3a_1^2$	25.81	25.09	25.05	25.755	25.610
	$1b_1^2$	26.31	25.98	25.46	26.254	26.280
	$1b_2^2$	25.65	25.10	25.17	25.616	25.517
	$1a_1 1b_1$	2.26	2.26	1.98	2.255	2.214
	$2a_1 1b_1$	18.93	18.72	18.06	18.897	18.802
	$3a_1 1b_1$	16.95	16.49	16.05	16.855	16.653
	$1a_1 1b_2$	1.53	1.53	1.34	1.534	1.511
	$2a_1 1b_2$	21.28	20.94	20.57	21.217	21.153
	$3a_1 1b_2$	17.78	17.35	17.28	17.765	17.707
	$1b_1 1b_2$	14.60	14.32	13.89	14.530	14.328
Triplets	$1a_1 2a_1$	1.54	1.53	1.41	1.544	1.543
	$1a_1 3a_1$	3.30	3.28	3.05	3.283	3.187
	$2a_1 3a_1$	8.49	8.25	8.29	8.479	8.422
	$1a_1 1b_1$	3.93	3.93	3.63	3.916	3.804
	$2a_1 1b_1$	9.40	9.19	9.12	9.378	9.336
	$3a_1 1b_1$	26.69	26.37	26.34	26.657	26.567
	$1a_1 1b_2$	2.69	2.69	2.49	2.685	2.629
	$2a_1 1b_2$	8.13	8.01	7.98	8.127	8.103
	$3a_1 1b_2$	23.84	23.40	23.59	23.817	23.711
	$1b_1 1b_2$	25.70	25.45	25.39	25.672	25.609
	$E^{(2)}$	362.01	356.43	351.485	361.393	359.787

[a] MP2-R12/A from Ref. [100].
[b] Nonlinearly optimised GTGs from Ref. [15]
[c] Using basis aug-cc-pCVTZ
[d] Using basis aug-cc-pCVTZ
[e] Using basis aug-cc-pCVDZ

Table 7.25: All-electron second-order correlation energy barriers to linearity for the water molecule. Energies are given in mE_h. Water geometries, which have been taken from Ref. [133], are given in tablenote [a].

Orbital basis (O,H)	VOE	KL	KQ	PQ
cc-pVDZ	1.541	0.397	−0.789	−1.631
cc-pVTZ	0.014	−0.560	−1.176	n/a
cc-pCVDZ	1.666	0.810	−0.620	−1.077
cc-pCVTZ	0.028	−0.399	−1.151	n/a
aug-cc-pVDZ	−0.399	−1.691	−2.245	−2.539
aug-cc-pVTZ (spd, sp)	−0.796	−1.442	−2.220	n/a
aug-cc-pVTZ	−1.092	−1.628	−2.095	n/a
aug-cc-pCVTZ (spd, sp)	−0.833	−1.352	−2.194	n/a
aug-cc-pCVQZ (spd, sp)	−0.704	−1.302	−2.191	n/a
aug-cc-pCVDZ	−0.311	−1.319	−2.053	−2.207
aug-cc-pCVDZ + ICP	−0.665	−1.664	−2.053	n/a
aug-cc-pCVTZ	−1.086	−1.475	−2.088	n/a

[a] Geometry, bent : $\angle$(HOH)=104.343° and r(O–H)=95.885 pm.
Geometry, linear : $\angle$(HOH)=180.000° and r(O–H)=93.411 pm.

be used for the pq-ansatz, the results listed for this ansatz are mainly included for reference. The correlation energies for the two different geometries of water are not discussed and are therefore given in Table B.17 of appendix B

In the upper part of Table 7.25, we give correlation energy barriers obtained with some small cc-pVXZ and cc-pCVXZ basis sets. Among these estimates both positive and negative values are observed. To second order, the correction made to the barrier due to electron–electron correlation is approximately $-2.1\,mE_h$ (see below), implying that the barrier is lowered. All our estimates using conventional MP2 get this wrong, and predict a heightening rather than a lowering of the barrier. The kl-ansatz performs slightly better and correctly predicts a lowering of the barrier when the larger TZ basis sets are used, but the magnitude predicted for the barrier, is far off. For the kq-ansatz, the barrier is predicted to be lowered for all basis sets, but also in this case the magnitude of the correction is wrong.

Proceeding with the aug-cc-pVXZ and aug-cc-pCVXZ basis sets, we see that all estimates correctly predict a lowering of the barrier, although the magnitude in some cases is still far off. For the virtual orbital expansion, for instance, we only recover half of the true barrier correction. With the kl-ansatz the performance is somewhat better and we note, especially, that the different basis sets produce very similar barrier estimates. The best estimate is probably obtained with *internal*

Table 7.26: Core (top) and valence (bottom) contributions to the second-order correlation energy barrier to linearity for the water molecule. The basis sets used are aug-cc-pCVTZ (A) and aug-cc-pCVQZ(spd,sp) (B). For the energy conversion we have used $1\,\mathrm{mE_h} = 219.47463\,\mathrm{cm^{-1}}$.

	Single-point energy/$\mathrm{mE_h}$		Barrier	
	Bent geom.	Linear geom.	$\mathrm{mE_h}$	$\mathrm{cm^{-1}}$
A	−61.4412271	−61.9452909	−0.5041	−110.6
B	−61.5362531	−62.0436242	−0.5074	−111.4
A	−299.9515832	−301.5353845	−1.5838	−347.6
B	−299.0833648	−300.7673288	−1.6839	−369.6

Counterpoise-correction (ICP) and the basis set aug-cc-pVDZ, in which case nearly 80% of the true barrier correction is recovered.

Internal Counterpoise-correction specifies that the linear and the bent water molecules are calculated in *exactly* the same basis set. Thus, when we straighten the bent molecule, duplicate hydrogen basis functions are maintained in the bent positions, and vice versa when the linear molecule is bent. This ensures a more balanced description of the two geometries.

While even the best estimate using the kl-ansatz is only modest, the kq-ansatz is seen to perform well for all basis sets. Even for the smallest of the basis sets, aug-cc-pVDZ, the kq-ansatz overshoots the magnitude of the barrier by less than 7%, which is quite remarkable.

Our best estimate of the all-electron energy barrier is $-2.088\,\mathrm{mE_h}$ and is obtained with the aug-cc-pCVTZ basis set. Since this basis set gives the lowest correlation energy for the two water geometries, it is reasonable to assume that it gives the best barrier estimate. When we split up the estimates in core and valence contributions, however, we see that the aug-cc-pCVQZ(spd,sp) basis set gives a slightly better description of the core correlation. The core and valence contributions for the aug-cc-pCVTZ and aug-cc-pCVQZ(spd,sp) basis sets are given in Table 7.26.

Although the latter performs slightly better for core correlation, we see that the former performs far better for valence correlation, probably due to the f-functions on oxygen and d-functions on hydrogen. The additional flexibility provided by these functions is very important, especially for the bent geometry. Since the aug-cc-pCVQZ(spd,sp) basis set lacks these functions, the description of the linear geometry becomes better, and as a consequence, the estimate of the valence contribution to the barrier becomes too large.

It is difficult to say how well our estimate of the core and valence contributions is converged. Since an internal counterpoise-correction makes no difference for the

Table 7.27: Core (top) and valence (bottom) contributions to the second-order correlation energy barrier (E/cm^{-1}) to linearity for the water molecule. A comparison with literature data. Basis sets are specified in the text. Entries are listed chronologically.

Authors	$\Delta E^{(2)}$[core]
This work	
kq-ansatz with basis aug-cc-pCVQZ(spd,sp)	−111
Valeev *et al.* [133]	
MP2-R12/A with basis K2^{1h}	−110
Tarczay *et al.* [132]	
MP2-R12/A with basis K2	−109
MP2 with basis K2	−106
	$\Delta E^{(2)}$[valence]
This work	
kq-ansatz with basis aug-cc-pCVTZ	−348
Valeev *et al.* [133]	
MP2-R12/A with basis K4^{3i}	−357
MP2 with basis K4^{3i}	−325
CBS limit[a]	−353
Tarczay *et al.* [132]	
MP2-R12/B with basis K2 + ICP	−344

[a] Using a two-point extrapolation of type $E_{\mathrm{CBS}} = E_X + aX^{-3}$ with the basis sets aug-cc-pV{5,6}Z+ICP.

kq-ansatz when the aug-cc-pCVDZ basis set is used, however, it seems reasonable to assume that the larger aug-cc-pCVTZ basis provides a well-balanced and good estimate of the barrier.

In Table 7.27 we compare our best estimates of the core and valence contributions to the barrier with literature data. The best estimates found in literature have been obtained using MP2-R12 methods and large basis sets denoted K2, K2^{1h}, and K4^{3i}. In (oxygen, hydrogen) quality these basis sets are $(15s9p7d5f, 9s7p5d)$, $(15s9p7d5f3g1h, 9s7p5d3f1g)$, and $(19s13p11d9f7g5h3i, 13s11p9d7f5g3h)$, respectively.

For core correlation, the GTG and MP2-R12/A approaches give similar estimates of the barrier, and when the MP2-R12/A method is combined with the larger K2^{1h} basis set, the difference is no more than $1\,\mathrm{cm}^{-1}$. Note, also, that the barrier difference is only $3\,\mathrm{cm}^{-1}$ between the MP2 and the MP2-R12/A methods when the K2 basis set is used. This good performance for the conventional MP2 approach is most likely

related to cancellation of errors.

Although the aug-cc-pCVQZ basis set give an unbalanced valence description of the two water geometries, this is probably not the case for the description of the core. Opening for the possibility, however, we suggest that the core correlation correction of the barrier is in the range $-111.0 \pm 0.5\,\mathrm{cm}^{-1}$.

For valence energy, Table 7.27 shows that the different approaches produce quite different estimates of the barrier. Note, for instance, that Valeev *et al.* [133] obtained a barrier estimate of only $-325\,\mathrm{cm}^{-1}$ using conventional MP2 and the large K4^{3i} basis set, which is some $30\,\mathrm{cm}^{-1}$ off the limit suggested in their paper. The valence estimate of the barrier is therefore very sensitive to the quality of the basis set, as ought to be expected from the high degree of rehybridisation involved when the molecule is made linear. As shown by Tarczay *et al.* [132], the conventional MP2 calculations are especially sensitive to this rehybridisation, and barrier estimates should therefore preferably be made in basis sets employing ICP.

The MP2-R12/A estimate of the barrier using the large K4^{3i} set is possibly the current best estimate of the barrier. If the three i-orbitals on oxygen and the three h-orbitals on hydrogen are removed, however, the barrier estimate changes by as much as $6\,\mathrm{cm}^{-1}$ to $-363\,\mathrm{cm}^{-1}$. It is therefore reason to question how well the estimate of $-357\,\mathrm{cm}^{-1}$ is converged. Based on the results obtained in this work, we suggest that the barrier of $-357 \pm 5\,\mathrm{cm}^{-1}$, suggested by Valeev and co-workers are changed to $-353 \pm 5\,\mathrm{cm}^{-1}$. The total correction made to the barrier to linearity by the core and valence correlation energies then become $-464 \pm 5\,\mathrm{cm}^{-1}$ or $-2.11 \pm 0.02\,\mathrm{mE_h}$.

7.9 The rotational barriers of hydrogen peroxide

Since the results obtained for the water molecule are quite encouraging, we proceed by studying the rotational barriers of the hydrogen peroxide molecule. The stable conformation of hydrogen peroxide is a *gauche* conformation in which the dihedral angle is approximately 113° [135]. The molecule may be rotated around the oxygen–oxygen bond, and under a full rotation, a barrier is crossed for the *cis* and *trans* conformations. In this section we estimate the height of these two barriers at the second-order level of theory.

As the purpose is mainly to check whether our GTG-MP2 approach is successful for systems of this size, we have not used accurate geometries for the three conformations, but crude estimates obtained from a conventional MP2 optimisation using the basis set aug-cc-pVDZ. The bond lengths and angles obtained in this optimisation, are summarised as in Table 7.28.

Before we look at the GTG results, we study the correlation energy barriers using conventional MP2 and the four basis set series cc-pVXZ, cc-pCVXZ, aug-cc-pVXZ, and aug-cc-pCVXZ. The results are given in Table 7.29. The single-point correlation energies used to compute these barriers are given in Appendix B as Table B.18.

Table 7.28: Bond length and bond angles used for the three hydrogen peroxide conformations in the study of the rotational barriers. Bond lengths are given in pico-meter and angles in degrees.

	r(O–O)	r(O–H)	$\angle$(HOO)	$\angle$(dihedral)
cis	145.79	96.44	103.87	0.0
gauche	145.05	96.44	99.33	114.2
trans	146.09	96.35	97.69	180.0

We start by investigating the estimates of the *cis* barrier. Table 7.29 shows that all four basis set series agree on the sign of the barrier correction, but not on the magnitude. While the cc-pVXZ series seems to stabilise around $+0.1\,\mathrm{mE_h}$ as the cardinal number X is increased, the cc-pCVXZ and aug-cc-pVXZ series are decreasing rather steadily, and for $X = 5$, the barrier estimates are approximately $+0.05\,\mathrm{mE_h}$ for both series. For the aug-cc-pCVXZ series, on the other hand, the barrier increases with increasing X for low values of X, but decreases for $X : Q \to 5$, and ends at $+0.024\,\mathrm{mE_h}$. Since the aug-cc-pCVXZ series of basis sets are the highest saturated, we consider the estimate of $+0.024\,\mathrm{mE_h}$ to be the best estimate of the barrier. We therefore conclude that that the correction due to the correlation energy leads to a slightly increased *cis* barrier.

For the *trans* barrier correction, we also note that the different series agree on the sign, but not entirely on the magnitude of the correction. The cc-pVXZ series is somewhat erratic and ends with an estimate of $-0.38\,\mathrm{mE_h}$, the cc-pCVXZ series has a rather stable estimate of $-0.44\,\mathrm{mE_h}$, and the aug-cc-pVXZ series is increasing and ends at $-0.38\,\mathrm{mE_h}$. The last series, aug-cc-pCVXZ, is steadily increasing, and ends at $-0.42\,\mathrm{mE_h}$, which we consider the best estimate of the *trans* barrier correction. As opposed to the *cis* correction, we see that the *trans* correction lowers the corresponding rotational barrier.

Using the aug-cc-pCV5Z basis set, the Hartree–Fock barriers are estimated to be 11.772 $\mathrm{mE_h}$ for the *cis* conformation and 2.102 $\mathrm{mE_h}$ for the *trans* conformation. To second-order, therefore, the rotational barriers become $11.80\,\mathrm{mE_h}$ and $2.53\,\mathrm{mE_h}$, respectively, or $2588\,\mathrm{cm^{-1}}$ and $554\,\mathrm{cm^{-1}}$.

In Table 7.30 we present barrier estimates obtained with the kl- and kq-ansätze and various basis sets. The single-point correlation energies used to compute the barriers are given in appendix B as Table B.19.

Some of the basis sets used in the GTG study have not been encountered earlier in this work, and require a short explanation. The basis set "aug-cc-pVDZ + aug-H", for instance, is the cc-pVDZ basis set augmented with extra functions for hydrogen. These extra functions are taken from aug-cc-pVDZ. Similarly, "aug-cc-pVDZ + d-

Table 7.29: All-electron correlation energy barriers ($E/\mathrm{mE_h}$) for rotating the *gauche* conformation of hydrogen peroxide into the *cis* or *trans* conformations. All energies are obtained using conventional MP2.

Basis	N_{bas}	*cis*	*trans*
cc-pVDZ	38	+0.289	−0.407
cc-pVTZ	88	+0.182	−0.415
cc-pVQZ	170	+0.099	−0.416
cc-pV5Z	292	+0.102	−0.375
cc-pCVDZ	46	+0.307	−0.409
cc-pCVTZ	114	+0.135	−0.440
cc-pCVQZ	228	+0.085	−0.444
cc-pCV5Z	400	+0.053	−0.441
aug-cc-pVDZ	64	−0.074	−0.323
aug-cc-pVTZ	138	+0.190	−0.357
aug-cc-pVQZ	252	+0.086	−0.355
aug-cc-pV5Z	414	+0.049	−0.378
aug-cc-pCVDZ	72	−0.060	−0.327
aug-cc-pCVTZ	164	+0.018	−0.384
aug-cc-pCVQZ	310	+0.030	−0.404
aug-cc-pCV5Z	522	+0.024	−0.424

aug-H" is the aug-cc-pVDZ basis set, supplemented with doubly-augmented functions taken from d-aug-cc-pVDZ.

Starting with the *cis* barriers again, we see that the barrier estimates are rather disappointing. For both the kl- and the kq-ansatz, the estimates are observed to be very sensitive to the basis set, and even for the two largest basis sets, aug-cc-pCVDZ and aug-cc-pVTZ(spd,sp), the barrier estimates differ considerably. Moreover, we also note that there are large differences *between* the ansätze, but this result is in agreement with earlier observations and less worrying.

If we consult Table B.19, we see that the basis set aug-cc-pVTZ(spd,sp) gives correlation energies that are some $8\,\mathrm{mE_h}$ lower than the energies obtained with the aug-cc-pCVDZ basis set. Although the aug-cc-pVTZ(spd,sp) basis was observed to give an unbalanced description of different water geometries (section 7.8.2), we choose to consider it the best basis set due to far better single-point energies. The *cis* barrier to rotation is therefore estimated to be $+0.093\,\mathrm{mE_h}$, or almost a factor four larger than the estimate obtained with conventional MP2.

Table 7.30: Hartree–Fock and all-electron correlation energy barriers ($E/\mathrm{mE_h}$) for rotating the *gauche* conformation of hydrogen peroxide into the *cis* or *trans* conformations. The *cis* and *trans* barriers are given in the upper and lower part of the table, respectively.

Basis	HF	VOE	KL	KQ
cc-pVDZ	+12.785	+0.289	+0.258	+0.815
cc-pVDZ + aug-H	+12.229	+0.140	−0.231	+1.116
cc-pVDZ + aug-O	+12.192	+0.006	+0.240	+0.298
aug-cc-pVDZ	+12.366	−0.074	+0.054	+0.333
aug-cc-pVDZ + d-aug-H	+12.392	−0.150	−0.001	+0.082
aug-cc-pCVDZ	+12.374	−0.060	+0.091	+0.241
aug-cc-pVTZ (spd,sp)	+12.145	+0.038	+0.027	+0.093
cc-pVDZ	+1.452	−0.407	−0.617	−0.252
cc-pVDZ + aug-H	+1.512	+0.246	+0.399	+0.367
cc-pVDZ + aug-O	+2.266	−0.468	−0.534	−0.414
aug-cc-pVDZ	+2.144	−0.323	−0.385	−0.246
aug-cc-pVDZ + d-aug-H	+2.167	−0.342	−0.404	−0.452
aug-cc-pCVDZ	+2.134	−0.327	−0.306	−0.294
aug-cc-pVTZ (spd,sp)	+2.376	−0.494	−0.281	−0.371

For the *trans* barrier, we see that the estimates are less sensitive to the basis set, that is, the relative differences between the barrier estimates are smaller. For the kq-ansatz, however, the difference for the two largest basis sets are still larger than appreciated. Again, regarding the aug-cc-pVDZ(spd,sp) basis as the better, we get $-0.37\,\mathrm{mE_h}$ as the estimate of the barrier. For the *trans* barrier, therefore, the GTG and VOE estimates are of the same order of magnitude.

Note, finally, that the correlation energy correction to the rotational barriers of hydrogen peroxide ($+0.02\,\mathrm{mE_h}$, $-0.42\,\mathrm{mE_h}$) are much smaller than the correlation energy correction to the barrier of linearity in the water molecule ($-2.1\,\mathrm{mE_h}$). Basis sets of much higher quality must therefore be used unless cancellation of errors are to be trusted. For the hydrogen peroxide conformations, there are also "long-range" effects involved which are not present in the water molecule. To get the rotational barriers accurate, therefore, more diffuse functions, and probably also functions of high angular momentum, are needed. Considering the small basis sets used in the GTG study, the poor performance is not surprising.

7.10 Energy recovery by different parts of the pair function

When Gaussian-type geminals was introduced in the expansion of pair functions in combination with the traditional orbital approximation [59], they were regarded as a supplement only. Since only the ij-ansatz was used at that time, the geminals indeed became a supplement, and the largest portion of the correlation energy, was for all calculations recovered by the virtual orbitals. When all three-electron integrals are calculated explicitly, we can only use basis sets with s-, p-, d-, and to some extent f-orbitals, due to high computation time. For such basis sets, the ij-ansatz proved to be of limited use, and this motivated us to generalise the geminal ansatz, first to the kl-ansatz, and then later to the kq- and pq-ansätze.

Whereas the geminal part of the pair function is properly regarded as a supplement when either the ij- or the kl-ansatz is used, this is not the case for the larger ansätze. To illustrate this, we have split the correlation energies for neon and water into VOE and GTG contributions, and calculated the portion of energy recovered by each of these terms alone. The VOE and GTG contributions for the neon atom are given in Table 7.31 as percentages.

We start by studying the percentages obtained with the kl-ansatz. Since only pairs of occupied orbitals are used in this ansatz, the amount of energy recovered by the geminals does not increase once the occupied orbitals have converged. After that, all improvement in the correlation energy can only come from the virtual orbitals expansion. To some extent, this may be observed in Table 7.31. For the cc-pVXZ series, for instance, the portion of the energy recovered by the GTG term decreases with increasing X, whereas the portion recovered by the VOE increases. The same relation holds for all the other basis set series, and for the largest basis set, aug-cc-pCV5Z, 98% of the energy is recovered by the VOE, and the GTGs is only needed for the last 2%, or 10 $\mathrm{mE_h}$. Note also, that for all basis sets the percentage recovered by the VOE is larger than the percentage recovered by the GTG.

With the kq-ansatz this situation is reversed, and for all basis sets, the largest portion of the energy is recovered by the GTG part. The difference is largest for small basis sets, but this is to be expected as the kq-ansatz does not need high angular momentum function to perform well. Since the GTG part recovers the larger portion of the energy, terms like supplement and correction would give an inaccurate description. Instead, the VOE term should in this case be regarded as the correction.

For the kq-ansatz, we note that the GTGs recover more than 83% of the correlation energy recovered by the full pair function for that basis set. If we move to the pq-ansatz this percentage increases to 99(!). For the pq-ansatz, therefore, the virtual orbital expansion only contribute with a very small amount of energy. Nevertheless, for our best neon energy, the VOE is responsible for the last, and very

Table 7.31: The percentage of the all-electron second-order correlation energy recovered for the neon atom by only the virtual orbital expansion part or the geminal part of the pair function relative to the amount of energy recovered when both are used.

	KL		KQ		PQ	
Orbital basis	VOE	GTG	VOE	GTG	VOE	GTG
cc-pVDZ	62	54	54	83	53	99.2
cc-pVTZ	79	47	73	93	72	99.4
cc-pVQZ	88	44	85	95	84	99.6
cc-pCVDZ	74	53	64	84	63	99.1
cc-pCVTZ	91	45	86	94	85	99.4
cc-pCVQZ	96	43	—	—	—	—
aug-cc-pVDZ	65	50	57	84	55	99.6
aug-cc-pVTZ	80	45	74	93	74	99.8
aug-cc-pVQZ	88	44	85	95	—	—
aug-cc-pCVDZ (sp)	60	61	46	83	44	99.5
aug-cc-pCVTZ (sp)	69	59	53	88	52	99.3
aug-cc-pCVQZ (sp)	69	59	53	89	52	99.2
aug-cc-pCV5Z (sp)	70	59	53	90	52	99.2
aug-cc-pCVDZ	75	49	67	85	65	99.6
aug-cc-pCVTZ (spd)	87	46	80	93	80	99.8
aug-cc-pCVQZ (spd)	89	46	83	94	—	—
aug-cc-pCVTZ	91	44	87	94	87	99.8
aug-cc-pCVQZ (spdf)	94	43	—	—	—	—
aug-cc-pCVQZ	96	43	—	—	—	—
aug-cc-pCV5Z	98	43	—	—	—	—

important, $1\,\mathrm{mE_h}$.

In Table 7.32, we give the corresponding VOE and GTG contributions for the water molecule. We do not go into details about these numbers, merely comment that they show exactly the same trends as the neon numbers.

Since the GTG part of the pair function is the one giving origin to three-electron integrals, this part should be kept at a minimum. To achieve this, and at the same time get high quality energy estimates, the virtual orbitals and geminals must be expanded in different one-electron basis sets. This would allow us to use much larger basis sets for the expansion of virtual orbitals, and at the same time smaller basis sets for the geminals. The need for this is commented several places in this work,

Table 7.32: The percentage of the all-electron second-order correlation energy recovered for the water molecule by only the virtual orbital expansion part or the geminal part of the pair function relative to the amount of energy recovered when both are used.

	KL		KQ		PQ	
Orbital basis	VOE	GTG	VOE	GTG	VOE	GTG
cc-pVDZ	69	50	61	86	60	98.1
cc-pCVDZ	77	49	71	87	70	98.1
aug-cc-pVDZ	70	47	63	87	62	99.1
aug-cc-pCVDZ (sp ,s)	66	57	54	83	52	97.8
aug-cc-pCVDZ (sp ,sp)	70	54	58	84	56	98.5
aug-cc-pCVDZ (spd,s)	79	47	71	86	70	98.6
aug-cc-pCVDZ	80	46	73	87	72	99.1
aug-cc-pCVTZ (sp ,s)	72	56	58	86	57	97.4
aug-cc-pCVTZ (sp ,sp)	76	52	64	86	62	98.6
aug-cc-pCVTZ (spd,s)	88	45	81	90	80	99.0
aug-cc-pCVTZ (spd,sp)	89	44	84	91	—	—
aug-cc-pCVTZ	92	42	90	92	—	—
aug-cc-pCVQZ (sp ,sp)	77	51	—	—	—	—

but in this section we have seen how unbalanced the pair function currently is with respect to energy contributions made by the orbital and geminal parts.

Note, finally, that even though the pair function seems to be well-balanced for the kl-ansatz, multiple basis sets are still very useful. While functions of high angular momentum may be needed for the virtual orbital part, for instance, they are most likely irrelevant for the occupied orbitals.

Chapter 8

Summary, conclusions, and future perspectives

In this thesis we have presented a new method for calculating highly accurate MP2 energies for atomic and molecular closed-shell systems. In order to obtain accurate energy estimates, we have included terms explicitly dependent on the inter-electronic distances r_{12} in the pair function. Our pair function is defined as

$$\tilde{u}_{ij}(1,2) = \underbrace{\sum_{a\geq b} c_{ij}^{ab}\phi_{ab}(1,2)}_{\text{orbital part}} + \underbrace{\sum_{v} c_{ij}^{v}\exp(-\gamma_v r_{12}^2)\sum_{x\geq y} c_{ij}^{xy}\tilde{\phi}_{xy}(1,2)}_{\text{geminal part}} \tag{8.1}$$

where the orbital part is the expansion of virtual orbitals used in conventional MP2 calculations, and the geminal part is an expansion of functions explicitly dependent on the inter-electronic distance r_{12}. In the geminal part, the $\tilde{\phi}_{xy}$ is a pair of Hartree–Fock orbitals or approximated Hartree–Fock orbitals, and $\exp(-\gamma_v r_{12}^2)$ is a Gaussian correlation factor (GCF) which ties a pair of orbitals $\tilde{\phi}_{xy}$ into a Gaussian-type geminal. The xy is a pair of non-specified summation indices that may be selected from the set $\{ij, kl, kq, pq\}$ where i, j, k, and l refer to occupied orbitals while p and q are general orbital indices. Whenever the indices p or q are used, the sum over orbitals may be replaced by a sum over atomic basis functions. A pair function in which the summation indices xy have been replaced by ij is referred to as the ij-ansatz, if xy is replaced by kl we get the kl-ansatz, and so forth.

The GTG-MP2 methods presented in this thesis may be regarded as an mixture/intermediate between the MP2-R12 method developed by Klopper and Kutzelnigg [6, 10, 11] and the Gaussian-type geminals (GTG) method developed by Szalewicz, Jeziorski, and others [12–15].

Klopper and Kutzelnigg define pair function similar to (8.1), but instead of using a sum over Gaussian correlation factors they use a single, linear r_{12} term. Moreover, they have restricted the summation indices xy to either of the forms ij or kl. While the linear r_{12} term has some theoretically appealing properties, the

Gaussian correlation factors have the advantage that they give integrals that may be evaluated analytically.

Szalewicz and co-workers do not use the orbital part in their pair function. Instead, they use a pure linear combination of GTGs in which all non-linear parameters are optimised. Their method leads to very accurate pair functions and pair energies for small systems, but is difficult to generalise to large molecules, partly due to the expensive non-linear optimisation.

To obtain pair energies, the pair functions must be optimised. This may be accomplished by minimising the strong orthogonality (SO) functional present in the variational formulation of MP2 theory

$$F_{ij}[\tilde{u}_{ij}] \propto \langle \tilde{u}_{ij}| \, Q_{\text{occ}} \left(f(1) + f(2) - \varepsilon_i - \varepsilon_j \right) Q_{\text{occ}} \, |\tilde{u}_{ij}\rangle + 2 \, \langle \tilde{u}_{ij}| \, Q_{\text{occ}} r_{12}^{-1} \, |\phi_{ij}\rangle \qquad (8.2)$$

leading to expensive three- and four-electron integrals. Klopper and Kutzelnigg avoid these integrals by introducing the resolution of the identity (RI) in several places. Using this identity has its price, however, and among other things, the upper-bound property of pair energies (see Equation 3.57) is lost.

Szalewicz and co-workers also avoid four-electron integrals, but achieve this by replacing the SO functional with their weak orthogonality (WO) functional

$$J_{ij}[\tilde{u}_{ij}] \propto \langle \tilde{u}_{ij}| \, \tilde{f}(1) + \tilde{f}(2) - \varepsilon_i - \varepsilon_j \, |\tilde{u}_{ij}\rangle + 2 \, \langle \tilde{u}_{ij}| \, Q_{\text{occ}} r_{12}^{-1} \, |\phi_{ij}\rangle \qquad (8.3)$$

where $\tilde{f}(1)$ and $\tilde{f}(2)$ are modified Fock operators defined as $\tilde{f} = f + \Delta_{ij} P_{\text{occ}}$, where Δ_{ij} is a level-shift given by $\Delta_{ij} = \frac{1}{2} \left(\varepsilon_i + \varepsilon_j - 2\varepsilon_1 \right) + \eta$. The level-shift parameter η may be greater than or equal to zero. While the WO functional maintains the upper-bound property of pair energies as shown in section A, it gives rise to expensive three-electron integrals.

The energies presented in this work have been obtained by minimising the WO functional of Szalewicz and co-workers. We only optimise linear parameters, however, and pair energies are therefore easily obtained by solving a set of linear equations. We still have to evaluate three-electron integrals, and to be able to calculate them effectively, we have developed a general scheme for symmetry-adapting many-electron integrals (section 5). This way, two- and three-electron integrals are calculated analytically within an Abelian subgroup of the true symmetry of the system. To speed up integral calculations further, we have also implemented an efficient parallelisation algorithm (section 6.6).

Even though we have used our explicitly correlated pair functions for obtaining accurate MP2 energies only, they may also be used to obtain molecular properties; either using the Hellman–Feynman approximation as done by Bakken *et al.* [136] for molecular geometric properties, or using explicit formulas as done by Bukowski *et al.* [137] for multipole moments.

The use of explicitly correlated basis functions is not limited to MP2 theory, but may also be developed for the coupled-cluster and CASPT2 theories, for example.

Table 8.1: Second-order correlation energies ($-E/\mathrm{mE_h}$) obtained in this work compared with current best estimates.

System	This work	Current best	Recovery
He	37.37729	37.37744	99.9996%
Be	76.355	76.358	99.996%
Ne	388.19	388.19	100%
He$\cdots$He	74.804	74.804	100%
H_2	34.252	34.252	100%
LiH	72.877	72.890	99.98%
HF	383.69	384.4	99.82%
H_2O[a]	361.39	361.92	99.85%
H_2O[b]	111.4	111.4	100%
H_2O[c]	347.6	357	97.4%

[a] Slightly different geometries.
[b] Core correction (in cm^{-1}) to the barrier to linearity.
[c] Valence correction (in cm^{-1}) to the barrier to linearity.

For the coupled-cluster singles and doubles theory Noga and co-workers [120, 138–141] have made an implementation in which the linear r_{12} terms are utilised (CCSD-R12), while Bukowski and co-workers [102] have made an implementation utilising Gaussian correlation factors (CCSD-GTG).

In this work we have shown that,when pair functions of the form (8.1) are optimised with the WO functional, high quality energies are obtained for both atoms and molecules. The orbital part of the pair functions has been expanded in standard one-electron basis functions. For hydrogen, helium, oxygen, and fluorine we have used the correlation consistent basis sets of Dunning and co-workers [65–69], and for lithium and beryllium we have used atomic natural orbitals (ANOs) developed by Roos and co-workers [72, 73]. The correlation function, which ties orbitals into geminals, has been chosen to be a nine-term expansion of Gaussian correlation factors having even-tempered exponents $\gamma_v \in \{1/9, 1/3, \ldots, 729\}$. No attempt has been made to optimise the non-linear exponents of either the GCFs or the one-electron basis sets, and the results presented here, merely show the potential of the pair functions of type (8.1) and not the ultimate performance.

In Table 8.1 we compare our best second-order correlation energies with the best estimates found in literature. For most of these systems, our correlation energies are excellent, and for four of them we also have the current best energy estimates. These estimates were all made using the pq-ansatz. The pq-ansatz has limited use, however, as it requires large equation systems to be solved. For the HF and water molecules, for instance, we were not able to use the basis set aug-cc-pCVTZ(spd,sp)

because of memory limit of 2 GB. For these systems, therefore, the pq-ansatz could not be used with a proper basis set and our best energy estimates were obtained with the kq-ansatz. The kq-ansatz does not suffer from large memory requirements, but to obtain accurate pair energies, the one-electron basis must include functions of higher angular momenta than is needed for the pq-ansatz. The three-electron integrals, however, become prohibitively expensive to compute when high angular momenta functions are included, and for the HF and water molecules we were not able to include enough basis functions to obtain correlation energies as good as the current best estimates obtained with the MP2-R12 method.

Originally, the geminal part of (8.1) was only intended to be a correction to the virtual orbital part. As discussed in section 7.10, however, the most of the correlation energy has usually been recovered by the geminal part rather than the virtual orbital part. This occurs for two reasons: First, we have introduced the kq- and pq-ansätze, which retrieve correlation energy much more efficiently than the originally proposed ij-ansatz. Secondly, we are restricted to using the same one-electron basis set for geminals and virtual orbitals. Whereas high angular momentum functions are needed to obtain good energy estimates with the virtual orbital expansion, such functions cannot generally be used because of three-electron integrals.

The use of a common one-electron basis for orbitals and geminals was particularly unfortunate for the study of the rotational barrier of the hydrogen peroxide molecule (section 7.9). Due to the expensive three-electron integrals, the largest basis set we could use was of quality $7s6p4d$ for oxygen and $4s3p$ for hydrogen. This basis set did neither contain flexible core functions nor a sufficient amount of polarisation functions, and the barrier could therefore only be described with moderate accuracy.

If the use of pair functions of type (8.1) is to become widespread, the one-electron basis sets used for geminals must be decoupled from the basis sets used for virtual orbitals. This will allow us to use large basis sets like aug-cc-pVQZ or aug-cc-pV5Z for the virtual orbital part and a smaller basis set, possibly containing only s-, p-, and d-orbitals, for the geminal part. Long-range correlation effects, therefore, may be described with the conventional part of the pair function, while short-range effects like core correlation may be described with geminals. Moreover, this approach will make it possible to design basis sets explicitly for geminals. As discussed by Noga and Valiron [142] in the framework of R12 theory, basis sets optimised for conventional calculations are not optimal for calculations employing explicitly correlated wave functions. This non-optimality is expected to be even more pronounced within GTG-MP2 theory and in particular for the kq-ansatz and pq-ansätze.

While basis set containing g- and h-orbitals may be needed in the virtual orbital expansion, they are not needed for the occupied Hartree–Fock orbitals. Use of a separate basis set for the occupied orbitals should therefore also be considered. Since the occupied orbitals are needed in the Fock operator, the projection operator, and the energy calculation, this will reduce the time spent in calculating three-electron

integrals significantly.

For almost all calculations presented in this work, the kl-ansatz performs poorly. From the neon results in Table 7.13, however, we know that the GTG-MP2 method with the kl-ansatz perform better than the MP2-R12 methods in the same one-electron. Obtaining good energies with the kl-ansatz is therfore only a question of using a sufficiently large basis for the virtual orbital expansion. As argued above, this will become possible when separate basis sets are used for different parts of the calculation.

Even though the use of multiple basis sets will allow calculations on larger molecules, the use of three-electron integrals will still limit the size of systems than can be treated. A remedy for this will be to introduce the resolution-of-the-identity (RI) in three-electron integrals, as discussed in section 3.5. The RI may be introduced at two different levels: In the pair function optimisation and in the energy calculation. In section 3.6, we showed that, if the RI is used in the optimisation, the time spent in calculating three-electron integrals change from an $\mathcal{O}(N_{\mathrm{GCF}}^2)$ process to an $\mathcal{O}(N_{\mathrm{GCF}})$ process. The error introduced in energies by using this approximation, however, is only quadratic in the error in the pair functions. If the RI is also used in the energy calculation, no three-electron integrals are needed.

As the GTG-MP2 method becomes applicable for larger systems, integrals should be prescreened. In section 6.7, we developed formulas for prescreening of two- and three-electron integrals except for kinetic energy integrals, and discussed what kind of performance improvement that can be expected. We have also argued (section 6.1) that the AO-formulation of the different ansätze is well-suited for to local methods such as the LMP2 method of Werner and co-workers [39, 40].

To improve the GTG-MP2 method presented in this work, one or more of the features discussed above must be implemented. In order of importance, these features are:

- Use different basis sets for geminals, virtual orbitals, and occupied orbitals
- Introduce the resolution-of-the-identity to avoid three-electron integrals
- Integral prescreening for better scaling with system size

where integral prescreening also includes local methods. If these techniques are implemented for the GTG-MP2 method, this method may turn out as the overall best method for retrieving dynamic correlation energies for both small and medium sized molecules.

Appendix A

Justification of the WO functional

In section 3.4.3 we showed that if the Hartree–Fock equations have been solved exactly, the strong orthogonality functional of Sinanoğlu

$$\begin{aligned} F_{ij}^{\mathcal{P}}[\tilde{u}_{ij}^{\mathcal{P}}] = \Lambda_{ij}^{\mathcal{P}} \big(& 2 \left\langle \tilde{u}_{ij}^{\mathcal{P}} \right| Q_{\mathrm{occ}} r_{12}^{-1} \left| \phi_{ij}^{\mathcal{P}} \right\rangle \\ & + \left\langle \tilde{u}_{ij}^{\mathcal{P}} \right| Q_{\mathrm{occ}} \left(f(1) + f(2) - \varepsilon_i - \varepsilon_j \right) Q_{\mathrm{occ}} \left| \tilde{u}_{ij}^{\mathcal{P}} \right\rangle \big) , \end{aligned} \tag{A.1}$$

represents a true upper bound to the exact pair energy. In this section we will show that the weak orthogonality functional of Szalewicz and co-workers

$$\begin{aligned} J_{ij}^{\mathcal{P}}[\tilde{u}_{ij}^{\mathcal{P}}] = \Lambda_{ij}^{\mathcal{P}} \big(& \left\langle \tilde{u}_{ij}^{\mathcal{P}} \right| f(1) + f(2) - \varepsilon_i - \varepsilon_j \left| \tilde{u}_{ij}^{\mathcal{P}} \right\rangle \\ & + \Delta_{ij} \left\langle \tilde{u}_{ij}^{\mathcal{P}} \right| P_{\mathrm{occ}}(1) + P_{\mathrm{occ}}(2) \left| \tilde{u}_{ij}^{\mathcal{P}} \right\rangle + 2 \left\langle \tilde{u}_{ij}^{\mathcal{P}} \right| Q_{\mathrm{occ}} r_{12}^{-1} \left| \phi_{ij}^{\mathcal{P}} \right\rangle \big) , \end{aligned} \tag{A.2}$$

in turn represents a true upper bound to the strong orthogonality functional

$$J_{ij}^{\mathcal{P}}[\tilde{u}_{ij}^{\mathcal{P}}] \geq F_{ij}^{\mathcal{P}}[\tilde{u}_{ij}^{\mathcal{P}}] \geq \epsilon_{ij}^{\mathcal{P}} \tag{A.3}$$

for all trial functions $\tilde{u}_{ij}^{\mathcal{P}}$. As we shall see, this proof assumes that the Hartree–Fock equations are solved exactly, but no further approximations have to be introduced.

Since the SO functional is expressed in terms of the functions $Q_{\mathrm{occ}}\tilde{u}_{ij}^{\mathcal{P}}$ rather than $\tilde{u}_{ij}^{\mathcal{P}}$, we start by decomposing the trial functions into two parts, one being strongly orthogonal to the occupied orbital

$$\tilde{u}_{ij} = \underbrace{Q_{\mathrm{occ}}\tilde{u}_{ij}}_{\tilde{u}_{ij}^{(1)}} + (1 - Q_{\mathrm{occ}})\tilde{u}_{ij} \tag{A.4}$$

Whether we work in the parity-adapted formalism or not does not affect the outcome, and since superscripts will be needed to distinguish between different pair function components, we ignore the parity adaption from here.

In order to prove (A.3), the pair function must be decomposed into mutually orthogonal spaces. This is fulfilled by the decomposition (A.4). Furthermore, as

we try to establish a relationship between the WO and SO functionals in which the difference is written in terms of expectation values, our subspaces should be closed under the operator $P_{\rm occ}(1)+P_{\rm occ}(2)$. This requirement is fulfilled by the first term of (A.4) but not the second. The latter term, therefore, has to undergo a new decomposition

$$(1-Q_{\rm occ})\tilde{u}_{ij} = \underbrace{P_{\rm occ}(1)P_{\rm occ}(2)\tilde{u}_{ij}}_{\tilde{u}^{(2)}_{ij}} + \underbrace{\left[P_{\rm occ}(1)+P_{\rm occ}(2)-2P_{\rm occ}(1)P_{\rm occ}(2)\right]\tilde{u}_{ij}}_{\tilde{u}^{(3)}_{ij}} \quad \text{(A.5)}$$

Combining decompositions (A.4) and (A.5) we write the pair function as

$$\tilde{u}_{ij} = \tilde{u}^{(1)}_{ij} + \tilde{u}^{(2)}_{ij} + \tilde{u}^{(3)}_{ij} \quad \text{(A.6)}$$

where the different components are given by

$$\tilde{u}^{(1)}_{ij} = Q_{\rm occ}\tilde{u}_{ij} \qquad \approx \text{double excitations} \quad \text{(A.7)}$$

$$\tilde{u}^{(2)}_{ij} = P_{\rm occ}(1)P_{\rm occ}(2)\tilde{u}_{ij} \qquad = \text{no excitation} \quad \text{(A.8)}$$

$$\tilde{u}^{(3)}_{ij} = \left[P_{\rm occ}(1)+P_{\rm occ}(2)-2P_{\rm occ}(1)P_{\rm occ}(2)\right]\tilde{u}_{ij} \qquad \approx \text{single excitations} \quad \text{(A.9)}$$

The pair function component $\tilde{u}^{(2)}_{ij}$ lies completely in the space spanned by the occupied orbitals. We may also regard the components $\tilde{u}^{(3)}_{ij}$ and $\tilde{u}^{(1)}_{ij}$ as single- and double-excitations respectively, but this analogy is, strictly speaking, only valid when the orbital basis is complete and pair functions can be fully expanded in it.

The components belonging to different subspaces are mutual orthogonal. Writing each components as $\tilde{u}^{(m)}_{ij} = \mathcal{O}^{(m)}\tilde{u}_{ij}$ where $\mathcal{O}^{(m)}$ is the projection operator associated with the mth subspace, we get

$$\left\langle \tilde{u}^{(m)}_{ij} | \tilde{u}^{(n)}_{ij} \right\rangle = \langle \tilde{u}_{ij}| \, \mathcal{O}^{(m)}\mathcal{O}^{(n)} \, |\tilde{u}_{ij}\rangle = \delta_{mn} \langle \tilde{u}_{ij}| \, \mathcal{O}^{(m)} \, |\tilde{u}_{ij}\rangle \quad \text{(A.10)}$$

The projection operators $\mathcal{O}^{(m)}$ may easily be identified from (A.7)–(A.9). Using the properties of these operators, we may also show that the pair function components are eigenfunctions of the projection operator $P_{\rm occ}(1)+P_{\rm occ}(2)$

$$\left[P_{\rm occ}(1)+P_{\rm occ}(2)\right]\left|u^{(m)}_{ij}\right\rangle = a_m \left|u^{(m)}_{ij}\right\rangle, \qquad a_m = \begin{cases} 0, & \text{for } m=1 \\ 2, & \text{for } m=2 \\ 1, & \text{for } m=3 \end{cases} \quad \text{(A.11)}$$

Inserting the decomposition (A.6) into the weak orthogonality functional

$$\begin{aligned} J_{ij}[\tilde{u}_{ij}] = \Lambda_{ij} \big(& \langle \tilde{u}_{ij}| \, f(1)+f(2)-\varepsilon_i-\varepsilon_j \, |\tilde{u}_{ij}\rangle \\ & + \Delta_{ij} \langle \tilde{u}_{ij}| \, P_{\rm occ}(1)+P_{\rm occ}(2) \, |\tilde{u}_{ij}\rangle + 2 \langle \tilde{u}_{ij}| \, Q_{\rm occ} r_{12}^{-1} \, |\phi_{ij}\rangle \big) \end{aligned} \quad \text{(A.12)}$$

and using relations (A.10) and (A.11) to simplify expressions, we get

$$\begin{aligned} J_{ij}[\tilde{u}_{ij}] = F_{ij}[\tilde{u}_{ij}] &+ \Lambda_{ij} \left\langle \tilde{u}_{ij}^{(2)} \right| f(1) + f(2) - \varepsilon_i - \varepsilon_j + 2\Delta_{ij} \left| \tilde{u}_{ij}^{(2)} \right\rangle \\ &+ \Lambda_{ij} \left\langle \tilde{u}_{ij}^{(3)} \right| f(1) + f(2) - \varepsilon_i - \varepsilon_j + \Delta_{ij} \left| \tilde{u}_{ij}^{(3)} \right\rangle \end{aligned} \tag{A.13}$$

where $F_{ij}[\tilde{u}_{ij}]$ is the strong orthogonality functional given in (A.1) but for non-parity-adapted pairs. Note that by virtue of the operator Q_{occ}, the only term *linear* in $\tilde{u}_{ij}$ is absorbed into the SO functional. In order to obtain (A.13), we have assumed that transition moments between different subspaces are zero

$$\left\langle \tilde{u}_{ij}^{(m)} \right| f(1) + f(2) \left| \tilde{u}_{ij}^{(n)} \right\rangle \approx 0 \quad \text{when} \quad m \neq n \tag{A.14}$$

If the Hartree–Fock equations have been solved exactly, (A.14) becomes an exact relation. This is trivial since the Fock operator and the projection operators $\mathcal{O}^{(m)}$ then commute

$$\mathcal{O}^{(m)} \left[f(1) + f(2) \right] \mathcal{O}^{(n)} = \delta_{mn} \mathcal{O}^{(m)} \left[f(1) + f(2) \right] \tag{A.15}$$

In order to prove that the weak orthogonality functional is an upper bound to the strong orthogonality functional, we must show that the second and third terms of (A.13) are both positive definite i.e. that

$$\left\langle \tilde{u}_{ij}^{(2)} \right| f(1) + f(2) - \varepsilon_i - \varepsilon_j + 2\Delta_{ij} \left| \tilde{u}_{ij}^{(2)} \right\rangle \geq 0 \tag{A.16}$$

$$\left\langle \tilde{u}_{ij}^{(3)} \right| f(1) + f(2) - \varepsilon_i - \varepsilon_j + \Delta_{ij} \left| \tilde{u}_{ij}^{(3)} \right\rangle \geq 0 \tag{A.17}$$

Using the definition of the level shift term Δ_{ij}

$$\Delta_{ij} = \frac{1}{2} \left(\varepsilon_i + \varepsilon_j - 2\varepsilon_1 \right) + \eta \tag{A.18}$$

where ε_1 is the energy of the lowest occupied orbital and η some nonnegative number having the dimension of energy, the positive definiteness of (A.16) is easily shown by rewriting the equation as

$$\begin{aligned} &\left\langle \tilde{u}_{ij}^{(2)} \right| f(1) + f(2) - \varepsilon_i - \varepsilon_j + 2\Delta_{ij} \left| \tilde{u}_{ij}^{(2)} \right\rangle \\ &\quad = \langle \tilde{u}_{ij} | \, \mathcal{O}^{(2)} \left(f(1) + f(2) - 2\varepsilon_1 + 2\eta \right) \mathcal{O}^{(2)} \, | \tilde{u}_{ij} \rangle \\ &\quad = \sum_{kl} \left| \langle \tilde{u}_{ij} | \phi_{kl} \rangle \right|^2 \left(\varepsilon_k + \varepsilon_l - 2\varepsilon_1 + 2\eta \right) \geq 0 \end{aligned} \tag{A.19}$$

which is manifestly nonnegative. Using simple quantum mechanical reasoning, (A.17) is also easily justified. Since any function in the 3rd subspace are orthogonal

to all doubly occupied states, we know that the $f(1)+f(2)$ expectation value must be bound from below by

$$\left\langle \tilde{u}_{ij}^{(3)} \right| f(1)+f(2) \left| \tilde{u}_{ij}^{(3)} \right\rangle \geq \left\langle \tilde{u}_{ij}^{(3)} \right| \varepsilon_{\mathrm{LUMO}} + \varepsilon_1 \left| \tilde{u}_{ij}^{(3)} \right\rangle \tag{A.20}$$

where $\varepsilon_{\mathrm{LUMO}}$ is the energy of the *lowest unoccupied molecular orbital* and e_1, as stated above, is the energy of the lowest occupied orbital. Inserting this result in (A.17) along with the explicit form of Δ_{ij} we get

$$\begin{aligned} &\left\langle \tilde{u}_{ij}^{(3)} \right| f(1)+f(2)-\varepsilon_i-\varepsilon_j+\Delta_{ij} \left| \tilde{u}_{ij}^{(3)} \right\rangle \\ &\quad \geq \left\langle \tilde{u}_{ij}^{(3)} \right| \varepsilon_{\mathrm{LUMO}} - \frac{1}{2}(\varepsilon_i+\varepsilon_j) + \eta \left| \tilde{u}_{ij}^{(3)} \right\rangle > 0 \end{aligned} \tag{A.21}$$

By relations (A.13), (A.19) and (A.21) we have shown that $J_{ij}[\tilde{u}_{ij}]$ will be a true upper bound to $F_{ij}[\tilde{u}_{ij}]$ for all trial functions. From this it follows that

$$J_{ij}[\tilde{u}_{ij}] \geq \epsilon_{ij} \tag{A.22}$$

If $\eta = 0$ the WO functional gives us the exact pair energy when the trial function equals the exact pair function or the exact pair function with any amount of $\varphi_1(1)\varphi_1(2)$ added to it. This may be written as $\tilde{u}_{ij} = u_{ij}(1,2) + \lambda\varphi_1(1)\varphi_1(2)$, where u_{ij} is the exact pair function and λ is arbitrary. The arbitrariness is caused by (A.19) which, for this particular choice of η, is invariant to changes in the direction of the lowest occupied orbitals. Once $\eta > 0$ however, this is no longer true and $J_{ij}[\tilde{u}_{ij}]$ equals the exact pair energy only when $\tilde{u}_{ij}$ is exactly equal to u_{ij}. Therefore, in minimising the WO functional with $\eta > 0$, the parameters in $\tilde{u}_{ij}$ take on such values as to satisfy not only the stationary condition (first order equation) but also the strong orthogonality condition

$$Q_{\mathrm{occ}} u_{ij} = u_{ij} \tag{A.23}$$

As we expand the pair function in a more flexible basis it will automatically become more strongly orthogonal to the occupied orbitals. This has one very important consequence. From (A.4) we see that if the SO condition is close to fulfilled, we may write $\tilde{u}_{ij} \approx \tilde{u}_{ij}^{(1)}$. This however, implies that $J_{ij}[\tilde{u}_{ij}] \approx F_{ij}[\tilde{u}_{ij}]$, and that the WO functional does a job nearly as good as the SO functional in optimising pair functions. When using the former to optimise pair functions, it is therefore of interest to know to what extent the SO condition is fulfilled. This may conveniently be measured by calculating the size of the $(1-Q_{\mathrm{occ}})\tilde{u}_{ij}$ component. Thus, for the pair of electrons i and j, we define the *SO measure* χ_{ij}^{SO} as

$$\begin{aligned} \langle \tilde{u}_{ij} | \tilde{u}_{ij} \rangle \chi_{ij}^{\mathrm{SO}} &= \langle (1-Q_{\mathrm{occ}})\tilde{u}_{ij} | (1-Q_{\mathrm{occ}})\tilde{u}_{ij} \rangle \\ &= \langle \tilde{u}_{ij} | \, P_{\mathrm{occ}}(1) + P_{\mathrm{occ}}(2) - P_{\mathrm{occ}}(1)P_{\mathrm{occ}}(2) \, | \tilde{u}_{ij} \rangle \end{aligned} \tag{A.24}$$

Originally, the programs used to obtain second-order energies for this thesis did not have the double-projected integrals available, and the SO measure were instead calculated as

$$\chi_{ij}^{\mathrm{SO}} \leq \frac{\langle \tilde{u}_{ij}| \, P_{\mathrm{occ}}(1) + P_{\mathrm{occ}}(2) \, |\tilde{u}_{ij}\rangle}{\langle \tilde{u}_{ij}|\tilde{u}_{ij}\rangle} \tag{A.25}$$

thus making the pair functions look less orthogonal to the occupied orbitals than they really are. This is clearly unfortunate if the SO measure is large, since this disables us to predict whether or not the WO functional represents a good approximation to the SO functional. Note that (A.23) will *not* be fulfilled if we use the SO functional to optimise pair functions, as the minimum value of $F_{ij}[\tilde{u}_{ij}]$, namely ε_{ij}, is attained when $\tilde{u}_{ij} = u_{ij}(1,2) + (1 - Q_{\mathrm{occ}})\chi$, where χ is an arbitrary function. In dealing with second-order energies, however, this does not represent a problem as Q_{occ} is present in the energy expression and projects out any SO violating components of the pair function. If the pair functions were to be used to obtain third-order energy corrections, on the other hand, one would have to project the strongly orthogonal component out of the function $\tilde{u}_{ij}^{\mathrm{min}}$ obtained in the minimisation process. This projection would then be an approximation to u_{ij} and could be used directly in the third-order energy expressions.

Using pair functions obtained from the WO functional to calculate higher-order energy corrections is not straight forward. Although the parameter η may be increased in order to make pair functions more strongly orthogonal, this eventually leads to a WO functional dominated by the level-shift term (the one involving Δ_{ij}). Such a functional will upon minimisation give pair functions that satisfy the strong orthogonality requirement very accurately at the expense of not precisely fulfilling the first-order perturbation equation [75]. Thus η must neither be too small nor too large. Unfortunately, there are no guidelines to follow as to which intermediate value of η is optimal. Therefore, when using pair functions obtained from the WO functional to calculate third-order energy corrections, Szalewicz *et al.* [45] recommend that the minimisation is performed with $\eta = 0$. The resulting pair functions are then orthogonalised to the occupied orbitals by a modified SO operator. We conclude this section by adding that if the pair functions are expanded in a complete basis, the energy corrections will be independent of η.

Appendix B

Supplementary tables

Table B.1: The size distribution of AO integrals for the *trans*-H_2O_2 molecule when using the cc-pVDZ basis and one GCF. The stack each integral belongs to is given by $\Delta = -\text{int}(\log_{10}|I_{\text{size}}|)$. Within each part of the table frequencies given on stacks 0–15 add up to 1 for each integral type.

	Δ	I21	I22	I2K1	I2K2	I2V1	I2V2	I2C0	I2C1	I3C1	I3E1	I3C2	I3E2	I32
$\gamma = \frac{1}{3}$	0	.0238	.0103	.0601	.0414	.3928	.2764	.0603	.0265	.0013	.0013	.0005	.0003	.0004
	1	.3354	.2445	.3186	.2982	.4531	.5169	.4472	.3674	.0513	.0513	.0273	.0187	.0211
	2	.4734	.5110	.4069	.4048	.0986	.1421	.3686	.4414	.3830	.3830	.3073	.2801	.2867
	3	.1018	.1559	.1457	.1799	.0215	.0290	.0680	.1031	.4028	.4028	.4485	.4729	.4640
	4	.0281	.0384	.0265	.0341	.0029	.0039	.0195	.0239	.1217	.1217	.1630	.1717	.1716
	5	.0033	.0057	.0042	.0054	.0002	.0004	.0024	.0036	.0300	.0300	.0411	.0438	.0434
	6	.0003	.0006	.0007	.0008	.0000	.0000	.0003	.0003	.0044	.0044	.0064	.0067	.0069
	7	.0000	.0000	.0000	.0001	.0000	.0000	.0000	.0000	.0007	.0007	.0010	.0011	.0011
	8	.0000	.0000	.0000	.0000	.0000	.0000	.0000	.0000	.0001	.0001	.0001	.0001	.0001
	9	.0000	.0000	.0000	.0000	.0000	.0000	.0000	.0000	.0000	.0000	.0000	.0000	.0000
	10	.0000	.0000	.0000	.0000	.0000	.0000	.0000	.0000	.0000	.0000	.0000	.0000	.0000
	11	.0000	.0000	.0000	.0000	.0000	.0000	.0000	.0000	.0000	.0000	.0000	.0000	.0000
	12	.0000	.0000	.0000	.0000	.0000	.0000	.0000	.0000	.0000	.0000	.0000	.0000	.0000
	13	.0000	.0000	.0000	.0000	.0000	.0000	.0000	.0000	.0000	.0000	.0000	.0000	.0000
	14	.0000	.0000	.0002	.0001	.0000	.0000	.0000	.0000	.0000	.0000	.0000	.0000	.0000
	15	.0338	.0335	.0372	.0353	.0309	.0313	.0336	.0338	.0048	.0048	.0047	.0046	.0048
$\gamma = 9$	0	.0001	.0001	.0009	.0019	.0035	.0008	.0603	.0006	.0000	.0000	.0000	.0000	.0000
	1	.0064	.0006	.0275	.0680	.1545	.0513	.4472	.0450	.0002	.0002	.0000	.0000	.0000
	2	.1319	.0499	.1709	.3592	.4700	.3449	.3686	.3301	.0147	.0147	.0033	.0002	.0000
	3	.4448	.3361	.3941	.3867	.2579	.4188	.0680	.4158	.1920	.1920	.0800	.0096	.0021
	4	.2737	.4079	.2739	.1092	.0720	.1196	.0195	.1242	.4318	.4318	.3616	.1098	.0444
	5	.0915	.1214	.0753	.0354	.0091	.0286	.0024	.0429	.2525	.2525	.3629	.3477	.2514
	6	.0153	.0428	.0160	.0070	.0023	.0054	.0003	.0075	.0838	.0838	.1400	.3357	.4032
	7	.0031	.0073	.0036	.0007	.0003	.0006	.0000	.0008	.0172	.0172	.0400	.1435	.2032
	8	.0002	.0009	.0005	.0000	.0000	.0000	.0000	.0000	.0027	.0027	.0063	.0403	.0747
	9	.0000	.0000	.0000	.0000	.0000	.0000	.0000	.0000	.0004	.0004	.0010	.0073	.0135
	10	.0000	.0000	.0000	.0000	.0000	.0000	.0000	.0000	.0000	.0000	.0001	.0011	.0025
	11	.0000	.0000	.0000	.0000	.0000	.0000	.0000	.0000	.0000	.0000	.0000	.0002	.0004
	12	.0000	.0000	.0000	.0000	.0000	.0000	.0000	.0000	.0000	.0000	.0000	.0000	.0000
	13	.0000	.0000	.0000	.0000	.0000	.0000	.0000	.0000	.0000	.0000	.0000	.0000	.0000
	14	.0000	.0000	.0000	.0000	.0000	.0000	.0000	.0000	.0000	.0000	.0000	.0000	.0000
	15	.0331	.0331	.0372	.0319	.0304	.0301	.0336	.0331	.0047	.0047	.0047	.0046	.0046
$\gamma = 243$	0	.0000	.0000	.0000	.0001	.0000	.0000	.0603	.0001	.0000	.0000	.0000	.0000	.0000
	1	.0001	.0000	.0002	.0052	.0004	.0002	.4472	.0001	.0000	.0000	.0000	.0000	.0000
	2	.0000	.0001	.0006	.1274	.0032	.0006	.3686	.0131	.0000	.0000	.0000	.0000	.0000
	3	.0053	.0010	.0250	.4303	.1193	.0341	.0680	.1869	.0003	.0003	.0001	.0000	.0000
	4	.1084	.0345	.1426	.2844	.4316	.3100	.0195	.4432	.0119	.0119	.0023	.0000	.0000
	5	.4002	.2920	.3769	.0989	.3064	.4397	.0024	.2251	.1610	.1610	.0596	.0001	.0000
	6	.3243	.4327	.2971	.0169	.0906	.1437	.0003	.0843	.4130	.4130	.3262	.0024	.0001
	7	.0992	.1455	.0925	.0044	.0147	.0355	.0000	.0109	.2813	.2813	.3844	.0385	.0017
	8	.0236	.0521	.0226	.0004	.0030	.0050	.0000	.0031	.0998	.0998	.1623	.2158	.0317
	9	.0056	.0078	.0044	.0000	.0004	.0008	.0000	.0003	.0237	.0237	.0502	.3899	.1907
	10	.0005	.0016	.0005	.0000	.0000	.0000	.0000	.0000	.0037	.0037	.0084	.2294	.3888
	11	.0000	.0000	.0000	.0000	.0000	.0000	.0000	.0000	.0005	.0005	.0015	.0942	.2508
	12	.0000	.0000	.0000	.0000	.0000	.0000	.0000	.0000	.0001	.0001	.0002	.0199	.1024
	13	.0000	.0000	.0000	.0000	.0000	.0000	.0000	.0000	.0000	.0000	.0000	.0044	.0233
	14	.0000	.0000	.0000	.0001	.0000	.0000	.0000	.0000	.0000	.0000	.0000	.0006	.0051
	15	.0328	.0328	.0375	.0319	.0303	.0303	.0336	.0328	.0047	.0047	.0047	.0047	.0055

Table B.2: The size distribution of AO integrals for the water dimer when using the cc-pVDZ basis and one GCF. The stack each integral belongs to is given by $\Delta = -\mathrm{int}(\log_{10}|I_{\mathrm{size}}|)$. Within each part of the table frequencies given on stacks 0–15 add up to 1 for each integral type.

	Δ	I21	I22	I2K1	I2K2	I2V1	I2V2	I2C0	I2C1	I3C1	I3E1	I3C2	I3E2	I32
$\gamma = \frac{1}{3}$	0	.0202	.0089	.0331	.0272	.1191	.0980	.0499	.0268	.0007	.0007	.0003	.0002	.0002
	1	.1157	.1065	.0971	.0919	.1963	.1243	.1807	.1087	.0199	.0199	.0136	.0108	.0093
	2	.1958	.1121	.1634	.1065	.2420	.2318	.2351	.1496	.0708	.0708	.0543	.0302	.0375
	3	.2447	.2452	.2518	.2178	.1568	.1712	.2146	.2510	.1574	.1574	.1135	.0805	.1107
	4	.1559	.1786	.1765	.1951	.0822	.1192	.1001	.1717	.2014	.2014	.1821	.1763	.1906
	5	.0742	.1041	.1008	.1313	.0458	.0718	.0491	.0833	.1651	.1651	.1693	.1891	.1859
	6	.0522	.0719	.0612	.0885	.0611	.0628	.0499	.0586	.1071	.1071	.1315	.1554	.1386
	7	.0583	.0679	.0440	.0579	.0436	.0540	.0480	.0555	.0725	.0725	.0909	.0995	.0884
	8	.0348	.0414	.0325	.0386	.0192	.0309	.0314	.0431	.0658	.0658	.0749	.0762	.0730
	9	.0176	.0270	.0136	.0186	.0048	.0069	.0141	.0198	.0563	.0563	.0639	.0658	.0619
	10	.0065	.0110	.0051	.0076	.0035	.0031	.0021	.0068	.0384	.0384	.0464	.0508	.0466
	11	.0020	.0023	.0026	.0034	.0024	.0029	.0020	.0024	.0184	.0184	.0257	.0296	.0255
	12	.0027	.0024	.0013	.0013	.0013	.0020	.0027	.0027	.0093	.0093	.0131	.0144	.0123
	13	.0013	.0015	.0001	.0001	.0000	.0001	.0013	.0013	.0062	.0062	.0078	.0080	.0072
	14	.0003	.0007	.0004	.0004	.0002	.0002	.0003	.0003	.0046	.0046	.0052	.0055	.0051
	15	.0178	.0186	.0164	.0138	.0215	.0209	.0189	.0183	.0061	.0061	.0074	.0077	.0071
$\gamma = 9$	0	.0001	.0001	.0009	.0016	.0017	.0008	.0499	.0006	.0000	.0000	.0000	.0000	.0000
	1	.0066	.0007	.0224	.0542	.0770	.0410	.1807	.0412	.0002	.0002	.0000	.0000	.0000
	2	.0831	.0450	.0722	.0761	.0729	.0767	.2351	.0892	.0089	.0089	.0023	.0001	.0000
	3	.0647	.0855	.0665	.1094	.1473	.1081	.2146	.0935	.0432	.0432	.0291	.0073	.0013
	4	.1493	.0950	.1475	.2000	.1881	.1898	.1001	.2016	.0690	.0690	.0560	.0230	.0202
	5	.1999	.2029	.1805	.1441	.1221	.1398	.0491	.1511	.1302	.1302	.0972	.0227	.0188
	6	.1224	.1497	.1337	.0699	.0622	.0919	.0499	.0781	.1550	.1550	.1529	.0588	.0400
	7	.0571	.0763	.0929	.0563	.0798	.0567	.0480	.0608	.1261	.1261	.1404	.1017	.0920
	8	.0835	.0608	.0790	.0925	.0916	.0922	.0314	.1051	.0916	.0916	.1062	.1122	.1101
	9	.0933	.1036	.0821	.0711	.0764	.0792	.0141	.0708	.0860	.0860	.0809	.1014	.1095
	10	.0634	.0692	.0614	.0554	.0383	.0637	.0021	.0516	.0867	.0867	.0861	.0853	.0914
	11	.0353	.0548	.0299	.0306	.0121	.0258	.0020	.0236	.0791	.0791	.0833	.0984	.0942
	12	.0121	.0235	.0098	.0110	.0059	.0084	.0027	.0073	.0543	.0543	.0699	.1123	.1112
	13	.0065	.0072	.0038	.0062	.0024	.0041	.0013	.0053	.0294	.0294	.0414	.1023	.1067
	14	.0032	.0054	.0012	.0020	.0015	.0013	.0003	.0015	.0157	.0157	.0218	.0713	.0821
	15	.0194	.0204	.0164	.0196	.0210	.0204	.0189	.0188	.0249	.0249	.0323	.1031	.1225
$\gamma = 243$	0	.0000	.0000	.0000	.0001	.0001	.0001	.0499	.0001	.0000	.0000	.0000	.0000	.0000
	1	.0001	.0000	.0003	.0048	.0003	.0002	.1807	.0002	.0000	.0000	.0000	.0000	.0000
	2	.0000	.0001	.0009	.0817	.0012	.0004	.2351	.0113	.0000	.0000	.0000	.0000	.0000
	3	.0074	.0004	.0206	.0604	.0725	.0286	.2146	.0929	.0003	.0003	.0000	.0000	.0000
	4	.0712	.0336	.0682	.1407	.0701	.0855	.1001	.0604	.0074	.0074	.0016	.0000	.0000
	5	.0691	.0917	.0598	.2018	.1330	.1052	.0491	.1717	.0405	.0405	.0249	.0001	.0000
	6	.1171	.0834	.1377	.1256	.1862	.1727	.0499	.1830	.0637	.0637	.0527	.0016	.0000
	7	.2161	.1910	.1796	.0561	.1290	.1462	.0480	.1090	.1192	.1192	.0884	.0186	.0011
	8	.1290	.1617	.1334	.0708	.0687	.0989	.0314	.0523	.1529	.1529	.1479	.0188	.0169
	9	.0623	.0840	.0926	.0940	.0624	.0548	.0141	.0778	.1299	.1299	.1431	.0348	.0187
	10	.0663	.0498	.0774	.0731	.0980	.0890	.0021	.0872	.0928	.0928	.1110	.0827	.0315
	11	.0964	.0936	.0830	.0444	.0732	.0700	.0020	.0686	.0785	.0785	.0797	.1013	.0792
	12	.0664	.0855	.0674	.0163	.0514	.0769	.0027	.0414	.0865	.0865	.0824	.1080	.1002
	13	.0486	.0554	.0403	.0064	.0202	.0354	.0013	.0159	.0812	.0812	.0840	.0871	.1083
	14	.0174	.0306	.0158	.0044	.0087	.0085	.0003	.0051	.0623	.0623	.0746	.0800	.0898
	15	.0326	.0391	.0231	.0192	.0251	.0277	.0189	.0231	.0848	.0848	.1096	.4671	.5541

Table B.3: The size distribution of AO integrals for the C_2 molecule using the cc-pVDZ basis and one GCF with exponent $\gamma = 9$. The stack each integral belongs to is given by $\Delta = -\text{int}(\log_{10}|I_{\text{size}}|)$. Within each part of the table frequencies given on stacks 0–15 add up to 1 for each integral type.

	Δ	I21	I22	I2K1	I2K2	I2V1	I2V2	I2C0	I2C1	I3C1	I3E1	I3C2	I3E2	I32
$R_{\text{C-C}} = 200\,pm$	0	.0002	.0002	.0007	.0009	.0011	.0006	.0744	.0004	.0000	.0000	.0000	.0000	.0000
	1	.0008	.0001	.0084	.0370	.0235	.0011	.5718	.0194	.0001	.0001	.0001	.0000	.0000
	2	.1086	.0238	.1232	.4989	.5420	.2576	.2415	.4102	.0076	.0076	.0013	.0001	.0000
	3	.5760	.4089	.4262	.3239	.3013	.5465	.0210	.4164	.2376	.2376	.0691	.0019	.0002
	4	.2115	.4173	.3036	.0465	.0372	.0984	.0004	.0601	.5614	.5614	.5282	.0804	.0198
	5	.0105	.0561	.0358	.0002	.0010	.0029	.0000	.0009	.1567	.1567	.3299	.4997	.3360
	6	.0002	.0009	.0043	.0001	.0000	.0002	.0000	.0005	.0139	.0139	.0466	.3375	.4794
	7	.0000	.0000	.0006	.0000	.0001	.0001	.0000	.0000	.0010	.0010	.0030	.0557	.1340
	8	.0000	.0000	.0000	.0000	.0000	.0000	.0000	.0000	.0000	.0000	.0002	.0028	.0087
	9	.0000	.0000	.0000	.0000	.0000	.0000	.0000	.0000	.0000	.0000	.0000	.0001	.0001
	10	.0000	.0000	.0000	.0000	.0000	.0000	.0000	.0000	.0000	.0000	.0000	.0000	.0000
	11	.0000	.0000	.0000	.0000	.0000	.0000	.0000	.0000	.0000	.0000	.0000	.0000	.0000
	12	.0000	.0000	.0000	.0000	.0000	.0000	.0000	.0000	.0000	.0000	.0000	.0000	.0000
	13	.0000	.0000	.0000	.0000	.0000	.0000	.0000	.0000	.0000	.0000	.0000	.0000	.0000
	14	.0000	.0000	.0000	.0000	.0000	.0000	.0000	.0000	.0000	.0000	.0000	.0000	.0000
	15	.0921	.0927	.0972	.0924	.0937	.0926	.0908	.0921	.0216	.0216	.0216	.0218	.0219
$R_{\text{C-C}} = 400\,pm$	0	.0002	.0002	.0005	.0009	.0007	.0003	.0378	.0004	.0000	.0000	.0000	.0000	.0000
	1	.0006	.0001	.0078	.0359	.0106	.0006	.0759	.0189	.0001	.0001	.0000	.0000	.0000
	2	.0600	.0232	.0435	.0260	.0392	.0409	.0848	.0568	.0049	.0049	.0011	.0000	.0000
	3	.0152	.0524	.0113	.0117	.0755	.0265	.1716	.0050	.0187	.0187	.0150	.0018	.0001
	4	.0239	.0061	.0349	.0738	.0822	.1223	.0957	.0646	.0169	.0169	.0146	.0144	.0105
	5	.0943	.0651	.0759	.0840	.0432	.0406	.0864	.0937	.0461	.0461	.0330	.0011	.0066
	6	.0551	.0921	.0564	.0254	.0366	.0397	.1082	.0316	.0649	.0649	.0641	.0107	.0039
	7	.0397	.0317	.0646	.0852	.0586	.0470	.1003	.0810	.0433	.0433	.0469	.0373	.0289
	8	.1378	.0807	.1195	.1648	.1594	.0909	.0578	.1489	.0626	.0626	.0498	.0252	.0354
	9	.1680	.1489	.1659	.1629	.1833	.1927	.0376	.1745	.0886	.0886	.0743	.0138	.0123
	10	.1488	.1744	.1475	.1223	.0977	.1373	.0242	.1205	.1256	.1256	.1062	.0421	.0285
	11	.0871	.1245	.0919	.0662	.0677	.0859	.0205	.0639	.1391	.1391	.1371	.0729	.0648
	12	.0458	.0576	.0411	.0276	.0300	.0454	.0061	.0303	.1086	.1086	.1264	.1151	.0989
	13	.0203	.0329	.0125	.0161	.0125	.0234	.0020	.0131	.0791	.0791	.0904	.1319	.1338
	14	.0086	.0131	.0007	.0033	.0026	.0060	.0004	.0031	.0690	.0690	.0741	.1197	.1244
	15	.0947	.0970	.1260	.0941	.1002	.1005	.0908	.0939	.1325	.1325	.1671	.4139	.4518
$R_{\text{C-C}} = 600\,pm$	0	.0002	.0002	.0005	.0009	.0007	.0003	.0261	.0004	.0000	.0000	.0000	.0000	.0000
	1	.0006	.0001	.0078	.0359	.0077	.0006	.0709	.0189	.0001	.0001	.0000	.0000	.0000
	2	.0600	.0232	.0435	.0260	.0418	.0409	.0284	.0568	.0048	.0048	.0010	.0000	.0000
	3	.0152	.0524	.0110	.0000	.0244	.0132	.0524	.0000	.0172	.0172	.0132	.0018	.0001
	4	.0000	.0000	.0000	.0000	.0312	.0446	.0368	.0000	.0082	.0082	.0114	.0144	.0105
	5	.0000	.0000	.0000	.0000	.0000	.0068	.0291	.0000	.0127	.0127	.0111	.0010	.0066
	6	.0000	.0000	.0003	.0005	.0018	.0000	.0397	.0005	.0093	.0093	.0127	.0000	.0000
	7	.0058	.0005	.0175	.0247	.0666	.0171	.0987	.0204	.0038	.0038	.0055	.0000	.0000
	8	.0288	.0204	.0328	.0594	.0298	.0667	.0393	.0516	.0107	.0107	.0052	.0000	.0000
	9	.0795	.0516	.0553	.0536	.0253	.0288	.0156	.0611	.0296	.0296	.0217	.0013	.0001
	10	.0216	.0620	.0287	.0048	.0099	.0175	.0167	.0048	.0400	.0400	.0400	.0106	.0080
	11	.0105	.0039	.0093	.0131	.0061	.0031	.0111	.0159	.0129	.0129	.0229	.0324	.0244
	12	.0180	.0157	.0151	.0168	.0161	.0130	.0338	.0175	.0122	.0122	.0112	.0098	.0197
	13	.0167	.0166	.0201	.0154	.0207	.0216	.0434	.0164	.0146	.0146	.0130	.0009	.0027
	14	.0140	.0178	.0126	.0112	.0127	.0172	.0639	.0120	.0163	.0163	.0159	.0053	.0024
	15	.7289	.7355	.7455	.7378	.7053	.7087	.3940	.7239	.8074	.8074	.8151	.9223	.9255

Table B.4: The size distribution of AO integrals for the C_2 molecule using the aug-cc-pVDZ basis and one GCF with exponent $\gamma = 9$. The stack each integral belongs to is given by $\Delta = -\mathrm{int}(\log_{10}|I_{\mathrm{size}}|)$. Within each part of the table frequencies given on stacks 0–15 add up to 1 for each integral type.

	Δ	I21	I22	I2K1	I2K2	I2V1	I2V2	I2C0	I2C1	I3C1	I3E1	I3C2	I3E2	I32
$R_{\text{C-C}} = 200\,pm$	0	.0000	.0000	.0002	.0003	.0004	.0002	.0522	.0001	.0000	.0000	.0000	.0000	.0000
	1	.0003	.0000	.0017	.0080	.0059	.0004	.5165	.0030	.0000	.0000	.0000	.0000	.0000
	2	.0307	.0037	.0468	.3701	.3366	.0847	.3246	.2542	.0009	.0009	.0002	.0000	.0000
	3	.5590	.2657	.3659	.4867	.5130	.6314	.0223	.5784	.0815	.0815	.0144	.0002	.0000
	4	.3068	.5716	.4009	.0509	.0743	.2008	.0002	.0790	.5592	.5592	.3394	.0136	.0022
	5	.0194	.0738	.0906	.0009	.0030	.0155	.0000	.0016	.3118	.3118	.5269	.2750	.1152
	6	.0001	.0015	.0062	.0000	.0003	.0001	.0000	.0002	.0268	.0268	.0954	.5476	.5397
	7	.0000	.0000	.0004	.0000	.0000	.0000	.0000	.0000	.0011	.0011	.0048	.1370	.2975
	8	.0000	.0000	.0000	.0000	.0000	.0000	.0000	.0000	.0000	.0000	.0002	.0077	.0258
	9	.0000	.0000	.0000	.0000	.0000	.0000	.0000	.0000	.0000	.0000	.0000	.0001	.0007
	10	.0000	.0000	.0000	.0000	.0000	.0000	.0000	.0000	.0000	.0000	.0000	.0000	.0000
	11	.0000	.0000	.0000	.0000	.0000	.0000	.0000	.0000	.0000	.0000	.0000	.0000	.0000
	12	.0000	.0000	.0000	.0000	.0000	.0000	.0000	.0000	.0000	.0000	.0000	.0000	.0000
	13	.0000	.0000	.0000	.0000	.0000	.0000	.0000	.0000	.0000	.0000	.0000	.0000	.0000
	14	.0000	.0000	.0000	.0000	.0000	.0000	.0000	.0000	.0000	.0000	.0000	.0000	.0000
	15	.0837	.0837	.0872	.0831	.0665	.0668	.0843	.0835	.0187	.0187	.0187	.0187	.0188
$R_{\text{C-C}} = 400\,pm$	0	.0000	.0000	.0001	.0001	.0001	.0000	.0216	.0001	.0000	.0000	.0000	.0000	.0000
	1	.0001	.0000	.0011	.0064	.0016	.0002	.1385	.0028	.0000	.0000	.0000	.0000	.0000
	2	.0128	.0034	.0144	.0491	.0278	.0089	.2777	.0449	.0005	.0005	.0001	.0000	.0000
	3	.0735	.0460	.0435	.1628	.1419	.0835	.2144	.1391	.0079	.0079	.0028	.0001	.0000
	4	.2042	.1428	.1165	.1954	.2498	.2247	.0789	.2054	.0494	.0494	.0232	.0024	.0008
	5	.1753	.2028	.2082	.1191	.1357	.1900	.0457	.1365	.1493	.1493	.1037	.0124	.0076
	6	.0928	.1340	.1387	.0578	.0504	.0807	.0574	.0621	.1842	.1842	.1811	.0495	.0285
	7	.0630	.0620	.0931	.0857	.0703	.0450	.0475	.0819	.1239	.1239	.1564	.1109	.0903
	8	.1026	.0814	.0945	.1043	.1106	.0946	.0203	.1051	.0792	.0792	.0900	.1221	.1266
	9	.0981	.1058	.0936	.0758	.0854	.1110	.0080	.0788	.0999	.0999	.0847	.0879	.1038
	10	.0597	.0777	.0592	.0412	.0361	.0558	.0037	.0398	.1123	.1123	.1102	.0794	.0754
	11	.0234	.0411	.0262	.0134	.0154	.0248	.0029	.0140	.0826	.0826	.1011	.1224	.1087
	12	.0074	.0132	.0087	.0040	.0042	.0082	.0009	.0043	.0421	.0421	.0604	.1401	.1395
	13	.0029	.0047	.0022	.0022	.0018	.0033	.0003	.0019	.0218	.0218	.0295	.1082	.1232
	14	.0012	.0019	.0002	.0005	.0004	.0008	.0001	.0004	.0140	.0140	.0173	.0639	.0781
	15	.0830	.0833	.0997	.0823	.0684	.0685	.0821	.0828	.0330	.0330	.0395	.1005	.1177
$R_{\text{C-C}} = 600\,pm$	0	.0000	.0000	.0001	.0001	.0001	.0000	.0165	.0001	.0000	.0000	.0000	.0000	.0000
	1	.0001	.0000	.0011	.0063	.0011	.0001	.0683	.0027	.0000	.0000	.0000	.0000	.0000
	2	.0128	.0033	.0138	.0438	.0208	.0077	.0884	.0428	.0004	.0004	.0001	.0000	.0000
	3	.0503	.0435	.0312	.0209	.0434	.0361	.1357	.0287	.0061	.0061	.0024	.0001	.0000
	4	.0242	.0279	.0262	.0501	.0879	.0745	.1092	.0427	.0167	.0167	.0131	.0024	.0008
	5	.0610	.0428	.0425	.0553	.0496	.0660	.0824	.0614	.0277	.0277	.0201	.0091	.0067
	6	.0464	.0616	.0451	.0579	.0475	.0380	.0673	.0529	.0506	.0506	.0424	.0082	.0091
	7	.0802	.0537	.0753	.0831	.0812	.0595	.0789	.0817	.0429	.0429	.0483	.0169	.0114
	8	.0715	.0816	.0966	.0820	.1005	.1128	.0449	.0801	.0553	.0553	.0463	.0190	.0219
	9	.0853	.0797	.0728	.0623	.0476	.0617	.0237	.0691	.0617	.0617	.0594	.0200	.0148
	10	.0495	.0682	.0599	.0395	.0454	.0461	.0133	.0394	.0755	.0755	.0700	.0375	.0348
	11	.0422	.0393	.0427	.0351	.0346	.0379	.0100	.0379	.0577	.0577	.0678	.0453	.0391
	12	.0289	.0376	.0315	.0238	.0259	.0355	.0099	.0255	.0492	.0492	.0512	.0512	.0557
	13	.0178	.0255	.0168	.0109	.0137	.0197	.0172	.0110	.0426	.0426	.0458	.0363	.0382
	14	.0079	.0111	.0114	.0046	.0050	.0071	.0335	.0048	.0355	.0355	.0398	.0395	.0390
	15	.4216	.4240	.4329	.4242	.3956	.3972	.2008	.4193	.4779	.4779	.4934	.7146	.7285

Table B.5: Second-order correlation energies ($-E/\mathrm{mE_h}$) for the helium atom. The entry marked with a dagger (†) failed to converge in the equation solver.

Orbital basis	VOE	KL	KQ	PQ
cc-pVDZ	25.8283396	33.7507519	36.7128111	36.9501418
cc-pVTZ	33.1375618	35.8656663	37.1832756	37.2997823
cc-pVQZ	35.4780039	36.7677458	37.3262452	37.3628376
cc-pV5Z	36.4065109	37.0944128	37.3630241	37.3738190
aug-cc-pVDZ(s)	11.4999266	29.3884687	36.9410031	37.0912806
aug-cc-pVTZ(s)	12.8983089	29.4829479	37.0531861	37.2166302
aug-cc-pVQZ(s)	13.2837987	29.5715668	37.2075987	37.3352629
aug-cc-pV5Z(s)	13.4357419	29.5903158	37.2353877	37.3613037
aug-cc-pV6Z(s)	13.4717990	29.5941402	37.2392707	37.3689399
aug-cc-pVDZ	26.9625116	35.2322784	37.1692450	37.2925905
aug-cc-pVTZ(sp)	31.1114901	35.7675026	37.2509427	37.3459518
aug-cc-pVQZ(sp)	32.0629483	35.9724312	37.3495672	37.3724487
aug-cc-pV5Z(sp)	32.3483217	36.0169177	37.3689839	37.3768968
aug-cc-pV6Z(sp)	32.4241476	36.0389875	37.3723078	37.3772022
aug-cc-pVTZ	33.6208150	36.5168146	37.2546865	37.3609842
aug-cc-pVQZ(spd)	35.0309781	36.8841931	37.3515670	37.3754901
aug-cc-pV5Z(spd)	35.4579308	36.9785018	37.3712882	37.3771734
aug-cc-pV6Z(spd)	35.5816092	37.0031851	37.3752050	37.3772866
aug-cc-pVQZ	35.7241295	37.0605428	37.3535817	37.3757587
aug-cc-pV5Z(spdf)	36.2915310	37.1854102	37.3719707	n/a
aug-cc-pV6Z(spdf)	36.4685698	37.2247233	37.3754580	n/a
aug-cc-pV5Z	36.5340057	37.2344197	37.3724829	n/a
aug-cc-pV6Z(spdfg)	36.7768787	37.2566701	†	n/a
aug-cc-pV6Z	36.8819326	37.3053519	n/a	n/a
d-aug-cc-pVDZ	27.0053301	35.2896959	37.1904140	37.3079330
d-aug-cc-pVTZ(sp)	31.1199958	35.7778669	37.2581569	37.3547094
d-aug-cc-pVQZ(sp)	32.0648825	35.9751658	37.3505827	37.3736193
d-aug-cc-pV5Z(sp)	32.3491615	36.0193452	37.3693452	37.3769670
d-aug-cc-pVTZ	33.6340446	36.5312307	37.2627313	37.3678115
d-aug-cc-pVQZ(spd)	35.0352615	36.8914008	37.3527960	37.3761708

Table B.6: Second-order correlation energies ($-E/\mathrm{mE_h}$) for the helium dimer. An inter-nuclear distance of $5.6\mathrm{a_0}$ was used.

Orbital basis	VOE	KL	KQ	PQ
cc-pVDZ	51.6634092	67.9745642	73.5603014	73.9383031
cc-pVTZ	66.2940279	71.8541489	74.4109357	74.6425264
cc-pVQZ	70.9843200	73.6154395	74.6964127	n/a
aug-cc-pVDZ(s)	22.9997077	59.3853235	73.9294819	74.2059079
aug-cc-pVTZ(s)	25.7937448	59.4093538	74.1438677	74.4535003
aug-cc-pVQZ(s)	26.5639368	59.5871140	74.4410613	74.6887158
aug-cc-pV5Z(s)	26.8677850	59.6246381	74.4976666	74.7393166
aug-cc-pV6Z(s)	26.9399968	59.6400197	74.5053953	74.7549872
aug-cc-pVDZ	53.9749009	70.6568190	74.4029833	74.6366350
aug-cc-pVTZ(sp)	62.2613806	71.6567364	74.5544924	74.7428267
aug-cc-pVQZ(sp)	64.1618525	72.0659499	74.7467067	74.7947802
aug-cc-pV5Z(sp)	64.7320344	72.1578087	74.7845331	74.8023462
aug-cc-pV6Z(sp)	64.8838531	72.2011736	74.7911152	74.8041685
aug-cc-pVTZ	67.2896986	73.1122844	74.5662835	74.7745032
aug-cc-pVQZ(spd)	70.1092366	73.8444521	74.7552083	n/a
aug-cc-pV5Z(spd)	70.9628443	74.0307299	74.7938016	n/a
aug-cc-pV6Z(spd)	71.2100451	74.0783222	74.8008871	n/a
aug-cc-pVQZ	71.4969535	74.1840905	74.7591960	n/a
d-aug-cc-pVDZ	54.0680050	70.7596231	74.4406590	74.6668764
d-aug-cc-pVTZ(sp)	62.2800868	71.6770247	74.5693601	74.7597793
d-aug-cc-pVQZ(sp)	64.1665903	72.0714322	74.7491134	74.7972713
d-aug-cc-pV5Z(sp)	64.7344929	72.1623792	74.7857329	74.8038410
d-aug-cc-pVTZ	67.3247445	73.1591661	74.5849510	n/a
d-aug-cc-pVQZ(spd)	70.1195356	73.8591108	74.7580983	n/a

Table B.7: Second-order correlation energies ($-E/\mathrm{mE_h}$) for the helium atom with a ghost basis at a distance of $5.6\,a_0$. Results for the pq-ansatz could not be obtained due to problems with singular matrices.

Orbital basis	VOE	KL	KQ
cc-pVDZ	25.8291499	33.7511534	36.7210450
cc-pVTZ	33.1385493	35.8665516	37.1849852
cc-pVQZ	35.4786865	36.7683524	37.3270348
aug-cc-pVDZ(s)	11.5020125	29.3891785	36.9421582
aug-cc-pVTZ(s)	12.8989897	29.4831533	37.0535724
aug-cc-pVQZ(s)	13.2840192	29.5717098	37.2076486
aug-cc-pV5Z(s)	13.4359002	29.5904548	37.2354038
aug-cc-pV6Z(s)	13.4719769	29.5943159	37.2392817
aug-cc-pVDZ	26.9701214	35.2400077	37.1698435
aug-cc-pVTZ(sp)	31.1132388	35.7696095	37.2514610
aug-cc-pVQZ(sp)	32.0634846	35.9731637	37.3496909
aug-cc-pV5Z(sp)	32.3485805	36.0175302	37.3690318
aug-cc-pV6Z(sp)	32.4243317	36.0393383	37.3723239
aug-cc-pVTZ	33.6228816	36.5191476	37.2553186
aug-cc-pVQZ(spd)	35.0319239	36.8857237	37.3517408
aug-cc-pV5Z(spd)	35.4584578	36.9792453	37.3713643
aug-cc-pV6Z(spd)	35.5818731	37.0034954	37.3752208
aug-cc-pVQZ	35.7251164	37.0620342	37.3537622
d-aug-cc-pVDZ	27.0164478	35.2959904	37.1898620
d-aug-cc-pVTZ(sp)	31.1222891	35.7802640	37.2586302
d-aug-cc-pVQZ(sp)	32.0655051	35.9759700	37.3506479
d-aug-cc-pV5Z(sp)	32.3494583	36.0199726	37.3693793
d-aug-cc-pVTZ	33.6396880	36.5369593	37.2643691
d-aug-cc-pVQZ(spd)	35.0367506	36.8935047	37.3529859

Table B.8: Energies ($-E/\mathrm{mE_h}$) for the helium atom with a ghost basis. The distance is given in $\mathrm{a_0}$. For the Hartree–Fock and the conventional MP2 calculations the basis set d-aug-cc-pV6Z was used. For the MP2 calculations with geminals the basis set was aug-cc-pVQZ(spd).

Distance	HF	VOE	KL	KQ
4.8	2861.6733399	36.8861319	36.8871824	37.3518463
5.0	2861.6733248	36.8858527	36.8867889	37.3518173
5.1	2861.6733195	36.8857270	36.8865972	37.3518029
5.2	2861.6733160	36.8856088	36.8864093	37.3517887
5.4	2861.6733127	36.8853923	36.8860502	37.3517625
5.6	2861.6733116	36.8851980	36.8857237	37.3517408
5.8	2861.6733107	36.8850228	36.8854403	37.3517244
6.0	2861.6733096	36.8848660	36.8852047	37.3517117
6.5	2861.6733017	36.8845547	36.8848036	37.3516838
7.0	2861.6732835	36.8843370	36.8845814	37.3516462
7.5	2861.6732712	36.8841744	36.8844489	37.3516130
8.0	2861.6732653	36.8840557	36.8843649	37.3516032
8.5	2861.6732554	36.8839780	36.8843103	37.3515814
∞	2861.6732130	36.8837739	36.8841931	37.3515670

Table B.9: Energies ($-E/\mathrm{mE_h}$) for the helium dimer. The internuclear distance is given in $\mathrm{a_0}$. For the Hartree–Fock and the conventional MP2 calculations the basis set d-aug-cc-pV6Z was used. For the MP2 calculations with geminals the basis set was aug-cc-pVQZ(spd).

Distance	HF	VOE	KL	KQ
4.8	5723.1434424	73.9024690	73.9312853	74.8357142
5.0	5723.2210981	73.8734973	73.9012405	74.8070068
5.1	5723.2480474	73.8616350	73.8887696	74.7952983
5.2	5723.2692552	73.8512219	73.8777133	74.7850491
5.4	5723.2990439	73.8340177	73.8591627	74.7681938
5.6	5723.3174243	73.8206645	73.8444521	74.7552083
5.8	5723.3287378	73.8102465	73.8327348	74.7451650
6.0	5723.3356857	73.8020764	73.8233696	74.7373594
6.5	5723.3434308	73.7883950	73.8072745	74.7244293
7.0	5723.3456547	73.7806083	73.7978805	74.7170954
7.5	5723.3462821	73.7759959	73.7922250	74.7128689
8.0	5723.3464568	73.7731682	73.7884353	74.7099956
8.5	5723.3464900	73.7713948	73.7852171	74.7080675

Table B.10: Interaction energies ($E/\mu\mathrm{E_h}$) for the helium dimer. The inter-nuclear distance is given in atomic units. For the Hartree–Fock and the conventional MP2 calculations the basis set d-aug-cc-pV6Z was used. For the MP2 calculations with geminals the basis set was aug-cc-pVQZ(spd).

Distance	HF	VOE	KL	KQ
4.8	−203.2374	130.2052	156.9205	132.0216
5.0	−125.5515	101.7919	127.6627	103.3722
5.1	−98.5916	90.1810	115.5752	91.6925
5.2	−77.3768	80.0043	104.8947	81.4717
5.4	−47.5815	63.2331	87.0623	64.6688
5.6	−29.1989	50.2685	73.0047	51.7267
5.8	−17.8836	40.2009	61.8542	41.7162
6.0	−10.9335	32.3444	52.9602	33.9918
6.5	−3.1726	19.2856	37.6673	21.0617
7.0	−.9123	11.9343	28.7177	13.8030
7.5	−.2603	7.6471	23.3272	9.6429
8.0	−.0738	5.0568	19.7055	6.7892
8.5	−.0208	3.4388	16.5965	4.9047

Table B.11: All-electron second-order correlation energies ($-E/\mathrm{mE_h}$) for the beryllium atom. The ANO basis sets are listed in appendix C. Basis sets marked with an asterisk (*) are used uncontracted.

Orbital basis		VOE	KL	KQ	PQ
ANO-1	(3s)	2.0500671	51.9700515	59.5924656	60.0480308
ANO-1	(4s)	3.7537654	52.5806604	61.1019983	62.1986634
ANO-1	(5s)	6.7935157	53.7589910	64.9110746	66.3533722
ANO-1	(6s)	14.8354794	55.6068514	65.9401855	67.0366919
ANO-1	(10s)*	15.6764185	55.6747570	66.0407661	67.4182203
ANO-1	(6s1p)	34.8606891	68.2236437	75.3069070	75.9839822
ANO-1	(6s2p)	36.4047854	68.4433675	75.4197070	76.1764601
ANO-1	(6s3p)	38.6340904	69.5358581	75.6998620	76.2464388
ANO-1	(6s4p)	42.0004484	70.2106081	75.7449296	76.2622820
ANO-1	(10s4p)*	42.8405675	70.2839948	75.8073821	76.2763501
ANO-1	(6s4p1d)	44.8933497	71.1359768	76.0720001	76.2985333
ANO-1	(6s4p2d)	45.4863128	71.2871452	76.0972040	76.3042673
ANO-1	(6s4p3d)	45.6132845	71.3525249	76.1077354	76.3071769
ANO-1	(10s4p3d)*	46.4532133	71.4272452	76.1668369	76.3168693
ANO-2	(14s)*	15.9116278	55.7636497	66.2388156	68.2173195
ANO-2	(14s4p)*[a]	43.0976956	70.3291847	75.8662703	76.3326173
ANO-2	(14s9p)*	64.0517928	74.1842257	75.9386530	76.3489560
ANO-2	(14s9p3d)*[b]	67.6725935	75.2720105	76.3140458	76.3554699
ANO-2	(14s9p4d)*	68.2785773	75.3927002	76.3178389	n/a
ANO-2	(14s9p4d3f)*	69.4012176	75.6215710	76.3454845	n/a

[a] Using the four p-orbitals from the ANO-1 basis set.
[b] Using the three d-orbitals from the ANO-1 basis set.

Table B.12: All-electron second-order correlation energies ($-E/\mathrm{mE_h}$) for the neon atom. A dagger (†) is given for calculations that failed to converge, and a double dagger (††) is given for calculations that are currently too computationally demanding. The (‡) is explained in the text.

Orbital basis	VOE	KL	KQ	PQ
cc-pVDZ	187.5671849	300.9758221	346.9322131	356.3721867
cc-pVTZ	277.2916007	350.3179262	380.6103510	383.9947580
cc-pVQZ	326.2584438	371.7724088	386.1863930	387.2971932
cc-pCVDZ	228.3024582	310.4283062	356.3977967	364.1591298
cc-pCVTZ	329.1000331	362.4669245	383.6677557	385.4860928
cc-pCVQZ	361.5148089	378.5113843	†	n/a
aug-cc-pVDZ	209.0598646	323.5838432	369.2693485	380.6600417
aug-cc-pVTZ	285.9063227	358.8924258	384.8629582	387.5515309
aug-cc-pVQZ	330.0104735	375.5079092	387.2148488	n/a
aug-cc-pCVDZ (sp)	157.7052447	265.2959277	344.3857403	356.1744428
aug-cc-pCVTZ (sp)	187.4763890	273.9064328	357.1121973	364.5434555
aug-cc-pCVQZ (sp)	190.9429692	275.7315810	358.5871838	365.7442404
aug-cc-pCV5Z (sp)	191.7427128	276.2621516	359.2356941	366.3603952
aug-cc-pCVDZ	249.8950577	333.1340121	375.0497838	384.5626936
aug-cc-pCVTZ (spd)	309.0780668	353.9141661	386.2315890	388.0079499
aug-cc-pCVQZ (spd)	319.3442255	358.2311241	387.1361791	n/a
aug-cc-pCV5Z (spd)	321.5666821	359.3687694		n/a
aug-cc-pCVTZ	337.2915361	370.7179317	387.1358532	388.1886004
aug-cc-pCVQZ (spdf)	354.1847489	377.1694689	†	n/a
aug-cc-pCVQZ	365.1575107	382.1186939	††	n/a
aug-cc-pCV5Z‡	375.9331092	385.5411256	††	n/a

Table B.13: Second-order correlation energies ($-E/\mathrm{mE_h}$) for the hydrogen molecule. An inter-nuclear distance of 74.08481 pm was used. Energies marked with a double-dagger (‡) undershoot the true energy, probably due to a non-positive-definite Fock operator.

Orbital basis	VOE	KL	KQ	PQ
cc pVDZ	26.3792393	31.6303701	33.5803206	33.8018975
cc-pVTZ	31.6790935	33.4759448	34.1512751	34.2262683
cc-pVQZ	33.1139759	33.9950799	34.2260982	n/a
aug-cc-pVDZ(s)	15.9526977	29.8195520	33.5348578	33.7942858
aug-cc-pVTZ(s)	17.9143332	30.0687929	33.8360853	34.1316651
aug-cc-pVQZ(s)	18.3559651	30.1145183	33.9337122	34.3231950‡
aug-cc-pV5Z (s)	18.4308635	30.1313834	33.9426885	34.3679945‡
aug-cc-pVDZ	27.2901476	32.7392165	33.8788877	34.0464343
aug-cc-pVTZ(sp)	29.8816660	33.3089378	34.1774876	34.2434412
aug-cc-pVQZ(sp)	30.4520480	33.4952722	34.2198759	34.2459881
aug-cc-pV5Z (sp)	30.6510425	33.5285683	34.2293332	34.2490788
aug-cc-pVTZ	31.9882134	33.8235774	34.2088953	34.2524911
aug-cc-pVQZ(spd)	32.7432582	34.0612479	34.2398888	n/a
aug-cc-pV5Z (spd)	32.9806260	34.1084555	34.2467649	n/a
aug-cc-pVQZ	33.2525468	34.1394478	34.2414171	n/a

Table B.14: All electron second-order correlation energies ($-E/\mathrm{mE_h}$) for the lithium hydride molecule with an inter-nuclear distance of r(Li–H)=159.5469 pm. Due to problems with singular matrices the pq-ansatz could not be used. Basis sets marked with an asterisk (*) are used uncontracted.

Orbital basis (Li,H)		VOE	KL	KQ
ANO-1	$(10s4p, 7s)^*$	28.9697878	58.1340277	70.5491681
ANO-1	$(10s4p3d, 7s)^*$	32.8310082	60.7579716	71.4194854
ANO-1	$(10s4p, 7s3p)^*$	40.7978142	63.7946890	72.3729029
ANO-1	$(10s4p3d, 7s3p)^*$	41.8034774	64.4968638	72.5106350
ANO-2	$(14s9p, 8s)^*$	49.9911124	63.8145582	70.8995447
ANO-2	$(14s9p4d, 8s)^*$	54.4061075	66.7187361	71.8082577
ANO-2	$(14s9p, 8s4p)^*$	61.7790297	69.5240877	72.6779843
ANO-2	$(14s9p4d, 8s4p)^*$	63.0587529	70.3822235	72.8090833
ANO-2	$(14s9p4d3f, 8s4p)^*$	63.6824982	70.7895194	72.8504877
ANO-2	$(14s9p4d, 8s4p3d)^*$	65.2430876	71.2024629	72.8636829
ANO-2	$(14s9p4d3f, 8s4p3d)^*$	65.4036246	71.3257233	72.8767305

Table B.15: All electron second-order correlation energies ($-E/\mathrm{mE_h}$) for the hydrogen fluoride molecule. For the structure we have used r(H–F)=91.6958 pm.

Orbital basis (F,H)	VOE	KL	KQ	PQ
cc-pVDZ	203.7801289	306.8868724	350.4820376	360.2138455
cc-pCVDZ	242.8538056	316.3286863	356.6340842	365.2383995
aug-cc-pVDZ	224.5636440	328.3577769	369.5061041	379.2051576
aug-cc-pCVDZ (sp , s)	173.7640838	270.1521942	342.2015061	353.9289289
aug-cc-pCVDZ (sp , sp)	181.8074065	277.4114011	347.2352492	359.9886782
aug-cc-pCVDZ (spd, s)	260.0109489	334.5857683	373.0188841	381.5940191
aug-cc-pCVDZ	263.7082488	337.7896370	374.0281698	382.0054614
aug-cc-pCVTZ (sp , s)	197.2089216	276.2098440	350.8738930	360.0519520
aug-cc-pCVTZ (sp , sp)	207.6018747	285.1132241	357.0505346	366.6610544
aug-cc-pCVTZ (spd, s)	309.1367529	351.2596695	381.3618637	383.6854768
aug-cc-pCVTZ (spd, sp)	313.5078326	354.7045289	382.3451163	n/a
aug-cc-pCVTZ (spd, spd)	317.0040330	357.3456341	382.6404160	n/a
aug-cc-pCVTZ	339.8909722	370.4108039	383.6904579	n/a
aug-cc-pCVQZ (sp , s)	200.4627606	277.7438019	352.0299913	361.1717311
aug-cc-pCVQZ (sp , sp)	212.0211688	287.4722186	358.6465526	367.9188748
aug-cc-pCVQZ (spd, s)	318.4742471	354.9366610	382.2475197	n/a
aug-cc-pCVQZ (spd, sp)	323.3147986	358.6534536	383.2213287	n/a
aug-cc-pCVQZ (spd, spd)	327.5312438	361.6761805	383.5292980	n/a

Table B.16: All electron second-order correlation energies ($-E/\mathrm{mE_h}$) for the water molecule. Except for the calculation marked with an [b], all geometries are as specified in tablenote [a].

Orbital basis (O,H)	VOE	KL	KQ	PQ
cc-pVDZ	203.9598954	298.0677188	334.2787467	342.9660027
cc-pCVDZ	241.3264464	307.0453161	339.1281887	346.6466825
aug-cc-pVDZ	221.8278994	315.7893544	349.9403721	357.7118544
aug-cc-pCVDZ (sp ,s)	171.6056913	258.9298023	320.6873018	332.6685883
aug-cc-pCVDZ (sp ,sp)	192.9769424	277.1660209	332.4220242	346.6383636
aug-cc-pCVDZ (spd,s)	249.8074029	317.4488319	351.7900855	359.3508897
aug-cc-pCVDZ	259.2360635	324.7248991	353.4825115	359.6559085
aug-cc-pCVTZ (sp ,s)	190.5105297	263.3925722	326.7113670	337.5135991
aug-cc-pCVTZ (sp ,sp)	217.6486357	285.8997955	341.1000204	352.5640490
aug-cc-pCVTZ (spd,s)	289.5892728	330.1781648	357.6645361	360.6535469
aug-cc-pCVTZ (spd,sp)	300.2146011	337.7533368	359.6505337	n/a
aug-cc-pCVTZ (spd,spd)	307.8619366	342.8268330	360.3492427	n/a
aug-cc-pCVTZ[b]	324.2788891	351.4845393	361.3928101	n/a
aug-cc-pCVQZ (sp ,s)	193.8448519	264.8357442	327.8663561	338.8423326
aug-cc-pCVQZ (sp ,sp)	223.4234073	288.9986733	342.9118133	n/a
aug-cc-pCVQZ (spd,s)	298.1965806	333.2011554	358.5168282	n/a
aug-cc-pCVQZ (spd,sp)	309.6164507	341.3354796	360.4936011	n/a

[a] Structure: $\angle$(HOH)=104.52° and r(O–H)=95.720 pm.
[b] Structure: $\angle$(HOH)=104.34° and r(O–H)=95.885 pm.

Table B.17: All electron second-order correlation energies ($-E/\mathrm{mE_h}$) for linear[a] and bent[b] structures of the water molecule. Geometries are taken from Ref. [133].

	Orbital basis (O,H)	VOE	KL	KQ	PQ
linear	cc-pVDZ	202.5506202	297.7685262	335.1683221	344.6981702
	cc-pVTZ	275.1860955	335.8536189	357.3103755	n/a
	cc-pCVDZ	239.7932936	306.3355532	339.8499531	347.8284880
	cc-pCVTZ	317.5979608	345.4894664	359.0211532	n/a
	aug-cc-pVDZ	222.3795193	317.6051626	352.3118494	360.3802954
	aug-cc-pVTZ (spd,sp)	258.4262031	329.5601977	360.3965522	n/a
	aug-cc-pVTZ	284.7503224	343.8506221	362.1609772	n/a
	aug-cc-pCVDZ	259.7010394	326.1707648	355.6626241	361.9945279
	aug-cc-pCVDZ + ICP	264.4372252	329.5539008	356.6938085	n/a
	aug-cc-pCVTZ (spd,sp)	301.1787044	339.2258233	361.9707977	n/a
	aug-cc-pCVTZ	325.3651259	352.9598414	363.4806754	n/a
	aug-cc-pCVQZ (spd,sp)	310.4454537	342.7557028	362.8109529	n/a
bent	cc-pVDZ	204.0913132	298.1654360	334.3788222	343.0676472
	cc-pVTZ	275.2005849	335.2938567	356.1342898	n/a
	cc-pCVDZ	241.4587978	307.1454273	339.2300260	346.7514592
	cc-pCVTZ	317.6257577	345.0909465	357.8706514	n/a
	aug-cc-pVDZ	221.9808397	315.9138760	350.0669050	357.8409535
	aug-cc-pVTZ (spd,sp)	257.6301690	328.1182590	358.1765303	n/a
	aug-cc-pVTZ	283.6584569	342.2230877	360.0664549	n/a
	aug-cc-pCVDZ	259.3897807	324.8516117	353.6098915	359.7872554
	aug-cc-pCVDZ + ICP	263.7726174	327.8895298	354.6404850	n/a
	aug-cc-pCVTZ (spd,sp)	300.3455303	337.8742016	359.7768385	n/a
	aug-cc-pCVTZ	324.2788891	351.4845393	361.3928101	n/a
	aug-cc-pCVQZ (spd,sp)	309.7415754	341.4537815	360.6196180	n/a

[a] Structure, bent : $\angle$(HOH)=104.343° and r(O–H)=95.885 pm.
[b] Structure, linear : $\angle$(HOH)=180.000° and r(O–H)=93.411 pm.

Table B.18: All-electron second-order correlation energies ($-E/\mathrm{mE_h}$) for the *cis*, *gauche*, and *trans* conformations of hydrogen peroxide. All energies were obtained using conventional MP2.

Basis	*cis*	*gauche*	*trans*
cc-pVDZ	390.5740485	390.8628834	391.2702935
cc-pVTZ	522.7329364	522.9151624	523.3307032
cc-pVQZ	596.2092874	596.3085115	596.7241990
cc-pV5Z	625.7749596	625.8768200	626.2523032
cc-pCVDZ	465.4366850	465.7438263	466.1525548
cc-pCVTZ	608.3992653	608.5340786	608.9745501
cc-pCVQZ	655.4359979	655.5209129	655.9650220
cc-pCV5Z	673.5691544	673.6217368	674.0628449
aug-cc-pVDZ	421.0351242	420.9615782	421.2846615
aug-cc-pVTZ	538.0707081	538.2607321	538.6181441
aug-cc-pVQZ	602.6217076	602.7073973	603.0620286
aug-cc-pV5Z	629.1126771	629.1611982	629.5393709
aug-cc-pCVDZ	495.9839828	495.9241639	496.2509231
aug-cc-pCVTZ	619.8469604	619.8648870	620.2485387
aug-cc-pCVQZ	660.7814651	660.8119266	661.2164110
aug-cc-pCV5Z	676.1555527	676.1791352	676.6030918

Table B.19: Hartree–Fock and all-electron second-order correlation energies ($-E/\mathrm{mE_h}$) for the *cis*, *gauche*, and *trans* conformations of hydrogen peroxide. The energies for these conformations are given in the top, middle, and bottom part of the table, respectively.

Basis	HF	VOE	KL	KQ
cc-pVDZ	150771.2012	390.5740485	577.3937636	643.1609623
cc-pVDZ + aug-H	150779.0404	399.7933716	585.7135006	655.0348786
cc-pVDZ + aug-O	150788.8281	419.3366570	606.9663333	668.4945075
aug-cc-pVDZ	150789.2442	421.0351242	608.5112712	670.4350304
aug-cc-pVDZ + d-aug-H	150789.3021	421.2967369	608.7188998	671.5634759
aug-cc-pCVDZ	150789.8267	495.9839700	623.5910010	676.9198280
aug-cc-pVTZ (spd,sp)	150823.3828	489.7217160	632.2016820	684.9133723
cc-pVDZ	150783.9858	390.8628834	577.6521101	643.9760662
cc-pVDZ + aug-H	150791.2695	399.9329510	585.4826804	656.1509016
cc-pVDZ + aug-O	150801.0203	419.3425454	607.2059955	668.7926730
aug-cc-pVDZ	150801.6102	420.9615782	608.5655580	670.7676936
aug-cc-pVDZ + d-aug-H	150801.6938	421.1463317	608.7177331	671.6450854
aug-cc-pCVDZ	150802.2004	495.9241672	623.6815021	677.1613079
aug-cc-pVTZ (spd,sp)	150835.5273	489.7595773	632.2288988	685.0062134
cc-pVDZ	150782.5339	391.2702935	578.2687393	644.2279227
cc-pVDZ + aug-H	150789.7578	399.6869763	585.0837837	655.7837852
cc-pVDZ + aug-O	150798.7539	419.8103951	607.7398724	669.2063081
aug-cc-pVDZ	150799.4666	421.2846615	608.9509079	671.0137681
aug-cc-pVDZ + d-aug-H	150799.5267	421.4885519	609.1220429	672.0972734
aug-cc-pCVDZ	150800.0666	496.2509232	623.9878765	677.4550080
aug-cc-pVTZ (spd,sp)	150833.1515	490.2536701	632.5102519	685.3771570

Appendix C

Listing of the ANO basis sets

Table C.1: Contraction matrix for the beryllium ANO-1 basis set given in Table C.2. The upper contraction block is for s-functions, the middle block is for p-functions and the lower contraction block is for d-functions

orb.1	orb.2	orb.3	orb.4	orb.5	orb.6
.00074493	-.0001427	.00015695	-.0001924	.00031124	-.0015720
.00572454	-.0011140	.00143307	-.0039778	.00436640	-.0060853
.02888438	-.0055613	.00562553	-.0015547	.00806211	-.0868722
.10711729	-.0218661	.03083988	-.1094019	.11885124	-.2255310
.28008888	-.0591129	.05111532	.09593658	.04010088	-1.689248
.44599943	-.1277397	.22985975	-1.147861	1.0707772	3.1302542
.28019932	-.1392613	.03609057	1.4866438	-1.879678	-1.852557
.01371755	.61480583	-1.639060	-.0525827	2.0015611	.72511480
-.0059191	.51190760	1.5342452	-1.350883	-2.549105	-.5918967
.00199796	-.0117939	.05893078	1.4017579	1.5882729	.27379324
.08652488	-.0268988	.59021034	-1.350149		
.32628265	-.8241012	.40781985	1.8100238		
.62511893	.22668606	-1.328299	-1.423157		
.13750967	.75535954	1.0185868	.74512678		
.27827904	-.9918512	.56070455			
.75227605	.45942600	-1.012287			
.15882957	.38362412	1.0974151			

Table C.2: The atomic natural orbital (ANO) basis sets used for hydrogen, lithium and beryllium in this work. The ANO-1 basis is taken from Ref.[73] while the ANO-2 basis is taken from Ref.[72]. The upper block is for s-function, the next block is for p-functions, and so forth.

Hydrogen		Lithium		Beryllium	
ANO-1	ANO-2	ANO-1	ANO-2	ANO-1	ANO-2
82.636374	188.61445	1359.4466	9497.9344	2732.3281	22628.599
12.409558	28.276596	204.02647	1416.8112	410.31981	3372.3181
2.8238540	6.4248300	46.549541	321.45994	93.672648	760.35040
.79767000	1.8150410	13.232594	91.124163	26.587957	211.74048
.25805300	.59106300	4.2861480	29.999891	8.6295600	67.223468
.08989100	.21214900	1.4955420	11.017631	3.0562640	23.372177
.03146200	.07989100	.54223800	4.3728010	1.1324240	8.7213730
	.02796200	.07396800	1.8312560	.18173200	3.4680910
		.02809500	.80226100	.05917000	1.4521440
		.00983300	.36264800	.02071000	.60861500
			.11399500		.25768600
			.05123700		.10417600
			.02246800		.04242700
			.00786000		.01484900
1.6625000	2.3050000	.38920000	13.119504	1.1677000	33.710184
.41560000	.80675000	.12170000	3.0774242	.36500000	8.0576495
.10390000	.28236200	.03800000	1.0988005	.11410000	2.8364714
	.09882700	.01190000	.43577840	.03570000	1.0999657
			.18024320		.44339640
			.07613330		.18222640
			.03254650		.07572410
			.01401820		.03168540
			.00490640		.01108990
	1.8190000	.34220000	.45000000	.54680000	1.4000000
	.72760000	.09170000	.15750000	.14650000	.49000000
	.29104000	.02460000	.05512500	.03930000	.17150000
			.01929380		.06002500
			.24000000		.50000000
			.09600000		.20000000
			.03840000		.08000000

List of acronyms

ANO	atomic natural orbital
AO	atomic orbital
aug-cc-pCVXZ	augmented cc-pCVXZ [basis]
aug-cc-pVXZ	augmented cc-pVXZ [basis]
BSSE	basis set superposition error
cc-pCVXZ	correlation consistent polarised core–valence X-tuple zeta [basis]
cc-pVXZ	correlation consistent polarised valence X-tuple zeta [basis]
CBS	complete basis set [model]
CCD	coupled-cluster doubles [model]
CCSD	coupled-cluster singles-and-doubles [model]
CCSD(T)	CCSD [model] with approximate triples correction
CI	configuration-interaction [model]
d-aug-cc-pVXZ	doubly augmented cc-pVXZ [basis]
DCD	double coset decomposition
DCR	double coset representative
DZ	double zeta [basis]
FCI	full CI [model]
GTO	Gaussian-type orbital [one-electron function]
GCF	Gaussian correlation factor [two-electron function]
GTG	Gaussian-type geminal [two-electron function]
HF	Hartree–Fock [model]
ICP	internal Counterpoise-correction
LHS	left hand side
LMP2	local MP2 [method]
MO	molecular orbital
MPn	nth-order Møller–Plesset [perturbation theory]

MRCI	multi-reference CI [model]
MP2-R12	MP2 with r_{12}-dependent basis function
MP2-R12/A	MP2-R12 standard approximation A
MP2-R12/B	MP2-R12 standard approximation B
MWO	modified weak-orthogonality
RHS	right hand side
RI	resolution of the identity
SCF	self-consistent field [model]
SO	a) symmetry orbital
	b) strong orthogonality
STO	Slater-type orbital
TZ	triple zeta [basis]
VOE	virtual orbital expansion
WO	weak orthogonality

References

[1] T. Helgaker, P. Jørgensen and J. Olsen, Molecular Structure Theory (John Wiley & Sons, Chichester, 2000).

[2] E. Hylleraas, Z. Phys. 54 (1929) 347.

[3] J. C. Slater, Phys. Rev. 31 (1928) 333.

[4] T. Kato, Comm. Pure Appl. Math. 10 (1957) 151.

[5] C. Schwartz, Phys. Rev. 126 (1962) 1015.

[6] W. Kutzelnigg, Theoret. Chim. Acta 68 (1985) 445.

[7] O. Sinanoğlu, Proc. Roy. Soc. London Ser. A 260 (1961) 379.

[8] O. Sinanoğlu, Phys. Rev. 122 (1961) 493.

[9] O. Sinanoğlu, J. Chem. Phys. 36 (1962) 3198.

[10] W. Klopper and W. Kutzelnigg, Chem. Phys. Lett. 134 (1986) 17.

[11] W. Kutzelnigg and W. Klopper, J. Chem. Phys. 94 (1991) 1985.

[12] K. Szalewicz, B. Jeziorski, H. J. Monkhorst and J. G. Zabolitzky, Chem. Phys. Lett. 91 (1982) 169.

[13] K. Szalewicz, B. Jeziorski, H. J. Monkhorst and J. G. Zabolitzky, J. Chem. Phys. 78 (1983) 1420.

[14] K. B. Wenzel, J. G. Zabolitzky, K. Szalewicz, B. Jeziorski and H. J. Monkhorst, J. Chem. Phys. 85 (1986) 3964.

[15] R. Bukowski, B. Jeziorski, S. Rybak and K. Szalewicz, J. Chem. Phys. 102 (1995) 888.

[16] E. K. U. Gross, E. Runge and O. Heinonen, Many Particle Theory, english ed. (Adam Hilger, Bristol, 1991).

[17] E. Merzbacher, Quantum Mechanics, 2nd ed. (John Wiley & Sons, New York, 1970).

[18] T. Helgaker, P. Jørgensen and J. Olsen, Molecular Structure Theory (John Wiley & Sons, Chichester, 2000).

[19] H. A. Bethe and E. E. Salpeter, Encyclopedia of Physics (Springer-Verlag, Berlin, 1957), Vol. 35, pp. 208–209.

[20] P. M. Morse and H. Feshbach, Methods of Theoretical Physics (McGraw-Hill, New York, 1953), pp. 1119–1120.

[21] P. O. Löwdin, in: Advances in chemical physics (Inter-science Publishers, New York, 1959), Vol. 2, pp. 207–322.

[22] E. Butkov, Mathematical Physics (Addison-Wesley, Reading, 1968).

[23] E. A. Hylleraas, Z. Phys. 65 (1930) 209.

[24] O. Sinanoğlu, Phys. Rev. 122 (1961) 491.

[25] B. Jeziorski and W. Kołos, Int. J. Quantum Chem. XII, Suppl. 1 (1978) 91.

[26] F. C. Sanders and C. W. Scherr, Phys. Rev. 181 (1969) 84.

[27] R. L. Matcha and W. Byers Brown, J. Chem. Phys. 48 (1968) 74.

[28] C. Møller and M. S. Plesset, Phys. Rev. 46 (1934) 618.

[29] T. Helgaker, P. Jørgensen and J. Olsen, Molecular Structure Theory (John Wiley & Sons, Chichester, 2000).

[30] W. M. Klopper, r_{12}–Dependent Wave Functions, Habilitationsschrift, November 1996, eidgenössischen Technischen Hochshule Zürich.

[31] D. C. Harris and M. D. Bertolucci, Symmetry and Spectroscopy (Dover, New York, 1978).

[32] T.-I. Shibuya and O. Sinanoğlu, Int. J. Quantum Chem. 7 (1973) 1145.

[33] T.-I. Shibuya and O. Sinanoğlu, Int. J. Quantum Chem. 7 (1973) 1159.

[34] O. Sinanoğlu, J. Chem. Phys. 36 (1962) 706.

[35] P. Pulay, Chem. Phys. Lett. 100 (1983) 151.

[36] P. Pulay and S. Sæbø, Theoret. Chim. Acta 69 (1986) 357.

[37] S. Sæbø and P. Pulay, J. Chem. Phys. 86 (1987) 914.

[38] S. Sæbø and P. Pulay, Ann. Rev. Phys. Chem. 44 (1993) 213.

[39] M. Schütz, G. Hetzer and H.-J. Werner, J. Chem. Phys. 111 (1999) 5691.

[40] G. Hetzer, M. Schütz, H. Stoll and H.-J. Werner, J. Chem. Phys. 113 (2000) 9443.

[41] V. Termath, W. Klopper and W. Kutzelnigg, J. Chem. Phys. 94 (1991) 2002.

[42] W. Klopper and C. C. M. Samson, J. Chem. Phys. 116 (2002) 6397.

[43] E. Eggarter and T. P. Eggarter, J. Phys. B: At. Mol. Phys. 11 (1978) 1157.

[44] E. Eggarter and T. P. Eggarter, J. Phys. B: At. Mol. Phys. 11 (1978) 2069.

[45] K. Szalewicz, J. G. Zabolitzky, B. Jeziorski and H. J. Monkhorst, J. Chem. Phys. 81 (1984) 2723.

[46] B. J. Persson and P. Taylor, Theoret. Chim. Acta 97 (1997) 240.

[47] P. Dahle and P. R. Taylor, Theoret. Chem. Acc. 105 (2001) 401.

[48] E. R. Davidson, J. Chem. Phys. 62 (1975) 400.

[49] P. R. Taylor, in: Lecture Notes in Quantum Chemistry, edited by B. Roos (Springer-Verlag, Berlin, 1992).

[50] P. R. Taylor, Theoret. Chim. Acta 69 (1986) 447.

[51] GREMLIN, a program for calculating integrals over Gaussian-Type geminals. Release 1.0 (2002). Written by P. Dahle and T. Helgaker.

[52] The MOLECULE integral program, J. Almlöf, University of Stockholm, Institute of Physics Report 74-29 (1974).

[53] R. Lindh, U. Ryu and L. B., J. Chem. Phys. 95 (1991) 5889.

[54] DALTON, a molecular electronic structure program. Release 1.2 (2001). Written by T. Helgaker, H. J. Aa. Jensen, P. Jørgensen, J. Olsen, K. Ruud, H. Ågren, A.A. Auer, K.L. Bak, V. Bakken, O. Christiansen, S. Coriani, P. Dahle, E. K. Dalskov, T. Enevoldsen, B. Fernandez, C. Hättig, K. Hald, A. Halkier, H. Heiberg, H. Hettema, D. Jonsson, S. Kirpekar, R. Kobayashi, H. Koch, K. V. Mikkelsen, P. Norman, M. J. Packer, T. B. Pedersen, T. A. Ruden, A. Sanchez, T. Saue, S. P. A. Sauer, B. Schimmelpfennig, K. O. Sylvester-Hvid, P. R. Taylor, and O. Vahtras, http:www.kjemi.uio.no/software/dalton/dalton.html.

[55] C. C. M. Samson and W. Klopper, Comp. Phys. Commun. 149 (2002) 1.

[56] S. F. Boys, Proc. Roy. Soc. London Ser. A 258 (1960) 402.

[57] K. Singer, Proc. Roy. Soc. London Ser. A 258 (1960) 412.

[58] W. A. Lester and M. Krauss, J. Chem. Phys. 41 (1964) 1407.

[59] B. J. Persson and P. Taylor, J. Chem. Phys. 105 (1996) 5915.

[60] SORE program. Written by W. M. Klopper.

[61] M. J. Bearpark, N. C. Handy, R. D. Amos and P. E. Maslen, Theoret. Chim. Acta 79 (1991) 361.

[62] PSI. Release 3.0 (2000). Written by T. D. Crawford, C. D. Sherrill, E. F. Valeev, *et. al.*, PSITECH, Inc., Watkinsville, GA 30677.

[63] W. Klopper, Chem. Phys. Lett. 186 (1991) 583.

[64] GEMINAL91, a program for performing explicitly correlated MBPT/CCSD calculations. Written by R. Bukowski, B. Jeziorski, S. Rybak, and K. Szalewicz.

[65] T. H. Dunning Jr., J. Chem. Phys. 90 (1989) 1007.

[66] R. A. Kendall, T. H. Dunning Jr. and R. J. Harrison, J. Chem. Phys. 96 (1992) 6796.

[67] D. E. Woon and T. H. Dunning Jr., J. Chem. Phys. 98 (1993) 1358.

[68] D. E. Woon and T. H. Dunning Jr., J. Chem. Phys. 100 (1994) 2975.

[69] D. E. Woon and T. H. Dunning Jr., J. Chem. Phys. 103 (1995) 4572.

[70] Basis sets were obtained from the Extensible Computational Chemistry Environment Basis Set Database, Version 7/30/02, as developed and distributed by the Molecular Science Computing Facility, Environmental and Molecular Sciences Laboratory which is part of the Pacific Northwest Laboratory, P.O. Box 999, Richland, Washington 99352, USA, and funded by the U.S. Department of Energy. The Pacific Northwest Laboratory is a multi-program laboratory operated by Battelle Memorial Institue for the U.S. Department of Energy under contract DE-AC06-76RLO 1830. Contact David Feller or Karen Schuchardt for further information., http:www.emsl.pnl.gov:2080/forms/basisform.html.

[71] D. Feller (unpublished).

[72] P.-O. Widmark, P.-Å. Malmqvist and B. O. Roos, Theoret. Chim. Acta 77 (1990) 291.

[73] K. Pierloot, B. Dumez, P.-O. Widmark and B. O. Roos, Theoret. Chim. Acta 90 (1995) 87.

[74] F. van Duijneveldt, IBM technical research report RJ945, 1970.

[75] K. Szalewicz, B. Jeziorski, H. J. Monkhorst and J. G. Zabolitzky, J. Chem. Phys. 79 (1983) 5543.

[76] I. Foster, Designing and Building Parallel Programs (Addison-Wesley (Online), http:www-unix.mcs.anl.gov/dbpp/, 1995).

[77] M. E. Colvin, C. L. Janssen, R. A. Whiteside and C. H. Tong, Theoret. Chim. Acta 84 (1993) 301.

[78] M. Feyereisen and R. A. Kendall, Theoret. Chim. Acta 84 (1993) 289.

[79] I. T. Foster, J. L. Tilson, A. F. Wagner, R. L. Shepard, R. J. Harrison, R. A. Kendall and R. J. Littlefield, J. Comput. Chem. 17 (1996) 109.

[80] R. J. Harrison, M. F. Guest, R. A. Kendall, D. E. Bernholdt, A. T. Wong, M. Stave, J. L. Anchell, A. C. Hess, R. J. Littlefield, G. L. Fann, J. Nieplocha, G. S. Thomas, D. Elwood, J. L. Tilson, R. L. Shepard, A. F. Wagner, I. T. Foster, E. Lusk and R. Stevens, J. Comput. Chem. 17 (1996) 124.

[81] P. Dahle, Beregning av store molekylers egenskaper ved hjelp av parallelle metoder., cand.scient. thesis, May 1996, university of Oslo.

[82] ERI, a program for calculating electron repulsion integrals. Written by T. Helgaker.

[83] M. Häser and R. Ahlrichs, J. Comput. Chem. 10 (1989) 104.

[84] J.J Dongarra, J.R. Bunch, C.B. Moler, G.W. Stewart, LINPACK users' guide. Society for Industrial and Applied Mathematics, Philadelphia, PA, USA, 1979, ISBN 0-89871-172-X.

[85] J. R. Bunch and L. Kaufman, Math. Comp. 37 (1977) 163.

[86] N. J. Higham, Linear Algebra App. 287 (1998) 181.

[87] J. S. Lee and S. Y. Park, J. Chem. Phys. 112 (2000) 10746.

[88] R. Bukowski, B. Jeziorski and K. Szalewicz, J. Chem. Phys. 104 (1996) 3306.

[89] J. R. Flores, J. Chem. Phys. 98 (1993) 5642.

[90] G. A. Petersson, A. Bennet, T. G. Tensfeldt, M. A. Al-Laham, W. A. Shirley and J. Mantzaris, J. Chem. Phys. 89 (1988) 2193.

[91] P. Malinowski, M. Polasik and K. Janowski, J. Phys. B: At. Mol. Phys. 12 (1979) 2965.

[92] N. W. Winter, V. McKoy and A. Laferriere, Chem. Phys. Lett. 6 (1970) 175.

[93] H. F. King, J. Chem. Phys. 46 (1967) 705.

[94] S. Y. Park and J. S. Lee, J. Chem. Phys. 116 (2002) 5389.

[95] S. B. Huh and J. S. Lee, J. Chem. Phys. 118 (2003) 3035.

[96] J. B. Anderson, J. Chem. Phys. 115 (2001) 4546.

[97] M. Jeziorska, R. Bukowski, W. Cencek, M. Jaszuński, B. Jeziorski and K. Szalewicz, Coll. Czech. Chem. Commun. 68 (2003) 463.

[98] W. Klopper, J. Chem. Phys. 115 (2001) 761.

[99] P. J. Mohr and B. N. Taylor, J. Phys. Chem. Ref. Data 28 (1999) 1713.

[100] W. Klopper, J. Chem. Phys. 102 (1995) 6168.

[101] M. Gutowski and G. Chał asińsky, J. Chem. Phys. 98 (1993) 5540.

[102] R. Bukowski, B. Jeziorski and K. Szalewicz, J. Chem. Phys. 110 (1999) 4165.

[103] J. Noga, D. Tunega, W. Klopper and W. Kutzelnigg, J. Chem. Phys. 103 (1995) 309.

[104] S. Salomonsen and P. Öster, Phys. Rev. **A** 41 (1990) 4670.

[105] S. S. Alexander, M. H. J. and S. K., J. Chem. Phys. 85 (1986) 5821.

[106] K. Janowski, D. Rutowska and A. Rutowski, J. Phys. B: At. Mol. Phys. 15 (1982) 4063.

[107] J. Komasa, W. Cencek and J. Rychlewski, Phys. Rev. **A** 52 (1995) 4500.

[108] P. Wind, W. Klopper and T. Helgaker, Theoret. Chem. Acc. 107 (2002) 173.

[109] I. Lindgren and S. Salomonsen, Phys. Scr. 21 (1980) 335.

[110] I. Lindgren and M. J., Atomic Many–Body Theory (Springer, New York, 1982).

[111] K. Janowski and P. Malinowski, Phys. Rev. **A** 21 (1980) 45.

[112] S. J. Chakravorty, S. R. Gwaltney, E. R. Davidson, F. A. Parpia and C. Froese-Fischer, Phys. Rev. **A** 47 (1993) 3649.

[113] W. Klopper and W. Kutzelnigg, J. Chem. Phys. 94 (1991) 2020.

[114] B. Jeziorski, K. Monkhorst, Hendrik J. Szalewicz and J. G. Zabolitzky, J. Chem. Phys. 81 (1984) 368.

[115] W. Cencek and W. Kutzelnigg, Chem. Phys. Lett. 266 (1997) 383.

[116] B. Jeziorski, R. Bukowski and K. Szalewicz, Int. J. Quantum Chem. 61 (1997) 769.

[117] R. N. Hill, Int. J. Quantum Chem. 68 (1998) 357.

[118] S. S. Alexander, M. H. J. and S. K., J. Chem. Phys. 87 (1987) 3976.

[119] W. Klopper, Mol. Phys. 99 (2001) 481.

[120] H. Müller, W. Kutzelnigg and J. Noga, Mol. Phys. 92 (1997) 535.

[121] K. B. Wenzel and J. G. Zabolitzky, J. Chim. Phys. 84 (1987) 691.

[122] L. Wallace, P. Bernath, W. Livingstone, K. Hinkle, J. Busler, B. Gou and K. Zhang, Science 268 (1995) 1155.

[123] T. Oka, Science 277 (1997) 328.

[124] O. L. Polyansky, N. F. Zobov, J. Tennyson, J. A. Lotoski and P. F. Bernath, J. Mol. Spectrosc. 184 (1997) 35.

[125] O. N. Ulenikov and G. A. Ushakova, J. Mol. Spectrosc. 117 (1986) 195.

[126] N. F. Zobov, O. L. Polyansky, C. R. Le Sueur and J. Tennyson, Chem. Phys. Lett. 260 (1996) 381.

[127] H. Partridge and D. W. Schwenke, J. Chem. Phys. 106 (1997) 4618.

[128] A. G. Császár, J. S. Kain, O. L. Polyansky, N. F. Zobov and J. Tennyson, Chem. Phys. Lett. 293 (1998) 317.

[129] A. G. Császár, J. S. Kain, O. L. Polyansky, N. F. Zobov and J. Tennyson, Chem. Phys. Lett. 312 (1999) 613.

[130] J. S. Kain, O. L. Polyansky and J. Tennyson, Chem. Phys. Lett. 317 (2000) 365.

[131] A. G. Császár, W. D. Allen and H. F. Schaefer III, J. Chem. Phys. 108 (1998) 9751.

[132] G. Tarczay, A. G. Császár, W. Klopper, V. Szalay, W. D. Allen and H. F. Schaefer III, J. Chem. Phys. 110 (1999) 11971.

[133] E. Valeev, W. D. Allen, H. F. Schaefer III and A. G. Császár, J. Chem. Phys. 114 (2001) 2875.

[134] A. K. Wilson, T. van Mourik and T. H. Dunning, J. Mol. Struct. THEOCHEM 388 (1997) 339.

[135] J. S. Lee, Chem. Phys. Lett. 359 (2002) 440.

[136] V. Bakken, T. Helgaker, W. Klopper and K. Ruud, Mol. Phys. 96 (1999) 653.

[137] R. Bukowski, B. Jeziorski and K. Szalewicz, J. Chem. Phys. 108 (1998) 7946.

[138] J. Noga, W. Kutzelnigg and W. Klopper, Chem. Phys. Lett. 199 (1992) 497.

[139] J. Noga and W. Kutzelnigg, J. Chem. Phys. 101 (1994) 7738.

[140] W. Klopper and J. Noga, J. Chem. Phys. 103 (1995) 6127.

[141] T. Helgaker, W. Klopper, H. Koch and J. Noga, J. Chem. Phys. 106 (1997) 9639.

[142] J. Noga and P. Valiron, Coll. Czech. Chem. Commun. 68 (2003) 340.